Experimental Determination
of Stray Load Losses in Cage Induction Machines

Vom Fachbereich Elektrotechnik und Informationstechnik
der Technischen Universität Darmstadt
zur Erlangung des akademischen Grades eines
Doktor-Ingenieurs (Dr.-Ing.)
genehmigte Dissertation

von

Dipl.-Ing. M´hamed Aoulkadi

geboren am 01.01.1972 in Douar Asila / Marokko

Acknowledgements

This work was carried out during the years 2002 to 2007, while I was working as research assistant at the Department of Electrical Energy Conversion at Darmstadt University of Technology.

Especially, I would like to thank my supervising professor, Prof. Dr.-Ing. habil. Dr. h.c. Andreas Binder, the head of the institute, for giving me the opportunity to carry out this work, for sharing his enormous expertise, for his guidance, patience and his support.

I would also like to express my deepest gratitude to Professor Dr.-Ing. Manfred Stiebler for taking on the role as second reader.

The research involved a lot of the measurements that had not been possible without the strong support of the mechanical and electrical workshop of the institute. I am deeply grateful for the support of the part of the crew in the workshops. I would like to thank all my colleagues at the institute for all their technical, professional and administrative support. I want to express my gratitude to all students, who participated in projects related to my PhD work.

I also wish to thank the colleagues of the company ELIN EBG-Motoren GmbH in Austria, the CEMEP members and the suppliers that accompanied the projects. These are ABB in Sweden, Electro-Putere in Romania, Leroy Somer in France, SEW-Eurodrive, Siemens and VEM in Germany.

The financial support given by the company ELIN EBG-Motoren GmbH and by CEMEP is also deeply acknowledged.

Finally, I owe my gratitude to my family, my parents, my friends, for all their support during my personal and professional education.

I am mostly indebted to the persons being closest to me, my wife Andrea and my children Amin and Iman, for their unremitting encouragement, patience and support.

I want to thank Allah for his help and his mercy.

Motivation

The present PhD thesis titled "*Experimental Determination of Stray Load Losses in Cage Induction Machines*" is based on two research projects and deals with the measurement of the stray load losses and the efficiency of the squirrel-cage induction machines.

From cost and competition reasons, the stator round wire winding is used in the grid-operated low-voltage squirrel-cage rotor asynchronous generators for 1.5 MW wind turbines. By overheating of the winding the high-utilized generator is endangered. The objective of the research project was to analyse the cause for high losses and overheating of the winding, to localise the sources and to develop measures to solve the problem.

The focus of the second research project was the measurement of the stray load losses in the grid-operated low-voltage standard TEFC induction machines. The well-known standardized methods like the input-output test (residual loss method), the calorimetric and the reverse rotation test acc. to the standards IEEE 112 or IEC 61972 needs expensive measurement equipments of high accuracy and a coupled load, take considerable time to perform the test and consume therefore more energy. With increasing efficiency, due to technical improvements, competition and environmental problems, a revision of these methods and of assigned fixed values for the stray load losses was necessary. Aim of this project was to find simple and economical alternative tests, applicable in manufacturer test field with reliable results also for high efficiency motors up to 95%…96%, with small amount of the stray load losses, where the input-output test is too inaccurate for the assessment of the stray load losses.

Abstract

With different purposeful measurements like for the stray load losses and the flux densities, on two low-voltage squirrel-cage rotor asynchronous generators for 1.5 MW wind turbines with different types of the stator winding (litz and round wire), the sources of the losses and the causes for the winding overheating are localized and defined. Different measures to reduce the stray load losses due the skin effect in the stator of the round wire winding generator are successfully tested and implemented in the manufacturing process. Thanks to these proven techniques the round wire winding is competitive to other expensive winding types. Analytical models for the estimation of the stator stray load losses due to the skin effect for profile, litz and round wire winding are compared to the measurements.

A survey on the cheap and simple methods to measure the stray load losses in squirrel-cage induction motors, apart from the standardized methods, results in three equivalent "no-load" methods, where no coupling and no dynamometer or torque-meter are needed. The strengths and weaknesses of the measurement methods were investigated and compared with the standardized input-output test (residual loss method) and the reverse rotation test (RRT) on 27 standard TEFC grid-operated cage induction motors (2-, 4- and 6-pole) with the current design of six European manufacturers with the rated power of 0.37 kW, 0.55 kW, 1.1 kW, 5.5 kW, 11 kW and 315 kW. It was concluded, that it is a benefit to add the eh-star method into the next edition of the future IEC 60034-2[*], as it is cheap, yielding comparable results with the input-output test, and is fitting better the purpose than RRT, which is already included in the standards. The theoretical background and the measurement procedure for the eh-star method are described in detail. Some analytical calculations were done, showing that theoretical prediction of the stray load losses correlates with the design and the measurement results.

[*]: The eh-star method was proposed on Dec. 2005 in IEC 60034-2 Ed. 4/1367/2nd draft [IEC 60034-2 draft]. May 2007 it was accepted and published on Sept. 2007 in IEC 60034-2-1, Edition 1.0 [IEC 60034-2-1].

Aufgabenstellung

Die vorliegende Arbeit "*Experimentelle Bestimmung der Zusatzverluste in Käfigläufer-Induktionsmaschinen*" basiert auf zwei Forschungsprojekten und befasst sich mit der Messung der Zusatzverluste und des Wirkungsgrades der Asynchronmaschinen mit Käfigläufer.

Aus Kosten- und Wettbewerbsgründen werden die Niederspannungs-Käfigläufer-Asynchrongeneratoren für 1.5 MW Windturbinen mit Runddraht-Träufelwicklungen im Stator ausgeführt. Durch Überhitzung ist die Wicklung der hoch ausgenutzten Maschinen gefährdet. Das Ziel des Forschungsprojekts war, die potentiellen Verlustquellen zu lokalisieren und zu analysieren sowie entsprechende Abhilfe-Maßnahmen zu entwickeln.

Im Rahmen des zweiten Forschungsprojekts stand die Messung der Zusatzverluste in netzgespeisten Niederspannungs-Normmotoren im Vordergrund. Die bekannten standardisierten Messmethoden in z.B. IEEE 112 oder IEC 61972, wie Input-output Test, kalorimetrische Messverfahren und der Reverse Rotation Test, sind aufwendig, und fordern teures Messequipment von hoher Genauigkeit sowie eine gekuppelte Lastmaschine. Sie benötigen mehr Zeit für die Durchführung der notwendigen Tests und verbrauchen deshalb mehr Energie. Aufgrund des technischen Fortschritts, aus Wettbewerbsgründen und wegen der zunehmenden Umweltprobleme werden effizientere Motorenreihen entwickelt. Damit war eine Revision dieser Messmethoden und des darin angenommenen festen Zuschlags für die Zusatzverluste notwendig. Ziel war es, ein einfaches, kostengünstiges alternatives Messverfahren zu finden, das leicht im Prüffeld des Herstellers anwendbar ist und zuverlässige Ergebnisse liefert, u.a. auch für Motoren mit einem Wirkungsgrad größer als 95 %. Input-output Tests (z.B. IEC 61972, IEEE-112-B) haben wegen der dafür zu hohen nötigen Genauigkeit der Messgeräte für die Aufnahme- und Abgabeleistung hier eine Grenze.

Kurzfassung

Durch gezielte Messungen, wie die der Zusatzverluste und der magnetischen Flussdichte an zwei 1.5 MW Niederspannungskäfigläufer-Windgeneratoren mit unterschiedlichen Stator-Wicklungsausführungen (Runddraht-Träufelwicklung und Litzenwicklung) konnten die Ursache, die Größe und der Ort der Zusatzverluste bestimmt werden. Verschiedene Abhilfe-Maßnahmen zur Reduzierung der Wicklungszusatzverluste infolge Stromverdrängung wurden erfolgreich getestet und in den Fertigungsprozess integriert. Dank dieser erprobten Techniken ist die Runddrahtwicklung konkurrenzfähig zu anderen teureren Wicklungsausführungen. Zur Abschätzung der Wicklungszusatz-verluste infolge Stromverdrängung wurde für jede Wicklungsausführung (Formspulenwicklung, Litzenwicklung, polumschaltbare und nicht polumschalt-bare Runddrahtwicklungen) ein Modell erstellt und mit der Messung verglichen.

Die Recherche über einfache und kostengünstige alternative Messverfahren zu den bereits genormten Messmethoden für die Bestimmung der Zusatz-verluste in Käfigläufer-Asynchronmaschinen ergab die Auswahl von drei „Leerlauf-Ersatzmethoden", in denen der Prüfling nicht mit einer Last gekuppelt werden muss und keiner kalibrierten Drehmomentenmesseinrichtung bedarf. Die Stärken und Schwächen dieser Messmethoden wurden untersucht. Die Messergebnisse an 27 Normmotoren von 6 europäischen Herstellern mit entsprechend unterschiedlichem Motor-Design mit Bemessungsleistungen von 0.37 kW, 0.55 kW, 1.1 kW, 5.5 kW, 11 kW und 315 kW zeigten, dass die eh-Stern Methode gute Übereinstimmung mit den Ergebnissen des Input-output Tests liefert. Der bereits genormte Reverse Rotation Test liefert in der Regel zu hohe Zusatzverluste. Da die eh-Stern Methode messtechnisch einfach und kostengünstig ist, und dazu vergleichbare Ergebnisse mit dem Input-output Test liefert, wurde sie in der Norm IEC 60034-2-1 aufgenommen. Der theoretische Hintergrund und das Messverfahren für die eh-Stern Methode sind in dieser Arbeit ausführlich beschrieben. Zur Abschätzung der Zusatzverluste wurden einige analytische Berechnungen durchgeführt, in denen der Einfluss des Motor-Designs gezeigt wurde, und die zum Teil gute Übereinstimmungen mit der Messung ergaben.

CONTENTS

1 INTRODUCTION

The workhorse in the drive system, namely the induction motor as squirrel-cage or wound rotor, is the most widely used electric motor type. Their application area is extensive as constant speed (grid fed) e.g. in pumps and wind generators, variable speed (inverter fed) e.g. in paper industry or high speed e.g. in tooling machinery, with some kW up to several MW.

A number of different types of electric motors exist. The vast majority of the motors used in industry are the standardized squirrel-cage induction motors due to their low cost, low-maintenance, high reliability and fairly high efficiency.

The losses including the stray load losses (additional losses) influence substantially the heating of the winding, worsen the torque characteristic at running up and reduce the efficiency of the induction machines. To improve the performance of the machines the place and the size of the losses including the stray load losses must be determined in order to reduce them. Owing to the competitiveness and the environmental problems, it has become more important to determine the losses and the efficiency of the motors.

But how to evaluate these motors of different manufacturers concerning their improved efficiency ? Of course several methods had been standardized for long in national and international standards e. g. IEC 60034-2 [IEC 60034-2], but with increased efficiency in the range of 95% and more some of these procedures were too inaccurate e.g. residual loss method (input-output test) acc. to IEEE 112-method B [IEEE 112] and others too expensive e.g. calorimetric method and needs a coupled load, take considerable time to perform the tests and consume therefore more energy. These standards use different ways to incorporate the stray load losses.

1.1 Challenge

Motor manufacturers are in a situation that any changing of the standards for efficiency determination methods requires retesting of currently and ongoing sold motor types, as generally a full occurrence-synchronisation between development of motors and standards is of "near zero" probability. The product lifetime of motors can be assumed of being significantly longer than ten years. The challenge for the responsibility of standardization experts is to find an alternative efficiency determination method with less expense, suitable in manufacturer test bays, but comparable results.

A close collaboration of the IEC standardization working groups, the national working groups and the industrial manufacturers organization (CEMEP: European Committee of Manufacturers of Electrical Machines and Power Electronics) brought up several parallel activities on efficiency motors. One of them was the collaboration with Universities in UK and Germany to find out,

- if additional measurement procedures for electric motor efficiency are available,
- if refinement of existing methods is necessary in mathematical, physical and technical way,

to show up strength and weakness of different methods and their practical existing limitations and to work out attainable accuracy in reality. This scientific work – in collaboration with CEMEP and the IEC Working group – was done between 2003…2005 and brought up several encouraging results, which have not been only discussed thoroughly within the standardization organizations and the industrial partners, but have been published also in the scientific community [Aoul 2005, Gera 2005, Zwan 2006].

Basically, one can resume, that some already known techniques have been "re-found", mainly the eh-star method [Jord 1967], which allowed much simpler way to measure stray load losses. This method – when being first presented to the public in the late Sixties – was not distributed broadly, as the calculation amount "post-processing", was rather time consuming, whereas the measurement procedure itself was simple. Nowadays with modern computers this calculation is done in the fraction of a heart-beat and can contribute to

efficiency evaluation even at values higher than 96 % without loading the machine with a coupled dynamometer, thus saving costs. An EXCEL sheet, which available overall, for the calculation and a guide-line [Guid 2005] for performing this test were provided. These results were welcome to the standardization working group and were presented and discussed on several meetings. As an answer to the challenge for the responsibility of standardization experts to find an alternative efficiency determination method with fewer amounts but comparable results, the eh-star method acc. to the proposed standard IEC 60034-2 Ed. 4 [IEC 60034-2 draft] can be such an optimal technical, feasible and economical alternative test. It needs usually an additional adjustable resistor for asymmetric feeding, which is cheaper than a calibrated load and torque measurement.

Obviously certain manufacturers are already well equipped with instrumentation e.g. acc. to IEEE-112 method-B standard and are not "open" for something "new". Due to experience with the new method within several companies, who took effort to evaluate the eh-star method in their test bay, the test time was calculated to be just 25 % to 30 % compared to the method according to IEC 61972, which leads at the end to a saving potential of ca. 10 Million Euros for the community. This result is a success to sensible standardization politics of the dedicated experts [Zwan 2006]. Nevertheless the already well-known and proven other test standards are still included and allow the manufacturer and customer to choose the negotiated method.

1.2 High efficiency is one of the tasks of the hour

Environmental problems – greenhouse gas emission, climate change, warming up of the earth – are topics we hear nearly every day discussed somewhere on TV, in newspapers or in the public. Growing earth population is of course one main driver as each individuum needs energy in on or other form. It is certain, everybody is concerned. How does everybody handle the "precious" energy in production and consumption ? How can society and each segment of it contribute to cope with these problems ? The standards e.g. by offering different reliable measurement methods and the standardization e.g. of industrial

equipment, namely the ubiquitous electric motors, can support our struggle for save future life.

Energy efficiency and the environment are inextricably linked i.e. in the ECCP (European Climate Change Program). In the actual and future electric energy market energy saving policies grows more and more important, having a big impact on industrial equipment and their standardization.

In the European Union, the rotating electrical machines needed in the industrial field applications transmit typically 60 %…70 % of the total absorbed electrical energy to mechanical energy. In the commercial sector, this percentage is up to 35 % [Bogl 2004]. So improvement of the motor efficiency is one of the tasks of the hour. In the last years, research and development into improving motor design construction and manufacturing techniques have resulted in improvements in efficiency, in costs reduction, reduction of environmental pollution and increasing of renewable energy sources, especially wind power as presented in Figure 1.1. Within only 20 years the energy yield increased by a factor of 100 (see Table 1.1) [BWE 2008].
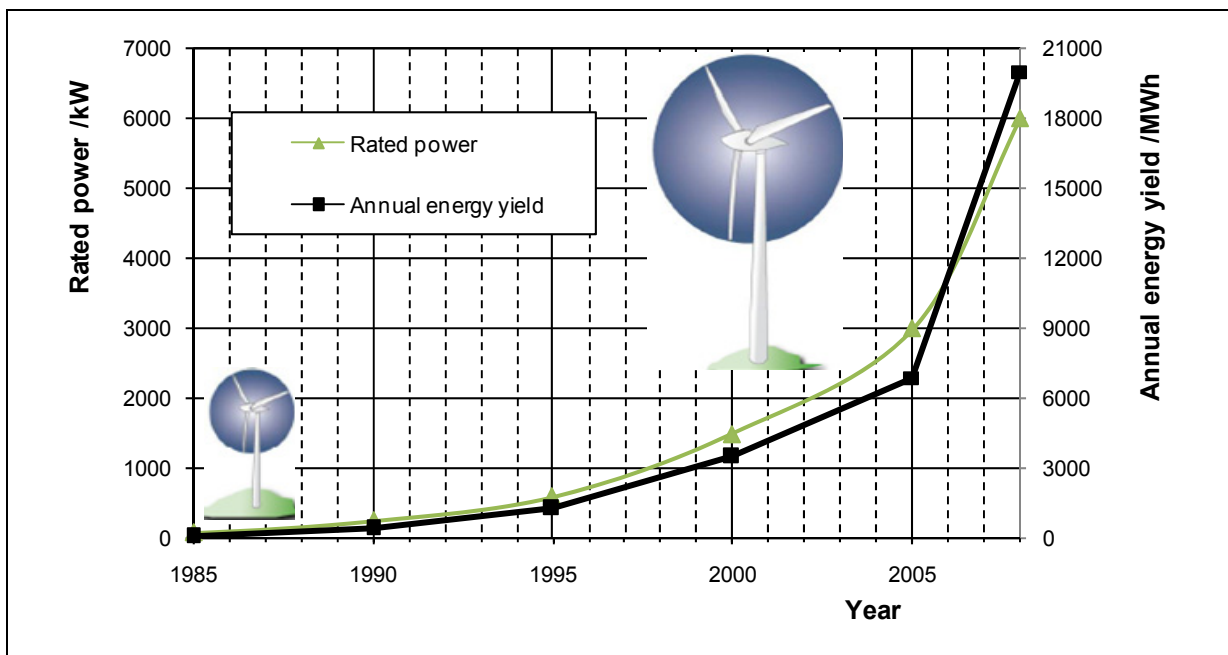
Figure 1.1: Development of the rated power and annual energy yield of the wind generators
          [BWE 2008]

The wind energy has grown strongly due to the development of the wind energy technology and increased number of installed wind turbines. Table 1.1 gives the development of the wind turbine size concerning the rated power, the rotor diameter and hub height between 1980 and 2008 [BWE 2008]. Larger turbines will be erected in the near future.

Year	1980	1985	1990	1995	2000	2005	2008
Rated power /kW	30	80	250	600	1500	3000	6000
Rotor diameter /m	15	20	30	46	70	90	126
Hub height /m	30	40	50	78	100	105	135
Annual energy yield /MWh	35	95	400	1250	3500	6900	approxim. 20000 [*)]

Table 1.1: Development of the wind turbine size [BWE 2008]

[*)]: Estimated value in [BWE 2008]. The combination of 6000 kW rated power and 20000 MWh energy yield is too optimistic, even for off-shore; this would mean 3333 full load hours per year.

To improve the efficiency, a "Voluntary Agreement" between the EC (European Commission) and CEMEP (European Committee of Manufacturers of Electrical Machines and Power Electronics) was made in the field of low voltage induction motors, where minimum nominal efficiencies were defined in classes EFF1 for high efficiency, EFF2 for improved efficiency and EFF3 for standard efficiency [Bert 2005, Auin 2001], as shown in Figure 1.4. The EFF-classes are meanwhile replaced by the efficiency classes IE1 – IE3 according to the new IEC 60034-30: 2008 [IEC 60034-30] presented in Figure 1.2. Due to their reduced losses, high efficiency motors IE3 and IE2 run at lower temperatures than equivalent standard motors IE1, which results in longer insulation and lubricant life and less downtime.

Note: The Voluntary Agreement was officially withdrawn when IEC 60034-30 came into effect.

Figure 1.3 shows how the weight of a 4 kW motor has been reduced over the last 60 years [Walt 1995] due to improved design and materials (magnetic steels, insulation, bearings…).
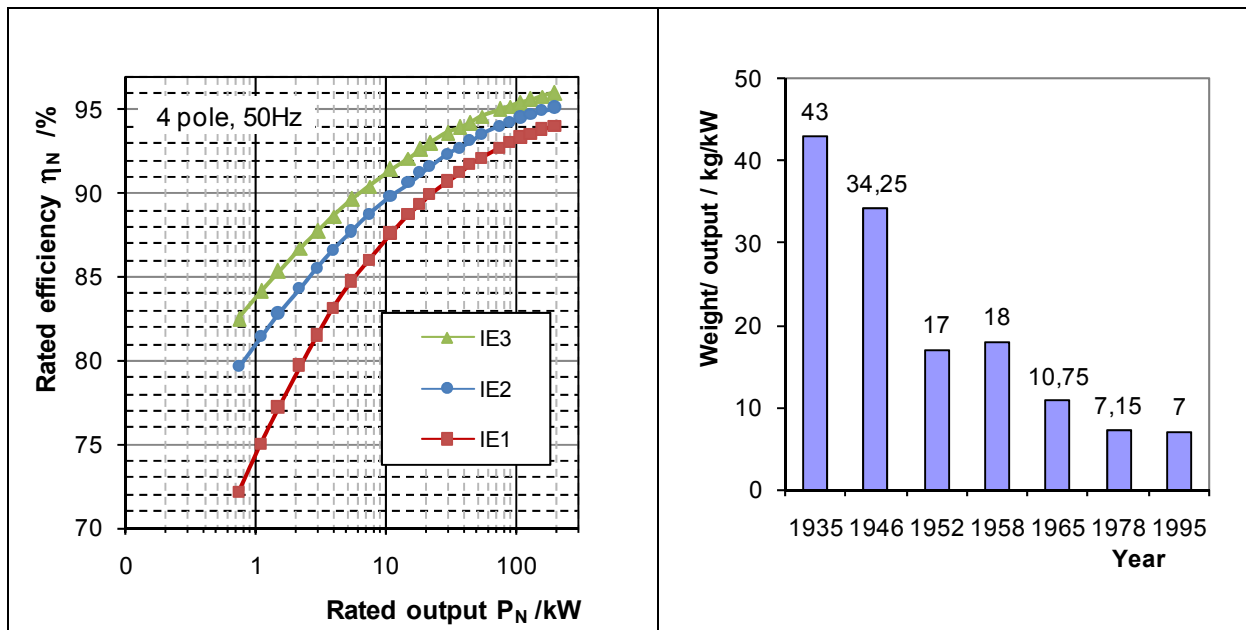
Figure 1.2: Nominal limits for Standard
Efficiency, for 4-pole motors 50 Hz,
according to IEC 60034-30
[IEC 60034-30]

Figure 1.3: Ratio of weight to output power
(kg/kW) for a 4 kW induction
motor 1935-1995 [Walt 1995]

1.3 Benefits of high efficiency motors to environment

Motors with improved efficiency EFF2 are 5 % and with premium efficiency
EFF1 are 30 % more expensive compared with the standard efficiency EFF3. As
the motor customers tend to make purchasing decisions based on lowest first
cost rather than life cycle cost, the market for EFF1-motors was below 7 % in
2004 [Zwan 2004]. The experiences in Europe and in other countries (USA,
Canada, and Australia) have shown that only by political support (financial
incentives or law) an essential market moving in this meaning can be reached
[VDE 2008]. The percentage of EFF3-motors decreased from 68 % in 1998
down to 8 % in 2004, which exceeds the target of the Voluntary Agreement of
CEMEP. A total sum of about 4 to 5 TWh of electrical energy was already saved
in 2004 in comparison to 1997 [Sand 2005, Zwan 2004].

Figure 1.4 shows the motor efficiency classes for 4-pole induction motors
again the rated power and the estimated energy saving potential with EFF1-

motors instead of EFF3-motors as percent of the electrical input power. The greatest energy saving potential by installed motors in the industrial sector is concentrated in power range of 1.1 to 37 kW due to the typical operating times per year [VDE 2008].
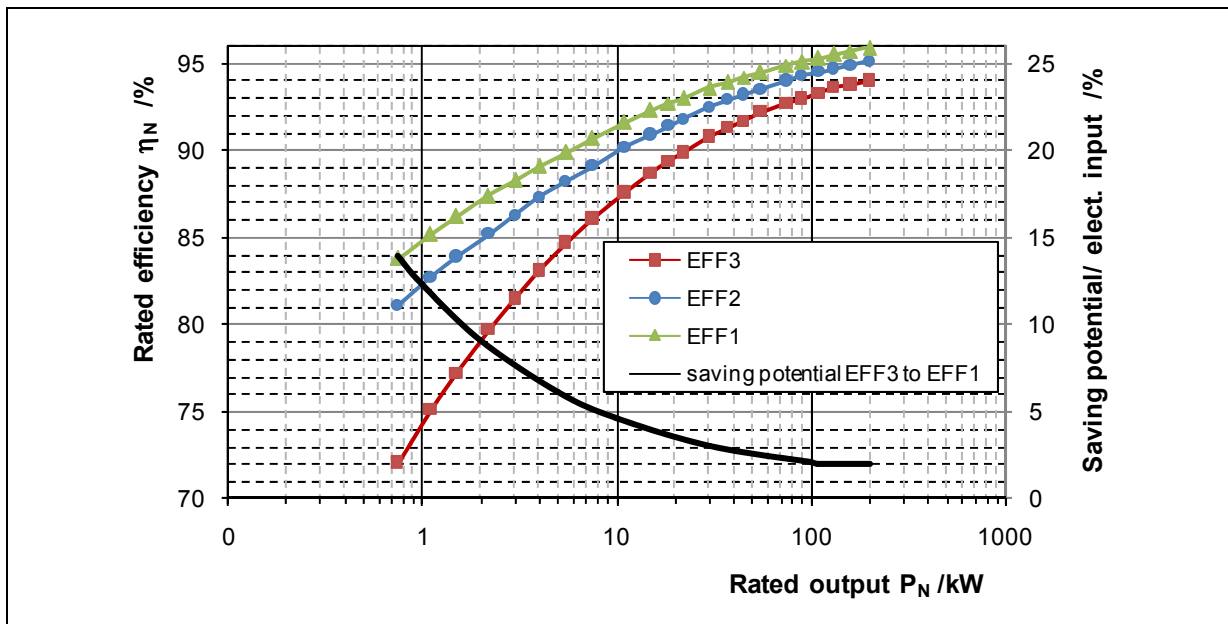
Figure 1.4: Motor efficiency classes and estimated energy saving potential with EFF1-motors instead of EFF3-motors as percent of the electrical input power [VDE 2008]

The pay-back periods in investments in energy efficient motor systems for new installations are in most cases relatively short, ranging at the actually given cost level for wages, materials and energy from 3 months to 3 years, depending on the motor type (EFF1 or EFF2) and on the real motor duty cycle, which determines energy costs. This pay-back period falls rather short, when compared with a typical motor life time of 20…30 years (and longer).

The implementation of modern efficient drive systems can save Europe over 200 TWh of electricity and 100 million tons of CO_2 emission annually, € 10 billion reduction per year in operating costs for industry, € 6 billion annual savings for Europe in reduced environmental costs, 45 GW reduction in the need for new power plant capacity over the next 20 years and 6 % reduction in Europe's energy imports [Keul 2005]. The high efficiency motors can contribute to the above noted energy savings by about 12 %, the use of variable speed by about 23 % and the improvements on the application side by 65 %.

But even concentrating here only on the efficiency of the motors itself, proves once again, that standards are important instruments to achieve technical, political and managerial objectives. The economical influence of the standards on technical development of induction motors has an ecological impact on our environment, which should not be under-estimated.

To get a feeling, how high efficient motors will contribute to save energy and greenhouse gas, let us look at the bare numbers of a simple calculation example: Electrical power consumption in Germany 2001 was 18 % of total energy consumption, resulting in 492 TWh (= 492 000 000 000 kWh). The industrial electrical energy consumption made up for 42.5 % (209 TWh). Conversion into mechanical energy came to 69 % of that (144 TWh), consumed by electric motors. With an average efficiency increase of 4 % of electromechanical energy conversion by premium efficiency motors, which we assume realized by only 50 % of installed drive power, one gets an energy saving of $0.04 \cdot 0.5 \cdot 144$ TWh = 2.9 TWh per year (8760 hours), which amounts to power delivery of a power plant with 2.9 TWh / 8760 h = 330 MW. Most power plants in Germany are thermal power plants. New plants have an optimum efficiency of 50 %, e.g. if a combined cycle plant is used. In this case the saving of thermal input power is 660 MW. In reality, many of German thermal power plants are still of older type with a lower efficiency, or they are operated not in the optimum point due to grid demands, so an overall average efficiency of only about 35 % is more close to the reality. Therefore the savings would even lead to a reduction of 943 MW thermal input power.

1.4 Structure of the thesis

The presented contribution "*Experimental Determination of Stray Load Losses in Cage Induction Machines*" is based on two research projects and focuses on the measurement methods to determine the stray load losses and the efficiency of grid-operated low-voltage squirrel-cage induction machines.

The PhD report consists of a summary and five chapters. Each chapter closes

with a short summary. The conclusions and the outlook of the thesis are summarized in the last Chapter 6. The thesis is structured as follows.

Chapter 2 gives an overview on the important efficiency measurement methods and explains how to determine the stray load losses in induction machines using different methods. Based on examples, obtainable accuracy, practically existing limitations, advantages and disadvantages of six different measurement methods are shown.

The focus of the third chapter is the eh-star method as an equivalent measurement method to determine the stray load losses. The theoretical background, the test procedure and the post-processing with different evaluation methods are described in detail.

Chapter 4 summarizes the test results from different measurement methods of different standard TEFC (totally enclosed, fan cooled) cage induction motors with rated power of 0.37 kW, 0.55 kW, 1.1 kW, 5.5 kW, 11 kW 315 kW, and of two 1500 kW wind generators.

The objective of chapter 5 is the analytical calculation of the stray load losses in the stator winding due to the skin effect. After a short summary on eddy currents, a comparison of the calculation models to the measurements for 1500 kW grid-operated cage induction generators with profile, litz and round wire windings is presented. Some measures to suppress stray load losses in the stator winding due to circulating currents are given. The chapter closes with an overview on main stray load loss components in 11 kW cage induction motors and comparison between measurement and analytical calculation.

The measurements on small motors were performed in the power lab of the *Department of Electrical Energy Conversion, Darmstadt University of Technology*, whereas the measurements on the 315 kW motor and the 1500 kW wind generators were performed in the manufacturer test field.

Note regarding the referred standards:

When referring to the standards, publications valid up to begin of 2006 were considered, since the experimental work was done up to end of 2005. Between

2006 and 2010 some standards were withdrawn and replaced by superseding publications. In chapter 7 Bibliography, Notes indicate where new standards came into effect in the meantime.

2 IMPORTANT MEASUREMENT METHODS FOR EFFICIENCY DETERMINATION

The present chapter provides an overview on the important efficiency measurement methods for induction machines. The main purpose is to determine the stray load losses (additional losses) by using different methods and procedures, and to compare the obtained results. The stray load losses are the remaining losses when subtracting from the total losses of an induction machine the sum of the friction and windage, the stator I^2R losses, the rotor I^2R losses and the iron losses. On the basis of examples six different measurement methods for the determination of the stray load losses of grid-operated induction machines will be compared. The advantages and disadvantages of these measurement methods will be discussed.

The six experimental measurement procedures are:

- the residual loss method acc. to IEC 61972 [IEC 61972] and IEEE 112-method B [IEEE 112]

- the reverse rotation test (RRT) acc. to the same standards,

- the eh-star method acc. to *Jordan* and *Richter* [Jord 1967, IEC 60034-2 draft],

- the equivalent no-load method acc. to *Bourne* [Bour 1989] and

- the equivalent no-load method acc. to *Rawcliffe* and *Menon* [Rawc 1952].

Note:
When referring to the residual loss method acc. to IEC 61972 [IEC 61972] and IEEE 112-method B [IEEE 112], the term for the test in view is "Input-output test with segregation of the losses and indirect measurement of the stray load losses", or residual loss method, as defined in 5.6 of IEC 60034-31 ("The

residual loss method in IEC 60034-2-1 is a defined calculation procedure for segregating the various types of losses from the raw data and smoothing the additional (stray-) load loss by linear regression analysis").

2.1 Motor efficiency

The efficiency η of an induction machine e.g. in motor operation is the ratio of the output power $P_{m,out}$ (the mechanical power on the motor shaft) to the input power $P_{e,in}$ (electrical power). It qualifies the degree for energetic conversion of electrical power $P_{e,in}$ into mechanical power $P_{m,out}$. The output power $P_{m,out}$ is equal to the input power $P_{e,in}$ minus the total losses P_d. Therefore, if two of the three variables (output power, input power, or total losses) are known, the efficiency η can be determined by one of the following equations:

$$\eta_{direct} = \frac{\text{output power}}{\text{input power}} = \frac{P_{m,out}}{P_{e,in}}, \tag{2.1}$$

$$\eta_{indirect} = \frac{\text{input power - total losses}}{\text{input power}} = \frac{P_{e,in} - P_d}{P_{e,in}}, \tag{2.2}$$

$$\eta_{indirect} = \frac{\text{output power}}{\text{output power + total losses}} = \frac{P_{m,out}}{P_{m,out} + P_d}. \tag{2.3}$$

According to (2.1) the efficiency η is determined directly by measurement of the input $P_{e,in}$ and output $P_{m,out}$ powers, and acc. to (2.2) and (2.3) the efficiency η is determined indirectly by the determination of the total losses P_d. The efficiency η of an induction motor depends, besides the motor design, the determination method, the instrumentation and measurement accuracies, on many parameters like the load condition (full or partial load), the winding temperature and the quality of the power supply including the frequency and other parameters [Auin 1999].

2.1.1 Efficiency determination methods

The efficiency determination methods vary greatly in terms of their complexity, overall performance and the suitability for the plant conditions. Experimentally it is not a simple task if it is to be performed with precision. The efficiency data provided by the manufacturers are measured or calculated according to different national and international standards. These standards use different ways and assumptions to incorporate the stray load losses, thus the efficiency values obtained from different testing standards can differ by several percent. This leads to problems in competition and to a perhaps confusing situation for manufacturers and customers.

With regard to the methods of evaluating the efficiency and particularly the stray load losses in induction motors, for the existing standards the following bodies are leading:

- the Institution of Electrical and Electronic Engineers (IEEE 112),

- the International Electrotechnical Commission (IEC 60034-2) and

- the Japanese Electrotechnical Commission (JEC 37).

Other national standards e.g. the Canadian CSA (C 390) are partly harmonised to one of these standards [Bogl 2004]. These standards provide several methods and procedures for efficiency measurements in accordance with the type and the machine rating, with the desired accuracy, etc. It is difficult to establish specific rules for efficiency determination. If there is no agreement between manufacturer and customer, the choice of measurement method will depend on the information required, the accuracy desired, the type and rating of the machine and the available test equipment, e.g. the supply, the load machine, the torque meter etc.

Some methods of the efficiency measurement and losses determination are presented in Figure 2.1 and can be grouped as follows:

- Input-output test e.g. acc. IEEE 112-method A

- Input-output test with segregation of the losses and indirect measurement of the stray load losses e.g. acc. IEEE 112-method B (residual loss method)

- Calorimetric method

- Electric power measurement under load with segregation of losses and direct measurement of the stray load losses e.g. acc. IEEE 112-method E

- Electric power measurement under load with segregation of losses and assumed value of the stray load losses e.g. acc. IEEE 112-method E1

As highlighted in Figure 2.1 the measurement of the stray load losses is the main purpose of this thesis.
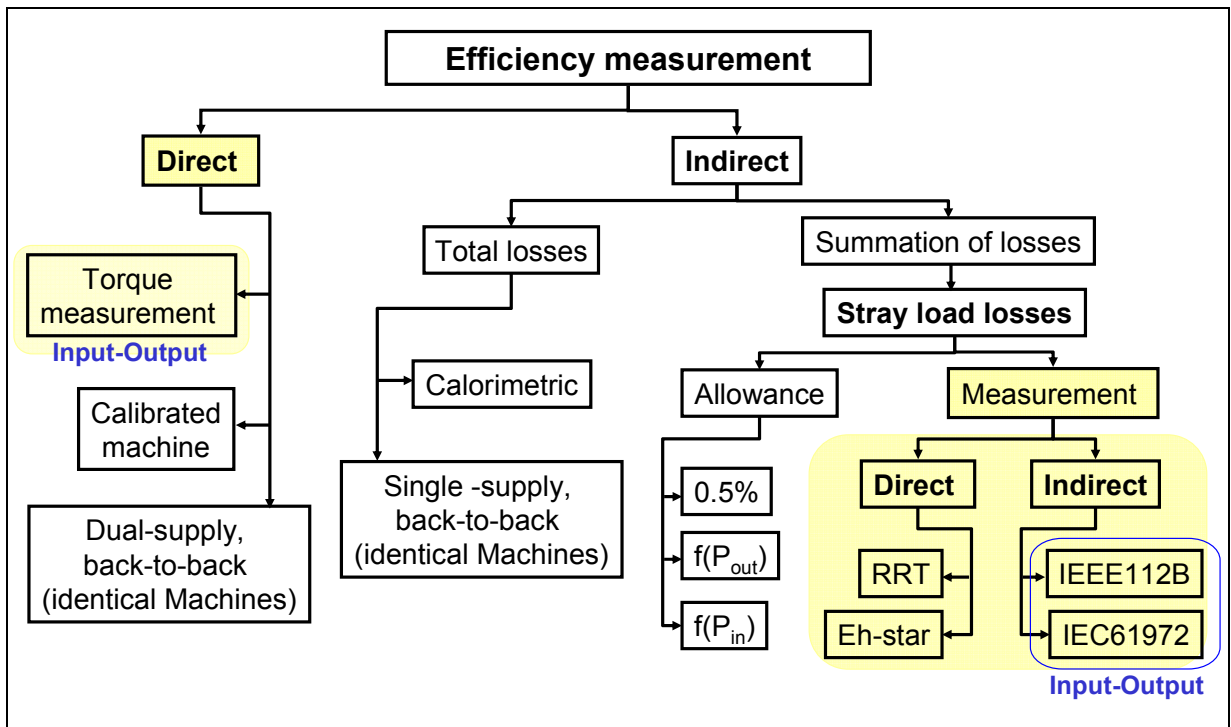
Figure 2.1: Efficiency determination methods

The main difference of the mentioned methods, beside measurement equipment and setup, is the determination of the stray load losses. The way to determine the stray load losses is the main focus of the next section. Some standards suggest various empirical factors. JEC 37 neglects completely the stray load losses. IEC 60034-2 [IEC 60034-2] assumes a fixed value of 0.5 % of the rated input power for the stray load losses. The National Electrical

Manufacturers Association NEMA MG1 [NEMA] recommends 1.2 % for induction motors rated less than 1850 kW, and 0.9 % for ratings 1850 kW and above. As an improvement, IEEE 112-method E1/F1 [IEEE 112] provides a variable portion of output power for the stray load losses, dependent on the machine ratings. This is listed in Table 2.1. Similarly, the new revision of the standard IEC 61972 [IEC 61972] provides a curve which is also a function of the motor ratings, as plotted in Figure 2.2.

Machine rating in kW	Stray loss/output
1 – 90	1.8 %
91 – 375	1.5 %
376 – 1850	1.2 %
> 1850	0.9 %
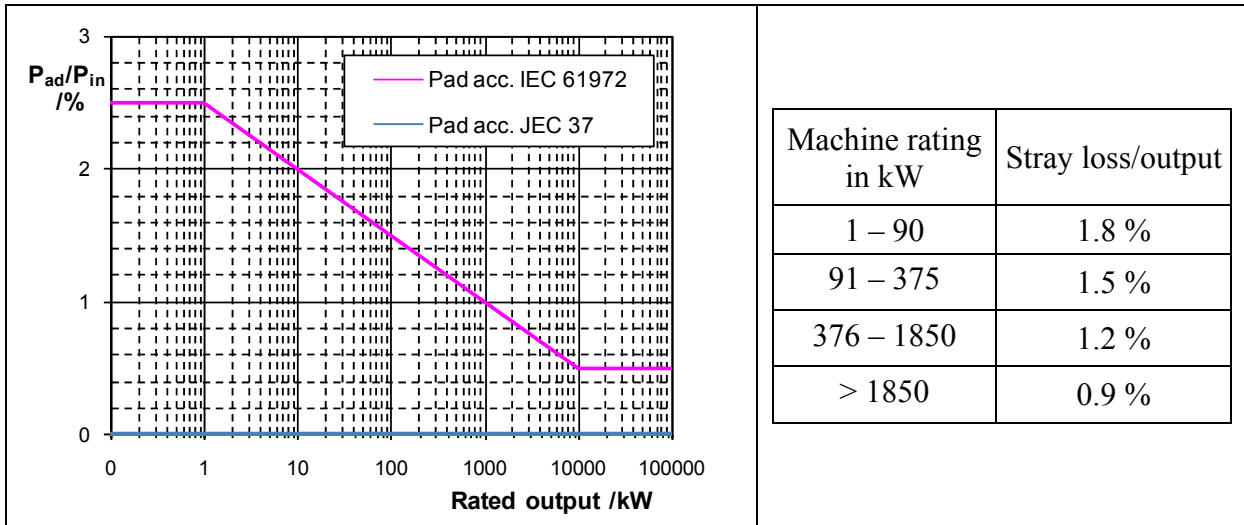
Figure 2.2: Assumed allowance for stray load losses in IEC 61972 and JEC 37

Table 2.1: Assigned values of stray load losses in IEEE 112

2.1.2 Uncertainty of directly measured efficiency

Because of unavoidable measurement errors, the direct efficiency η_{dir} determination by measuring input power $P_{e,in}$ and output power $P_{m,out}$ according to (2.1) is generally not accurate enough for motors of higher efficiency. Depending of the measurement accuracy of input $P_{e,in}$ and output $P_{m,out}$, the uncertainty of the directly measured efficiency $|\Delta\eta_{dir}|$ will vary with the real efficiency of the motor as

$$\left|\Delta\eta_{\text{dir}}\right| = \frac{P_{\text{m,out}}}{P_{\text{e,in}}} \cdot \left|\frac{\Delta P_{\text{m,out}}}{P_{\text{m,out}}}\right| + \frac{P_{\text{m,out}}}{P_{\text{e,in}}} \cdot \left|\frac{\Delta P_{\text{e,in}}}{P_{\text{e,in}}}\right| = \eta_{\text{dir}} \cdot \left(\left|\frac{\Delta P_{\text{m,out}}}{P_{\text{m,out}}}\right| + \left|\frac{\Delta P_{\text{e,in}}}{P_{\text{e,in}}}\right|\right). \qquad (2.4)$$

This impact is given for an error of 0.2 % in Table 2.2 and presented for other assumed errors in Figure 2.3. It is assumed that the input $P_{\text{e,in}}$ and output $P_{\text{m,out}}$ powers are measured with the same accuracy.

Real efficiency η_{real} /%	70	75	80	85	90	95	96	98	100
Mini measured η_{dir} /%	69.72	74.70	79.68	84.66	89.64	94.62	95.62	97.61	99.60
Maxi measured η_{dir} /%	70.28	75.30	80.32	85.34	90.36	95.38	96.38	98.39	100.4
|Uncertainty| /%	0.28	0.30	0.32	0.34	0.36	0.38	0.38	0.39	0.40

Table 2.2: Impact of 0.2 % error on the directly determined efficiency

For an assumed error of 0.2 % the measured efficiency can vary between 84.66 % and 85.34 % for a small motor with 85 % efficiency and between 95.62 % and 96.3 % for a large motor with 96 % efficiency. For a realistic error value of 0.5 % the uncertainty of the directly determined efficiency is higher with 0.85 % for the small motor and 0.96 % for the large one as shown in Figure 2.3.
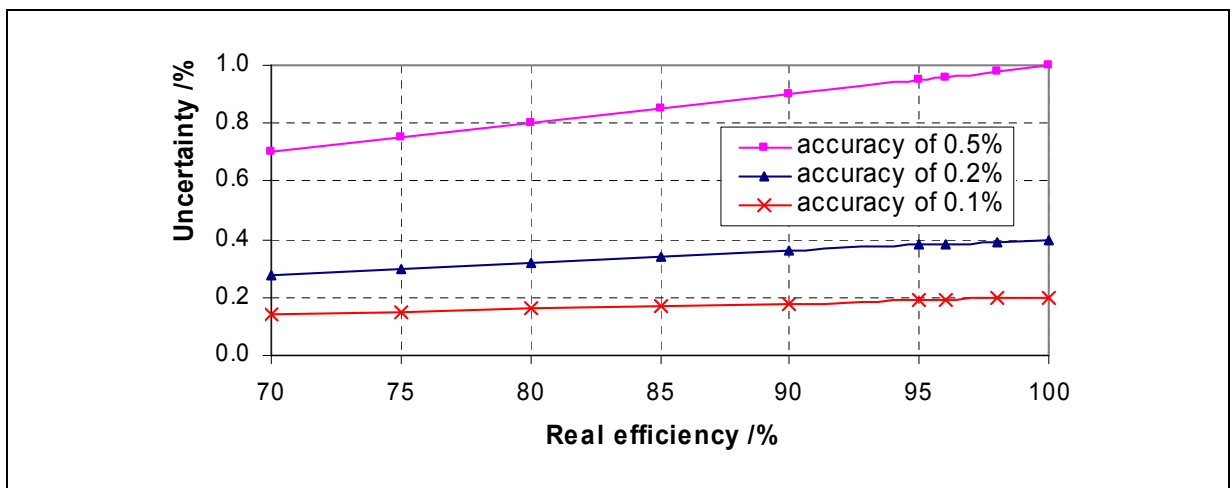
Figure 2.3: Impact of measurement error on the directly determined efficiency

2.1.3 Uncertainty of indirectly measured efficiency

The uncertainty of the indirectly measured efficiency $|\Delta\eta_{\text{indir}}|$ varies also with the accuracy of the measured total losses P_{d} and with the real efficiency of the motor as

$$\left|\Delta\eta_{\text{indir}}\right| = \frac{P_{\text{d}}}{P_{\text{e,in}}} \cdot \left|\frac{\Delta P_{\text{d}}}{P_{\text{d}}}\right| + \frac{P_{\text{d}}}{P_{\text{e,in}}} \cdot \left|\frac{\Delta P_{\text{e,in}}}{P_{\text{e,in}}}\right|. \tag{2.5}$$

With (2.6), the uncertainty of the indirectly measured efficiency $|\Delta\eta_{\text{indir}}|$ in (2.5) can be expressed as shown in (2.7)

$$\frac{P_{\text{d}}}{P_{\text{e,in}}} = 1 - \eta_{\text{indir}}, \tag{2.6}$$

$$\left|\Delta\eta_{\text{indir}}\right| = (1 - \eta_{\text{indir}}) \cdot \left(\left|\frac{\Delta P_{\text{d}}}{P_{\text{d}}}\right| + \left|\frac{\Delta P_{\text{e,in}}}{P_{\text{e,in}}}\right|\right). \tag{2.7}$$

Assuming that the measurement accuracy for the total losses P_{d} is the same as for the input power $P_{\text{e,in}}$, e.g. 0.2 %, the uncertainty of the indirectly determined efficiency $|\Delta\eta_{\text{indir}}|$, which decreases with higher efficiency, is smaller compared with the directly measured efficiency $|\Delta\eta_{\text{dir}}|$, which increases with higher efficiency, as shown in Figure 2.4 (see also [Auin 2001]). So the indirect efficiency determination seems to be useful for motors of higher efficiency, depending on the measurement accuracy of the total power losses P_{d}.
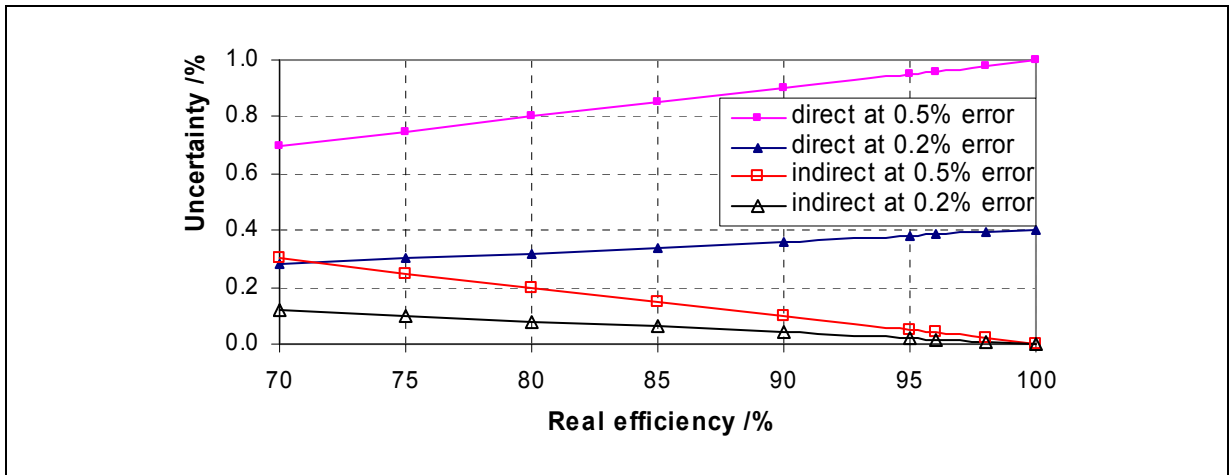
Figure 2.4: Impact of measurement error on the directly and indirectly determined efficiency

2.1.4 Uncertainty of measured total losses

The total losses P_d are given by the difference between the input $P_{e,in}$ and output $P_{m,out}$ acc. to (2.8). So the uncertainty in the determination of the total losses P_d depends on the measurement accuracy of these powers and on the real value of the efficiency as given in (2.11).

$$P_d = P_{e,in} - P_{m,out} \rightarrow \left|\Delta P_d\right| = \left|\Delta P_{e,in}\right| + \left|\Delta P_{m,out}\right|, \tag{2.8}$$

$$\left|\frac{\Delta P_d}{P_d}\right| = \left|\frac{\Delta P_{e,in}}{P_{e,in}}\right| \cdot \frac{P_{e,in}}{P_d} + \left|\frac{\Delta P_{m,out}}{P_{m,out}}\right| \cdot \frac{P_{m,out}}{P_d}. \tag{2.9}$$

With (2.10) the uncertainty $\left|\Delta P_d / P_d\right|$ can be expressed as shown in (2.11)

$$\frac{P_{e,in}}{P_d} = \frac{1}{1-\eta_{indir}}, \quad \frac{P_{m,out}}{P_d} = \frac{\eta_{indir}}{1-\eta_{indir}} \tag{2.10}$$

$$\left|\frac{\Delta P_d}{P_d}\right| = \left|\frac{\Delta P_{e,in}}{P_{e,in}}\right| \cdot \frac{1}{1-\eta_{indir}} + \left|\frac{\Delta P_{m,out}}{P_{m,out}}\right| \cdot \frac{\eta_{indir}}{1-\eta_{indir}}. \tag{2.11}$$

Figure 2.5 shows the impact of the measurement error on the determined total

losses P_d by the input-output test for different accuracy assumptions. It is assumed that the input $P_{e,in}$ and output $P_{m,out}$ powers are measured to the same accuracy.
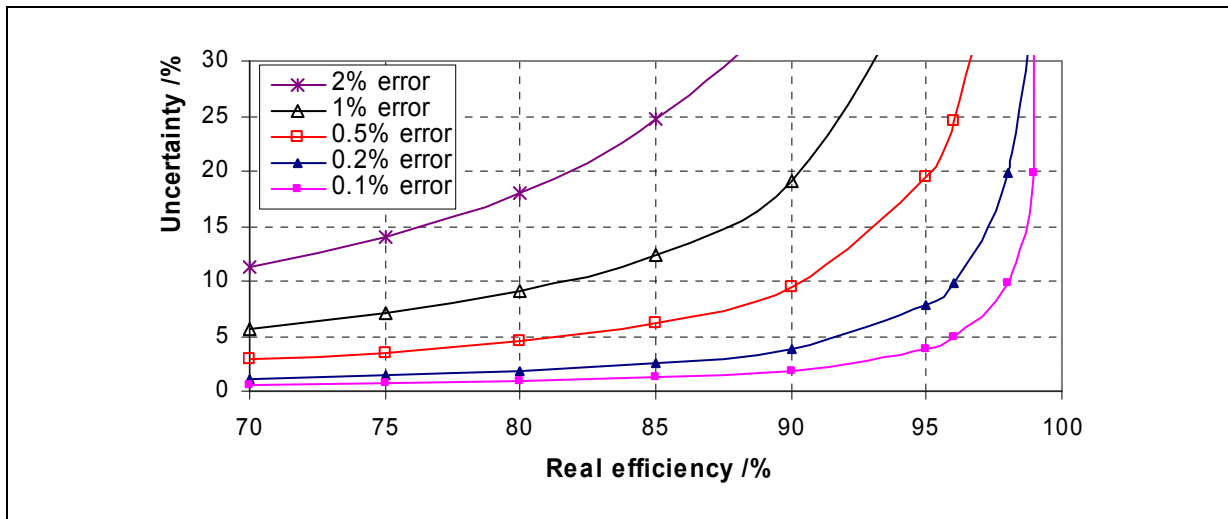
Figure 2.5: Impact of measurement error on the total loss determination with input-output test

As shown, there are problems for accurate determination of the total losses P_d by the input-output test (as difference of nearly equal quantities) in case of high efficiency. For example the maximum uncertainty in determination of the total losses is 24.5 % for an efficiency of 96 % due to an error of 0.5 %.

2.2 Measurement of stray load losses in induction machines

The stray load losses P_{ad} represent only a small fraction of the total power losses P_d, so they are difficult to predict analytically and difficult to measure accurately. A survey of the stray load losses P_{ad} in squirrel-cage induction motors was published by *Schwarz* [Schw 1964] and later by *Jimoh* et al [Jimo 1985]. The papers provided a comprehensive list of references to published works on the measurement of the losses, and discussed the origins of both the stray no-load and load losses. Various methods have been suggested for measuring the stray load losses of an induction machine in the literature, e.g. [Rawc 1952, Jimo 1985, Bird 1967, Mand 1979, Bour 1989], and in the

standards [IEEE 112, IEC 60034-2]. The suggested methods differ, apart from the physical model, in the complexity, the accuracy, the field suitability, the cost and regarding the load condition (full load, partial load and no-load).

A literature survey on cheap and simple methods to measure the stray load losses, apart from the standardized methods, reveals three "no-load" methods: the eh-star method of *Jordan* and *Richter* [Jord 1967], the equivalent no-load method of *Bourne* [Bour 1989] and the no-load method of *Rawcliffe* and *Menon* [Rawc 1952], which are investigated and compared with the standardized input-output test and the reverse rotation test acc. to IEC 61972 and IEEE 112.

The most used methods to measure the stray load losses can be subdivided in:
a) Direct measurement of the stray load losses:
- Reverse rotation test e.g. acc. IEEE 112-method E and IEC 61972.

- Eh-star method of *Jordan* and *Richter* [Jord 1967] acc. to [IEC 60034-2 draft].

b) Indirect measurement of the stray load losses:
- Input-output test with loss segregation (residual loss method) acc. to IEEE 112-method B and IEC 61972.

- Calorimetric method with segregation of the losses. The calorimeter test gives the total losses P_d of the machine, the stray load losses P_{ad} are determined by splitting the total losses P_d up into its various components. The stray load losses P_{ad} are defined as the difference between the calorimeter total losses P_d and the sum of the conventional losses P_Σ (stator I^2R loss, rotor I^2R loss, iron loss, and friction and windage losses).

The measurement of the stray load losses P_{ad} by the well-known input-output test in the residual loss method acc. to IEC 61972 and IEEE 112-method B, with the calorimetric and with the reverse rotation test acc. to the standards IEEE 112 or IEC 61972 needs calibrated measurement equipment of high accuracy and a coupled load, takes considerable time to perform the test and consumes therefore more energy. The eh-method acc. to the new proposed standard IEC 60034-2 Ed. 4, 2nd CDV [IEC 60034-2 draft] can be such an optimal technical, feasible

and economical alternative test. It is performed by asymmetric feeding of a three-phase induction machine without coupling the machine and without needing any dynamometer.

2.2.1 Accuracy of indirectly measured stray load losses

The stray load losses P_{ad} are defined, by indirect measurement, as the difference between the total losses P_d and the sum of the conventional losses P_Σ (2.12). Each uncertainty in these terms will lead to a significant error in the determination of the stray load losses P_{ad}. This error, given in (2.15), increases strongly with decreasing value of the stray load losses P_{ad}, e.g. in high efficiency motors (see Figure 2.9)

$$P_{ad} = P_d - P_\Sigma = P_{e,in} - P_{m,out} - P_\Sigma \ \rightarrow \ \left|\Delta P_{ad}\right| = \left|\Delta P_{e,in}\right| + \left|\Delta P_{m,out}\right| + \left|\Delta P_\Sigma\right|, \tag{2.12}$$

$$\left|\frac{\Delta P_{ad}}{P_{ad}}\right| = \left|\frac{\Delta P_{e,in}}{P_{e,in}}\right| \cdot \frac{P_{e,in}}{P_{ad}} + \left|\frac{\Delta P_{m,out}}{P_{m,out}}\right| \cdot \frac{\eta \cdot P_{e,in}}{P_{ad}} + \left|\frac{\Delta P_\Sigma}{P_\Sigma}\right| \cdot \frac{P_\Sigma}{P_{ad}} \tag{2.13}$$

Using (2.14) the uncertainty can be expressed as given in (2.15)

$$P_\Sigma = P_{e,in} - \eta \cdot P_{e,in} - P_{ad} \ \rightarrow \ \frac{P_\Sigma}{P_{ad}} = \frac{P_{e,in}(1-\eta)}{P_{ad}} - 1 \tag{2.14}$$

$$\left|\frac{\Delta P_{ad}}{P_{ad}}\right| = \left(\left|\frac{\Delta P_{e,in}}{P_{e,in}}\right| + \eta \cdot \left|\frac{\Delta P_{m,out}}{P_{m,out}}\right|\right) \cdot \frac{P_{e,in}}{P_{ad}} + \left|\frac{\Delta P_\Sigma}{P_\Sigma}\right| \cdot \left(\frac{P_{e,in}(1-\eta)}{P_{ad}} - 1\right). \tag{2.15}$$

The first summand in (2.15) (see also (2.17)) represents the error of the total losses P_d and the second summand represents the error of the sum of the conventional losses P_Σ. The error of the total power losses P_d influences the results of the determined stray load losses P_{ad} more than the error of the sum losses P_Σ as shown in Figure 2.6 for an assumed value of the stray load losses P_{ad} of 0.5 % of the input power $P_{e,in}$ and for the same accuracy of

$$\left| \Delta P_{e,in} / P_{e,in} \right| = \left| \Delta P_{m,out} / P_{m,out} \right| = \left| \Delta P_{\Sigma} / P_{\Sigma} \right| = 0.2 \%.$$
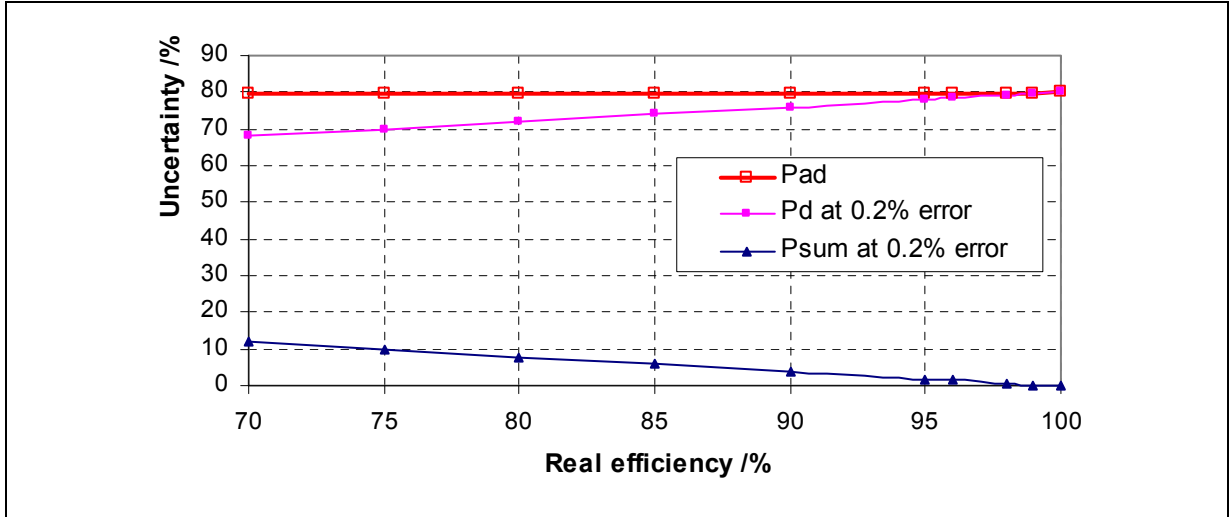
Figure 2.6: Impact of measurement error in the total and the sum losses on the stray load loss for an assumed value of the stray load losses of 0.5 % of the input power

As shown in Figure 2.6 the error of the total losses P_d influences the results of the determined stray load losses P_{ad} more than the error of the sum of the conventional losses P_{Σ}. In order to obtain an accurate result of the measured stray load losses P_{ad}, by indirect methods, we have to look for the methods where the total power losses P_d are measured more accurately e.g. by the calorimetric method. The impact of the measurement error in the total power losses P_d on the stray load losses P_{ad} is derived in (2.17) and presented, for different accuracy assumptions, as function of the ratio of the stray load losses P_{ad} to the total losses P_d in Figure 2.7 and Table 2.3.

$$P_{ad} = P_d - P_{\Sigma} \ \rightarrow \ \left| \Delta P_{ad} \right| = \left| \Delta P_d \right| + \left| \Delta P_{\Sigma} \right|, \tag{2.16}$$

$$\left| \frac{\Delta P_{ad}}{P_{ad}} \right| = \left| \frac{\Delta P_d}{P_d} \right| \cdot \frac{P_d}{P_{ad}} + \left| \frac{\Delta P_{\Sigma}}{P_{\Sigma}} \right| \cdot \frac{P_{\Sigma}}{P_{ad}} = \left| \frac{\Delta P_d}{P_d} \right| \cdot \frac{P_d}{P_{ad}} + \left| \frac{\Delta P_{\Sigma}}{P_{\Sigma}} \right| \cdot \left(\frac{P_d}{P_{ad}} - 1 \right). \tag{2.17}$$
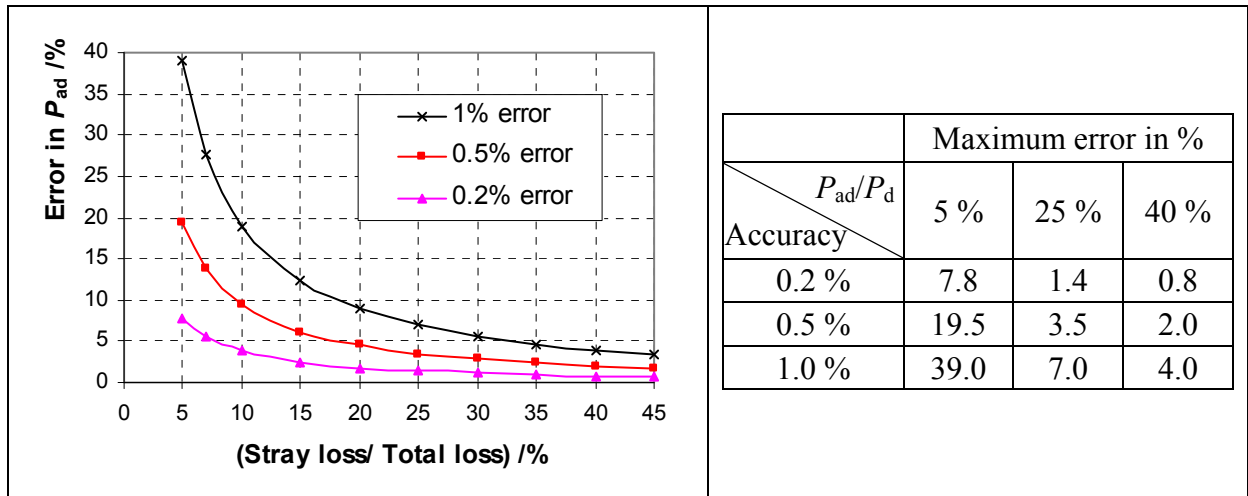
Figure 2.7: Maximum error of indirectly determined stray load losses as function of the accuracy in total losses

Table 2.3: Maximum error of stray load losses as function of the accuracy in total losses

The maximum error depends on the portion of the stray load losses P_{ad} related to the total losses P_d (see also Figure 2.8). For an assumed realistic portion of 25 % ($= P_{ad}/P_d$) and a measurement accuracy of 1 % ($= |\Delta P_d / P_d| = |\Delta P_\Sigma / P_\Sigma|$), the maximum error of 7 % is much lower than with the input-output test, where the input $P_{e,in}$ and output $P_{m,out}$ powers and the losses P_Σ are measured to the same accuracy.

With (2.18) the uncertainty in (2.15) can be expressed as function of the efficiency and the portion of the stray load losses P_{ad} related to the total losses P_d as given in (2.19) and presented in Figure 2.8

$$P_{e,in} = P_d /(1-\eta) \tag{2.18}$$

$$\left|\frac{\Delta P_{ad}}{P_{ad}}\right| = \left(\left|\frac{\Delta P_{e,in}}{P_{e,in}}\right| + \eta \cdot \left|\frac{\Delta P_{m,out}}{P_{m,out}}\right|\right) \cdot \frac{P_d}{P_{ad}(1-\eta)} + \left|\frac{\Delta P_\Sigma}{P_\Sigma}\right| \cdot \left(\frac{P_d}{P_{ad}} - 1\right). \tag{2.19}$$
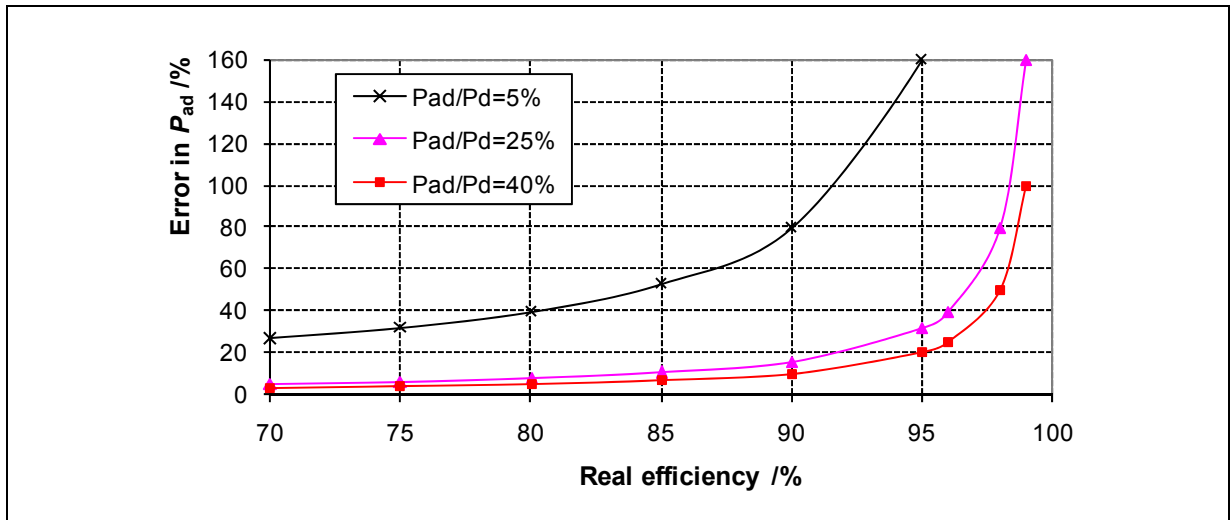
Figure 2.8: Maximum error of indirectly determined stray load losses as function of the efficiency at 0.2 %-accuracy

As shown the maximum error depends on the efficiency and on the portion of the stray load losses P_{ad} related to the total losses P_d. For an assumed realistic portion of 25 % (= P_{ad}/P_d) and a measurement accuracy of 0.2 % (= $\left|\Delta P_{e,in} / P_{e,in}\right|$ = $\left|\Delta P_{m,out} / P_{m,out}\right| = \left|\Delta P_{\Sigma} / P_{\Sigma}\right|$), the error in determination of the stray load losses P_{ad} at an efficient motor with 96 % efficiency is significantly ca. 40 % and ca. 6 % at an efficiency of 75 %.

Figure 2.9 and Table 2.4 show the impact of the measurement error on the determined stray load losses P_{ad} by the input-output test for different accuracy assumptions. It is assumed that the input $P_{e,in}$ and output $P_{m,out}$ and the losses P_{Σ} are measured to the same accuracy (e.g. $\left|\Delta P_{e,in} / P_{e,in}\right|$ = $\left|\Delta P_{m,out} / P_{m,out}\right|$ = $\left|\Delta P_{\Sigma} / P_{\Sigma}\right| = 0.2\,\%$). For a high efficiency motor, where the stray load losses P_{ad} are assumed to be 0.5 % of the input power $P_{e,in}$, the error in determination of the stray load losses P_{ad} is with ca. 40 % high already under premise of the highest measurement accuracy of 0.1 %. For smaller motors with the stray load losses P_{ad} of about 3 % of the input power $P_{e,in}$, the error is 13 % with the usual accuracy of 0.2 %.
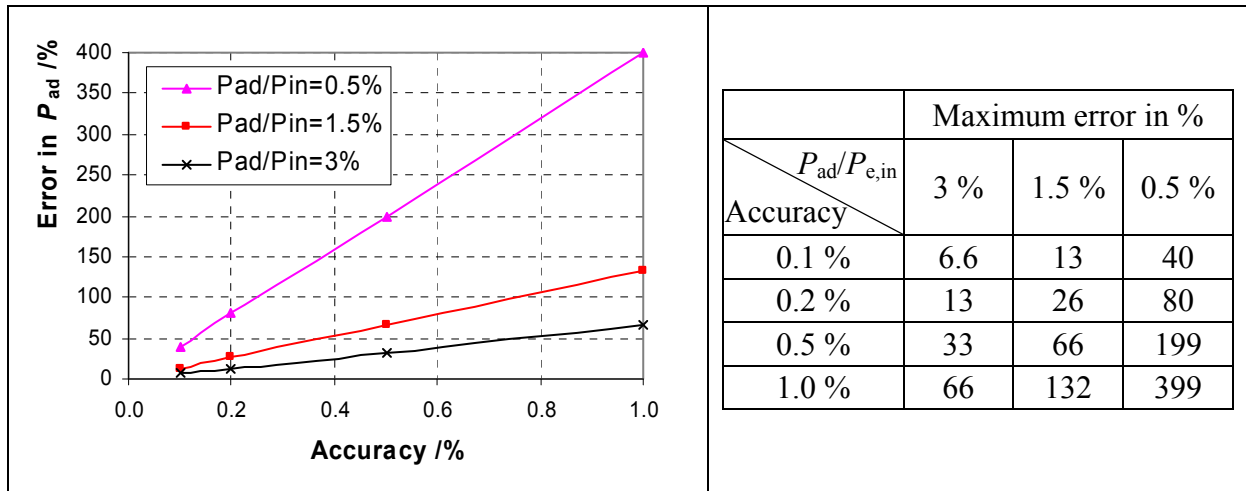
Figure 2.9: Maximum error of indirectly determined stray load losses as function of the accuracy

Table 2.4: Maximum error of indirectly determined stray load losses

	Maximum error in %		
$P_{ad}/P_{e,in}$ / Accuracy	3 %	1.5 %	0.5 %
0.1 %	6.6	13	40
0.2 %	13	26	80
0.5 %	33	66	199
1.0 %	66	132	399

In equation (2.12) the output power $P_{m,out}$ can be expressed with the efficiency η. The stray load losses P_{ad} acc. to (2.12) are then

$$P_{ad} = P_d - P_\Sigma = P_{e,in} - P_{m,out} - P_\Sigma = P_{e,in} - \eta \cdot P_{e,in} - P_\Sigma \; . \tag{2.20}$$

The maximum error in the stray load losses is

$$\left|\Delta P_{ad}\right| = \left|\Delta P_{e,in}\right| + P_{e,in} \cdot \left|\Delta\eta\right| + \eta \cdot \left|\Delta P_{e,in}\right| + \left|\Delta P_\Sigma\right|. \tag{2.21}$$

With (2.14) the uncertainty in the stray load losses can be written as function of variation of the efficiency $\left|\Delta\eta\right|$, due to an error in the measurement or to an improvement of the efficiency e.g. due to the design changes, as:

$$\left|\frac{\Delta P_{ad}}{P_{ad}}\right| = \left(\left|\frac{\Delta P_{e,in}}{P_{e,in}}\right| + \left|\Delta\eta\right| + \eta \cdot \left|\frac{\Delta P_{e,in}}{P_{e,in}}\right|\right) \cdot \frac{P_{e,in}}{P_{ad}} + \left|\frac{\Delta P_\Sigma}{P_\Sigma}\right| \cdot \left(\frac{P_{e,in}(1-\eta)}{P_{ad}} - 1\right). \tag{2.22}$$

Figure 2.10 and Table 2.5 show the maximum error of the indirectly determined stray load losses as function of the efficiency-variation at 0.2 %-accuracy. For the calculation, it is assumed that the input $P_{e,in}$ power and the losses P_Σ are measured to the same accuracy of 0.2 %. For an efficiency variation $\left|\Delta\eta\right| = 0$ %, the equation (2.22) is similar to (2.15) for the same

accuracy $\left|\Delta P_{e,in} / P_{e,in}\right| = \left|\Delta P_{m,out} / P_{m,out}\right|$ and the maximum error in the determined stray load losses is 80 % for an assumed stray load losses value of 0.5 % of the input power $P_{e,in}$. An increasing of $\left|\Delta\eta\right| = 0.5$ % step leads to 180 % error. The error increases with higher efficiency, especially when the stray load losses P_{ad} are very small.

0.2 %-Accuracy	Maximum error in %		
$P_{ad}/P_{e,in}$ $\left|\Delta\eta\right|$	3 %	1.5 %	0.5 %
0.0 %-Step	13	26	80
0.3 %-Step	23	46	140
0.5 %-Step	30	60	180
1.0 %-Step	46	93	280
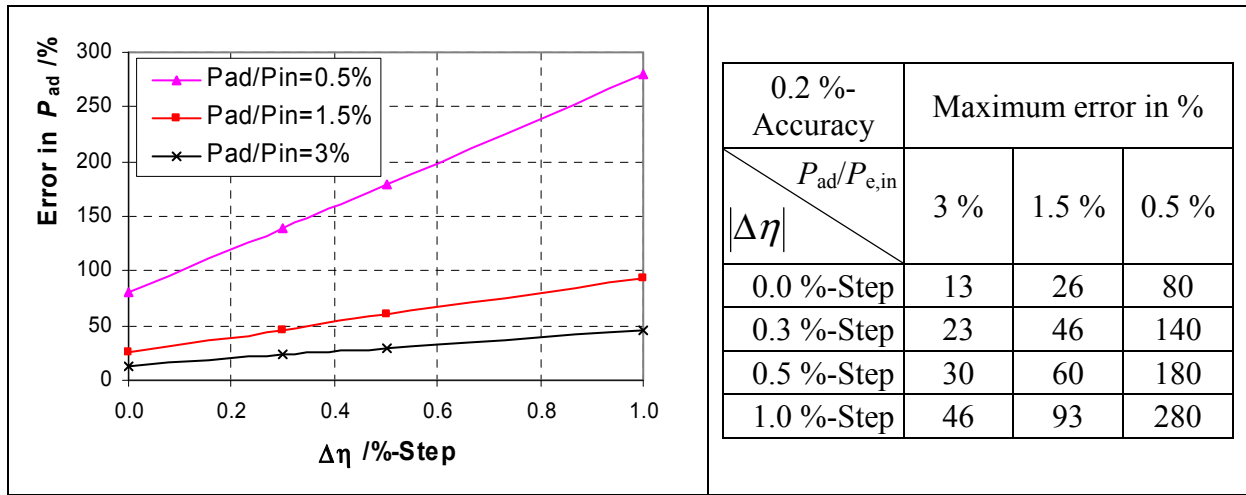
Figure 2.10: Maximum error of indirectly determined stray load losses as function of the efficiency-variation at 0.2 %-accuracy

Table 2.5: Maximum error of stray load losses as function of the efficiency-variation

Because of the unavoidable measurement errors, the indirect determination of the stray load losses P_{ad} by measuring the input $P_{e,in}$ and output $P_{m,out}$ powers is generally not accurate enough with small values of the stray load losses P_{ad} e.g. for high efficiencies. Therefore the direct measurement methods of the stray load losses P_{ad} could be useful at high efficiencies.

2.2.2 Some stray load loss measurement methods in the literature

Apart from the well-known methods to measure the stray load losses P_{ad} in squirrel-cage induction motors like the input-output test (residual loss method), the calorimetric method and the reverse rotation test, there are in the literature and the standards other methods [Schw 1964, Jimo 1985, IEEE 112] e.g.:

- Dual supply back-to-back test (duplicate machines) [IEC 60034-2-1]

- Differential dynamometer [IEEE 112]

- Mechanical/electrical differential (two identical machines) [Bird 1964, IEEE 112]

- Back-to-back [IEEE 112],

which are complicated, expensive or inaccurate though standardised. There are also other methods, which were investigated by one or other authors like:

a) DC/AC short circuit method of *Richter* [Rich 1936]

b) Thermocouples-calorimetric method of *Keve* [Keve 1973]

c) Input-output at reduced voltage method of *Mandi* [Mand 1962]

d) Eh-star method of *Jordan* and *Richter* [Jord 1967]

e) Equivalent no-load method of *Rawcliffe* and *Menon* [Rawc 1952]

f) and the equivalent no-load method of *Bourne* [Bour 1989].

The selected methods a) ... c) will be shortly introduced here, and the methods d) ... f) will be investigated and compared to some standards.

2.2.2.1   DC/AC short circuit method of *Richter*

It consists of three separate tests [Rich 1936]:

1) *Removed rotor test* for the determination of the fundamental frequency stray load losses in the stator $P_{ad,s}$ like the standardised reverse rotation test acc. to [IEEE 112].

2) *DC field test*, where two stator phases are fed by an equivalent direct current while the rotor is driven by an auxiliary motor at synchronous speed. The equivalent direct current corresponds to the peak value of the corresponding alternating load current. The mechanical power required to drive the rotor, which is measured e.g. by dynamometer, covers the friction and windage losses, the fundamental frequency rotor losses and the high frequency stray load losses in the rotor $P_{ad,r}$.

3) *AC short circuit test* similar to the standardised locked rotor test. The measured input power minus the winding losses in the stator is assumed to be equal to the fundamental frequency rotor losses in the DC field test.

The friction and windage losses are taken from the no-load test. The stray load losses P_{ad} are the sum of the fundamental $P_{ad,s}$ and the high frequency $P_{ad,r}$ stray load losses.

For an equivalent method the real physical load situation of the machine is missing (e.g. saturation). The rotor flux is higher compared with the standardized RRT. Like with the RRT the iron losses in the stator core P_{Fe} are neglected due to the strongly reduced voltage, and the synchronous speed is slightly higher than the rated speed, giving slightly higher stray load losses P_{ad}. Coupling of the machine with the driver and use of the calibrated dynamometer are necessary. The measurement of the mechanical power by dynamometer suffers from uncertainty. The biggest error can occur by the determination of the temperature in the rotor cage.

The *Richter*'s test was investigated by more than one author e.g. *Mandi* [Mand 1962] and compared with the RRT (DC/RRT = 1.44).

2.2.2.2   **Thermocouples-calorimetric method of *Keve***

The test [Keve 1973] is based on the relationship between the heating, due to the losses, and the temperature rise of the housing (enclosure). Since the power losses of the test machine are dissipated in form of heat, the energy transferred through the housing is a measure of the power losses produced inside the housing. It uses, for totally enclosed surface cooled machines, 4 thermocouples distributed at the housing circumference: 2 thermocouples on the none drive end and 2 thermocouples on the drive end. For the determination of the stray load losses P_{ad} the average value of the housing temperature rise $\Delta\vartheta_{G,av}$ from the 4 thermocouples is taken. The "total heat" P_d comprises the stator and the rotor resistive losses, the iron losses and the inner friction losses (no external fan losses). The inner friction losses can be measured at no-load without the fan.

It requires three separate tests:

1) *No-load test* without the fan to get the inner friction losses.

2) Normal *no-load test* at three voltages 80 %, 100 % and 120 % of the rated voltage. Each test points should be run until thermally stable condition is reached. The measured curve $\Delta\vartheta_{G,av} = f(P_d)$ is plotted. In this curve the measured value of the inner friction losses, $\Delta\vartheta_{G,av} = 0$ K, is defined to be negative. To smoothe the three no-load run-values a regression line $P_{d,0\_regr}$ through the inner friction losses is developed. The regression line $P_{d,0\_regr}$ is extrapolated to the highest value.

3) *Test under load* at rated voltage at three load currents 80 %, 100 % and 120 % of the rated current. Each test point should be run until thermally stable condition is reached. The measured three values are plotted in the same curve $\Delta\vartheta_{G,av} = f(P_d)$. To smoothe the three load-run values a regression line $P_{d,load\_regr}$ through the measured points at no-load for rated voltage is developed. The regression line $P_{d,load\_regr}$ is extrapolated to the highest value.

As the stray load losses increase the housing temperature rise the slope of the regression line $P_{d,load\_regr}$ is bigger than that of line the regression $P_{d,0\_regr}$. Thus the differences between both lines are the stray load losses P_{ad}.

A curve of the resulting stray load losses P_{ad} against the current squared I_s^2 is developed. With the linear regression line $P_{ad}(I_s^2)$ the value of the stray load losses $P_{ad,N}$ at the rated current $I_{s,N}$ is derived.

Physically it is an exact method. The measurement of the mechanical power is not needed, but a load machine and the test with removed fan are necessary. The result depends mainly on the accuracy of the temperature measurement i.e. the measurement should be done, like in the calorimetric method, in a "calorimetric"-chamber. The measurements take considerable time, as the thermal stability is necessary for each no-load and load point. To improve the accuracy of the regression lines the set of runs shall be increased from (3 no-load, 3 load) to (6 no-load, 6 load). This extends the test time. Apart from the site the thermal stability at overload depends on the insulation and on the thermal reserve of the motor.

Keve has compared its results for two motors (low-voltage 4 kW, high-voltage 460 kW) only with the eh-star method. It is interesting to compare it with the input-output test for the small one. However the ratio of additional losses for eh-star/thermocouples-calorimetric = 1.2 … 1.4, as the eh-star test was

done only for one load point at high voltage where the ratio of positive to negative sequence current = 0.5 … 3.4 was too high.

2.2.2.3 *Mandi* -Input-output test at reduced voltage

The test [Mand 1962] is similar to the standardised input-output test but at reduced voltage of 25 % rated voltage at rated current, the slip should be in the range of 10 %. The measurement at 25 % rated voltage needs a smaller dynamometer of ca. 12.5 % rated power, and yields a bigger percentage "stray load loss/input power", so the error is by factor 4 smaller than at rated voltage. Thus the accuracy of the input-output test is improved. The stable operation at reduced voltage and bigger slip of ca. 10 % is obtained by the controlled dynamometer machine. Due to the reduced speed at reduced voltage the friction losses are corrected by an exponent of 3.11 ! Also the iron losses must be corrected and taken as load-dependent. To correct the high frequency stray load losses in the rotor $P_{ad,r}$ to the rated speed, the fundamental frequency stray load losses in the stator $P_{ad,s}$ are taken from the removed rotor test.

The accuracy of the input-output test is improved. Due to the small load machine, this may be useful for large machines. For an equivalent method the real physical load situation of the machine is missing (e.g. saturation), due to the reduced flux of only 25 % rated flux. The test speed is lower than the rated speed, giving slightly different stray load losses P_{ad}. Coupling of the machine with a load and the use of calibrated dynamometer are necessary. The removed rotor test is also needed.

Mandi has compared its results for a 125 kW motor with the DC/AC short circuit method of *Richter,* where good coincidence was observed, and with RRT, where the RRT values were too small.

2.2.3 Residual loss method acc. to IEC 61972

The IEC 61972 standard [IEC 61972] defines the stray load losses P_{ad} acc. to (2.12) as the difference between the total measured losses P_d and the sum of the

conventional losses P_Σ consisting of the no-load (iron P_{Fe} and friction P_{fw}) and $I^2 R$ load losses, so the residual stray load losses P_{ad} of the machine (stator and rotor together) are determined indirectly as

$$
\begin{aligned}
P_{\text{ad}} = P_{\text{d}} - P_\Sigma &= P_{\text{e,in}} - P_{\text{m,out}} - P_\Sigma \\
&= P_{\text{e,in}} - P_{\text{m,out}} - P_{\text{Cu,s}} - P_{\text{Fe}}(U_{\text{i}}) - P_{\text{Cu,r}} - P_{\text{fw}},
\end{aligned}
\tag{2.23}
$$

where $\underline{U}_{\text{i}}$ is the reduced inner phase voltage across the equivalent iron resistance R_{Fe} which takes the resistive voltage drop in the primary winding into account (Figure 2.11)

$$
U_{\text{i}} = U_{\text{r}} = \sqrt{(U_{\text{s}} - \sqrt{3}/2 \cdot R_{\text{LL}} \cdot I_{\text{L}} \cdot \cos\varphi)^2 + (\sqrt{3}/2 \cdot R_{\text{LL}} \cdot I_{\text{L}} \cdot \sin\varphi)^2} \tag{2.24}
$$

To simplify the calculation the reactive voltage drop in the stator stray reactance $X_{\text{s}\sigma}$ is neglected, as its determination needs extra measurement and calculation.

Figure 2.11: T-equivalent circuit of the induction machine with consideration of the load dependent iron losses

The stray load losses P_{ad} are obtained from a linear regression analysis for six different load points to reduce the effect of random measurement errors. These smoothed stray load losses data $P_{\text{ad,c}}$ are used to calculate the final value of the stray load and total losses and the efficiency for a given load point.

This standard is recommended for polyphase squirrel-cage induction motors with rated power in the range 1 kW…150 kW. It requires four tests:

1) *No-load test:* For the determination of the iron P_{Fe}, friction and windage P_{fw} losses and the no-load current, the motor - supplied with the rated voltage and the rated frequency - runs without mechanical load until both the temperature and the input power have stabilized. Between two consecutive measurements spaced out of 30 min, the input power shall not increase over 3 %. Then a variable voltage test is performed.

2) *Rated load temperature test:* For the determination of the rated data, the machine is coupled to a dynamometer load (Figure 2.12) and operated at rated load (rated output power), until a thermally stable condition is reached. The tested motor temperature shall not change by more than 1 °C, measured each 30 min.

3) *Test under load:* For the determination of the stray load losses and the efficiency, the machine is loaded by a dynamometer by six decreasing load torque values, beginning with 150 % down to 25 % of rated torque. The temperature of the stator winding shall be within 5 °C of the hottest temperature reading, recorded during the rated load temperature test prior to the start of this test.

4) *Dynamometer correction:* Correction for the windage and bearing loss torque of the used dynamometer and the coupling. It consists of two measurements:

a) *Dynamometer coupled*: The motor runs at the rated voltage and the rated frequency, coupled to the dynamometer with the dynamometer armature circuit open (Figure 2.12).

b) *Motor uncoupled*: The motor runs at rated voltage and rated frequency, uncoupled from the dynamometer.

The difference of both tests is then used to correct the dynamometer scale.

A test bench where the tested induction motor (IM) is coupled to a dynamometer load is presented in Figure 2.12. The power flow during the input-output test in motor operation is given in Figure 2.14.
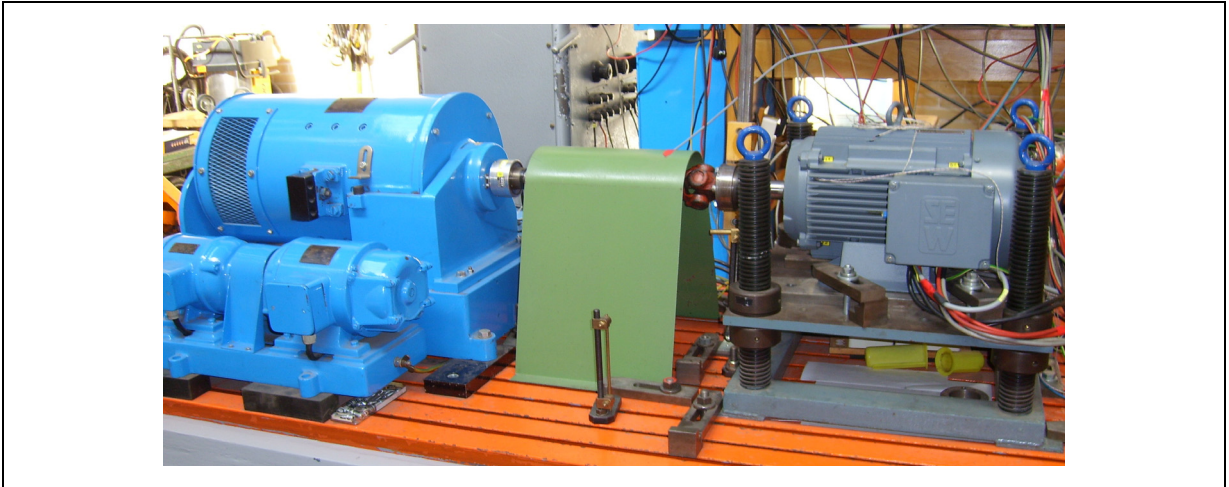
Figure 2.12: Test bench: coupled IM with dynamometer for the input-output test and the RRT

2.2.4 Residual loss method acc. to IEEE 112-Method B

The residual loss method acc. to IEEE 112-method B [IEEE 112] allows – like the IEC 61972 – an indirect access to the stray load losses P_{ad} from the measured input $P_{e,in}$ and output $P_{m,out}$ powers acc. to (2.23). It is recommended for three-phase cage induction motors with rated power in the range 1 kW…190 kW and is similar to the standard IEC 61972. The two standards are different in the procedure to obtain the stray load losses P_{ad}. The main differences are the determination of the winding temperature and the consideration of the iron losses P_{Fe} (see Figure 2.13).
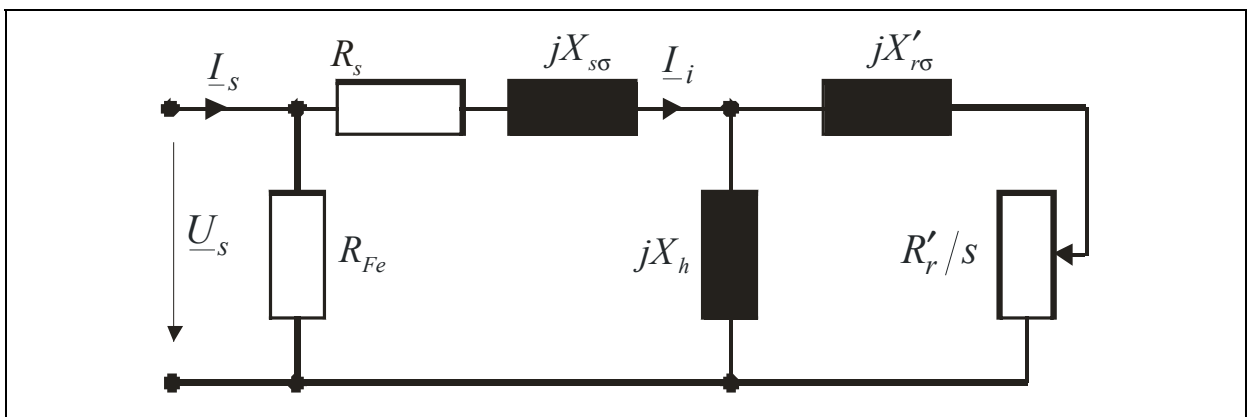
Figure 2.13: T-equivalent circuit of induction machine with consideration of the iron losses acc. to IEEE 112-method B
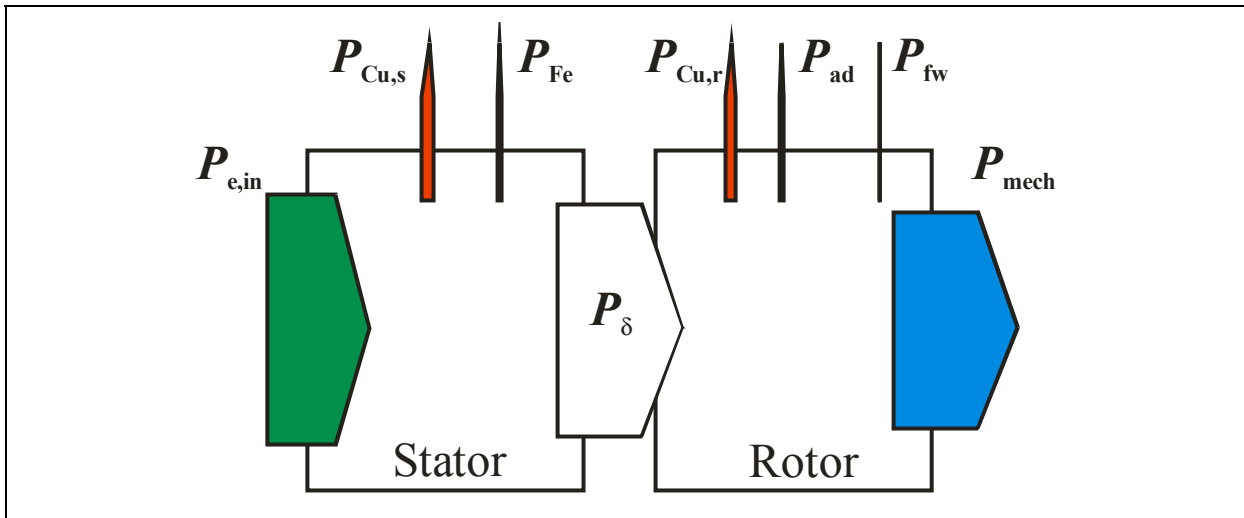
Figure 2.14: Power flow in motor operation acc. to IEEE 112-method B

Acc. to IEEE 112-method B the instruments shall be calibrated, within 12 months, indicating limits of the error no greater than ± 0.2 % of full scale. If the dynamometer output measurements are used, the coupling and bearing friction losses must be compensated for. Properly sized dynamometers should be used, such that the coupling, friction, and windage losses of the dynamometer measured at the rated speed of the machine being tested should not be greater than 15 % of the rated output of the machine being tested; and the dynamometer should be sensitive to a change of the torque of 0.25 % of the rated torque. The dynamometer correction test is not generally necessary when the load on the test machine is measured using a torque transducer in line with the shaft of the machine because the low coupling losses do not significantly affect the efficiency [IEEE 112].

2.2.5 Comparison of IEEE 112-Method B and IEC 61972

A comparison of the input-output test acc. to the standards IEEE 112-method B and IEC 61972 is given in Table 2.6.

	Residual loss method (Input-output test)	
	IEEE 112-method B	**IEC 61972**
Temperature of the stator winding	Thermocouples	Interpolated resistance
Iron losses	Load independent, taken at rated voltage	Load dependent, taken from $P_{Fe}(U_i)$ curve
Friction losses from	Lower voltage range	50% or less of rated voltage
Correlation coeff. R	> 0.9	> 0.95
Temp. variation for begin of the test under load	Within 10 °C	Within 5 °C
Instrument transformers accuracy	± 0.3 %	± 0.2 %
Speed accuracy	± 1 rpm	0.1 %
Copper coefficient	234.5	235

Table 2.6: Comparison of the residual loss method acc. to IEEE 112-method B and IEC 61972

The main differences between both standards are the winding temperature determination (see Figure 2.15) and the consideration of the load dependent iron losses P_{Fe} (see Figure 2.16). The standard IEC 61972 uses for the temperature the interpolation between the measured resistances and considers the iron losses P_{Fe} to be dependent on the load. The iron losses P_{Fe} of the desired load point are taken from the curve $P_{Fe}(U_i)$ at reduced inner voltage U_i which takes the resistive voltage drop in the primary winding into account. This effect is stronger for small motors with relatively bigger stator resistance. In fact the iron losses P_{Fe} depend also on the lamination temperature [Bogl 2004, Auin 1999]. Therefore the no-load test, to measure the iron and the friction and windage losses, should be done after the rated load temperature test (heat run test) as the machine is warm and the bearing losses are stabilized. The IEEE 112-method B considers the iron losses P_{Fe} at no load and the rated voltage to be independent of the load. The same iron losses value P_{Fe} is used for all load points.
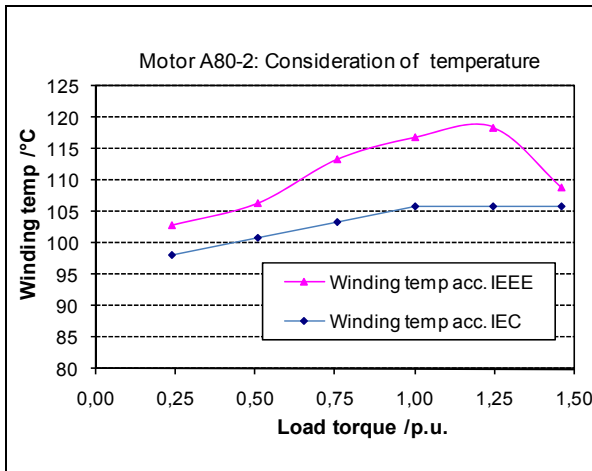
Figure 2.15: Linear interpolation of the
winding temperature acc. to IEC
61972 and the thermocouples
temperat. acc. to IEEE 112-B for
1.1 kW 2-pole motor "A80-2"
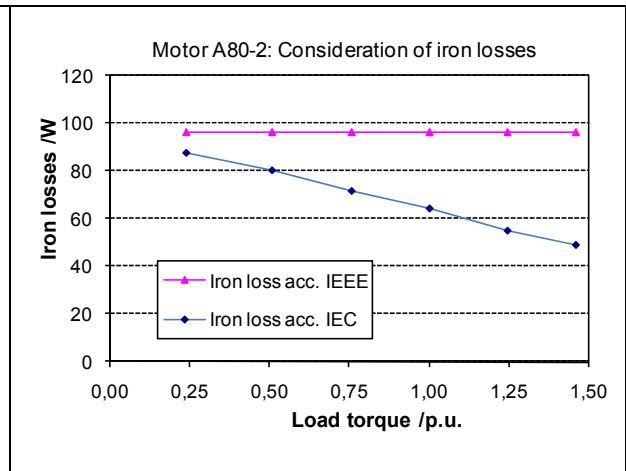
Figure 2.16: Consideration of the iron losses
P_{Fe} acc. to IEC 61972 and acc. to
IEEE 112-B for 1.1 kW 2-pole
motor "A80-2"

Table 2.7 shows the difference between both standardised methods, considering as example a small motor of 1.1 kW 2-pole "A80-2", where the influence of the stator resistance on the internal voltage U_i is big. The measured Pad and the smoothed (corrected) stray load losses $P_{ad,c}$ as function of square of the torque in Figure 2.17 and Figure 2.18 show, that negative stray load losses are determined with IEEE 112-method B (Figure 2.17). Here the wrong assumption of the load-independent iron losses causes the wrong results.

1.1 kW 2-pole motor: "A80-2"	IEEE 112-method B	IEC 61972
Winding temperature rise /K	92.4	81.4
Electrical input /W	1433	1433
Iron losses /W	96	64
Stray load losses/P_{in} /%	-0.08	1.17
Efficiency P_{out}/P_{in} /%	75.85	76.56
Correlation coefficient R	0.139	0.986

Table 2.7: Loss segregation acc. to IEEE 112-method B and IEC 61972 in comparison

Figure 2.17: Measured stray load losses acc.
        to IEEE 112-method B for 1.1 kW
        2-pole motor "A80-2"

Figure 2.18: Measured stray load losses acc.
        to IEC 61972 for 1.1 kW 2-pole
        motor "A80-2"

(Subscript c for corrected: Linear regression line without offset)

The IEEE 112-method B is less accurate concerning the iron losses P_{Fe}, especially for small motors with their rather big stator resistance R_s. Concerning the temperature the IEC 61972 method is less accurate due to use of the interpolated values, but no thermocouples are needed in the stator winding, which simplifies the test procedure.

2.2.6 Reverse rotation test

The so called *Morgan* test is an "equivalent method" to measure the stray load losses acc. to IEEE 112 [IEEE 112], which is also quoted in [IEC 61972] and [IEC 60034-2 draft], consists of two separate measurements, after the no-load current is determined from the no-load test:

1) *Removed rotor test:* The stator stray load losses $P_{ad,s}$ occurring at fundamental frequency are determined.

2) *Reverse rotation test:* The stator and the rotor stray load losses $P_{ad,r}$, occurring at high frequencies (e.g. slot frequency), are determined by the reverse rotation test at slip $s = 2$.

In the determination of the stray load losses P_{ad} the iron losses P_{Fe} in the stator and in the rotor (by 2 times stator frequency !) are completely neglected due to the strongly reduced voltage.

A linear regression analysis of the *log* of the powers (rotor mechanical and stator electrical power) vs. the *log* of the currents is used to smoothe the test values. If the measured data are accurate, each curve will conform to a square-law relationship between the powers and the currents. Thus, the correlation factor from the regression and the exponent for each curve both serve as indicators of the measurement accuracy.

The stray load losses P_{ad} are the sum of the fundamental $P_{ad,s}$ and the high frequency $P_{ad,r}$ stray load losses at given stator current

$$P_{ad} = P_{ad,s} + P_{ad,r} .$$
(2.25)

2.2.6.1   Removed rotor test

The stator stray load losses occurring at the fundamental frequency are determined at rated current. Reduced voltage of ca. 10 % - 30 % of rated voltage is applied to the stator-winding terminals to get the rated current, due to the low main flux of about 10 % of the rated main flux, as the rotor is removed. During this test, the bearing brackets and other structural parts, in which eddy current might be induced, shall be in place.

The stray load losses $P_{ad,s}$ are derived from the power flow acc. to Figure 2.19. The electrical input $P_{e,in}$ minus the stator winding losses $P_{Cu,s}$ at the test temperature is equal to the fundamental frequency stray load losses $P_{ad,s}$. The iron losses in the stator core P_{Fe} are neglected due to the reduced voltage ($P_{Fe} \sim B^2$, $B \sim U$). The fundamental frequency stray load losses $P_{ad,s}$ are given in (2.26) and presented in Figure 2.22:

$$P_{ad,s} = P_{e,in} - P_{Cu,s} - P_{Fe} \cong P_{e,in} - P_{Cu,s} .$$
(2.26)
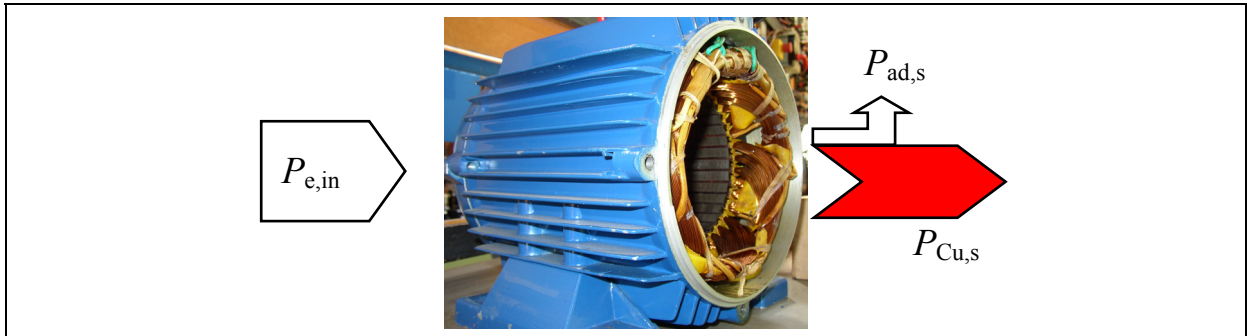
Figure 2.19: Power flow in the removed rotor test acc. to IEEE 112

2.2.6.2   Reverse rotation test

The stray load losses occurring at high frequencies $P_{ad,r}$ are determined by the reverse rotation test (RRT) at slip $s = 2$. With the machine completely assembled, due to the low main flux at slip $s = 2$, a reduced balanced polyphase voltage (ca. 10% - 30% of rated voltage) at rated frequency is applied at the stator winding terminals to get rated current. The rotor is driven by e.g. a dc-motor at synchronous speed in the direction opposite to the stator field rotation, as shown in Figure 2.20. The electrical input $P_{e,in}$ to the stator winding is measured. The mechanical power required to drive the rotor is also measured with a sensitive dynamometer both with and without the current in the stator winding as P_{mech} and P_{fw}, respectively.
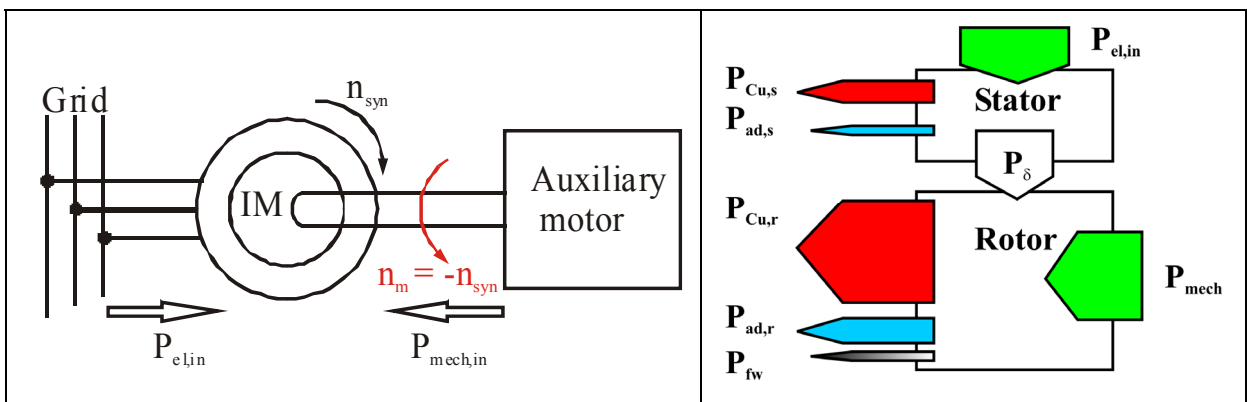
Figure 2.20: Simplified test setup of the reverse rotation test (IM: induction motor)

Figure 2.21: Power flow in the reverse rotation test

Using the RRT-power flow, shown in Figure 2.21, the higher frequencies stray load losses $P_{ad,r}$ are determined. Also here the iron losses in the stator and the rotor core P_{Fe} are neglected due to the reduced voltage ($P_{Fe} \sim B^2$, $B \sim U$). The stray load losses $P_{ad,r}$ are given in (2.27) and shown in Figure 2.22.

$$P_{ad,r} = (P_{mech} - P_{fw}) - (P_{e,in} - P_{Cu,s} - P_{ad,s}).$$

(2.27)
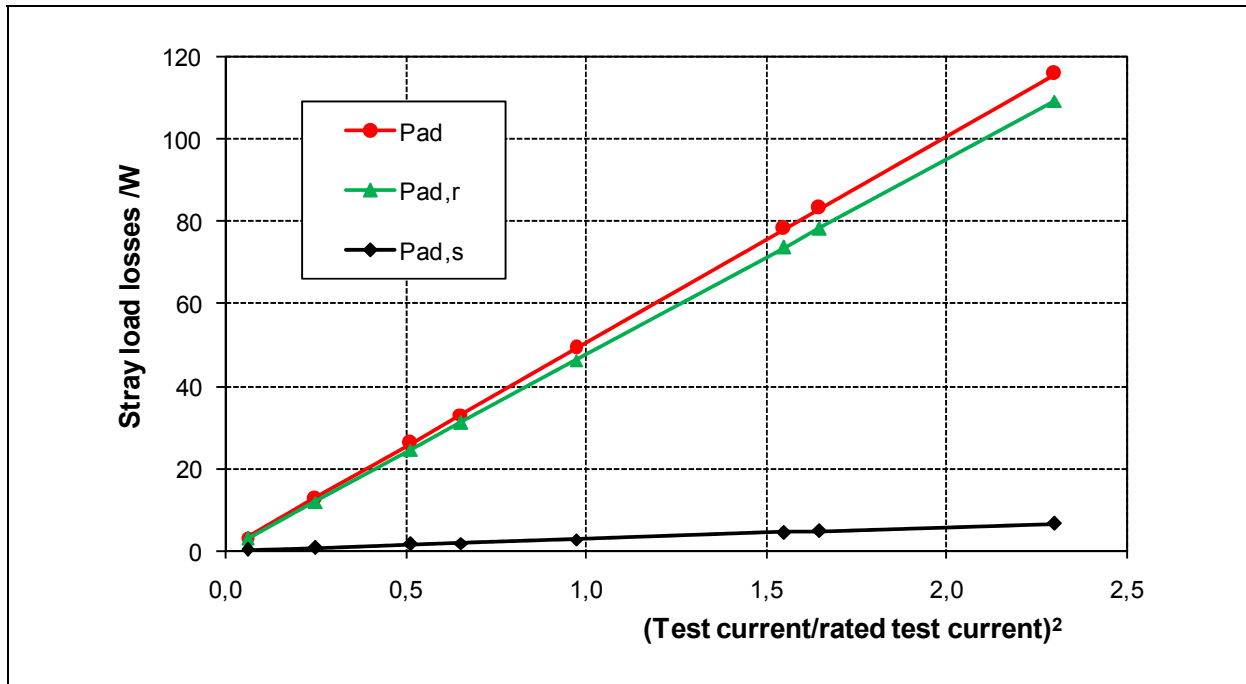
Figure 2.22: Measured stray load losses acc. to the reverse rotation test of a 1.1 kW 2-pole motor "C80-2"

2.2.7 Eh-star-circuit Method

The eh-star-circuit method [Jord 1967, IEC 60034-2 draft], which is described in detail in the next chapter, is performed by asymmetric feeding of a three-phase induction machine (squirrel cage or wound rotor) without coupling of the machine and without needing any dynamometer (Figure 2.23). The asymmetrical operation is obtained by operating the stator winding in star connection, where two machine phases U and W are connected in parallel through an auxiliary *ohmic* resistance R_{eh} of a value similar to the motor short

circuit impedance Z_{sc} (Figure 2.23). This resistance shall be adjusted, so that the positive sequence current $I_{s,1}$ stays below 30% of negative sequence current $I_{s,2}$, and the speed stays in the range of typically rated speed. The star-point must not be connected to earth to avoid zero-sequence currents. For the test bench one needs an auxiliary resistance R_{eh} and a switch S for switching from three-phase starting of the tested machines to single phase operation (Figure 2.23). As the negative sequence dominates, the machine may be assumed to be mainly operating under inverse field conditions, similar to the reverse rotation test (RRT). Thus the negative sequence losses corresponding to the slip $s_2 = (2 - s) \approx 2$ should be nearly the same as at the same current under the reverse rotation test conditions, but without needing any dynamometer. A second advantage of the eh-star-circuit in comparison to the RRT is the fact that the positive sequence current system of ca. 25 % … 30 % of the negative sequence current excites a main flux of about the same order, which resembles more the full flux operation at the rated slip than the RRT does. Another advantage of the eh-star-circuit in comparison to the RRT is that the removed rotor test is not necessary. The stray load losses are evaluated directly from the load flow calculation for the T-equivalent circuit (Figure 2.11) with consideration of the iron losses P_{Fe}, which must be known from a prior no-load test. Hence the stray load losses $P_{ad,asym}$ of the asymmetrically fed machine - as the sum of additional losses of the positive $P_{ad,1}$ and negative $P_{ad,2}$ sequence system - are given by the power balance (2.28), where $P_{\delta,1}$ and $P_{\delta,2}$ are the air gap power of the positive and negative sequence system and s is the slip. The output power is zero, because the motor is not coupled to a mechanical load. Only the friction and windage losses P_{fw} and the stray load losses $P_{ad,asym}$ are loading the machine (Figure 2.24).

$$P_{ad,asym} = P_{ad,1} + P_{ad,2} = (1-s) \cdot (P_{\delta,1} - P_{\delta,2}) - P_{fw}. \qquad (2.28)$$

The eh-star measurement circuit is presented in Figure 2.23, whereas in the Figure 2.24 the power flow of the decomposed positive and negative sequence systems is illustrated.
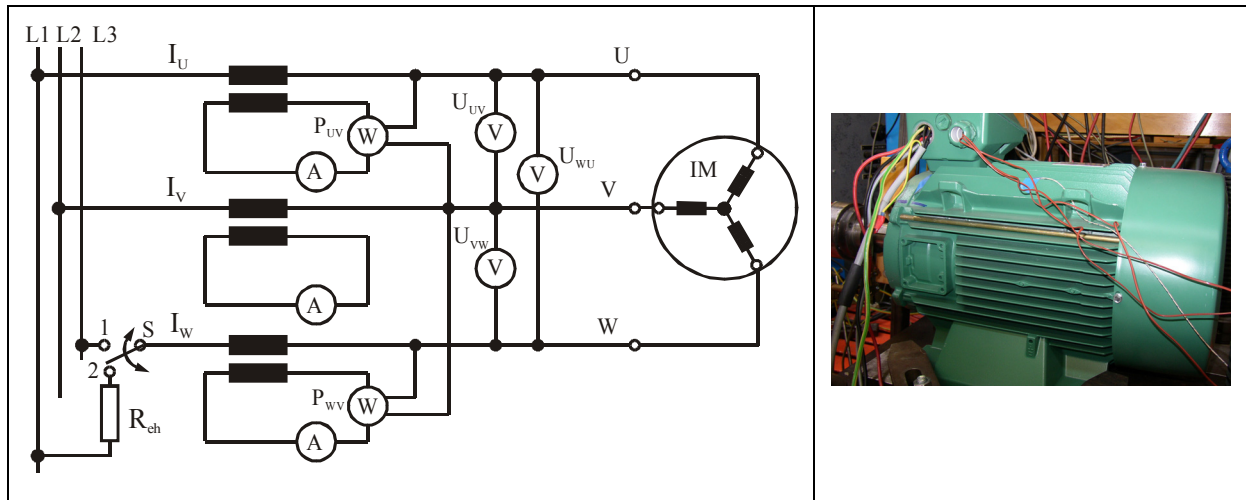
Figure 2.23: Eh-star measurement circuit with uncoupled induction machine (IM) and the test bench
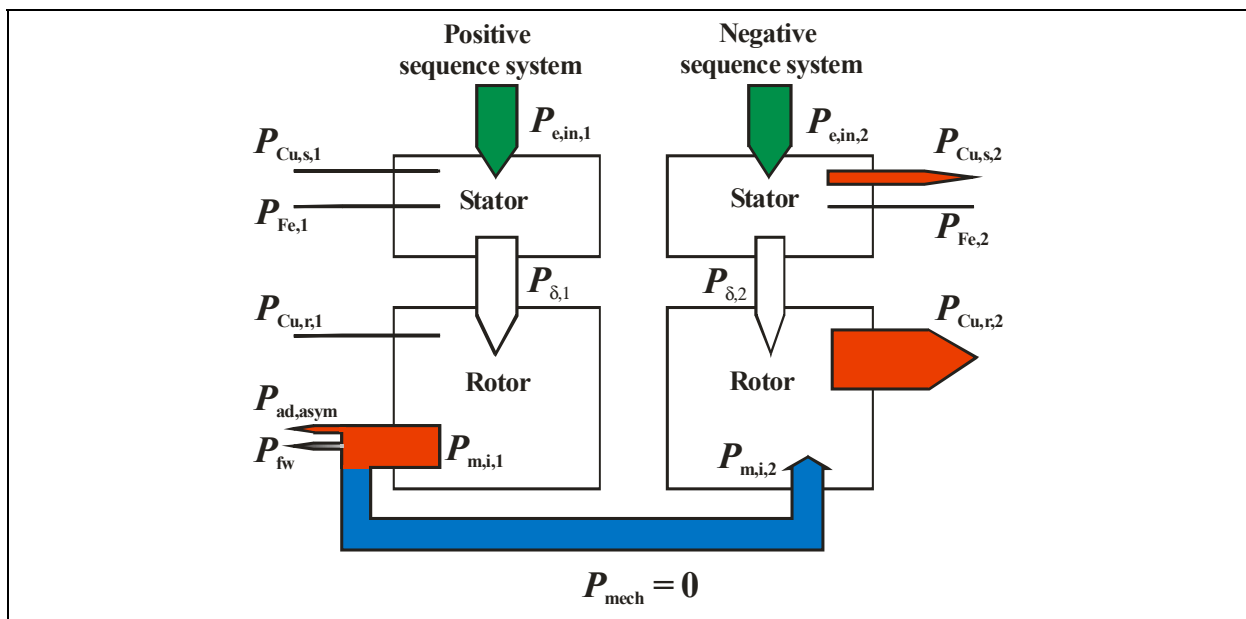
Figure 2.24: Power flow of the positive and the negative sequence systems in eh-star test

Figure 2.25 shows an example of the measured values P_{ad} and the smoothed data $P_{ad,c}$ of the stray load losses without the offset for an 11 kW, 4-pole motor "A160-4". As the offset is omitted, the slope of the regression-line 132.8 W is the stray load losses at the rated load.
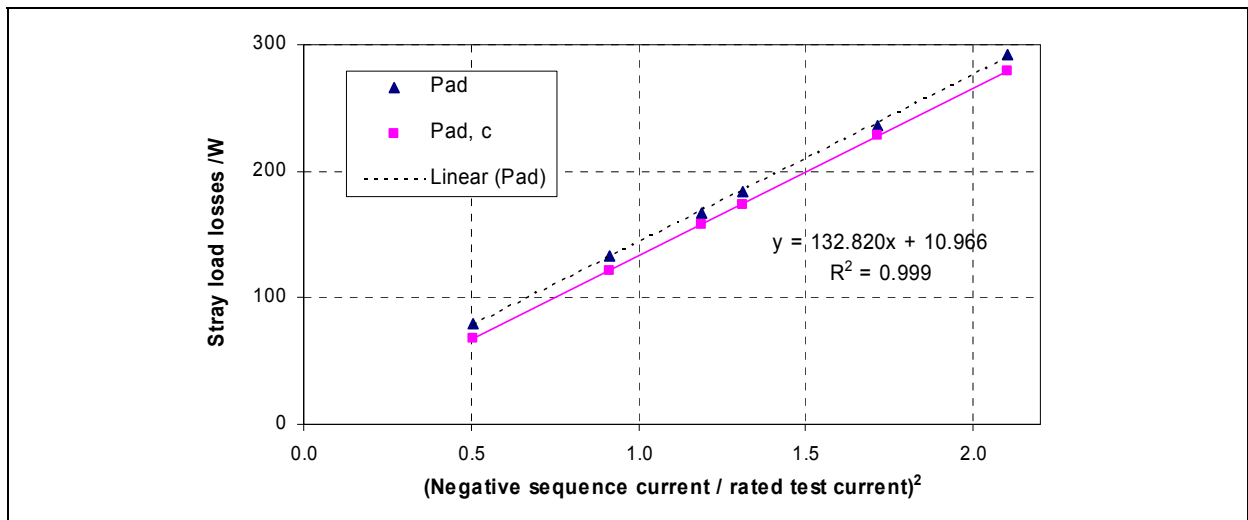
Figure 2.25: Measured stray load losses acc. to eh-star test of a 11 kW 4-pole motor "A160-4"
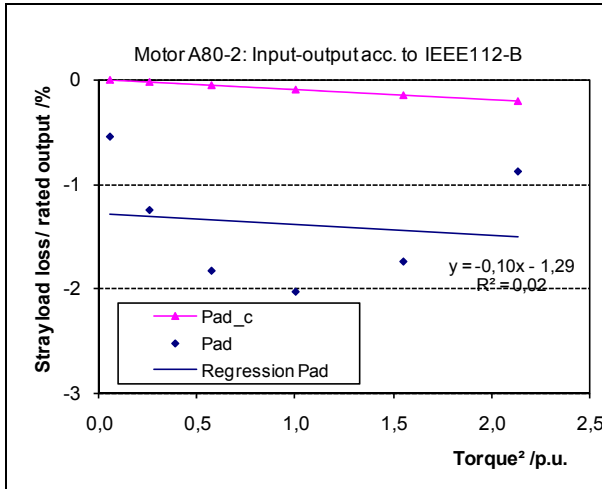(Subscript c for corrected: Linear regression line without offset)

2.2.8 Equivalent no-load method of *Bourne*

This test [Bour 1989] is simple to perform and is similar to the standardised no-load test [IEEE 112, IEC 61972], but with more test points at high no-load current. Like the eh-star test it does not need any coupling of the machine, but does not consider the stray load losses due to the rotor field harmonics, as the rotor fundamental current is not flowing at no-load. To measure the loss component in delta-connected winding due to circulating current of 3-times the stator frequency f_s , caused by the saturation harmonic, the measurement was done in delta-connection for all motors. For one 11 kW, 4-pole motor the measurement was done in delta- and in star-connection to compare the results. The difference of the stray load losses was negligible.

Before beginning the no-load test, the no-load losses have to be stabilised at rated frequency and rated voltage. The test comprises a minimum number of 15 values of the voltage, including 150 % of the rated current down to 20 % of the rated voltage. The test shall be carried out as quickly as possible to avoid strong temperature change in the stator winding, with the readings taken in descending order of the voltage. The power flow at the no-load test is shown in Figure 2.26.
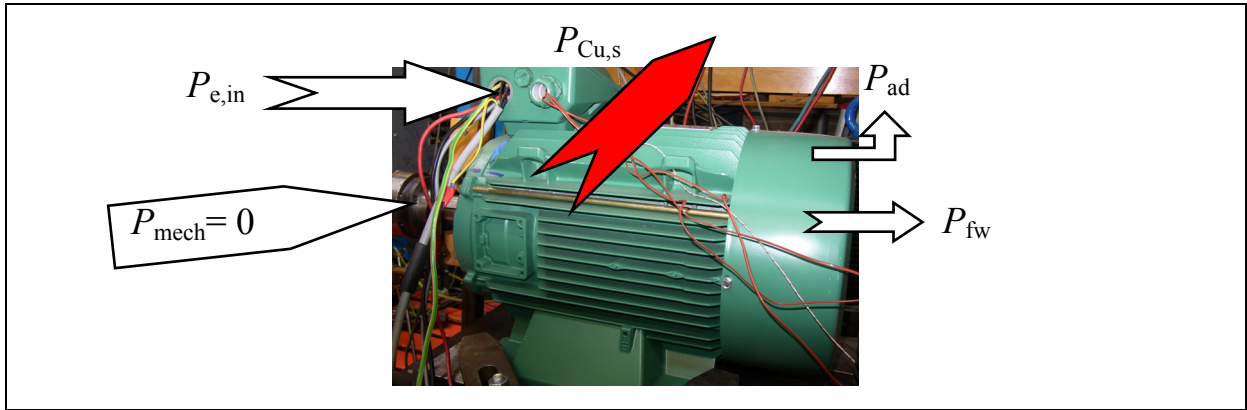
Figure 2.26: Power flow of the uncoupled induction motor at the no-load test acc. to *Bourne*

Subtracting the no-load winding losses $P_{Cu,s}$ (at test temperature) from the no-load electrical input power $P_{e,in}$, acc. to Figure 2.26, gives the sum of the friction, windage, iron losses and stray no-load losses $P_{Fe+fw+ad}$ as

$$P_{Fe+fw+ad} = P_{e,in} - P_{Cu,s}.$$ (2.29)

A curve of the remaining losses $P_{Fe+fw+ad}$ against the voltage squared U^2 is plotted as shown in Figure 2.27.
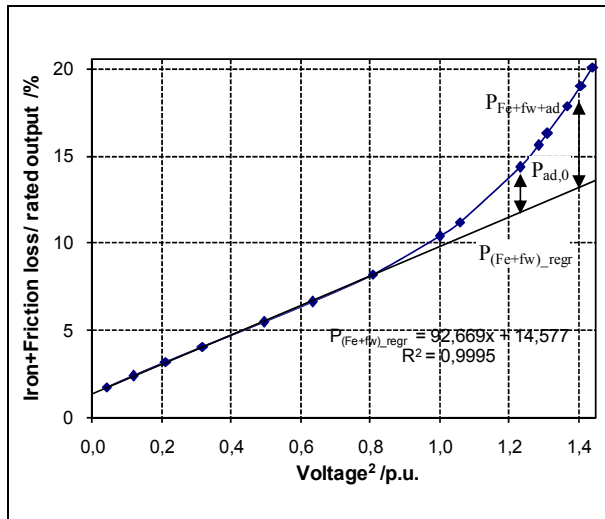
Figure 2.27: No-load losses segregation acc. to equivalent no-load method of *Bourne* for 1.1 kW 2-pole motor "C80-2"
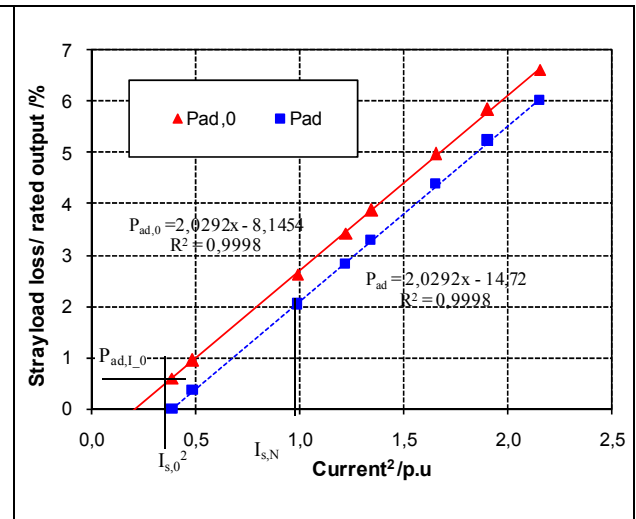
Figure 2.28: Stray load losses acc. to equivalent no-load method of *Bourne* for 1.1 kW 2-pole motor "C80-2"

A straight line (regression line) $P_{(Fe+fw)\_regr}$ for the values of the voltage below about 80 % of the rated voltage is developed, so that the correlation coefficient R of the regression line is above 0.98. The regression line $P_{(Fe+fw)\_regr}$ is extrapolated to the highest measured voltage value. As illustrated in the Figure 2.27 the difference between the measured losses curve $P_{Fe+fw+ad}$ above the rated voltage and the losses from the regression line $P_{(Fe+fw)\_regr}$ are the stray load losses $P_{ad,0}$

$$P_{ad,0} = P_{Fe+fw+ad} - P_{(Fe+fw)\_regr}. \tag{2.30}$$

The stray load losses value P_{ad,I_0} at the no-load current $I_{s,0}$ determined at the rated voltage is considered as offset, which is omitted as given in (2.31). As presented in Figure 2.28 a curve of the resulting stray load losses P_{ad} against the current squared I_s^2 is developed

$$P_{ad} = P_{ad,0} - P_{ad,I\_0}. \tag{2.31}$$

With the linear regression line $P_{ad}(I_s^2)$ the value of the stray load losses $P_{ad,N}$ at the rated current $I_{s,N}$ is derived (dashed line in Figure 2.28).

For a better representation, the stray load losses P_{ad} are plotted in dependence of the square of the test current vs. the square of the rated test current $(I_t / I_{t,N})^2$ in Figure 2.29. The test current I_t is determined from the stator current I_s and the no-load current $I_{s,0}$ at the rated voltage. The Figure 2.27 - Figure 2.29 show the procedure to determine the stray load losses from the equivalent no-load measurement method for a 2-pole squirrel cage test motor of 1.1 kW "C80-2". For this example the determined stray load losses at rated load are 23 W.
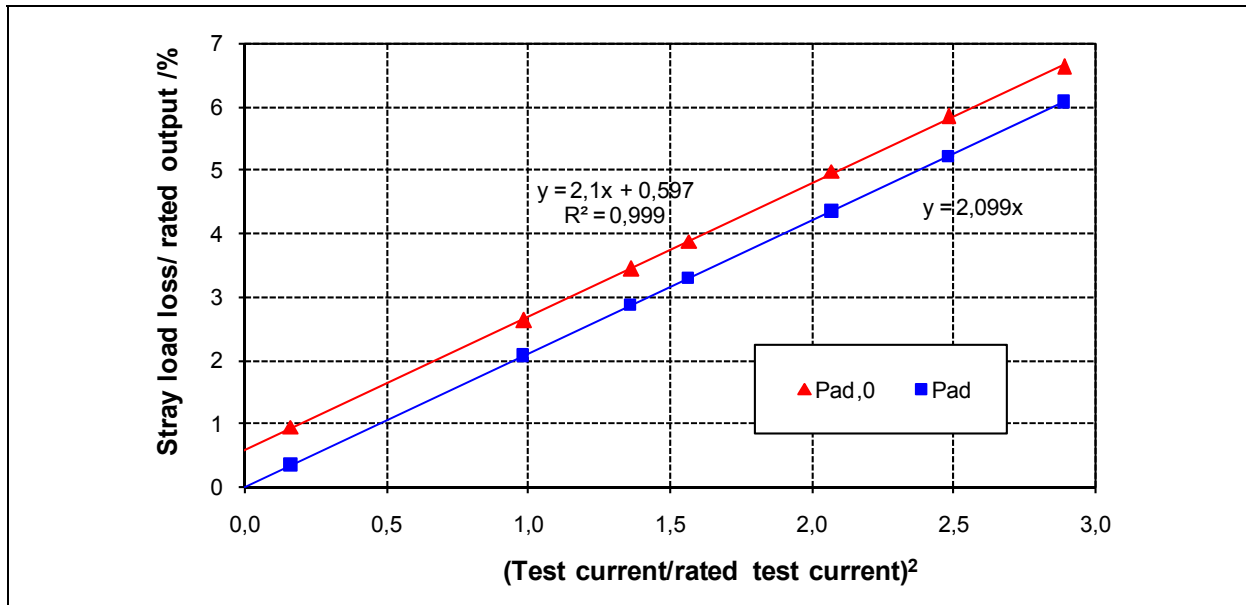
Figure 2.29: Measured stray load losses vs. square of test current acc. to equivalent no-load method of *Bourne* for 1.1 kW 2-pole motor "C80-2"

2.2.9 **Equivalent no-load method of *Rawcliffe* and *Menon***

Rawcliffe and *Menon* have developed "A simple new test for harmonic-frequency losses in a.c. machines" [Rawc 1952]. The *Rawcliffe*'s test is a no-load test, which is similar to the standardised no-load test, where the machine is uncoupled. The values ($s \cdot U^2$) determined from the product of the slip s and the square of the voltage U^2 must be plotted against the voltages U and extrapolated to zero voltage as shown in Figure 2.30 and Figure 2.31. The value ($s \cdot U^2$) representing the power transferred to the rotor "air gap power" covers the friction P_{fw} and the harmonic $P_{hf,measur}$ losses. The usual no-load power/voltage curve $P_{Fe+fw}(U)$ is used to put a scale on the $s \cdot U^2(U)$ curve. The value ($s \cdot U^2$) at zero voltage is equivalent to the friction losses P_{fw} as derived from the power/voltage curve $P_{Fe+fw}(U)$. The measured harmonic-frequency losses $P_{hf,measur}$ e.g. at the rated voltage are the difference between the value ($s \cdot U^2$) at the rated voltage and the constant value ($s \cdot U^2$) at zero voltage (Figure 2.31):

$$P_{\text{hf,measur}} \cong (s \cdot U^2)|_{\text{rated voltage}} - (s \cdot U^2)|_{\text{zero voltage}}$$

$$= \left((s \cdot U^2)|_{\text{rated voltage}} - (s \cdot U^2)|_{\text{zero voltage}}\right) \cdot \frac{P_{\text{fw}}}{(s \cdot U^2)|_{\text{zero voltage}}} \qquad (2.32)$$

$$= P_{\text{e,in}} - P_{\text{Cu,s}} - P_{\text{Fe,s}} - P_{\text{fw}}.$$

The resulting harmonic-frequency losses P_{hf} should be corrected to the calculated secondary hysteresis (torque) losses at fundamental frequency $P_{\text{Fe,hy,r,calcul}}$ as

$$P_{\text{hf}} = P_{\text{hf,measur}} + P_{\text{Fe,hy,r,calcul}}. \qquad (2.33)$$

This additional calculation of the secondary hysteresis losses $P_{\text{Fe,hy,r,calcul}}$ is a blemish on this test, as any inaccuracy in these calculations will be reflected in the final result. Of course the design data of the machine must be available for the calculation ! The resistive losses and the slip must be measured accurately. The extrapolation of the $(s \cdot U^2)$/voltage curve to zero voltage to determine the friction losses and so the scale-factor is also problematic (Figure 2.30) and each inaccuracy will influence the result as the results are most accurate when the windage and the harmonic losses are roughly of the same order [Rawc 1952, Taeg 1987]. For 5 slip-ring induction motors (ca. 3 -15 kW) *Rawcliffe* and *Menon* have compared the results of the new test with the "*Linke* auxiliary drive test" [Link 1907] and with the "*Hoseason* double fed and standstill tests" [Hose 1923], which are applicable only to a slip-ring induction motors, and found good agreement. For 8 squirrel-cage motors, the agreement with the calculation was less good, due to certain simplifying assumptions in the calculation. *Taegen* and *Walczak* [Taeg 1987] have compared the measured stray load losses of an 11 kW squirrel-cage motor at no-load (auxiliary driven laminated rotor without windings and slots) and under full-load with the *Rawcliffe*'s test. For semi-closed stator slots with unskewed rotor slots, the *Rawcliffe*'s test results deviate by 19 % ... 44 % at no-load and by -32 % ... -57 % at full-load. For open stator slots with skewed rotor slots, the *Rawcliffe*'s test results deviate by -18 % ... 34 % at no-load and by -49 % ... -55 % at full-load.

To check the reliability of the *Rawcliffe*'s test some measured motors acc. to

the standardized no-load test are evaluated acc. to the *Rawcliffe*'s method without calculation of the secondary hysteresis losses $P_{Fe,hy,r,calcul}$. The results were not encouraging; for some motors the evaluation was not possible as the slip of the machine is zero or the values are erratic as shown in Figure 2.32 and Figure 2.33. The finding is close to the investigation of *Taegen* and *Walczak* [Taeg 1987]. So this method should not be recommended for stray load losses assessment.
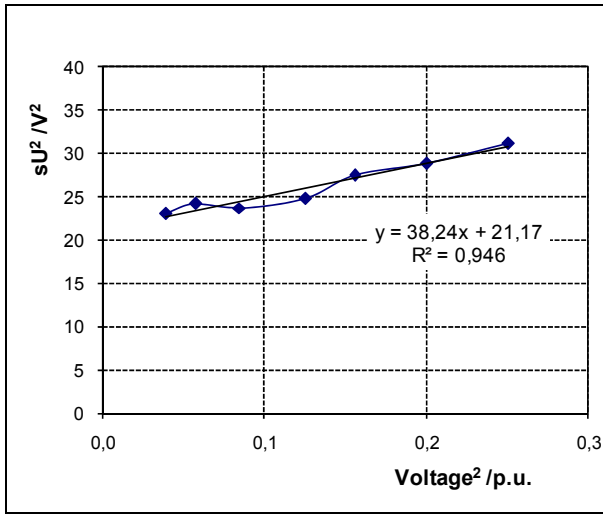
Figure 2.30: Determination of the scaling factor acc. to the equivalent no-load method of *Rawcliffe* for 1.1 kW 2-pole motor "C80-2"
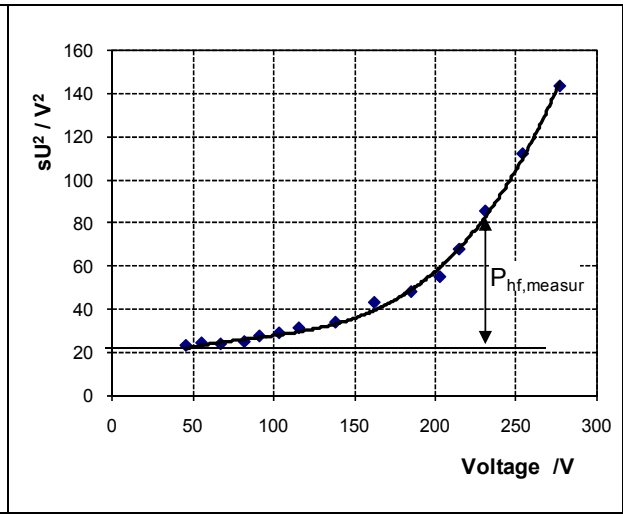
Figure 2.31: Stray load losses acc. to the equivalent no-load method of *Rawcliffe* for 1.1 kW 2-pole motor "C80-2"

In the example of the Figure 2.30 the zero-crossing of the curve is 21.17 V^2. With the determined friction and windage losses P_{fw} of 14.58 W acc. to IEC 61972 the scale factor is

$$\frac{P_{fw}}{(s \cdot U^2)|_{\text{zero voltage}}} = \frac{14.58 \text{ W}}{21.17 \text{ V}^2} = 0.688 \frac{\text{W}}{\text{V}^2}.$$ (2.34)

The measured harmonic-frequency losses $P_{hf,measur}$ e.g. at rated voltage are

$$P_{\text{hf,measur}} = \left((s \cdot U^2)\big|_{\text{rated voltage}} - (s \cdot U^2)\big|_{\text{zero voltage}} \right) \cdot \frac{P_{\text{fw}}}{(s \cdot U^2)\big|_{\text{zero voltage}}} \qquad (2.35)$$

$$= (85 \text{ V}^2 - 21.17 \text{ V}^2) \cdot 0.688 \text{ W/V}^2 = 44 \text{ W}.$$

For comparison the measured value of the stray load losses P_{ad} at rated load acc. to IEC 61972 is 50 W.

For the examples in Figure 2.32 and Figure 2.33 negative values of the stray load losses P_{ad} are obtained as the slip s is close to zero.
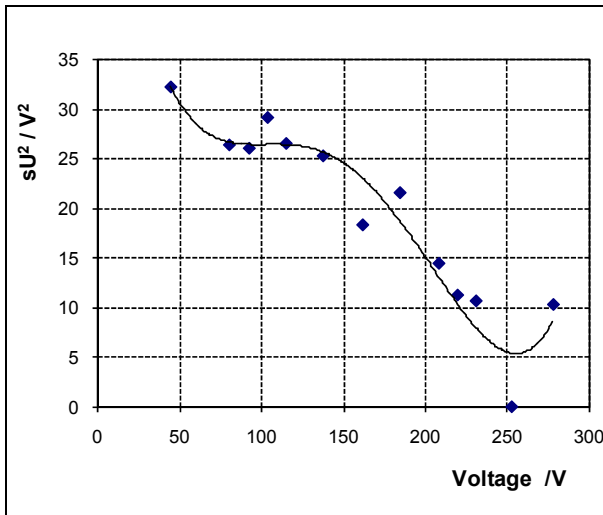
Figure 2.32: Stray load losses acc. to the equivalent no-load method of *Rawcliffe* for 11 kW 2-pole motor "D160-2"
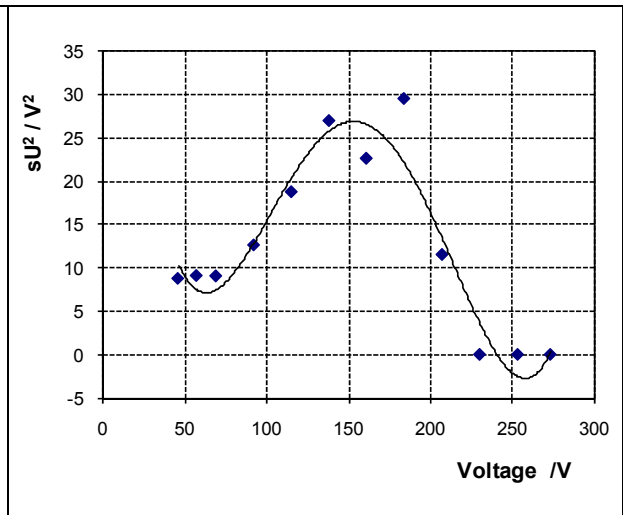
Figure 2.33: Stray load losses acc. to the equivalent no-load method of *Rawcliffe* for 11 kW 4-pole motor "E160-4"

2.3 Advantages and disadvantages of compared test methods

The advantages (+) and disadvantages (-) of the investigated test methods are summarized in this section.

2.3.1 Direct methods for the total losses determination

The advantages (+) and disadvantages (-) of the input-output tests (residual loss method) acc. to IEC 61972 and IEEE 112-method B are

+ Real physical behaviour due to the direct losses assessment from the input-output test.

+ IEC 61972 considers the load-dependent iron losses.

- IEEE 112-method B considers the iron losses to be independent of the load, so wrong results for small motors (with big stator resistance) are obtained.

- IEC 61972 and IEEE 112-method B consider the friction and windage losses to be independent of the changing speed during the load test, this leads to a small error in the stray load losses especially for motors with higher slip.

- Coupling of the machine with the load and the use of calibrated dynamometer are necessary.

- Since losses are the difference of nearly equal input/ output power quantities, the upper limit of efficiency to be evaluated with sufficient accuracy should be 95%...96% .

- Procedure takes considerable time.

2.3.2 Indirect methods for the total losses determination

The advantages (+) and disadvantages (-) of the indirect methods for the total losses determination using equivalent methods for the stray load losses will be listed for each test in following.

1) Reverse rotation test

+ Physically correct determination of the fundamental stray load losses in the stator at the removed rotor test (except the neglect of – small – iron losses).

- The consideration of the load-independent friction and windage losses affects the efficiency determination (e.g. IEEE 112-method E and IEC 61972) but not the stray load losses.

- Coupling of the machine with the load and the use of calibrated dynamometer are necessary.

- No real physical load situation of the machine.

- At the slip $s = 2$ the magnetisation current is small, so too low main flux and no main flux iron saturation. The zig-zag stray flux dominates.

- Different harmonic slip s_v of - in single layer winding dominating - 5th and 7th air gap field harmonic at the slip $s = 2$ and rated slip $s_N \approx 0$ causes different stray load losses.

- RRT yields generally too high stray load losses.

- Two test procedures are necessary.

2) Eh-star test

+ No coupling of the machine with the load and no dynamometer are needed.

+ Simple and short test.

+ No difference of nearly equal power quantities to be measured, so no efficiency limit.

± Main flux too small, but is bigger than at RRT due to the positive sequence system.

- No real physical load situation of the machine.

- Complicated theory behind.

- Auxiliary power resistor R_{eh} and may be a switch for the symmetric start-up are necessary, the latter especially with smaller motors (with bigger motors the switch and resistor might be omitted).

- Loss component due to 3-times stator frequency f_s circulating current in delta-connected winding, caused by the saturation harmonic, is not included (but is usually small at not too high saturation).

3) Equivalent no-load method

+ No coupling of the machine with the load and no dynamometer are necessary.

+ Very simple method.

+ Fundamental stator current effects (e.g. current displacement) are considered.

- No real physical load situation of the machine.

- Rotor fundamental current is missing, so the stray load losses due to the rotor field harmonics are missing.

- Machine is highly saturated, so the main flux dependent stray load losses are bigger than at rated condition.

- Voltage must be higher than the rated voltage to reach the rated current at the no-load.

- Resistive losses must be measured accurately.

- High frequency losses mainly localized in the rotor, so the rotor fundamental current may be of minor influence.

A comparison of the useful methods to determine the stray load losses is presented in Table 2.8. The evaluation of the measurement is not included in this comparison, because usually computers are applied for this purpose.

Tests	Input-output test (Residual loss method)	Reverse rotation test	Eh-star test
Standard	IEC 61972 and IEEE 112-method B	IEC 61972 and IEEE 112	IEC 60034-2 Ed.4, 2nd CDV
Measurement of electrical values	High accuracy	High accuracy	High accuracy
Measurement of Torque	High accuracy	High accuracy	NA
Cost of torque device	Expensive	Expensive	NA
Cost of adjustable resistor + Switch	NA	NA	Low to Medium
Measurement of speed	High accuracy	High accuracy	Medium accuracy
Load machine + equipment	Highly expensive	Highly expensive	NA
Mechanical adjustment	Additional time	Additional time	NA
Calibration of torque device	Additional time	Additional time	NA
Demounting & mounting of rotor	NA	Additional time	NA
Measurement time	Long	Medium	Short
Energy consumption	Highly	High	Low
Environmental impact	Highly	High	Low
Resulting cost	Highly	High	Low
Industrial application	Complicated	Complicated	Simple
Reliability related to Input-output test	--	Bad	Good
Sensitivity on measurement errors	High	High	Medium

Table 2.8: Comparison of the investigated methods (NA: not applicable or not needed)

2.4 Conclusion

The methods for determining the efficiency of induction machines are based on different theoretical models and different assumptions. Therefore, it is not reasonable to make a comparison between the values of the efficiency obtained

by different methods. As the direct determination of the efficiency (measurement of the input and output power) suffers from the measurement uncertainty, it is – naturally – limited for motors of high efficiency. The indirect method is less sensitive to measurement errors and seems to be, depending on the measurement accuracy of the total power losses P_d, useful also for higher efficiency machines.

In the efforts to improve the efficiency of the induction machine also the stray load losses should be taken into account. Because of the unavoidable measurement errors, the indirect determination of the stray load losses P_{ad} by measuring the input $P_{e,in}$ and output $P_{m,out}$ power is generally not accurate enough for small value of the stray load losses P_{ad} e.g. at high efficiencies. Therefore the direct measurement methods of the stray load losses P_{ad} could be useful at high efficiencies. The strengths and weaknesses of different determination methods and their practical existing limitations is discussed. A simple and fast test, like the eh-star method, is required for the stray load losses P_{ad} measurement e.g. during the process of the optimisation of the motor design.

3   EH-STAR METHOD

In this chapter the theoretical background, the test procedure and the post-processing of measured data of the eh-star method, as an equivalent measurement method to determine the stray load losses, will be described in detail. Different evaluation methods will be investigated by theoretical and measurement examples. The impact of different parameters on the eh-star method will be shown.

The eh-star method, introduced by *Jordan* and *Richter* [Jord 1967], utilizes an asymmetric feeding of a three-phase induction machine (squirrel-cage or wound rotor) without coupling of the machine and without needing any dynamometer. The asymmetrical operation is obtained by operating the stator winding in star connection from a single phase voltage source. Two machine phases *U* and *W* are connected in parallel through an auxiliary *ohmic* resistance R_{eh} of a value similar to the motor short circuit impedance. This resistance shall be adjusted, so that the positive sequence current I_1 stays below 30 % of the negative sequence current I_2, and the speed stays in the range of typically rated speed. The star-point must not be connected to earth to avoid zero-sequence currents. A switch *S* for switching from three-phase starting of the tested machines to single phase operation (Figure 3.2) is needed. So the abbreviation „eh" explains the operation: *Einphasig* (single phase), *Hilfswiderstand* (auxiliary resistance).

The determination of the stray load losses must be done from the measured losses by decomposition into the positive and the negative sequence losses. The negative sequence losses at slip $2 - s \cong 2$ correspond to the stray load losses, similar to the standardized reverse rotation test. For this evaluation, the phase angles of the measured currents and voltages must be known. In addition to the

results of the eh-star measurement, one needs the measurement of the stator resistance and the temperature and the measurement results of the no-load test (iron losses and friction and windage losses).

The conditions of the eh-star test can be summarized as:

-   The feeding of the induction machine by an asymmetrical 3-phase current system, via single phase with the auxiliary resistance R_{eh}.

-   The rotor speed should be near the rated speed, so that the slip of the inverse field is nearly $s \approx 2$. So the inverse field rotates with the slip $s_2 = (2 - s) \approx 2$ like in the reverse rotation test (RRT) according to the standard IEEE 112, but without need of coupling the machine with the dynamometer.

-   The rotor current of the inverse system at slip $s \approx 2$ simulates the load condition as at the RRT. So only the stray load losses due to the negative sequence system I_2 are considered for the final result.

-   The positive sequence component I_1 shall be small to keep the motor rotating, so that the conditions of the RRT are simulated.

3.1 Theoretical background

Like in the reverse rotation test, the broad saddle due to additional asynchronous parasitic torque in the motor torque-speed characteristic is used for determining the additional losses P_{ad}. These additional torques M_{ad}, which are always braking and which are recognized in the slip region $s > 1$ as a strong increase of the torque (Figure 3.1), have always been brought into connection with the additional losses [Rogo 1925, Drey 1928, Neuh 1964].

First it will be described theoretically, how the harmonic fields and thus consequent additional losses are acting in the induction machines, where the stator winding is connected in eh-star circuit by an auxiliary resistance (Figure 3.2). We assume, as a simplification, that the magnetic circuit is not too much saturated. Thus it may be permissible to superimpose the harmonic fields of different frequencies and wave lengths to get their effects.
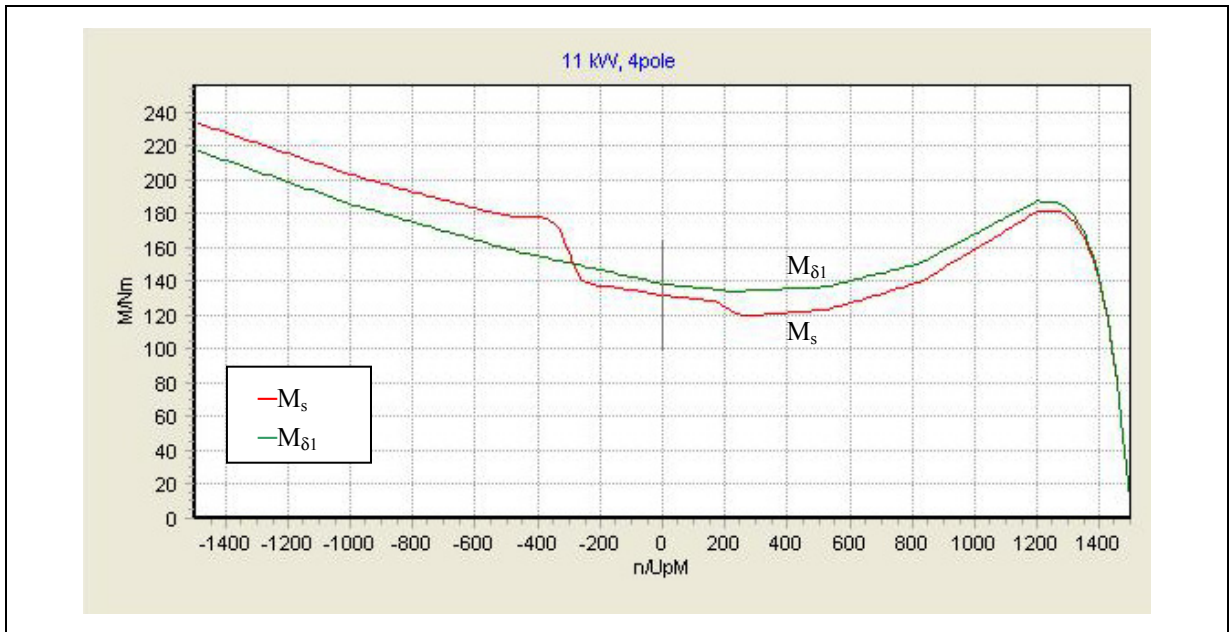
Figure 3.1: Calculated torque-speed characteristic of an 11 kW 4-pole cage induction motor
"D160-4". M_s is the shaft torque and $M_{\delta 1}$ is the fundamental torque. The
calculation is done with KLASYS [KLASYS].
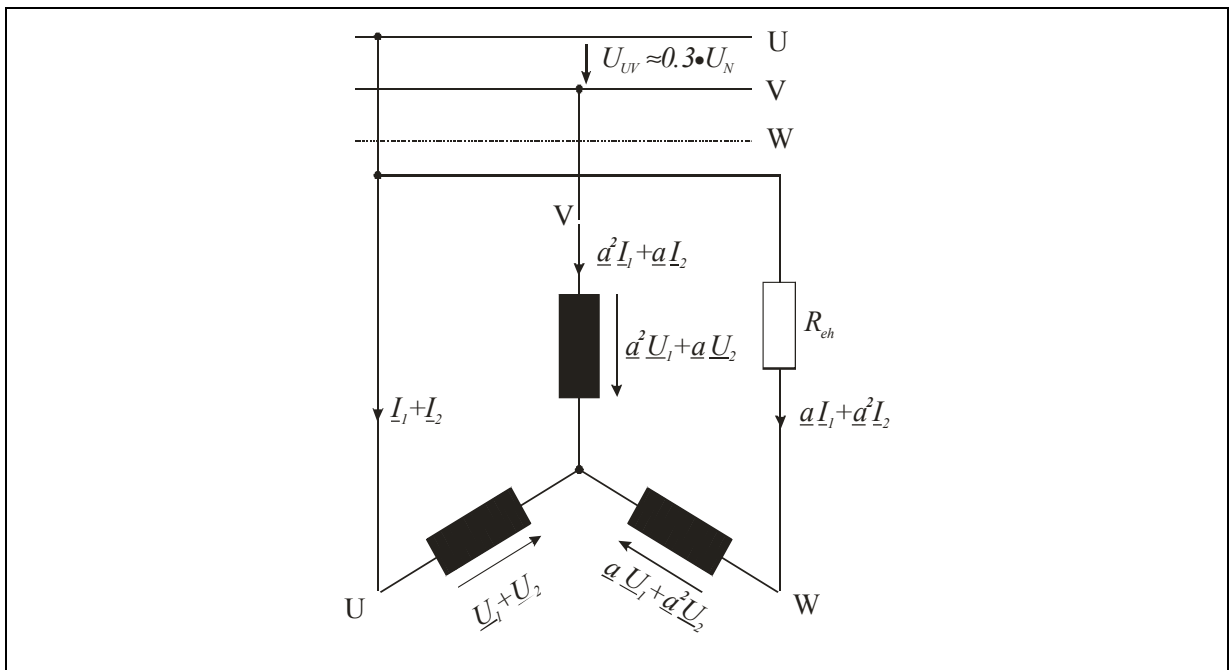
Figure 3.2: Eh-star circuit with the auxiliary resistance R_{eh}

$\underline{I}_1$: positive sequence current, $\underline{I}_2$: negative sequence current, $\underline{U}_1$: positive
sequence voltage, $\underline{U}_2$: negative sequence voltage, $\underline{a}$ is the phase shifter by
120°: $\underline{a} = e^{j2\pi/3}$.

For the symmetrically fed induction machines the relation between the additional losses P_{ad} and the torque M at a slip s has been already derived in [Jord 1965, Neuh 1964]:

$$M = \frac{p}{\omega} \cdot \sum_{v=p}^{\infty} P_{\delta v} - \frac{p}{\omega} \cdot \frac{P_{ad}}{1-s} + \frac{s}{1-s} \cdot \sum_{v \neq p}^{\infty} \frac{p}{v} \cdot M_{\delta v} - \frac{s}{1-s} \cdot \sum_{\mu_p = p}^{\infty} \frac{p}{\mu_p} \cdot M_{\delta \mu_p} \qquad (3.1)$$

with p the number of pole pairs, ω the angular frequency, P_δ the air gap power, v the ordinal number of stator harmonic field and μ the ordinal number of rotor harmonic field caused by the vth stator harmonic field. Torque M comprises the shaft torque M_s plus the friction and windage torque M_{fw}. The term $(\frac{p}{\omega} \cdot \frac{P_{ad}}{1-s})$ denotes the braking torque due to the additional losses, the component $M_{\delta v}$ is the torque of the stator field harmonics and the torque $M_{\delta \mu_p}$ comprises the components of the rotor field harmonics. These rotor field harmonics are excited by the rotor fundamental current, which is caused by the stator fundamental field.

The additional losses are in that case

$$P_{ad} = \sum_{v \neq p}^{\infty} P_{Cu,r,v} + \sum_{v=p}^{\infty} \sum_{\mu_v = v}^{\infty} P_{Cu,sf,\mu_v} \,, \qquad (3.2)$$

with $\sum_{v \neq p}^{\infty} P_{Cu,r,v}$ the losses due to stator field harmonics in the rotor cage and in the rotor iron, whereas $\sum_{v=p}^{\infty} \sum_{\mu_v = v}^{\infty} P_{Cu,sf,\mu_v}$ are the higher frequency losses in the stator winding and the stator iron due to the rotor field harmonics of frequencies f_{s,μ_v}, which differ from the stator grid frequency f_s

$$f_{s,\mu_v} = \left[1 + \frac{\mu_v - v}{p} \cdot (1-s) \right] \cdot f_s \,. \qquad (3.3)$$

The asymmetrically fed three-phase induction machine is considered, according to the rules of symmetrical components, as superposition of two

equivalent symmetric induction machines, of which one is fed by the positive sequence system and the other by the negative sequence system [Kova 1962]. The internal torque components of both machines (which are acting in opposite directions) will be added as $(M_1 - M_2)$. The positive sequence machine (subscript 1) is fed by the positive sequence three-phase symmetric voltage system $\underline{U}_1$ (phase sequence U-V-W). Hence the negative sequence machine, which is fed by the negative sequence three-phase symmetric voltage system $\underline{U}_2$ (phase sequence U-W-V) is driven by the positive sequence machine against its own rotating air gap field. Thus the positive sequence machine operates at slip $s_1 = s$, whereas the negative sequence machine operates at slip $s_2 = 2 - s$. The speed of the machine is given by the torque of the positive M_1 and the negative M_2 sequence system and the friction and windage torque M_{fw}. At machine no-load the shaft torque M_s, which is given by the positive M_1 and negative M_2 sequence internal (air gap) torque and the friction and windage torque M_{fw}, is zero:

$$M_s = M_1 - M_2 - M_{fw} = 0 \quad \Rightarrow \quad M_1 - M_2 = M_{fw} . \tag{3.4}$$

For the positive sequence machine – operating at $\underline{U}_1$ – we get the internal torque M_1 acc. to (3.1) at the slip $s_1 = s$:

$$M_1 = \frac{p}{\omega} \cdot \sum_{v=p}^{\infty} P_{\delta v,1} - \frac{p}{\omega} \cdot \frac{P_{ad,1}}{1-s} + \frac{s}{1-s} \cdot \sum_{v \neq p}^{\infty} \frac{p}{v} \cdot M_{\delta v,1} - \frac{s}{1-s} \cdot \sum_{\mu_p = p}^{\infty} \frac{p}{\mu_p} \cdot M_{\delta \mu_p,1} . \tag{3.5}$$

With (3.1) and

$$\frac{s_2}{1-s_2} = \frac{2-s}{1-2+s} = -\frac{2-s}{1-s}$$

$$\frac{1}{1-s_2} = \frac{1}{1-2+s} = -\frac{1}{1-s} , \tag{3.6}$$

we get the internal torque M_2, for the negative sequence machine, operating at the slip $s_2 = 2 - s$

$$M_2 = \frac{p}{\omega} \cdot \sum_{v=p}^{\infty} P_{\delta v,2} + \frac{p}{\omega} \cdot \frac{P_{ad,2}}{1-s} - \frac{2-s}{1-s} \cdot \sum_{v \neq p}^{\infty} \frac{p}{v} \cdot M_{\delta v,2} + \frac{2-s}{1-s} \cdot \sum_{\mu_p=p}^{\infty} \frac{p}{\mu_p} \cdot M_{\delta \mu_p,2}. \quad (3.7)$$

With (3.4), (3.5) and (3.7) we get for the friction and windage torque M_{fw}

$$M_{fw} = \frac{p}{\omega} \cdot \sum_{v=p}^{\infty} (P_{\delta v,1} - P_{\delta v,2}) - \frac{p}{\omega} \cdot \frac{P_{ad,1} + P_{ad,2}}{1-s} + M_E, \quad (3.8)$$

where the component M_E the error term in the harmonic torque is

$$M_E = \sum_{v \neq p}^{\infty} \frac{p}{v} \cdot \left(\frac{s}{1-s} \cdot M_{\delta v,1} + \frac{2-s}{1-s} \cdot M_{\delta v,2} \right) +$$
$$+ \sum_{\mu_p=p}^{\infty} \frac{p}{\mu_p} \cdot \left(\frac{s}{1-s} \cdot M_{\delta \mu_p,1} + \frac{2-s}{1-s} \cdot M_{\delta \mu_p,2} \right). \quad (3.9)$$

The total additional losses of the asymmetrically feed machine $P_{ad,asym}$ are therefore the sum of the additional losses $P_{ad,1}$ of the positive and $P_{ad,2}$ of the negative sequence system

$$P_{ad,asym} = P_{ad,1} + P_{ad,2} = (1-s) \cdot \sum_{v=p}^{\infty} (P_{\delta v,1} - P_{\delta v,2}) - P_{fw} + P_E, \quad (3.10)$$

Where, with the mechanical speed $(\omega/p) \cdot (1-s)$, the friction and windage losses P_{fw} are

$$P_{fw} = \frac{\omega}{p} \cdot (1-s) \cdot M_{fw}, \quad (3.11)$$

and the error term of the higher harmonic field power P_E is

$$P_E = \frac{\omega}{p} \cdot (1-s) \cdot M_E. \quad (3.12)$$

The losses P_E contain components which are the sums in (3.9). At slip $s \leq 0.15$ the expression $(1-s)$ is near unity, the harmonic torque components

$M_{\delta v,1}$, $M_{\delta \mu_p,1}$ at slip s and $M_{\delta v,2}$, $M_{\delta \mu_p,2}$ at slip $(2-s)$ are small, and the values of $1/v$, $1/\mu_p$ decrease with increasing ordinal numbers very fast and with alternating sign, so the infinite sums are small compared to the rest terms in (3.10) [Jord 1965]. Therefore the losses P_E are neglected. This is especially valid, when the 5th and 7th harmonic ($v = -5, v = 7$) are small in case of pitched coils e.g. with two-layer windings, which suppress these two harmonics. This precondition is also of advantage in the reverse rotation test, to get the similar additional losses at the slip $s = 2$ as at the rated speed [Morg 1939, Chal 1963, IEEE 112]. Regarding the magnitude of the neglected value of the losses P_E one has to look into detail from case to case. Hence the equation (3.10) gives a simple expression for determination of the additional losses of the asymmetrically fed induction machines. The corresponding calculated torque-speed characteristic is shown in Figure 3.3.
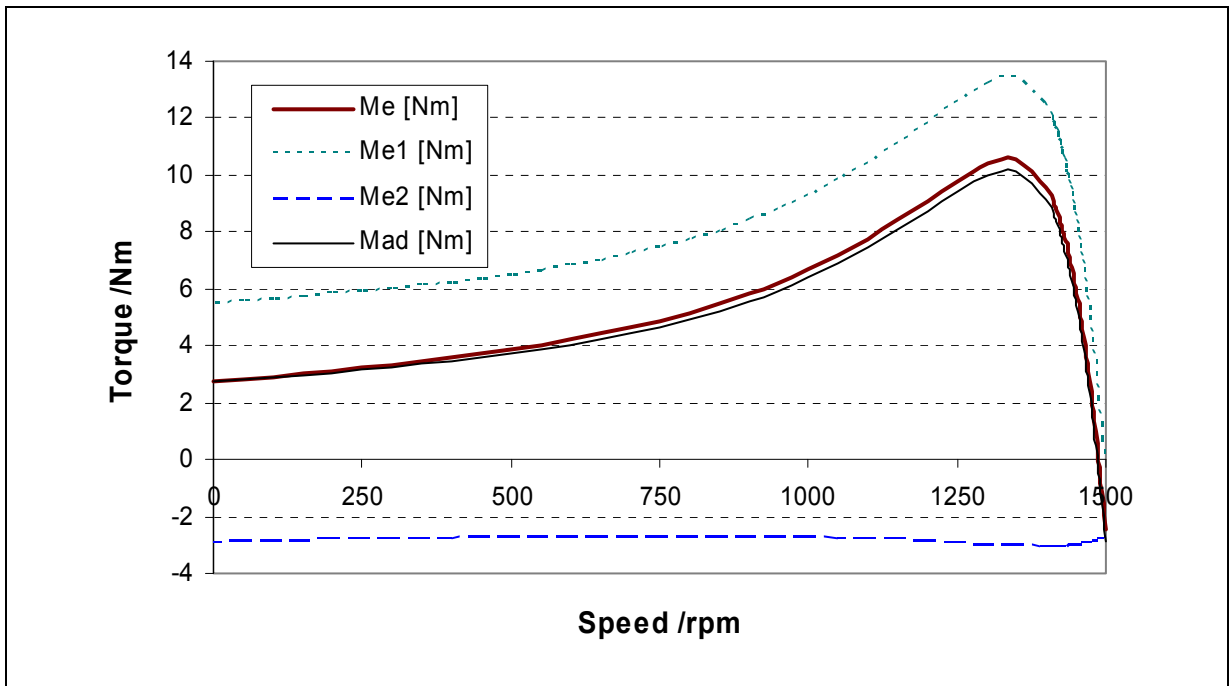
Figure 3.3: Calculated electromagnetic internal torque of positive M_{e1}, negative M_{e2}, resulting M_e and braking torque due the stray load losses M_{ad} in eh-star operation at reduced voltage for an 11 kW 4-pole motor.

For the calculation, Figure 3.3, it was assumed that the harmonic torque

components are negligible, $\sum\limits_{\nu \neq p}^{\infty} \dfrac{p}{\nu} \cdot M_{\delta\nu} = 0$ and $\sum\limits_{\mu_p = p}^{\infty} \dfrac{p}{\mu_p} \cdot M_{\delta\mu_p} = 0$, due to the

alternating sign of the ordinal numbers ν and μ and the rapid decrease of the values $1/\nu$, $1/\mu_p$ with increasing ordinal numbers.

For the determination of the additional losses $P_{ad,asym}$ of the asymmetrically fed machine acc. to the equation (3.10) the friction and windage losses P_{fw} and the difference of the air gap power of the positive $P_{\delta,1}$ and negative $P_{\delta,2}$ sequence system are needed.

The air gap power (internal power) of the positive $P_{\delta,1}$ and negative $P_{\delta,2}$ sequence system are calculated from the corresponding positive and negative components as

$$P_{\delta,1} = 3 \cdot \mathrm{Re}\{\underline{U}_{i,1} \cdot \underline{I}_{i,1}^{*}\} \tag{3.13}$$

$$P_{\delta,2} = 3 \cdot \mathrm{Re}\{\underline{U}_{i,2} \cdot \underline{I}_{i,2}^{*}\} \tag{3.14}$$

where $\underline{U}_i$ is the inner phase voltage at the equivalent iron resistance R_{Fe} and $\underline{I}_i$ is the inner phase current "behind" the iron resistance R_{Fe} (Figure 3.4).
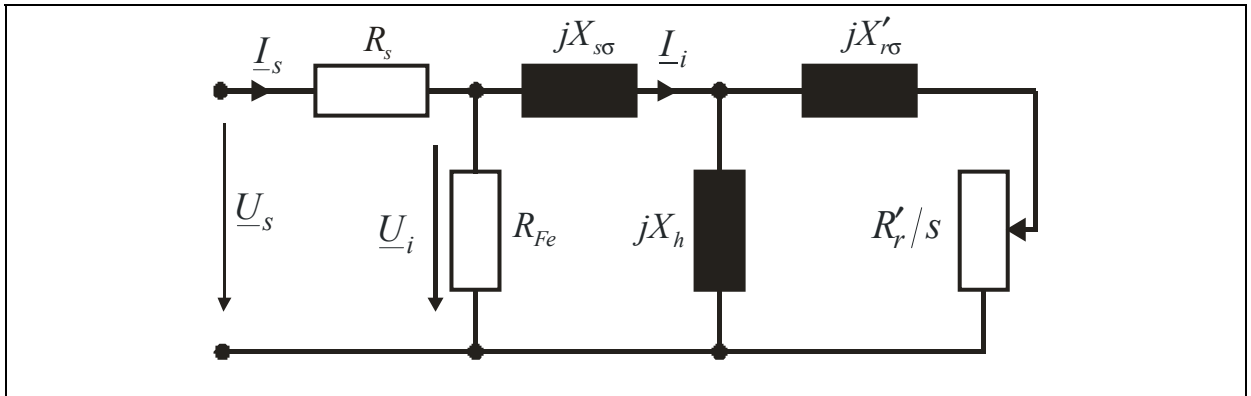
Figure 3.4: T-equivalent circuit of induction machine with consideration of the iron losses

Considering that the internal power contains not only the fundamental air gap power but also the small part of the harmonic air gap power supplied from the grid, this internal power equals exactly the expression $\sum\limits_{\nu = p}^{\infty} P_{\delta\nu}$ of equation (3.1). Therefore the difference of (3.13) and (3.14) delivers already the desired value

$\sum\limits_{v=p}^{\infty}(P_{\delta v,1} - P_{\delta v,2})$ for determination of the additional losses $P_{ad,asym}$ of the asymmetrically fed machine:

$$P_{ad,asym} = (1-s)\cdot\left(3\cdot\mathrm{Re}\{\underline{U}_{i,1}\cdot\underline{I}_{i,1}^{*}\} - 3\cdot\mathrm{Re}\{\underline{U}_{i,2}\cdot\underline{I}_{i,2}^{*}\}\right) - P_{fw}. \qquad (3.15)$$

To calculate the air gap power $P_{\delta,1}$ of the positive and $P_{\delta,2}$ of the negative sequence system and hence the additional losses P_{ad}, the determination of the real and imaginary parts of the complex phasors of the three-phase voltages and currents from measured r.m.s. values is necessary. The detailed calculation is shown in the following section.

3.2 Determination of current phasors by different methods

The determination of the real and the imaginary parts of the complex phasors of the three-phase voltages and currents from the measured r.m.s. values is necessary to evaluate the stray load losses in eh-star method by post-processing of the measured data. Depending on the nature of the auxiliary impedance - purely resistive or complex - different methods A, A1, B and C are presented, which yield identical results for ideal *ohmic* resistance R_{eh}.

The decomposition of the current phasors into the real part (subscript: *r*) and the imaginary part (subscript: *i*) from the measured phase currents depends on the measured input power and on the decomposed voltages. So the real and imaginary part of the three phase currents can be calculated by different methods:

1. Method A is acc. to the new edition of the standard IEC 60034-2 [IEC 60034-2 draft]. It is based on the measured motor input power $P_{e,in}$ and the power losses P_{eh} within the resistance R_{eh} for carrying out the loss separation (see Figure 3.5). This method is useful in case of resistive $\underline{Z}_{eh} = R_{eh}$ and slightly resistive-inductive or resistive-capacitive impedance $\underline{Z}_{eh} = Z_{eh}\cdot\mathrm{e}^{j\varphi_{eh}}$ with a phase angle $-10° \leq \varphi_{eh} \leq 10°$.

2. <u>Method A1</u>, where the voltage and the current in the resistance R_{eh} are assumed to be in phase $\varphi_{eh} = 0°$ (or $\varphi_{eh} = 180°$, when choosing opposite voltage and current reference arrows). So the measurement of the input power $P_{e,in}$ is not necessary, but a purely *ohmic* auxiliary resistance R_{eh} should be used.

The value of the resistance $R_{eh} = \text{Re}\{\underline{Z}_{eh}\}$ has to be determined as average value of the measured resistance at the beginning, $R_{eh,begin}$, and at the end, $R_{eh,end}$, of the measurement to take the increase of the resistance R_{eh} due to thermal influence of the current flow into account. The auxiliary resistance R_{eh} should therefore be chosen with sufficient thermal rating, so that it is not much influenced thermally by the current flow during the test.

3. *Method B* may be applied with *ohmic*-inductive or the *ohmic*-capacitive impedance $\underline{Z}_{eh}$. The **two** line-to-line motor input power values P_{e,in_UV} and P_{e,in_WV} measured independently in *Aron*-circuit are needed (see Figure 3.5). For the evaluation of the stray load losses no information about the nature of the impedance $\underline{Z}_{eh}$ (inductor, capacitor or resistor) is necessary. The impedance value $\underline{Z}_{eh}$ does not influences numerically the calculation result.

4. *Method C* is very similar to method B, but instead of the **two** line-to-line motor input power values P_{e,in_UV} and P_{e,in_WV} measured independently in *Aron*-circuit only the measured total motor input power $P_{e,in}$ ($= P_{e,in\_UV} + P_{e,in\_WV}$) is needed.

From the calculated real and imaginary parts of the voltages and currents the positive and negative sequence air gap power $P_{\delta,1}$ and $P_{\delta,2}$ are calculated to evaluate the stray load losses P_{ad}. From that the check input power P_{cont} can be recalculated in order to check it with the measured input power $P_{e,in}$. The calculated - control - input power P_{cont} is a good indicator for the accuracy of the calculation model for the loss balance, including $\underline{Z}_{eh}$, and of the measurement. The calculated check power P_{cont} should not deviate from the measured input power $P_{e,in}$ by more than 1 %. Otherwise it indicates that the calculation model is

not representing the reality, e.g. that the determined phase angles of the voltages and the currents are not correct or the used auxiliary impedance $\underline{Z}_{eh}$ is highly resistive-inductive or highly resistive-capacitive.
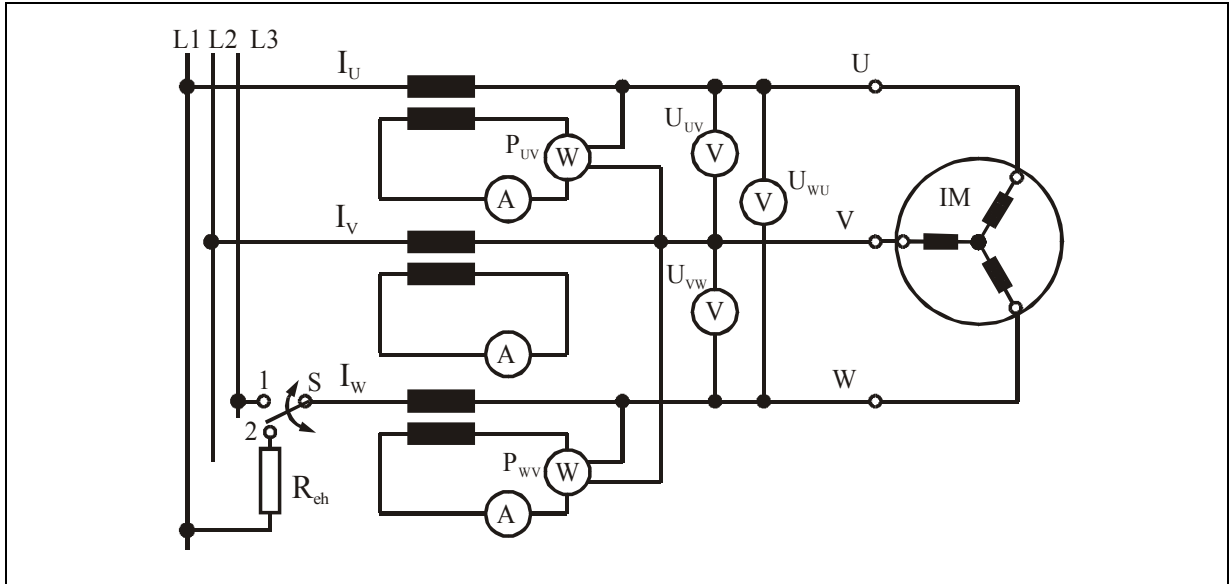
Figure 3.5: Eh-star measurement circuit with uncoupled induction machine (IM)

3.2.1 Decomposition of voltages into real and imaginary parts

The decomposition of the voltage phasors into the real part (subscript: r) and the imaginary part (subscript: i) from the measured r.m.s. voltages is independent of the measured input power (see (3.22)…(3.25)). The input variables are the measured line-to-line voltages (Figure 3.5) U_{UV}, U_{VW}, U_{WU}. The unknowns are the real parts $U_{UV,r}$, $U_{VW,r}$, $U_{WU,r}$ and the imaginary parts $U_{UV,i}$, $U_{VW,i}$, $U_{WU,i}$. We choose the line-to-line voltage U_{UV} to be real (3.21). The unknowns are determined by solving the system of the equations (3.16)…(3.21).

$$U_{UV}^2 = U_{UV,r}^2 + U_{UV,i}^2 \tag{3.16}$$

$$U_{VW}^2 = U_{VW,r}^2 + U_{VW,i}^2 \tag{3.17}$$

$$U_{WU}^2 = U_{WU,r}^2 + U_{WU,i}^2 \tag{3.18}$$

$$U_{UV,r} + U_{VW,r} + U_{WU,r} = 0 \tag{3.19}$$

$$U_{UV,i} + U_{VW,i} + U_{WU,i} = 0 \tag{3.20}$$

$$U_{UV,r} = U_{UV} \; ; \; (U_{UV,i} = 0). \tag{3.21}$$

From the set of the six equations (3.16)…(3.21) we determine the unknowns with the solutions (3.22)…(3.25). The U-W-V voltage system (anti-clockwise) is chosen, therefore the voltage $U_{WU,i}$ in (3.23) is positive.

$$U_{WU,r} = \frac{U_{VW}^2 - U_{WU}^2 - U_{UV}^2}{2 \cdot U_{UV}} \tag{3.22}$$

$$U_{WU,i} = \pm\sqrt{U_{WU}^2 - U_{WU,r}^2} = \sqrt{U_{WU}^2 - U_{WU,r}^2} \tag{3.23}$$

$$U_{VW,r} = -U_{UV,r} - U_{WU,r} \tag{3.24}$$

$$U_{VW,i} = -U_{WU,i}. \tag{3.25}$$

Note:

The U-V-W voltage system leads to other algorithms in the post-processing for the stray load losses.

3.2.2 Decomposition of currents into real and imaginary parts

The decomposition of the phase currents into the real and the imaginary parts depends on the measured input power and on the decomposed voltages. So the real and imaginary part of the three phase currents $I_{U,r}$, $I_{V,r}$, $I_{W,r}$, $I_{U,i}$, $I_{V,i}$, $I_{W,i}$ as six unknowns can be calculated by the different methods A, A1, B and C. For the six unknown currents only five equations (3.26)…(3.30) are given, so a 6th equation - depending on the used method - is necessary to solve the system of the equations.

For the star-connection, where the star point is not connected, the following equations for the currents are given:

$$I_U^2 = I_{U,r}^2 + I_{U,i}^2 \tag{3.26}$$

$$I_V^2 = I_{V,r}^2 + I_{V,i}^2 \tag{3.27}$$

$$I_W^2 = I_{W,r}^2 + I_{W,i}^2 \tag{3.28}$$

$$I_{U,r} + I_{V,r} + I_{W,r} = 0 \tag{3.29}$$

$$I_{U,i} + I_{V,i} + I_{W,i} = 0. \tag{3.30}$$

Note:

The solutions of the currents are chosen so that the current $\underline{I}_{Grid} = -\underline{I}_V$ lags behind the voltage $\underline{U}_{UV} = \underline{U}_{Grid}$ (Figure 3.6) and the currents I_1 of the positive and I_2 of the negative sequence system lag behind the voltages U_1 of the positive and U_2 of the negative sequence system (resistive-inductive behaviour).
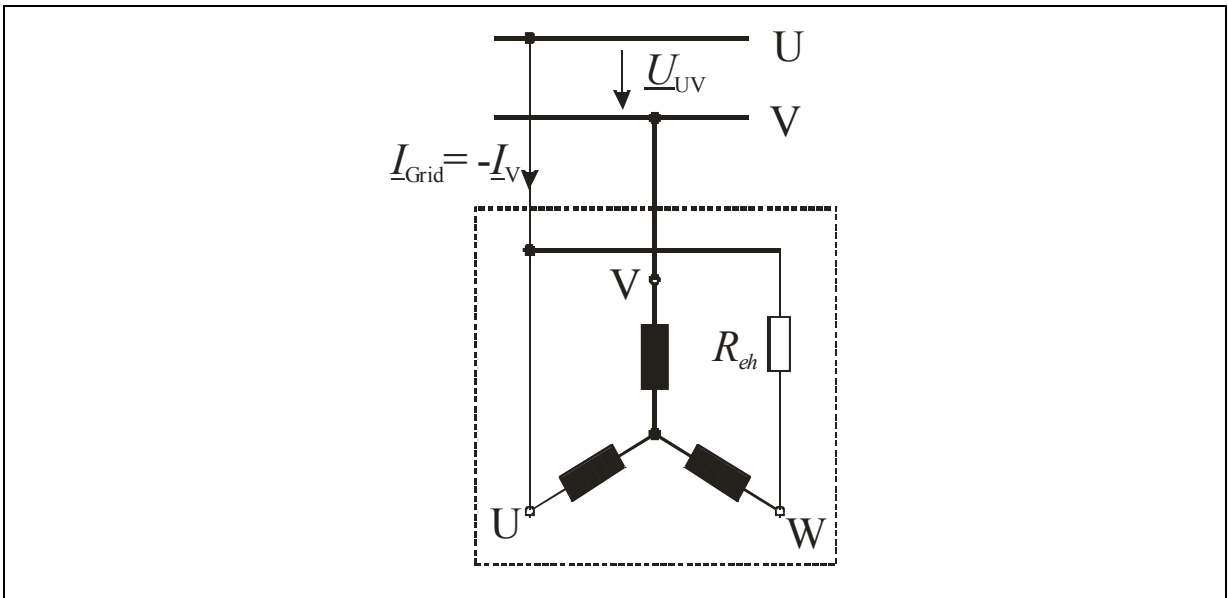
Figure 3.6: Simplified eh-star circuit

The active power P_{Grid} is calculated from the circuit in Figure 3.6 as the sum

of the motor input power $P_{e,in}$ and the power loss P_{eh} within the auxiliary resistance R_{eh}:

$$P_{Grid} = P_{eh} + P_{e,in} = \text{Re}\{\underline{U}_{UV} \cdot \underline{I}_{Grid}^*\}. \tag{3.31}$$

With the current $\underline{I}_{Grid} = -\underline{I}_V$ and the voltage $\underline{U}_{UV} = U_{UV,r}$, $(U_{UV,i} = 0)$ the current $I_{V,r}$ is derived as:

$$P_{Grid} = P_{eh} + P_{e,in} = -\text{Re}\{\underline{U}_{UV} \cdot \underline{I}_V^*\} = -U_{UV,r} \cdot I_{V,r} \tag{3.32}$$

$$I_{V,r} = -(P_{eh} + P_{e,in})/U_{UV,r}. \tag{3.33}$$

Note:

There is more than one way (algorithm) to solve the set of the current equations (3.26)…(3.30) depending on which current is firstly derived see e.g. (3.36) and (3.57). So one solution only is presented in the following.

3.2.2.1 Method A

Method A uses the measured motor input power $P_{e,in}$ and the power loss P_{eh} within the auxiliary resistance R_{eh}. From the set of six equations (3.26)…(3.34) the six current components are derived:

$$I_{V,r} = \frac{-(P_{e,in} + P_{eh})}{U_{UV}} \tag{3.34}$$

$$I_{V,i} = \sqrt{I_V^2 - I_{V,r}^2} \tag{3.35}$$

$$I_{U,r} = \frac{(I_W^2 - I_U^2 - I_V^2) \cdot I_{V,r}}{2 \cdot I_V^2} +$$

$$+ \sqrt{\frac{(I_W^2 - I_U^2 - I_V^2)^2 \cdot I_{V,r}^2}{4 \cdot I_V^4} - \frac{(I_W^2 - I_U^2 - I_V^2)^2 - 4 \cdot I_{V,i}^2 \cdot I_U^2}{4 \cdot I_V^2}} \tag{3.36}$$

$$I_{U,i} = \frac{\left(I_W^2 - I_U^2 - I_V^2\right) - 2 \cdot I_{U,r} \cdot I_{V,r}}{2 \cdot I_{V,i}} \tag{3.37}$$

$$I_{W,r} = -I_{U,r} - I_{V,r} \tag{3.38}$$

$$I_{W,i} = -I_{U,i} - I_{V,i}. \tag{3.39}$$

3.2.2.2 Method A1

As the auxiliary impedance $\underline{Z}_{eh}$ is assumed to be purely *ohmic*, we choose the complex voltage phasor at the resistance R_{eh} acc. to the chosen arrow reference system as:

$$-\underline{U}_{WU} = R_{eh} \cdot \underline{I}_W. \tag{3.40}$$

The solution of the six unknown current components is determined by (3.26)…(3.30), (3.40) as:

$$I_{W,r} = -U_{WU,r} / R_{eh} \tag{3.41}$$

$$I_{W,i} = -U_{WU,i} / R_{eh} \tag{3.42}$$

$$I_{V,r} = \frac{(I_U^2 - I_W^2 - I_V^2) \cdot I_{W,r}}{2 \cdot I_W^2} - \\ \sqrt{\frac{(I_U^2 - I_W^2 - I_V^2)^2 \cdot I_{W,r}^2}{4 \cdot I_W^4} - \frac{(I_U^2 - I_W^2 - I_V^2)^2 - 4 \cdot I_{W,i}^2 \cdot I_V^2}{4 \cdot I_W^2}} \tag{3.43}$$

$$I_{V,i} = \frac{(I_U^2 - I_W^2 - I_V^2) - 2 \cdot I_{W,r} \cdot I_{V,r}}{2 \cdot I_{W,i}} \tag{3.44}$$

$$I_{U,r} = -I_{V,r} - I_{W,r} \tag{3.45}$$

$$I_{\mathrm{U,i}} = -I_{\mathrm{V,i}} - I_{\mathrm{W,i}}.$$

(3.46)

3.2.2.3   Method B

Method B uses the independently measured **two** line-to-line motor input power values $P_{\mathrm{e,in\_UV}}$ and $P_{\mathrm{e,in\_WV}}$ without any information about the value and the losses of the impedance $\underline{Z}_{\mathrm{eh}}$. The power is measured in *Aron*-circuit with phase *V* as common phase (Figure 3.5):

$$P_{\mathrm{e,in\_U}V} = U_{\mathrm{UV,r}} \cdot I_{\mathrm{U,r}} + U_{\mathrm{UV,i}} \cdot I_{\mathrm{U,i}} = U_{\mathrm{UV,r}} \cdot I_{\mathrm{U,r}}$$

(3.47)

$$P_{\mathrm{e,in\_WV}} = -U_{\mathrm{VW,r}} \cdot I_{\mathrm{W,r}} - U_{\mathrm{VW,i}} \cdot I_{\mathrm{W,i}}.$$

(3.48)

From (3.47) the current $I_{\mathrm{U,r}}$ is derived:

$$I_{\mathrm{U,r}} = P_{\mathrm{e,in\_UV}} / U_{\mathrm{UV,r}}.$$

(3.49)

From (3.48), (3.28) and (3.17) the current $I_{\mathrm{W,r}}$ is derived:

$$I_{\mathrm{W,r}} = \frac{-P_{\mathrm{e,in\_WV}} \cdot U_{\mathrm{VW,r}}}{U_{\mathrm{VW}}^2} + \sqrt{\frac{P_{\mathrm{e,in\_WV}}^2 \cdot U_{\mathrm{VW,r}}^2}{U_{\mathrm{VW}}^4} - \frac{P_{\mathrm{e,in\_WV}}^2 - U_{\mathrm{VW,i}}^2 \cdot I_{\mathrm{W}}^2}{U_{\mathrm{VW}}^2}}$$

(3.50)

$$I_{\mathrm{W,i}} = (-P_{\mathrm{e,in\_WV}} - U_{\mathrm{VW,r}} \cdot I_{\mathrm{W,r}}) / U_{\mathrm{VW,i}}$$

(3.51)

$$I_{\mathrm{U,i}} = \left((I_{\mathrm{V}}^2 - I_{\mathrm{W}}^2 - I_{\mathrm{U}}^2) - 2 \cdot I_{\mathrm{W,r}} \cdot I_{\mathrm{U,r}} \right) / (2 \cdot I_{\mathrm{W,i}}).$$

(3.52)

In method B one equation more than unknown parameters exists. To fulfil (3.29) and (3.30) the „the sum of currents is zero" condition. The currents $I_{\mathrm{V,r}}$ and $I_{\mathrm{V,i}}$ are determined as:

$$I_{\mathrm{V,r}} = -I_{\mathrm{U,r}} - I_{\mathrm{W,r}}$$

(3.53)

$$I_{V,i} = -I_{U,i} - I_{W,i}.$$ (3.54)

The conditions (3.26) and (3.27) are not used here, so the calculated results of the phase currents I_U and I_V may differ slightly from the measured values I_U and I_V.

3.2.2.4   Method C

For method C the measured total motor input power $P_{e,in}$ is used, without any information about the value and losses of the impedance $\underline{Z}_{eh}$. The measured total motor input power $P_{e,in}$ is given as:

$$\begin{aligned}P_{e,in} &= P_{e,in\_UV} + P_{e,in\_WV} \\ &= U_{UV,r} \cdot I_{U,r} + U_{UV,i} \cdot I_{U,i} - U_{VW,r} \cdot I_{W,r} - U_{VW,i} \cdot I_{W,i}\end{aligned}$$ (3.55)

With (3.21) and (3.28) we write (3.55) as:

$$(P_{e,in} - U_{UV} \cdot I_{U,r} + U_{VW,r} \cdot I_{W,r})^2 - U_{VW,i}^2 \cdot (I_W^2 - I_{W,r}^2) = 0.$$ (3.56)

In equation (3.56) the currents $I_{U,r}$ and $I_{W,r}$ are unknown. From the set of equations (3.26)…(3.30) the current $I_{U,r}$ is determined:

$$\begin{aligned}I_{U,r} = \;&\frac{(I_V^2 - I_W^2 - I_U^2) \cdot I_{W,r}}{2 \cdot I_W^2} + \\ &+ \sqrt{\frac{(I_V^2 - I_W^2 - I_U^2)^2 \cdot I_{W,r}^2}{4 \cdot I_W^4} - \frac{(I_V^2 - I_W^2 - I_U^2)^2 - 4 \cdot I_U^2 \cdot (I_W^2 - I_{W,r}^2)}{4 \cdot I_W^2}}\end{aligned}$$ (3.57)

With (3.57) and the abbreviation $b = (I_V^2 - I_W^2 - I_U^2)$ the equation (3.56) is rewritten as:

$$\begin{aligned}&\left[P_{e,in} - U_{UV} \cdot \left(\frac{b \cdot I_{W,r}}{2 \cdot I_W^2} + \sqrt{\frac{b^2 \cdot I_{W,r}^2}{4 \cdot I_W^4} - \frac{b^2 - 4 \cdot I_U^2 \cdot (I_W^2 - I_{W,r}^2)}{4 \cdot I_W^2}}\right) + U_{VW,r} \cdot I_{W,r}\right]^2 + \\ &- U_{VW,i}^2 \cdot (I_W^2 - I_{W,r}^2) = 0\end{aligned}$$ (3.58)

In equation (3.58) only the current $I_{W,r}$ is unknown and it may be solved e.g. by Matlab or Maple...

The current $I_{W,i}$ is then calculated as:

$$I_{W,i} = -\sqrt{I_W^2 - I_{W,r}^2} \, . \tag{3.59}$$

Using (3.52), (3.53), (3.54) the currents $I_{U,i}$, $I_{V,r}$, $I_{V,i}$ are calculated.

The equation (3.58) can be written as 4th order polynomial (3.60). The equation (3.60) can be solved e.g. by Matlab or Maple or by iteration with the *Durand-Kerner* method [see Appendix: *Durand-Kerner*]

$$a_4 \cdot I_{W,r}^4 + a_3 \cdot I_{W,r}^3 + a_2 \cdot I_{W,r}^2 + a_1 \cdot I_{W,r} + a_0 = 0 \, . \tag{3.60}$$

The coefficients $a_4 \ldots a_0$ have then to be determined from the known parameters in the following (without derivation).

$$
\begin{aligned}
a_4 &= g^2 - n \cdot m^2 \\
a_3 &= 2 \cdot g \cdot h + 4 \cdot U_{UV} \cdot P_{e,in} \cdot n \cdot m \\
a_2 &= h^2 + 2 \cdot f \cdot g - m^2 \cdot c - 4 \cdot U_{UV}^2 \cdot P_{e,in}^2 \cdot n \\
a_1 &= 2 \cdot f \cdot h + 4 \cdot U_{UV} \cdot P_{e,in} \cdot c \cdot m \\
a_0 &= f^2 - 4 \cdot U_{UV}^2 \cdot P_{e,in}^2 \cdot c \, .
\end{aligned}
\tag{3.61}
$$

With the following abbreviations:

$$
\begin{aligned}
a &= (I_V^2 - I_W^2 - I_U^2)/(2 \cdot I_W^2) \\
b &= (I_V^2 - I_W^2 - I_U^2) \\
c &= (4 \cdot I_U^2 \cdot I_W^2 - b^2)/(4 \cdot I_W^2) \\
d &= I_U^2 / I_W^2 \\
e &= U_{UV}^2 \cdot (2 \cdot a - d) \\
f &= P_{e,in}^2 - U_{VW,i}^2 \cdot I_W^2 + U_{UV}^2 \cdot c
\end{aligned}
\tag{3.62}
$$

$$g = e + U_{\mathrm{VW}}^2 - 2 \cdot U_{\mathrm{UV}} \cdot U_{\mathrm{VW,r}} \cdot a$$

$$h = 2 \cdot P_{\mathrm{e,in}} \cdot U_{\mathrm{VW,r}} - 2 \cdot U_{\mathrm{UV}} \cdot P_{\mathrm{e,in}} \cdot a$$

$$m = 2 \cdot a \cdot U_{\mathrm{UV}}^2 - 2 \cdot U_{\mathrm{UV}} \cdot U_{\mathrm{VW,r}}$$

$$n = a^2 - d \; .$$

With the determined real and imaginary parts of the complex phasors of the three-phase voltages and currents from measured r.m.s. values, the air gap power $P_{\delta,1}$ of the positive and $P_{\delta,2}$ of the negative sequence system and therefore the additional losses P_{ad} will be calculated. The detailed calculation is shown in the following section.

3.3 Determination of stray load losses

The determination of the stray load losses must be done from the measured losses by decomposition into the positive and negative sequence losses. The negative sequence losses at the slip $2 - s \cong 2$ correspond to the stray load losses, similar to the standardised reverse rotation test. For this evaluation, the phase angles of the measured currents and voltages must be known. This can be done by the calculation with the previously presented methods.

Figure 3.7 gives an overview on the post-processing algorithms for the eh-star method. In Figure 3.7 the indication "*Ohmic* R_{eh}" corresponds to $\underline{Z}_{\mathrm{eh}} = Z_{\mathrm{eh}} \cdot \mathrm{e}^{\mathrm{j}\varphi_{\mathrm{eh}}}$ with a phase angle $-10° \leq \varphi_{\mathrm{eh}} \leq 10°$ and the indication "purely *ohmic* R_{eh}" corresponds to $\varphi_{\mathrm{eh}} = 0°$ (see chapter 3.2).
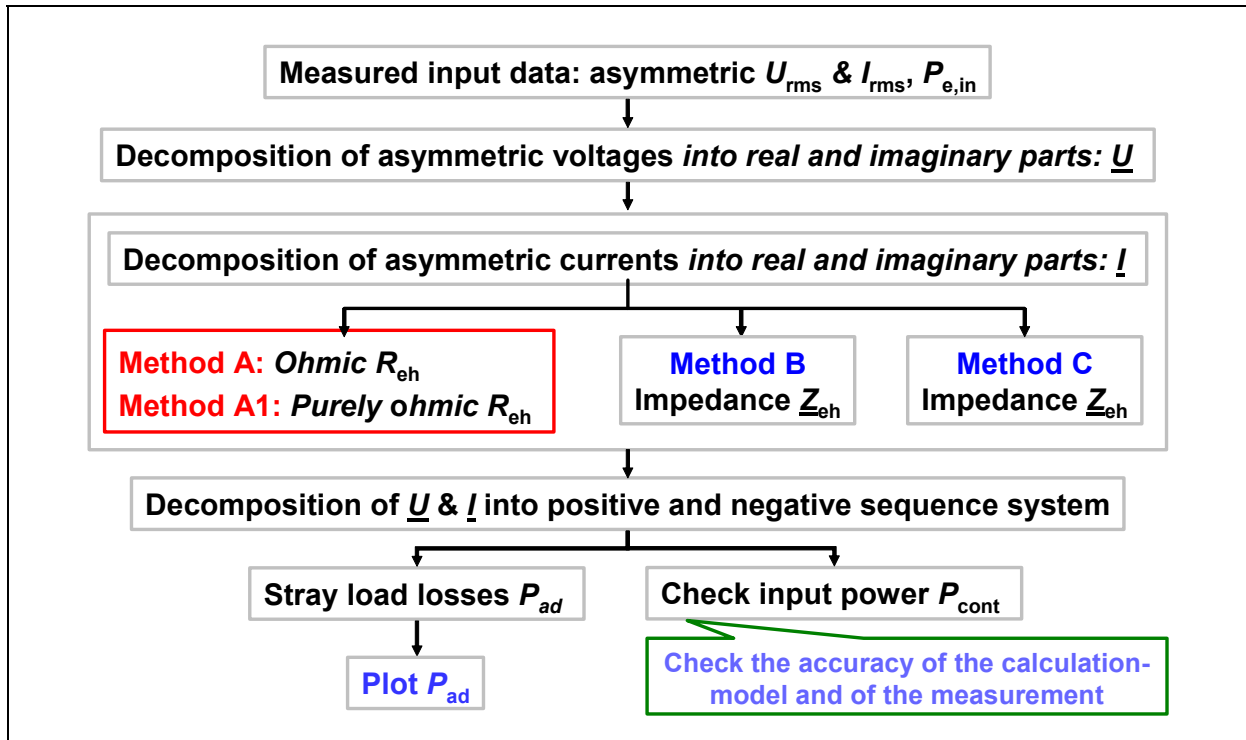
Figure 3.7: Overview on the post-processing in eh-star method

To determine the additional losses P_{ad} of the asymmetrically fed induction machine, the equivalent circuit of the induction machine (Figure 3.8) for the positive and negative sequence system is used.
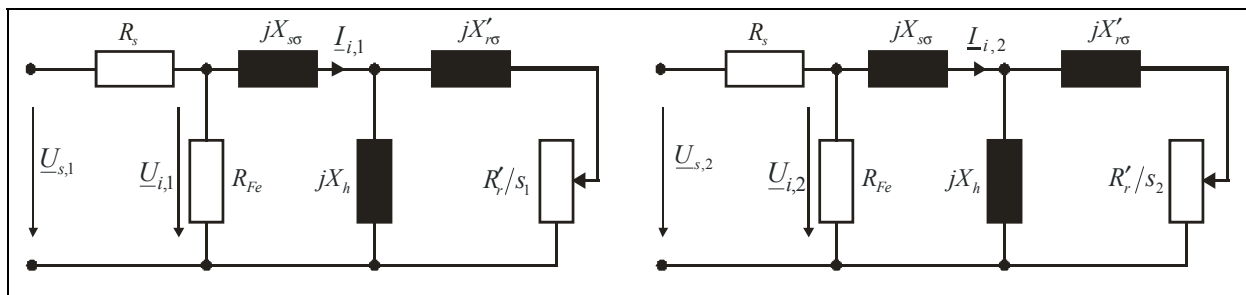
Figure 3.8: T-equivalent circuit of the induction machine with consideration of iron losses for the positive and negative sequence system

The inner line-to-line voltages $\underline{U}_i$ across the equivalent iron resistance R_{Fe} are determined by the voltage drop at the stator resistance R_s from the complex line-to-line voltages and currents:

$$\underline{U}_{\text{iUV}} = \underline{U}_{\text{UV}} + R_{\text{s}} \cdot (\underline{I}_{\text{V}} - \underline{I}_{\text{U}}) \tag{3.63}$$

$$\underline{U}_{\text{iVW}} = \underline{U}_{\text{VW}} + R_{\text{s}} \cdot (\underline{I}_{\text{W}} - \underline{I}_{\text{V}}) \tag{3.64}$$

$$\underline{U}_{\text{iWU}} = \underline{U}_{\text{WU}} + R_{\text{s}} \cdot (\underline{I}_{\text{U}} - \underline{I}_{\text{W}}). \tag{3.65}$$

The zero-sequence system of currents is zero, as the star-point is not connected to earth. The separation into the positive $\underline{U}_{\text{iLL},1}$ and negative $\underline{U}_{\text{iLL},2}$ sequence components of the inner line-to-line voltage is necessary due to the asymmetric voltage system:

$$\underline{U}_{\text{iLL},1} = (1/3) \cdot (\underline{U}_{\text{iUV}} + \underline{a} \cdot \underline{U}_{\text{iVW}} + \underline{a}^2 \cdot \underline{U}_{\text{iWU}}) \tag{3.66}$$

$$\underline{U}_{\text{iLL},2} = (1/3) \cdot (\underline{U}_{\text{iUV}} + \underline{a}^2 \cdot \underline{U}_{\text{iVW}} + \underline{a} \cdot \underline{U}_{\text{iWU}}) \tag{3.67}$$

where $\underline{a}$ is the phase shifter by $120°$: $\underline{a} = \text{e}^{\text{j}2\pi/3}$.

Using the positive $\underline{U}_{\text{i},1}$ and negative $\underline{U}_{\text{i},2}$ sequence components of the inner phase voltage $\underline{U}_{\text{i}}$

$$\underline{U}_{\text{i},1} = \text{e}^{-\text{j}\pi/6} \cdot \underline{U}_{\text{iLL},1} / \sqrt{3} \tag{3.68}$$

$$\underline{U}_{\text{i},2} = \text{e}^{\text{j}\pi/6} \cdot \underline{U}_{\text{iLL},2} / \sqrt{3}, \tag{3.69}$$

we determine the asymmetrical inner phase voltages:

$$\underline{U}_{\text{iU}} = \underline{U}_{\text{i},1} + \underline{U}_{\text{i},2} \tag{3.70}$$

$$\underline{U}_{\text{iV}} = \underline{a}^2 \cdot \underline{U}_{\text{i},1} + \underline{a} \cdot \underline{U}_{\text{i},2} \tag{3.71}$$

$$\underline{U}_{\text{iW}} = \underline{a} \cdot \underline{U}_{\text{i},1} + \underline{a}^2 \cdot \underline{U}_{\text{i},2} \tag{3.72}$$

and the inner phase currents "behind" the iron resistance R_{Fe}:

$$\underline{I}_{\text{iU}} = \underline{I}_{\text{U}} - \underline{U}_{\text{iU}} / R_{\text{Fe}} \tag{3.73}$$

$$\underline{I}_{iV} = \underline{I}_V - \underline{U}_{iV} / R_{Fe} \tag{3.74}$$

$$\underline{I}_{iW} = \underline{I}_W - \underline{U}_{iW} / R_{Fe} . \tag{3.75}$$

The positive $\underline{I}_{i,1}$ and negative $\underline{I}_{i,2}$ sequence components of the inner phase currents are:

$$\underline{I}_{i,1} = (\underline{I}_{iU} + \underline{a} \cdot \underline{I}_{iV} + \underline{a}^2 \cdot \underline{I}_{iW}) / 3 \tag{3.76}$$

$$\underline{I}_{i,2} = (\underline{I}_{iU} + \underline{a}^2 \cdot \underline{I}_{iV} + \underline{a} \cdot \underline{I}_{iW}) / 3 . \tag{3.77}$$

With the equations (3.68), (3.69), (3.76) and (3.77) the air gap power of the positive and the negative sequence system $P_{\delta,1}$ and $P_{\delta,2}$ is given as:

$$P_{\delta,1} = 3 \cdot \mathrm{Re}\{\underline{U}_{i,1} \cdot \underline{I}_{i,1}^*\} = P_{e,in,1} - P_{Cu,s,1} - P_{Fe,1} \tag{3.78}$$

$$P_{\delta,2} = 3 \cdot \mathrm{Re}\{\underline{U}_{i,2} \cdot \underline{I}_{i,2}^*\} = P_{e,in,2} - P_{Cu,s,2} - P_{Fe,2} . \tag{3.79}$$

The air gap power $P_{\delta,1}$ of the positive and $P_{\delta,2}$ of the negative sequence system are calculated from the corresponding positive and negative power components $P_{e,in,1}$ and $P_{e,in,2}$ by subtracting the stator copper losses $P_{Cu,s}$ and the iron losses P_{Fe}. The iron losses P_{Fe} we get from the prior no-load test.

Hence the stray load losses $P_{ad,asym}$ of the asymmetrically fed machine - as the sum of the additional losses of the positive $P_{ad,1}$ and the negative $P_{ad,2}$ sequence system - are given by the power balance (3.80). The output power is zero, because the motor is not coupled to a mechanical load. Only the friction and windage losses P_{fw} and the additional losses $P_{ad,asym}$ are loading or braking the machine.

$$P_{ad,asym} = P_{ad,1} + P_{ad,2} = (1-s) \cdot (P_{\delta,1} - P_{\delta,2}) - P_{fw} . \tag{3.80}$$

In the linear range of the torque-slip-characteristic between the no-load ($s = 0$) and typically twice rated slip ($2 \cdot s_N$) the torque M is proportional to the

slip s and proportional to the rotor current (load current) I_r' (Figure 3.9). For the asymmetrically fed machine (uncoupled machine) the rotor current I_r' may be taken as equivalent of the torque M, which ranges between $0 \le I_r' \le I_{rN}'$ for $0 \le M \le M_N$. The negative sequence current component $I_{i,2}$ at slip $s \cong 2$ corresponds to the rotor current $\underline{I}_r' \cong -\underline{I}_{i,2}$. So the negative sequence system represents the equivalent motor load of the uncoupled machine: $I_{i,2} \approx I_r' \sim M$. Due to the dominating negative sequence current $I_{i,2} \gg I_{i,1}$ - like in the RRT - ($s_2 = 2 - s \approx 2$) the stray load losses of the negative sequence system $P_{ad,2}$ are taken as the equivalent stray load losses P_{ad}.
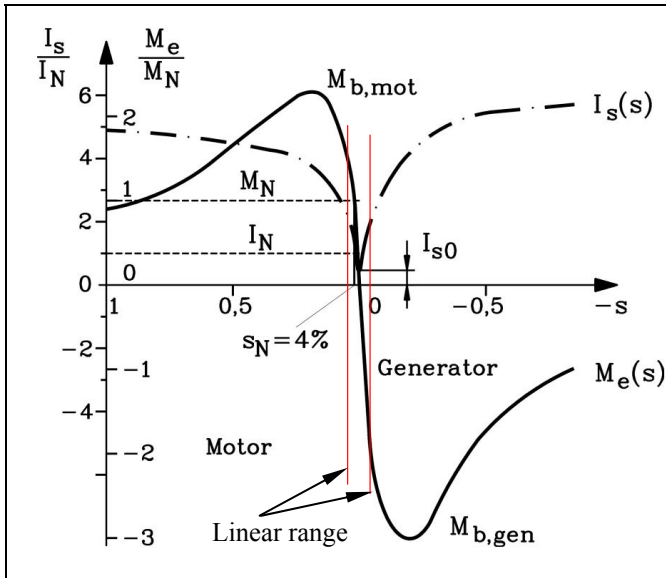
Figure 3.9: Torque-slip- and current-slip-characteristics of induction machine
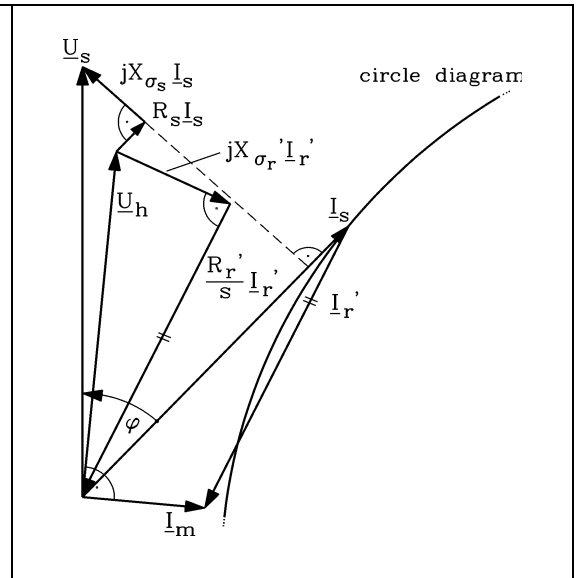
Figure 3.10: Phasor diagram of induction machine

Assuming that the stray load losses P_{ad} depend on the square of stator current [Rogo 1925, Morg 1939, Chal 1963] we get, with the relationships $P_{ad,2} \sim I_{i,2}^2$ and $P_{ad,1} \sim I_{i,1}^2$, the stray load losses:

$$P_{ad} = P_{ad,2} = P_{ad,asym} \cdot I_{i,2}^2 / (I_{i,1}^2 + I_{i,2}^2). \tag{3.81}$$

3.3.1 Plotting of the stray load losses

With the assumption of a right angle between the magnetizing current $\underline{I}_m$ and the rotor current $I_r^{'}$ in the phasor diagram of the induction machine for motor operation (Figure 3.10) the rated test current I_{tN} is determined from the rated current I_N and the no-load current I_0 as

$$I_{tN} = \sqrt{I_N^2 - I_0^2} \ . \tag{3.82}$$

As the rated torque is proportional to the rated rotor current $M_N \sim I_{rN}^{'}$, we get

$$I_{rN}^{'} \cong \sqrt{I_N^2 - I_0^2} = I_{tN} \ . \tag{3.83}$$

The stray load losses $P_{ad,2} = P_{ad}$ are plotted versus the square of the ratio of the negative sequence current $I_{i,2}$ related to the rated test current I_{tN} (Figure 3.11), which corresponds to the square of the per unit torque $(I_{i,2}/I_{tN})^2 \sim (M/M_N)^2$.

The stray load losses data shall be smoothed by using the linear regression analysis for 6 different test points to reduce the effect of random errors in the test measurements. The offset of the straight line has to be neglected - like in IEEE 112 Method B -, as at zero torque, which corresponds with zero load current and hence zero negative sequence current, the stray load losses shall be zero. The stray load losses for rated load $(I_{i,2}/I_{tN} = 1)$ are the slope of the regression-line (Figure 3.11).
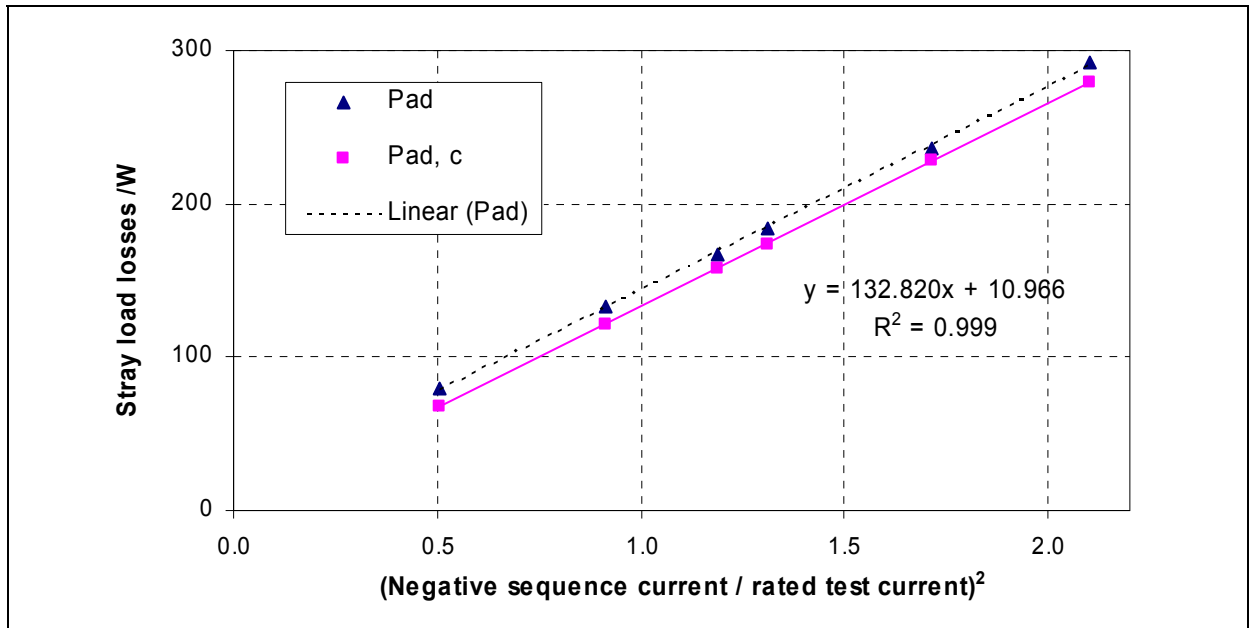
Figure 3.11: Measured stray load losses of a 11 kW 4-pole motor "A160-4"
(Subscript c for corrected: Linear regression line without offset)

Figure 3.11 shows an example of the measured values P_{ad} and the smoothed data $P_{ad,c}$ of the stray load losses without the offset for an 11 kW, 4-pole motor "A160-4". As the offset is omitted, the value on slope of the regression-line 132.8 W is the stray load loss at rated load.

3.3.2 Determination of the check input power

With the calculated positive and negative sequence air gap power $P_{\delta,1}$ and $P_{\delta,2}$, respectively, according to the power flow in the positive and the negative sequence system in Figure 3.12, the check input power P_{cont} can be determined in order to check it with the measured input power $P_{e,in}$.

$$
\begin{aligned}
P_{cont} &= (P_{\delta,1} + P_{\delta,2}) + P_{Fe} + P_{Cu,s} \\
&= (P_{\delta,1} + P_{\delta,2}) + (U_{iU}^2 + U_{iV}^2 + U_{iW}^2)/R_{Fe} + R_s \cdot (I_U^2 + I_V^2 + I_W^2)
\end{aligned}
\tag{3.84}
$$

The check input power P_{cont} as sum of the all loss components must be theoretically identical with the input power $P_{e,in}$, and should not deviate from the measured input power $P_{e,in}$ for a good test evaluation results by more than 1 %.

If not, it indicates, that the calculation model is not representing the reality, e.g. that the determined phase angles of the voltages and the currents are not correct or the used auxiliary impedance $\underline{Z}_{eh}$ is highly resistive-inductive or highly resistive-capacitive, or there is an error in the measurement setup.
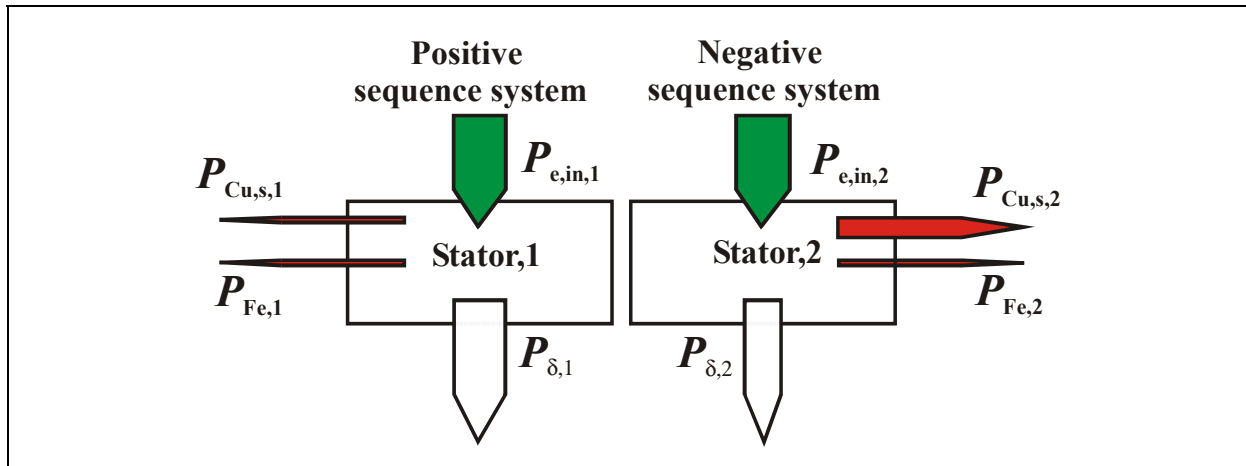
Figure 3.12: Power flow of the positive and the negative sequence system

3.4 Test procedure

The machine stator winding has to be connected in star. So the rated data of the machine are referred to the star connection. The star-point must not be connected to earth to avoid zero-sequence currents. The measurement setup of the eh-star test, where the induction motor is uncoupled, is shown in Figure 3.13.
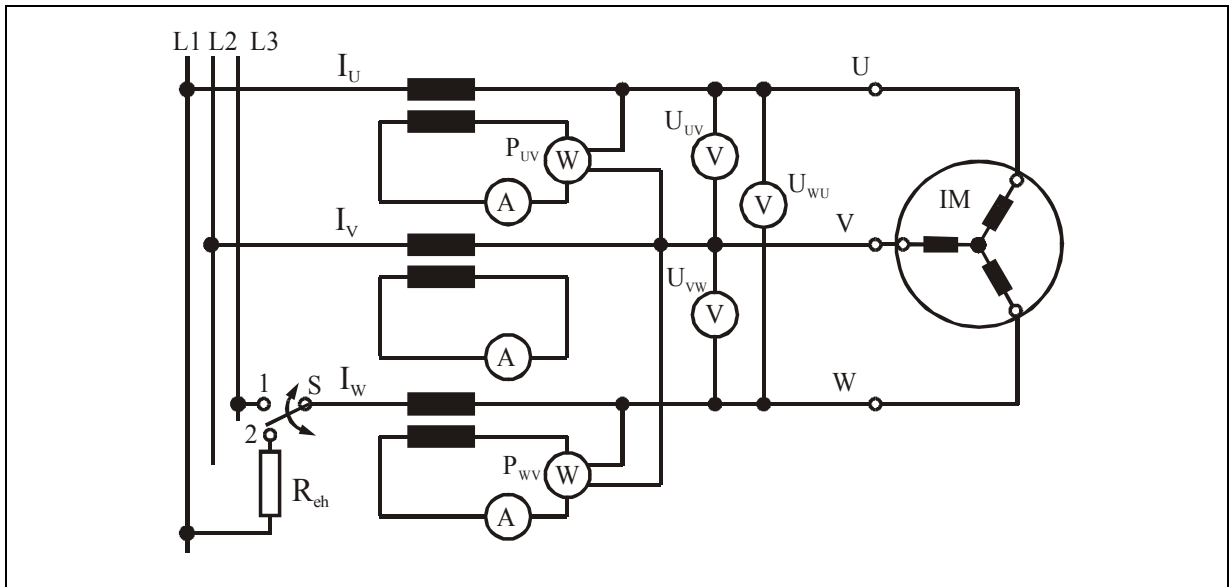
Figure 3.13: Eh-star measurement circuit

3.4.1 Requirements for the measurement

For the measurement following requirements are needed:

- A variable transformer (e.g. rotary transformer) capable to vary the supply voltage of the machine from typically 25 % to the rated phase voltage U_{Nph} and the supply current to 150 % rated phase current I_N of the machine. Such voltage supply is typically used for the no-load test as described in IEC 61972.

- The voltage waveform of the open circuit voltage supply shall comply with the demands of the harmonic voltage factor (HVF), defined in IEC 60034-1 [IEC 60034-1], clause 6.2.1.1 for the thermal test IEC 60034-1, cl. 7.3.1: HVF ≤ 0.015.

- An auxiliary resistor R_{eh}, capable of up to 150 % rated phase current I_N of the machine. The resistance should be about the short circuit impedance Z_{sc} of the motor, which is typically 20 % of the rated impedance, $R_{eh} = 0.2 \cdot U_{N,ph} / I_N$, and shall be adjusted, so that the positive sequence current I_1 stays below 30 % of the negative sequence current I_2 and the speed stays in the range of the typical motor speed near the rated speed. The

resistance R_{eh} should therefore be chosen with sufficient thermal rating, so that it is not much influenced thermally by the current flow during the test.

- A power switch S for larger motors. Smaller motors should usually start-up with the resistor R_{eh} already connected (switch S in position 2, see Figure 3.13). In this case the switch is not needed. But it depends on the motor design, some motors could not start-up with the resistor R_{eh} already connected !

- Measurement devices for the three line-to-line r.m.s. voltages U_{UV}, U_{VW}, U_{WU} at the motor terminals U, V, W.

- Measurement devices for the three phase r.m.s. currents I_U, I_V, I_W.

- Measurement devices to measure the electrical machine input power $P_{e,in}$ with *Aron-* circuit at the machine terminals "behind" the auxiliary resistor R_{eh}.

- Measurement device to measure the resistances.

- Measurement device to measure the speed.

The accuracy of the measurement devices shall comply with the demands for the load test and efficiency determination of the induction machines as described in IEC 61972.

Note:

It is not recommended to determine the winding temperature from the reading of thermocouples, due to the unequal heating of the three phases, if their positions are unknown (see Figure 3.40). Only if the positions of the thermocouples are exactly known, then the use of the thermocouples could be possible.

Note:

As the asymmetrically fed induction machines generate a pulsating torque component of double supply frequency, which is only filtered out by the rotor's inertia, bigger machines (e.g. above 500 Nm rated torque) might be put on rubber elements or a damping pad during the eh-star test to avoid

transmission of the vibrations from the machine into the surrounding adjacent test bed. But as the tested machine is operated at reduced supply voltage, the torque oscillation is small, so that usually damping pads may be not necessary even for bigger machines.

3.4.2 Measurement procedure

Before starting the eh-star test the uncoupled machine should have run already for certain time to get stable no-load losses. The no-load losses are considered stabilised when the no-load power input varies by 3 % or less, when measured at two successive 30 min intervals [IEC 61972].

1. According to the circuit in Figure 3.13 the line-to-line resistance R_{VW} at cold machine is measured to get the 20°C resistance value ($R_{VW,20°C}$).

2. The no-load losses should be stable at no-load in symmetric operation at rated voltage U_N and rated frequency. The temperature of the winding should be stable and is about the typical temperature of the motor at no-load. At the end of the no-load test the line-to-line resistance R_{VW} is measured. This resistance will be taken as the resistance $R_{VW,begin}$ before the beginning of the eh-star test; i.e. the next steps shall be carried out as quickly as possible.

3. The motor is started in star connection at no load in symmetric operation (switch S in position 1, see Figure 3.13) at reduced voltage (e.g. at 25 % … 40 % of the rated voltage U_N) up to about synchronous speed.

4. After start-up phase W is disconnected from the grid via the switch S (S in position 2, see Figure 3.13) and an auxiliary *ohmic* resistance R_{eh} is put between the phases U and W. Hence the motor is fed from the phases U and V with reduced voltage at rated frequency and is rotating at about the rated speed (single phase operation with auxiliary resistance: eh-star).

Note:

If the supply voltage is too low, the torque of the machine is too small. The machine will break down from the synchronous to very low speed and may overheat. With the above recommended voltage U_{UV} between the phases U

and V and the resistance value R_{eh} the machine will operate at line frequency with the speed in the range of the typical motor speed near the rated speed.

5. Due to the asymmetric feeding the three phase currents I_{U}, I_{V}, I_{W} are different, with typical values between 130 % ... 70 % of average value $I_{\text{av}} = (I_{\text{U}} + I_{\text{V}} + I_{\text{W}})/3$, see example in Table 3.1. The current I_{V} in phase V is the maximum and the current I_{W} in phase W is the smaller one. During the test the supply voltage $U_{\text{LL}} = U_{\text{UV}}$ shall vary for at least six test points. The test points shall be chosen to be approximately equally spaced between 150 % and 75 % of the rated phase current I_{N} measured in phase V (I_{V}). When starting the test one should begin with the highest current ($I_{\text{V}} = 1.5 \cdot I_{\text{N}}$) and proceed in descending order to the lowest current ($I_{\text{V}} = 0.75 \cdot I_{\text{N}}$) to limit the variation of the temperature.

6. For each test point the values of the three phase currents I_{U}, I_{V}, I_{W}, the three line-to-line voltages U_{UV}, U_{VW}, U_{WU}, the electrical motor input power $P_{\text{e,in}}$ and the speed n are measured, preferably simultaneously to get high accuracy.

7. At the end of the eh-star test the motor is switched off and the line-to-line resistance $R_{\text{VW,end}}$ is measured.

Note:

For evaluation of the stray load losses acc. to the method A or the method A1 (see section 3.2) the value of the auxiliary resistance R_{eh} is needed if an auxiliary impedance $\underline{Z}_{\text{eh}} = Z_{\text{eh}} \cdot e^{j\varphi_{\text{eh}}}$ is used. The value of the resistance $R_{\text{eh}} = \text{Re}\{\underline{Z}_{\text{eh}}\}$ has to be determined as average value of the measured resistance $R_{\text{eh,begin}}$ at the beginning and $R_{\text{eh,end}}$ at the end of the measurement to take the increase of the resistance R_{eh} due to thermal influence of the current flow during the test into account.

3.4.3 Example

The test object called "A160-4" is a four pole standard induction motor, frame size 160 mm, totally enclosed, fan cooled, 400 V Y, 50 Hz, 11 kW, 21.6 A.

From the rated data of the motor in star connection the value of the auxiliary resistance R_{eh} will be determined. With the phase voltage $U_{Nph} = U_N / \sqrt{3} = 400 / \sqrt{3} = 230.9 \text{ V}$ and the phase current $I_{Nph} = I_N = 21.6 \text{ A}$, the rated impedance Z_N of the motor is determined as $Z_N = U_{Nph}/I_{Nph} = 230.9/21.6 = 10.7$ Ohm. The value of the auxiliary resistance R_{eh} should be about the value of the short circuit impedance Z_{sc} of the motor: $R_{eh} = Z_{sc} = 0.2 \cdot Z_N = 2.1$ Ohm.

The measured data for the 6 test points during the eh-star test are given in Table 3.1. Figure 3.19 shows the phasor diagram of the measured unbalanced voltages and currents, corresponding to the first load point in Table 3.1. The corresponding phasor diagram of the positive and negative sequence system is presented in Figure 3.20.

	Test point	1	2	3	4	5	6
Line to line voltage	U_{UV} /V	152.48	140.23	125.01	120.12	107.16	82.7
Line to line voltage	U_{VW} /V	166.26	152.81	136.26	130.89	116.76	89.94
Line to line voltage	U_{WU} /V	47.49	42.82	37.33	35.56	30.95	22.3
Phase current	I_U /A	27.267	24.719	21.688	20.706	18.245	13.807
Phase current	I_V /A	32.549	29.452	25.787	24.609	21.661	16.397
Phase current	I_W /A	22.361	20.134	17.488	16.622	14.437	10.371
Input power	$P_{e,in}$ /W	2456.7	2050.5	1600	1469.4	1155.42	684.81
Speed	n /rpm	1467.5	1466.7	1466.4	1466.3	1465.3	1461.3
Line to line resistance at begin	$R_{VW, begin}$ /Ω	0.7375					
Line to line resistancat end	$R_{VW, end}$ /Ω	0.771					

Table 3.1: Measured data at the eh-star test for an 11 kW 4-pole motor "A160-4"

From the measured resistances $R_{VW,begin}$ at the beginning and $R_{VW,end}$ at the end of the test a linear interpolation between the first load point $I_V/I_N = 1.5$ and the fifth load point $I_V/I_N = 1.0$ is used to determine the stator winding temperature for the test points in between (see Table 3.3 and Figure 3.14), which is needed for the losses evaluation.
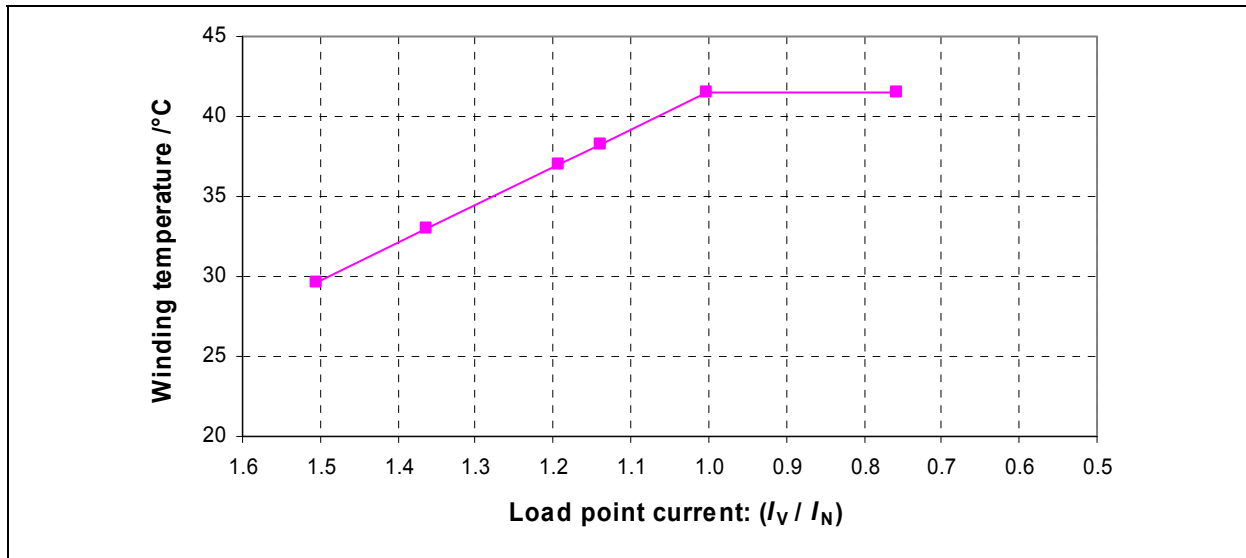
Figure 3.14: Linear interpolation of the winding temperature for an 11 kW 4-pole motor "A160-4"

In addition, for the evaluation of the stray load losses, the 20°C-value of the stator resistance $R_{s,20}$, the iron losses P_{FeN} and the no-load current I_0 at rated voltage, the friction and windage losses P_{fwN} at synchronous speed must be known from the no-load test according to IEC 61972 (see Table 3.2). To plot the stray load losses P_{ad} the rated test current $I_{tN} = \sqrt{I_N^2 - I_0^2}$ is determined acc. to (3.82) from the rated current I_N and the no-load current I_0.

Phase resistance at 20°C	Iron losses	Friction and windage losses	No-load current	Rated test current
$R_{s,20}$ /Ω	P_{FeN} /W	P_{fwN} /W	I_0 /A	I_{tN} /A
0.3623	312	71	10.9	18.6

Table 3.2: Measurement data from the no-load test for an 11 kW 4-pole motor "A160-4"

In Table 3.3 the positive and the negative sequence impedances , the ratio of the negative sequence current I_2 related to the rated test current I_{tN}, the ratio of the positive sequence current I_1 related to the negative sequence current I_2, which is smaller than 30 %, and the stray load losses P_{ad} are presented. The evaluation is done e.g. according to method A (see section 3.2).

Test point	1	2	3	4	5	6
Winding temperature /°C	30	33	37	38	42	42
I_2/I_{tN}	1.45	1.31	1.14	1.09	0.96	0.71
I_1/I_2	0.217	0.219	0.223	0.225	0.232	0.259
I_1 /A	5.88	5.37	4.77	4.59	4.14	3.45
I_2 /A	27.04	24.44	21.36	20.36	17.85	13.29
U_1 /V	63.85	58.46	51.86	49.73	44.11	33.48
U_2 /V	36.35	33.71	30.41	29.32	26.48	21.04
Z_1 /Ω	10.86	10.89	10.88	10.84	10.65	9.72
Z_2 /Ω	1.34	1.38	1.42	1.44	1.48	1.58
P_{ad} /W	292.8	236.2	184	167.5	133.7	79.6
$P_{ad,corrected}$ /W	278.9	227.9	174.1	158.1	121.6	67.3

Table 3.3: Eh-star loss evaluation acc. to method A for an 11 kW 4-pole motor "A160-4"

The impedances and the Voltage-Current-Curve of the positive and the negative sequence components are given in Figure 3.15 and Figure 3.16 for the measured example. The characteristics show that the negative sequence system is unsaturated, whereas the positive sequence system is slightly, but not significantly, saturated. A small negative sequence current I_2 reflects a higher negative sequence impedance Z_2.
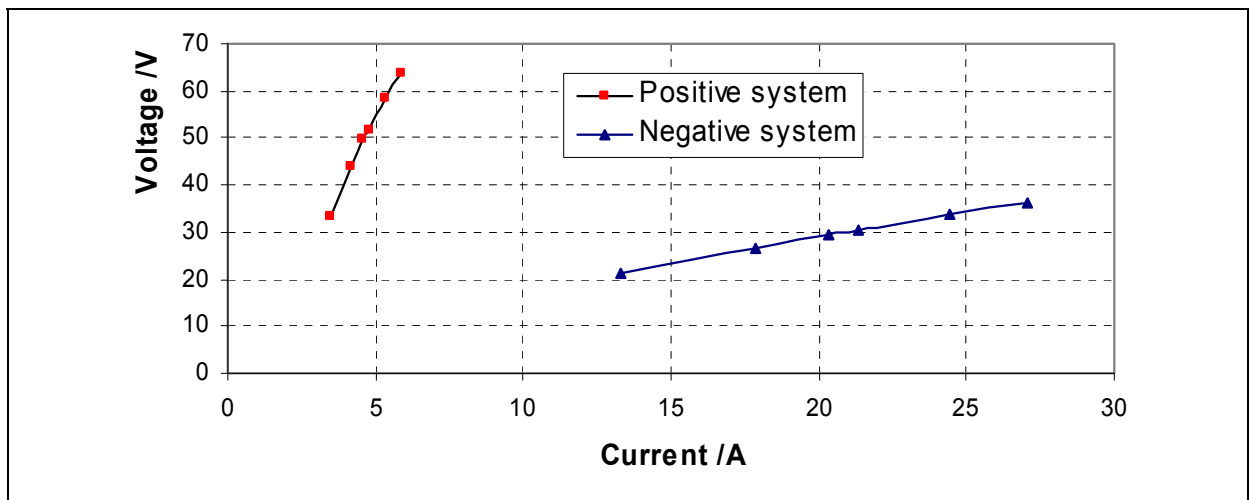
Figure 3.15: Voltage-Current-Characteristics of the positive and negative sequence system for an 11 kW 4-pole motor "A160-4"
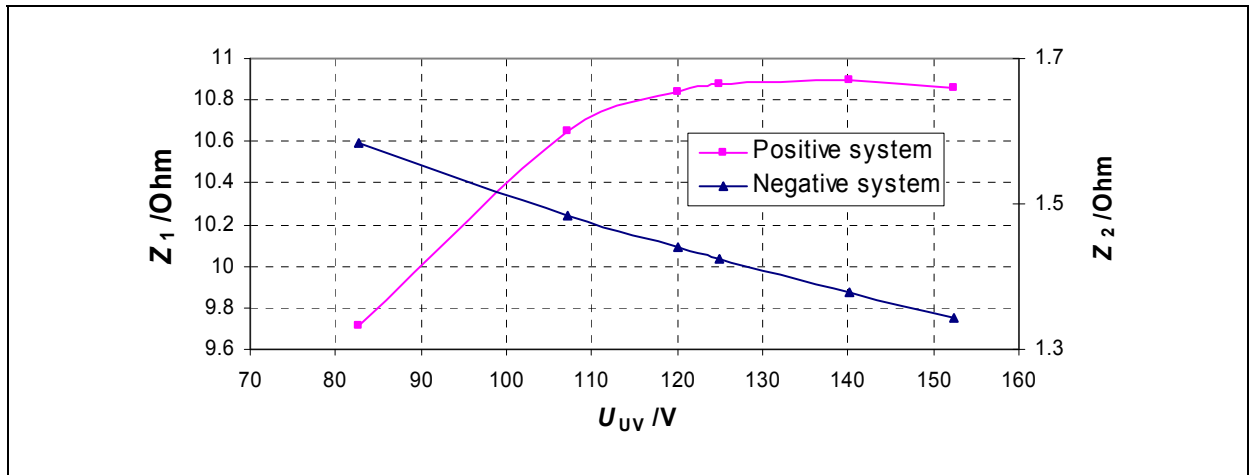
Figure 3.16: Impedances of the positive and negative sequence system as function of the
supply voltage U_{UV} for an 11 kW 4-pole motor "A160-4"

The stray load losses P_{ad} are plotted versus the square of the ratio of the negative sequence current I_2 related to the rated test current I_{tN}, which corresponds to the square of the per unit torque $(I_2/I_{tN})^2 \sim (M/M_N)^2$. The stray load losses data shall be smoothed (corrected) by using the linear regression analysis for the six test points to reduce the effect of random errors in the test measurement. The offset must be omitted, as at zero torque, which corresponds to the zero load current and hence zero negative sequence current, the stray load losses shall be zero. The stray load losses for rated load are taken from the slope ($P_{ad} = 132.8$ W) of the regression-line (Figure 3.17). The evaluation is summarized in Figure 3.18.

Figure 3.17: Measured stray load losses of an 11 kW 4-pole motor "A160-4"
(Subscript c for corrected: Linear regression line without offset)

	Method A	load point	1	2	3	4	5	6
Input data	rated line- line voltage	U_N [V]	400,0	400,0	400,0	400,0	400,0	400,0
	rated line current	I_N [A]	21,62	21,62	21,62	21,62	21,62	21,62
	no-load line current	I_0 [A]	10,92	10,92	10,92	10,92	10,92	10,92
	frequency	f [Hz]	50	50	50	50	50	50
	number of poles	2p	4	4	4	4	4	4
	line- line voltage	U_{UV} [V]	152,48	140,23	125,01	120,12	107,16	82,7
	line- line voltage	U_{VW} [V]	166,26	152,81	136,26	130,89	116,76	89,94
	line- line voltage	U_{WU} [V]	47,49	42,82	37,33	35,56	30,95	22,3
	phase current	I_{Uph} [A]	27,267	24,719	21,688	20,706	18,245	13,807
	phase current	I_{Vph} [A]	32,549	29,452	25,787	24,609	21,661	16,397
	phase current	I_{Wph} [A]	22,361	20,134	17,488	16,622	14,437	10,371
	input power	$P_{e,in}$ [W]	2456,7	2050,5	1600	1469,4	1155,42	684,81
	speed	n [rpm]	1467,5	1466,7	1466,4	1466,3	1465,3	1461,3
	phase resistance @ 20°C	$R_{s, 20°C}$ [Ω]	0,362301	0,362301	0,362301	0,362301	0,362301	0,36230067
	line- line resistance @ 20°C	$R_{VW, 20°C}$ [Ω]	0,710781					
	line- line resistance @ begin	$R_{VW, begin}$ [Ω]	0,73749					
	line- line resistance @ end	$R_{VW, end}$ [Ω]	0,770816					
	core losses	P_{FeN} [W]	312,41	312,41	312,41	312,41	312,41	312,41
	friction & windage losses	P_{fwN} [W]	71,38	71,38	71,38	71,38	71,38	71,38

Output data	eh-resistance (operating)	R_{eh} [Ω]	2,1238	2,1268	2,1346	2,1393	2,1438	2,1502
	winding temperature	temp [°C]	29,58	32,98	37,01	38,30	41,54	41,54
	positive sequence current	I_1 [A]	5,8784	5,3657	4,7681	4,5856	4,1404	3,4453
	negative sequence current	I_2 [A]	27,0377	24,4424	21,3614	20,3620	17,8526	13,2873
	ratio (positive/negative)	I_1 / I_2	0,2174	0,2195	0,2232	0,2252	0,2319	0,2593
	rated test current	I_{tN} [A]	18,6595	18,6595	18,6595	18,6595	18,6595	18,6595
	stray load losses	P_{add} [W]	292,8050	236,1909	184,0135	167,4715	133,6884	79,5636
	check of real power	P_{cont} [W]	2457,53	2051,23	1600,59	1469,95	1155,86	685,05
		$(I_2/I_{tN})^2$	2,0996	1,7159	1,3106	1,1908	0,9154	0,5071
	stray load losses @ I_{tN}	Intercept B	10,9656		Slope A	**132,8205**	Correlat. Fact	0,99960
	corrected stray load losses	$P_{add, c}$ [W]	278,872	227,904	174,070	158,163	121,581	67,350

Figure 3.18: Eh-star evaluation sheet acc. to method A for an 11 kW 4-pole motor "A160-4"

Figure 3.19 shows the phasor diagram of the measured voltages and currents, corresponding to the first load point (I_2/I_{tN} = 1.45) in Table 3.1, for an 11 kW 4-pole motor "A160-4". The corresponding phasor diagram of the positive and negative sequence system is given in Figure 3.20, where a resistive-inductive behaviour is shown.
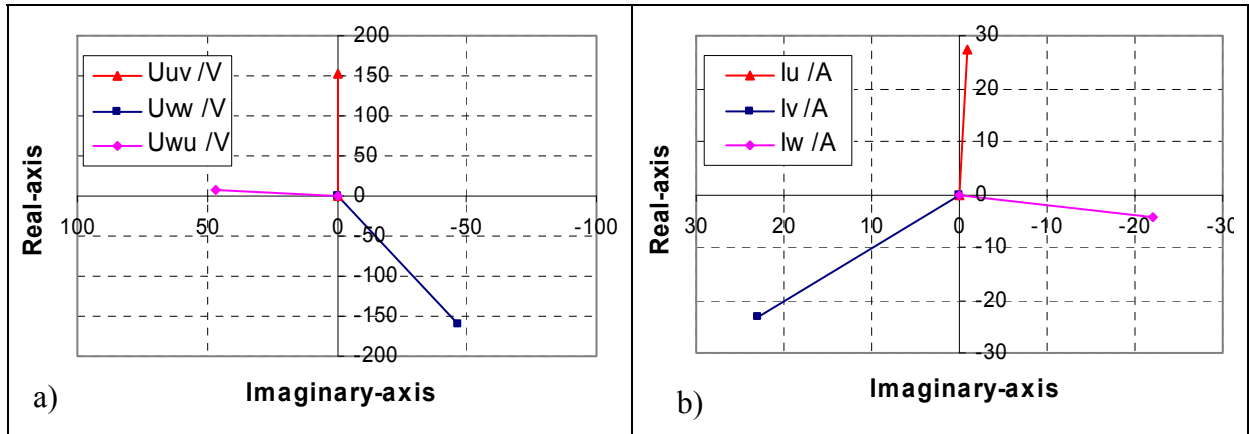
Figure 3.19: Phasor diagram of measured voltages and currents at (I_2/I_{tN} = 1.45) for an 11 kW 4-pole motor "A160-4"   a) Line to line voltages   b) Phase currents
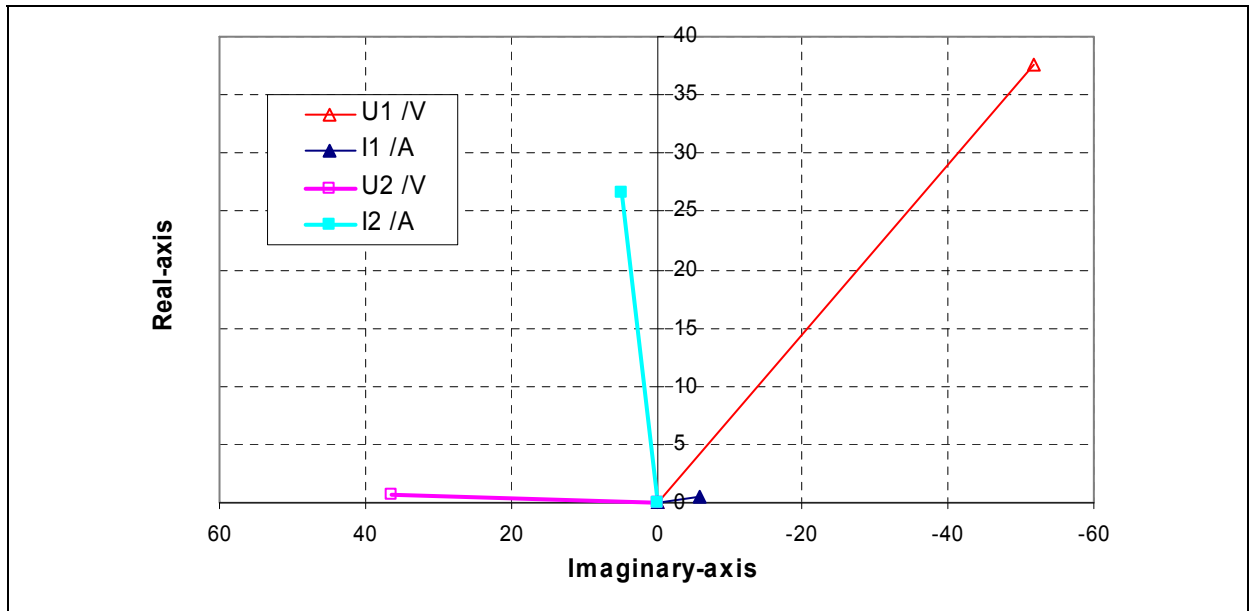
Figure 3.20: Phasor diagram of the positive and negative sequence system at (I_2/I_{tN} = 1.45) for an 11 kW 4-pole motor "A160-4"

Figure 3.21 shows the waveform of the stator currents and the voltages during the eh-star test for an 11 kW 4-pole motor "A160-4". In the shape of the

waveform the effect of the slot harmonics is visible.
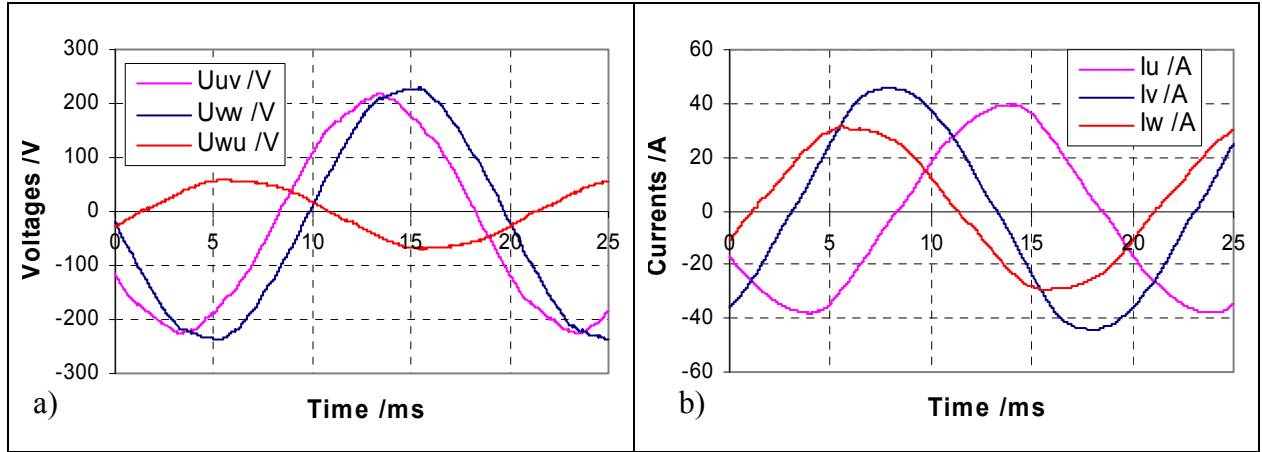
Figure 3.21: Measured waveform of the stator currents and voltages at eh-star test for an 11 kW 4-pole motor "A160-4". The variables are successively measured, thus no information about the phase angle   a) Waveform of the stator line to line voltages b) Waveform of the stator phase current

3.5 Theoretical model

With the theoretical model a fictive motor with known parameters and loss balance is simulated at eh-star measurement conditions. This model is needed e.g. to check the different post-processing methods A, A1, B and C with the mathematically exact results of the simulation and to check the influence of different types of the auxiliary impedances on the stray load loss result.

The theoretical model of the asymmetrically fed induction machine is considered, according to the rules of the symmetrical components, as superposition of two equivalent symmetric induction machines, of which one is fed by a positive sequence system at slip $s_1 = s$ and the other by a negative sequence system at slip $s_2 = 2 - s$. The impedances $\underline{Z}_1(s_1)$ of the positive and $\underline{Z}_2(s_2)$ of the negative sequence system for the theoretical model depend on slip s, which is determined by the load of the motor. The load is given by the friction and windage losses P_{fw} and the stray load losses $P_{ad,r}$ due to the rotor movement. The stator stray load losses due to skin-effect in the stator winding do not brake the rotor and may be considered in an equivalent circuit as "equivalent series

resistance" $R_{ad,s}$ in series with the stator phase resistance R_s.
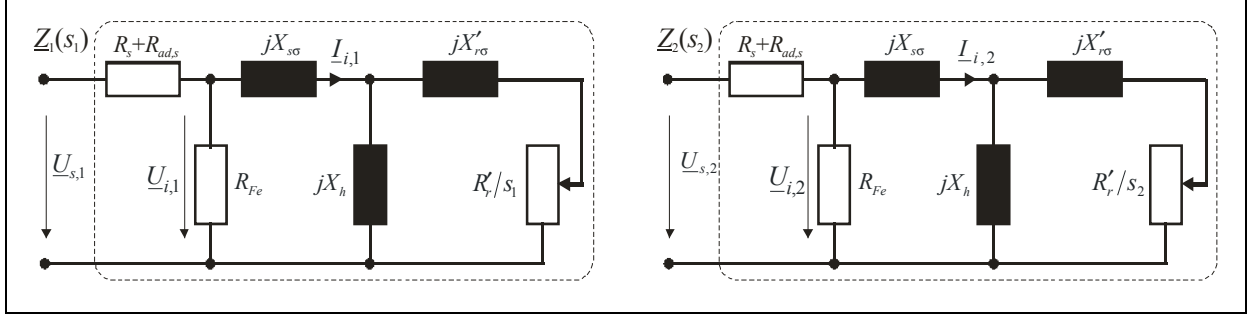
Figure 3.22: T-equivalent circuit of the theoretical model for the positive and the negative sequence system

The impedances $\underline{Z}_1(s_1)$ of the positive and $\underline{Z}_2(s_2)$ of the negative sequence system are calculated as:

$$\underline{Z}_1(s_1) = R_s + R_{ad,s} + \frac{jX_s R_{Fe} \cdot (R'_{r1} + j \cdot s_1 \cdot \sigma_1 \cdot X'_{r1})}{(R_{Fe} R'_{r1} - s_1 \cdot \sigma_1 \cdot X_s X'_{r1}) + j \cdot (s_1 \cdot R_{Fe} X'_{r1} + X_s R'_{r1})} \quad (3.85)$$

$$\underline{Z}_2(s_2) = R_s + R_{ad,s} + \frac{jX_s R_{Fe} \cdot (R'_{r2} + j \cdot s_2 \cdot \sigma_2 \cdot X'_{r2})}{(R_{Fe} R'_{r2} - s_2 \cdot \sigma_2 \cdot X_s X'_{r2}) + j \cdot (s_2 \cdot R_{Fe} X'_{r2} + X_s R'_{r2})} \quad (3.86)$$

with the leakage coefficients $\sigma_1(s_1)$ of the positive and $\sigma_2(s_2)$ of the negative sequence systems

$$\sigma_1(s_1) = 1 - \frac{X_h^2}{X_s X'_{r1}} \quad (3.87)$$

$$\sigma_2(s_2) = 1 - \frac{X_h^2}{X_s X'_{r2}} \quad (3.88)$$

and the reactances X_s of the stator and of the rotor $X'_{r1}(s_1)$ at slip s_1 and $X'_{r2}(s_2)$ at slip s_2

$$X_s = X_{s\sigma} + X_h \quad (3.89)$$

$$X'_{r1}(s_1) = X'_{r\sigma1} + X_h \quad (3.90)$$

$$X'_{r2}(s_2) = X'_{r\sigma2} + X_h. \tag{3.91}$$

In addition to the impedance of the T-equivalent circuit in Figure 3.22 the auxiliary impedance $\underline{Z}_{eh}$ in Figure 3.23 must be considered to determine the unknown currents and voltages.
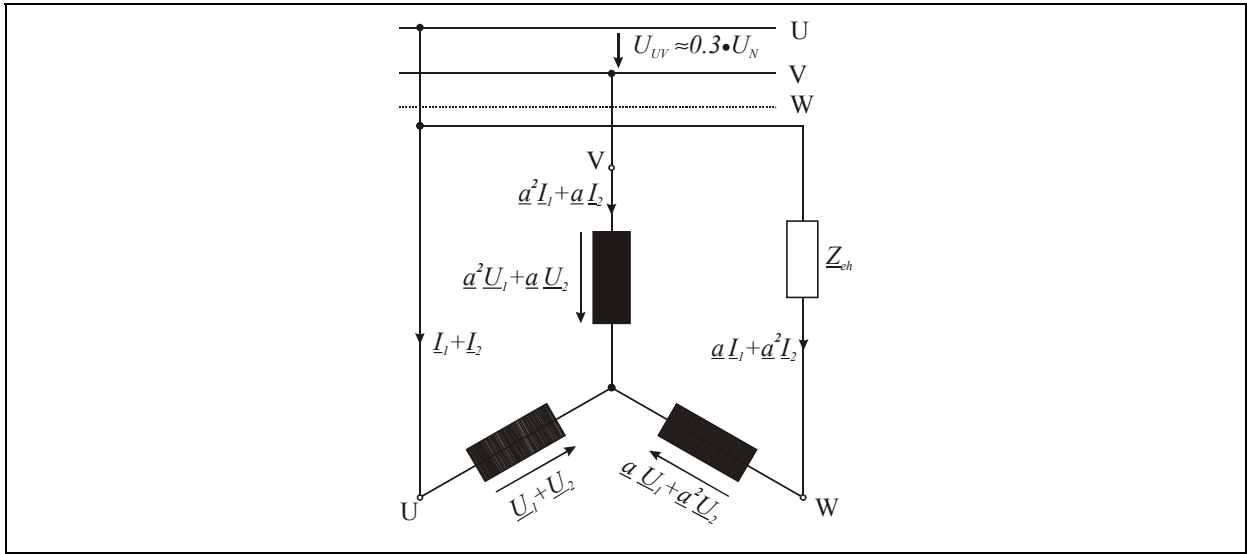
Figure 3.23: Eh-star circuit

The currents $\underline{I}_{s,1}$ of the positive and $\underline{I}_{s,2}$ of the negative sequence system and the phase currents $\underline{I}_W$ and $\underline{I}_V$ are calculated from the impedances $\underline{Z}_1$ of the positive and $\underline{Z}_2$ of the negative sequence system acc. to Figure 3.22, the "given" stator voltage U_{UV} and the auxiliary impedance $\underline{Z}_{eh}$ according to the Figure 3.23 as:

$$\underline{I}_{s,1} = \frac{U_{UV}}{3} \cdot \frac{(1-\underline{a}) \cdot \underline{Z}_{eh} - 3\underline{a} \cdot \underline{Z}_2}{3 \cdot \underline{Z}_1 \underline{Z}_2 + \underline{Z}_{eh} \cdot (\underline{Z}_1 + \underline{Z}_2)} \tag{3.92}$$

$$\underline{I}_{s,2} = \frac{U_{UV}}{3} \cdot \frac{(1-\underline{a}^2) \cdot \underline{Z}_{eh} - 3\underline{a}^2 \cdot \underline{Z}_2}{3 \cdot \underline{Z}_1 \underline{Z}_2 + \underline{Z}_{eh} \cdot (\underline{Z}_1 + \underline{Z}_2)} \tag{3.93}$$

$$\underline{I}_W = -\frac{U_{UV}(\underline{a} \cdot \underline{Z}_1 + \underline{a}^2 \cdot \underline{Z}_2)}{3 \cdot \underline{Z}_1 \cdot \underline{Z}_2 + \underline{Z}_{eh}(\underline{Z}_1 + \underline{Z}_2)} \tag{3.94}$$

$$\underline{I}_V = -\frac{\underline{U}_{UV}(\underline{Z}_1 + \underline{Z}_2 + \underline{Z}_{eh})}{3 \cdot \underline{Z}_1 \cdot \underline{Z}_2 + \underline{Z}_{eh}(\underline{Z}_1 + \underline{Z}_2)}. \tag{3.95}$$

The phase current $\underline{I}_U$ is resulting as

$$\underline{I}_U = -\underline{I}_V - \underline{I}_W. \tag{3.96}$$

With the calculated phase current $\underline{I}_W$, the three phase voltages $\underline{U}_U$, $\underline{U}_V$, $\underline{U}_W$

$$\underline{U}_U = (\underline{U}_{UV} + \underline{Z}_{eh} \cdot \underline{I}_W)/3 \tag{3.97}$$

$$\underline{U}_V = (-2 \cdot \underline{U}_{UV} + \underline{Z}_{eh} \cdot \underline{I}_W)/3 \tag{3.98}$$

$$\underline{U}_W = (\underline{U}_{UV} - 2 \cdot \underline{Z}_{eh} \cdot \underline{I}_W)/3 \tag{3.99}$$

and the phase voltages $\underline{U}_1$ of the positive and $\underline{U}_2$ of the negative sequence system

$$\underline{U}_1 = (\underline{U}_U + \underline{a} \cdot \underline{U}_V + \underline{a}^2 \cdot \underline{U}_W)/3 = -(\underline{a} \cdot \underline{U}_{UV} + \underline{a}^2 \cdot \underline{Z}_{eh} \cdot \underline{I}_W)/3 \tag{3.100}$$

$$\underline{U}_2 = (\underline{U}_U + \underline{a}^2 \cdot \underline{U}_V + \underline{a} \cdot \underline{U}_W)/3 = -(\underline{a}^2 \cdot \underline{U}_{UV} + \underline{a} \cdot \underline{Z}_{eh} \cdot \underline{I}_W)/3 \tag{3.101}$$

are derived.

With the decomposed voltages $\underline{U}_1$ of the positive and $\underline{U}_2$ of the negative sequence system, the phase voltages $\underline{U}_U$, $\underline{U}_V$, $\underline{U}_W$ and therefore the "given" voltage U_{UV} can be recalculated to check the calculation model.

$$\underline{U}_U = \underline{U}_1 + \underline{U}_2 \tag{3.102}$$

$$\underline{U}_V = \underline{a}^2 \cdot \underline{U}_1 + \underline{a} \cdot \underline{U}_2 \tag{3.103}$$

$$\underline{U}_W = \underline{a} \cdot \underline{U}_1 + \underline{a}^2 \cdot \underline{U}_2. \tag{3.104}$$

From the equations (3.102) and (3.103) the "given" supply voltage U_{UV} is calculated as:

$$\underline{U}_{UV} = \underline{U}_U - \underline{U}_V = (1 - \underline{a}^2) \cdot \underline{U}_1 + (1 - \underline{a}) \cdot \underline{U}_2 \tag{3.105}$$

The terminal power data from a 2-wattmeter-measurement-method are given in the following:

$$P_{e,in} = P_{e,in\_UV} + P_{e,in\_WV}$$
$$= U_{UV,r} \cdot I_{U,r} + U_{UV,i} \cdot I_{U,i} - U_{VW,r} \cdot I_{W,r} - U_{VW,i} \cdot I_{W,i}$$

(3.106)

The input and output data for the theoretical model of a 315 kW 4-pole motor (TEFC) are give in Table 3.4.

Input data			→ Model →	Output data		
Rated line-to-line voltage	u_N / p.u.	1		Line-to-line voltage	U_{UV} /V	282.2
Rated line current	i_N / p.u.	1		Line-to-line voltage	U_{VW} /V	331.3
No-load line current	i_0 / p.u.	0.27		Line-to-line voltage	U_{WU} /V	88.9
Number of poles	$2p$	4		Phase current	I_U /A	458.2
Frequency	f /Hz	50		Phase current	I_V /A	521.2
Rated iron losses	P_{FeN} / P_N	0.008		Phase current	I_W /A	355.5
Rated friction & windage losses	P_{fwN} / P_N	0.004		Motor input power	$P_{e,in}$ /kW	48.92
Stator phase resistance	$r_{s,\,20°C}$ / p.u.	0.008		input power UV	P_{e,in_UV}/kW	125
Skin-effect_stator	$r_{ad,s}$ / p.u.	0		input power WV	P_{e,in_WV}/kW	-76.1
Stator stray inductance	$x_{s\sigma}$ / p.u.	0.077		Eh-resistance	R_{eh} /Ω	0.25
Magnetizing inductance	x_h / p.u.	3.16		Eh-reactance	X_{eh} /Ω	0
Rotor resistance ($s = 1$)	$r'_{r,\,20°C,\,s=1}$ /p.u.	0.022		Pos. seq. impedance	Z_1 /Ω	1.29
Rotor resistance ($s = 0$)	$r'_{r,\,20°C,\,s=0}$ /p.u.	0.006		Neg. seq. impedance	Z_2 /Ω	0.18
Rotor stray inductance	$x'_{r\sigma}$ / p.u.	0.137		Pos. seq. current	I_1 /A	95
Eh-impedance	Z_{eh} /Ω	0.25		Neg. seq. current	I_2 /A	440
Eh-phase angle	φ_{eh} /°	0		Pos. seq. voltage	U_1 /V	123
Line-to-line voltage	U_{UV} /V	282.2		Neg. seq. voltage	U_2 /V	81
Speed	n /rpm	1490		Internal Torque	M_e /Nm	121
Winding temperature	ϑ /°C	30		Stray load losses	P_{ad} /kW	16.89

Table 3.4: Input and output data for theoretical model of a 315 kW 4-pole motor "A317-4"

3.5.1 Loss balance of the positive and the negative sequence system

The input power of the positive and negative sequence system are:

$$P_{e,\,in,1} = 3 \cdot \text{Re}\{\underline{U}_1 \cdot \underline{I}_1^*\} \tag{3.107}$$

$$P_{e,\,in,2} = 3 \cdot \text{Re}\{\underline{U}_2 \cdot \underline{I}_2^*\} \tag{3.108}$$

where $\underline{I}^*$ is the conjugate complex value of the current $\underline{I}$.

The stator copper losses of the positive and negative sequence system are:

$$P_{Cu,\,s,1} = 3 \cdot R_s \cdot \left|\underline{I}_1\right|^2 \tag{3.109}$$

$$P_{Cu,\,s,2} = 3 \cdot R_s \cdot \left|\underline{I}_2\right|^2. \tag{3.110}$$

With the inner voltages of the positive and the negative sequence system the iron losses are respectively determined:

$$P_{Fe,1} = 3 \cdot \left|\underline{U}_{i,1}\right|^2 / R_{Fe} \tag{3.111}$$

$$P_{Fe,2} = 3 \cdot \left|\underline{U}_{i,2}\right|^2 / R_{Fe}. \tag{3.112}$$

The input powers of the positive and the negative sequence system minus the stator losses (the copper and the iron losses) of the positive and the negative sequence system respectively gives the air gap power of the positive and negative sequence system:

$$P_{\delta,1} = P_{e,\,in,1} - P_{Cu,\,s,1} - P_{Fe,1} \tag{3.113}$$

$$P_{\delta,2} = P_{e,\,in,2} - P_{Cu,\,s,2} - P_{Fe,2}. \tag{3.114}$$

The rotor copper losses of the positive and the negative sequence system are:

$$P_{Cu,\,r,1} = s_1 \cdot P_{\delta,1} \tag{3.115}$$

$$P_{\text{Cu, r,2}} = s_2 \cdot P_{\delta,2} .$$ (3.116)

The remaining inner mechanical power of the positive and the negative sequence system results in:

$$P_{\text{m, i,1}} = (1 - s_1) \cdot P_{\delta,1}$$ (3.117)

$$P_{\text{m, i,2}} = (1 - s_2) \cdot P_{\delta,2} .$$ (3.118)

The resulting braking losses, the additional losses $P_{\text{ad,asym}}$ of the asymmetrically fed machine and the friction and windage losses P_{fw}, must equal the inner mechanical power:

$$P_{\text{ad,asym}} = P_{\text{m,i,1}} - \left| P_{\text{m,i,2}} \right| - P_{\text{fw}} .$$ (3.119)

The mechanical output power on the shaft is zero as the machine is uncoupled.

An example of the loss balance is given for the measured load point at $I_2/I_{\text{tN}} = 1$ in Table 3.5 and presented in Figure 3.24.

Table 3.5 shows that the winding losses of the negative sequence system are the dominating part of the absorbed power. With 69 % of the electrical input power the rotor winding losses of the negative sequence system $P_{\text{Cu,r,2}}$ dominate, as they are directly proportional to the respective slip ($s_2 \approx 2$), followed by the stator winding losses $P_{\text{Cu,s,2}}$ of the negative sequence system, due to the higher negative sequence current I_2.

In Figure 3.24 the quantitative power flow of the positive and the negative sequence system for the data in Table 3.5 is shown. The mechanical output power on the shaft P_{mech} is zero as the motor is uncoupled.

		Power in W	$P_x/P_{el,in}$ /%
Input power	$P_{e,in}$	21124	100
Input power of positive	$P_{e,in,1}$	10409.66	49.28
and negative sequence system	$P_{e,in,2}$	10714.34	50.72
Copper losses in stator of positive	$P_{Cu,s,1}$	89.93	0.43
and negative sequence system	$P_{Cu,s,2}$	3352.32	15.87
Iron losses of positive	$P_{Fe,1}$	122.73	0.58
and negative sequence system	$P_{Fe,2}$	51.00	0.24
Air gap power of positive	$P_{\delta,1}$	10197.00	48.27
and negative sequence system	$P_{\delta,2}$	7311.03	34.61
Copper losses in rotor of positive	$P_{Cu,r,1}$	67.98	0.32
and negative sequence system	$P_{Cu,r,2}$	14573.31	68.99
Inner mechanical power of positive	$P_{m,i,1}$	10129.02	47.95
and negative sequence system	$P_{m,i,2}$	-7262.29	-34.38
Friction and windage losses	P_{fw}	1286.67	6.09
Asymmetrical additional losses	$P_{ad,asym}$	1580.06	7.48

Table 3.5: Measured loss balance of the positive and negative sequence system and the ratio of the powers to the input power of a 315 kW 4-pole motor "A317-4"
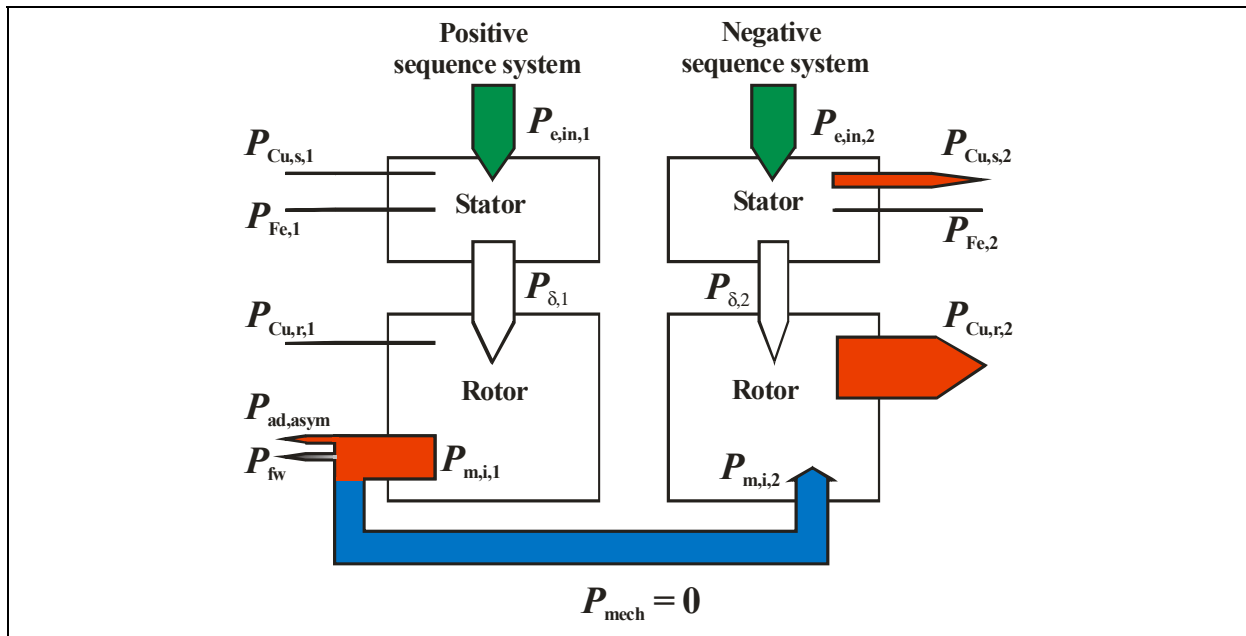
Figure 3.24: Power flow of the positive and negative sequence system of a 315 kW 4-pole motor"A317-4"

The resulting inner mechanical power $P_{m,i,1}$ of the positive sequence system covers the additional losses $P_{ad,asym}$ of the asymmetrically fed machine, the friction and windage losses P_{fw} and supplies the negative sequence system with $P_{m,i,2}$. The losses as percentage of the electrical input power for the data in Table 3.5 are shown in Figure 3.25. It can be seen that most of the total input power is absorbed as winding losses in the rotor and in the stator.
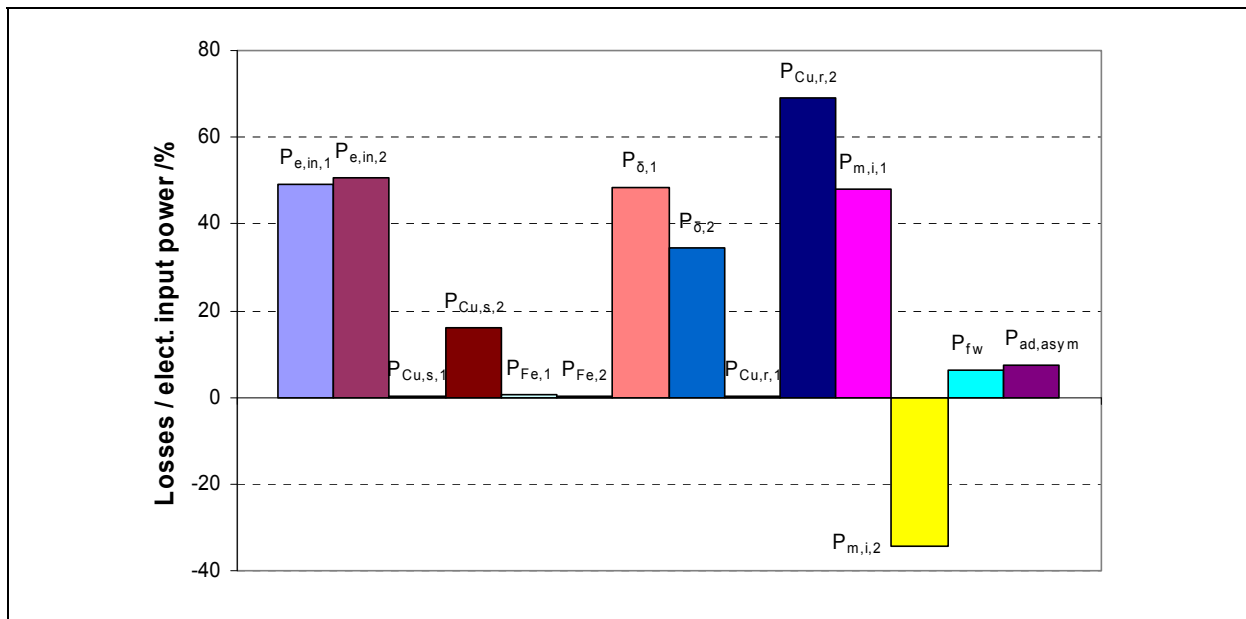
Figure 3.25: Measured loss balance of the positive and negative sequence system as percentage of the electrical input power of a 315 kW 4-pole motor "A317-4"

3.5.2 Characteristics of the positive and negative sequence system

Figure 3.26 shows the calculated characteristics of the current I and the electromagnetic internal torque M_e of the positive and the negative sequence system at fixed supply voltage $U_{UV} = 282.2$ V and at an auxiliary resistance $\underline{Z}_{eh} = R_{eh} = 0.25$ Ohm for a 315 kW 4-pole induction motor according to the data in Table 3.4 by variation of the slip s. The calculation is done at reduced supply voltage U_{UV}.
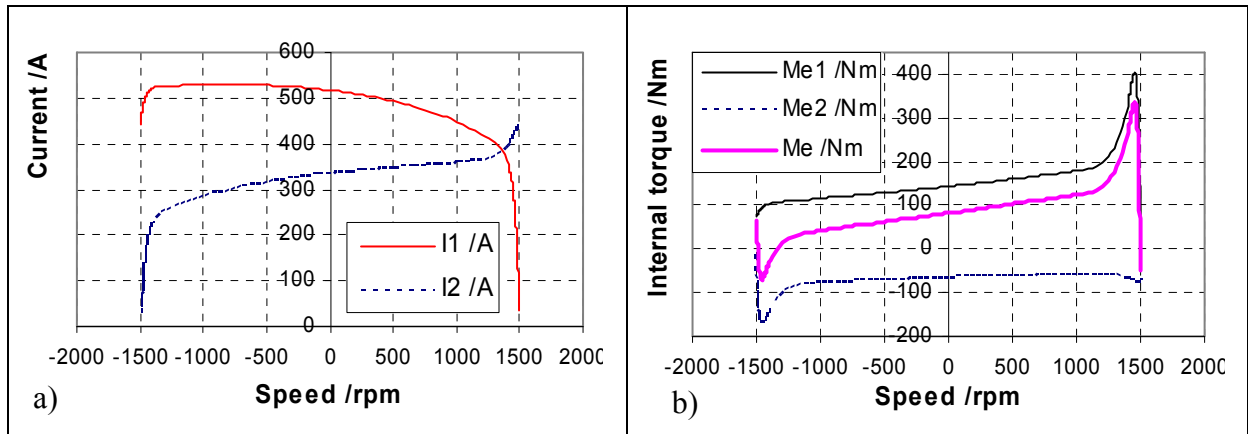
Figure 3.26: Characteristics of the calculated positive and negative sequence system of a 315 kW 4-pole motor "A317-4" a) Current   b) Electromagnetic internal torque

In the range between rated speed and synchronous speed (Figure 3.26a) the negative sequence current I_2 is bigger than the positive sequence current I_1, so that the ratio $I_1/I_2 < 0.3$, outside this range the positive sequence current I_1 dominates. The electromagnetic internal torque of the positive sequence system M_{e1} is reduced by the braking negative sequence component M_{e2}, this yields reduced resulting electromagnetic internal torque M_e (Figure 3.26b).

3.5.3 Influence of the auxiliary resistance on the positive and the negative sequence system at fixed slip

Figure 3.27a gives the calculated voltage U_1 of the positive and U_2 of the negative sequence for a 315 kW 4-pole induction motor by variation of the auxiliary resistance R_{eh} with the assumption that the slip s and the supply voltage U_{UV} are constant. Figure 3.27b shows the calculated positive M_{e1} and negative M_{e2} sequence internal torque and the resulting torque M_e. Of course in reality the slip s is not constant, as with varying current the electromagnetic torque varies too, which has to balance the load torque due to the friction, windage losses and the stray load losses. In Figure 3.27c the Voltage-Current-Curve of the positive and the negative sequences, due to varying the resistance R_{eh}, are depicted.
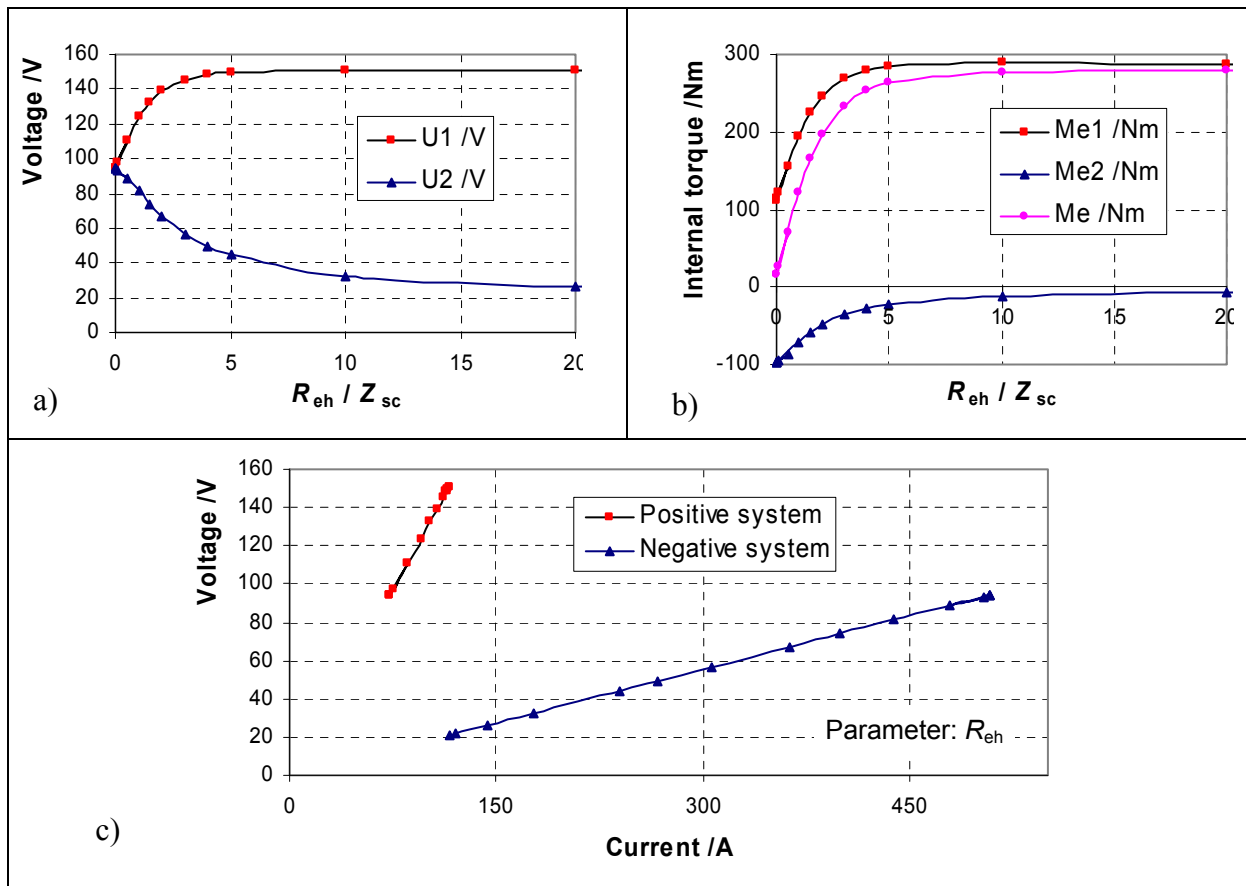
Figure 3.27: Influence of the resistance R_{eh} on the calculated positive and negative sequence system of a 315 kW 4-pole motor "A317-4" a) Voltage   b) Electromagnetic internal torque c) Voltage-Current-Curve
(Z_{sc}: short circuit impedance)

For a resistance value $R_{eh} = 0$ the voltages U_1 of the positive and U_2 of the negative sequence system are equal. If the resistance R_{eh} increases to large values, the positive sequence voltage U_1 increases and the negative sequence voltage U_2 decreases significantly (Figure 3.27a). A small eh-resistance value produces a high negative torque component M_{e2} and high torque pulsations. It is quite possible not to have enough net positive torque M_{e1} to overcome the friction and windage torque as the positive torque component M_{e1} is typically heavily reduced by the reduced supply test voltage U_{UV} and by the effective reduction in positive sequence voltage U_1 (Figure 3.27b). The impedances of the positive and the negative sequence systems are constant, as the slip s is assumed to be constant, as shown in the Voltage-Current-Curve by varying the resistance R_{eh} (Figure 3.27c).

In Figure 3.28 the calculated positive I_1, negative I_2 sequence current and the ratio I_1/I_2 by variation of the auxiliary resistance R_{eh} at fixed slip s and supply voltage U_{UV} are presented. The value of the auxiliary resistance R_{eh} adjusts the proportion of positive I_1 to negative I_2 sequence currents. High resistance values make the two current components closer to each other with the extreme being a phase open circuit ($R_{eh} \rightarrow \infty$), which would result in equal positive I_1 and negative I_2 sequence current components. The lower the value of this resistance, the higher is the difference in magnitude between the negative I_2 and positive I_1 sequence current components (Figure 3.28).
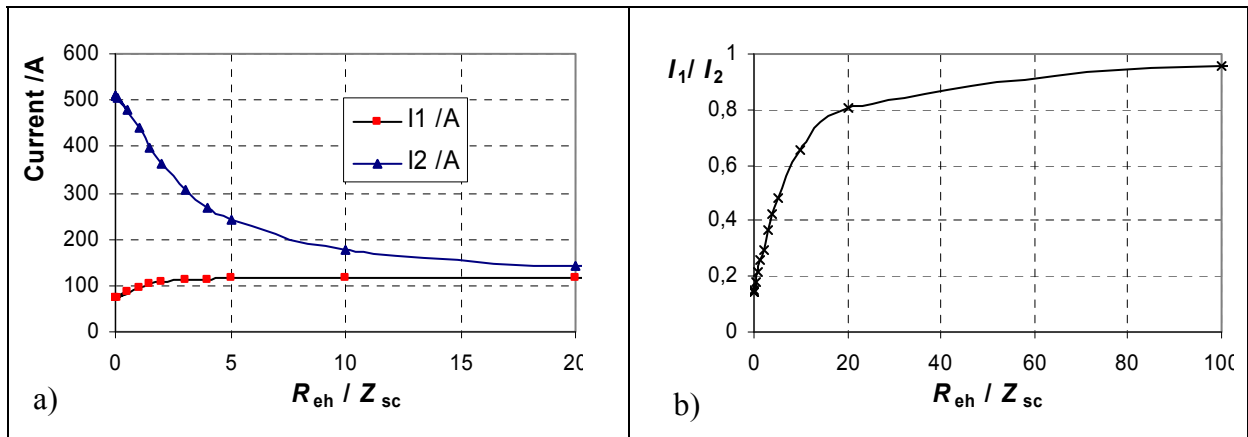
Figure 3.28: Influence of the resistance R_{eh} on the calculated positive and negative sequence system of a 315 kW 4-pole motor "A317-4" a) Current b) Ratio of currents (Z_{sc}: short circuit impedance)

Figure 3.29 shows the calculated ratio of the positive I_1 and negative I_2 sequence currents for a small 11 kW and a big 1 MW 4-pole motor for variation of the auxiliary resistance R_{eh} at constant slip s and supply voltage U_{UV}. The ratio of the currents I_1/I_2 of the big motor is smaller than that of the small one. With increased value of the auxiliary resistance R_{eh} the ratio I_1/I_2 tends to unity.
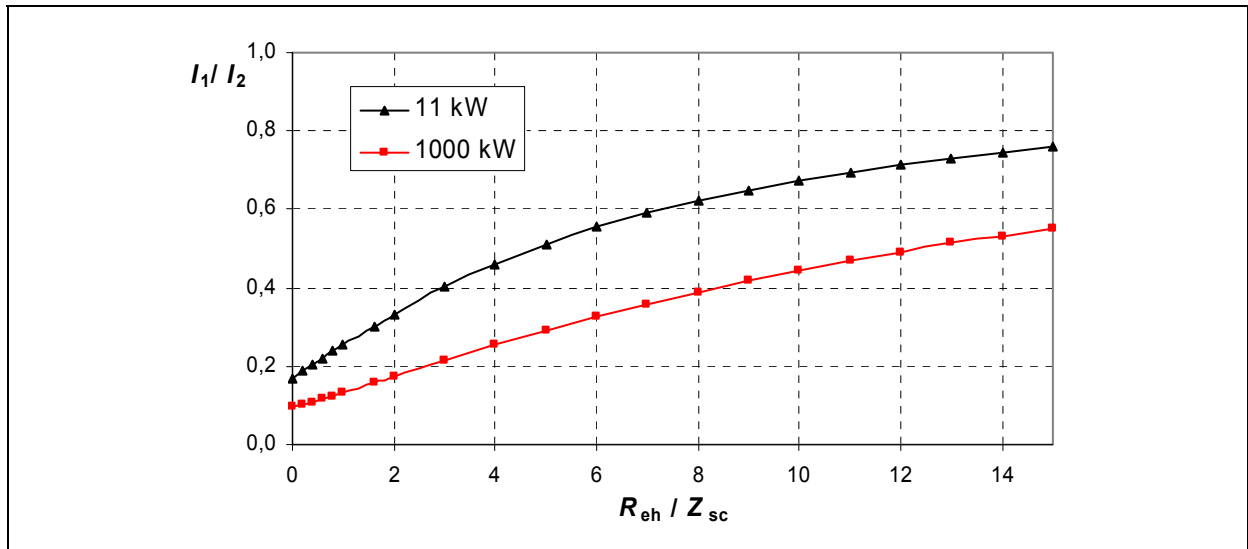
Figure 3.29: Influence of the resistance R_{eh} on the calculated ratio of positive and negative
sequence currents of an 11 kW and a 1000 kW 4-pole motors
(Z_{sc}: short circuit impedance)

3.5.4 Influence of the auxiliary resistance on the positive and the negative sequence system at varying slip

As mentioned earlier, the slip is not constant in reality, as with varying current the electromagnetic torque varies too, which has to balance the load torque due to the friction, windage losses and the stray load losses. The varying slip s was taken from the measurement on an 11 kW 4-pole motor and used for the calculation in Table 3.6 and in Figure 3.30a.

R_{eh} /Ohm	5.3	3.7	2.5	1.3	1.15
R_{eh} / Z_{sc}	2.12	1.48	1.0	0.52	0.46
Speed /rpm	1483.2	1468.7	1451.3	1422.2	1387.8
I_1 / I_2 measured	0.19	0.21	0.248	0.29	0.40
I_1 / I_2 calculated	0.158	0.207	0.251	0.32	0.40

Table 3.6: Influence of the resistance R_{eh} on the positive and negative sequence system of an
11 kW 4-pole motor "E160-4", comparison of the measurement and the
calculation

At small values of the auxiliary resistance R_{eh} the small positive sequence

voltage U_1 leads to a small torque ($P_{ad,1} \sim I_1^2$) and to big slip s due to the friction load, hence increasing the positive sequence current I_1, so the ratio I_1/I_2 increases. If the resistance R_{eh} increases to large values, the positive sequence voltage U_1 increases, so the slip s decreases to zero (Figure 3.30b). The negative sequence voltage U_2 decreases significantly and so does the negative sequence current I_2, hence the ratio I_1/I_2 increases again. At an infinite value of the resistance R_{eh} the ratio $I_1/I_2 = 1$ (Figure 3.28b and Figure 3.29), so there exists a value R_{eh}, where the ratio I_1/I_2 is minimum (Figure 3.30a). The impact of the resistance value on the slip s at eh-star measurement is given in Figure 3.30b.
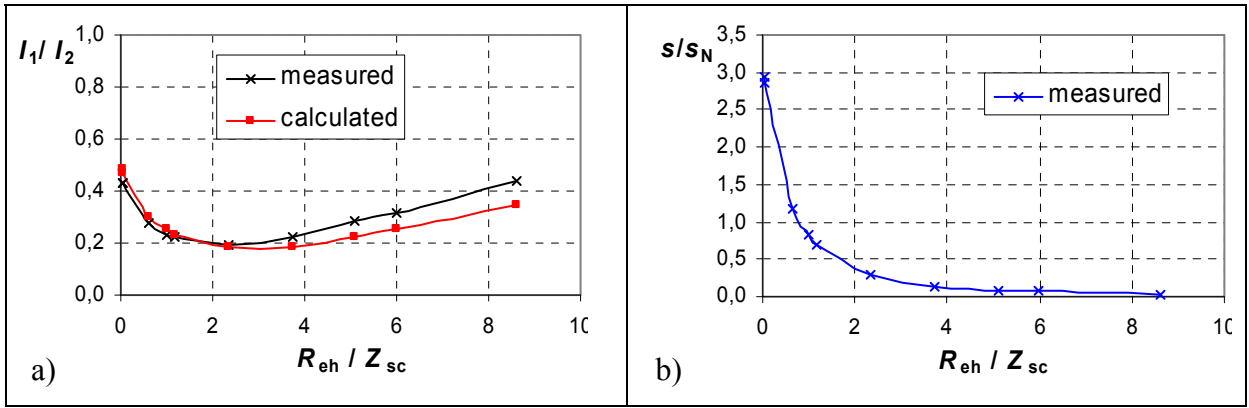
Figure 3.30: Influence of the resistance R_{eh} on the positive and negative sequence system of an 11 kW 4-pole motor "A160-4"   a) comparison of measured and calculated ratio of currents   b) Ratio of slip at eh-measurement related to the rated slip (Z_{sc}: short circuit impedance)

3.5.5 Influence of the phase angle of the auxiliary impedance on the positive and the negative sequence system at fixed slip

For the calculated data in Table 3.4 resistive auxiliary impedance $\underline{Z}_{eh} = R_{eh} = 0.25$ Ohm, $\varphi_{eh} = 0°$ is assumed. Figure 3.31 shows the influence of the phase angle φ_{eh} of the auxiliary impedance $\underline{Z}_{eh} = Z_{eh} \cdot e^{j\varphi_{eh}}$ on the positive and the negative sequence system at constant slip s and supply voltage U_{UV} for the example of a 315 kW 4-pole motor "A317-4" given in Table 3.4 if the really used impedance $\underline{Z}_{eh} = Z_{eh} \cdot e^{j\varphi_{eh}}$ is either resistive-inductive $\varphi_{eh} > 0°$ or

3 Eh-star method

resistive-capacitive $\varphi_{eh} < 0°$. The deviation is related to the values at $\varphi_{eh} = 0°$ and calculated for example for an assumed phase angle $\varphi_{eh} = 10°$ as:

$$\Delta U_1\mid_{\varphi=10°} = (U_1\mid_{\varphi=10°} - U_1\mid_{\varphi=0°})/U_1\mid_{\varphi=0°}. \tag{3.120}$$

In case of slightly resistive-capacitive or slightly resistive-inductive behaviour $-10° \leq \varphi_{eh} \leq 10°$ the deviation of the positive sequence voltage U_1 is smaller than 1.5 % whereas the negative sequence voltage U_2 varies within 4.5 %. The variation of the ratio of currents I_1/I_2 is smaller than 3 %. The influence of the high resistive-capacitive impedance on the positive and the negative sequence system at constant slip s and supply voltage U_{UV} is much higher than the influence of the resistive-inductive behaviour, especially for the negative sequence system.
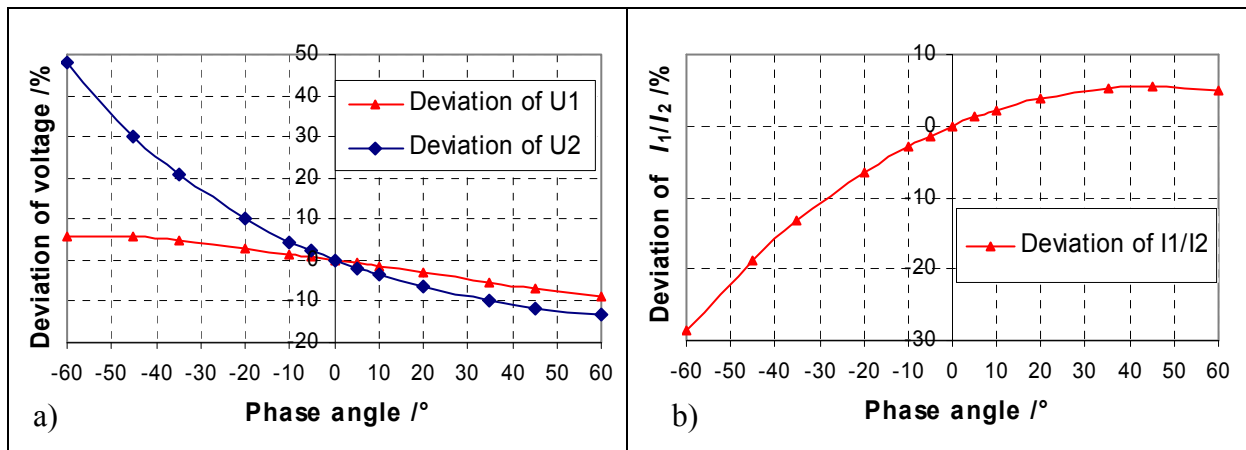
Figure 3.31: Influence of the phase angle φ_{eh} of the auxiliary impedance on the calculated positive and negative sequence system of a 315 kW 4-pole motor "A317-4"
a) Deviation of voltages   b) Deviation of ratio of currents
The deviation is related to the values at $\varphi_{eh} = 0°$

3.5.6 Influence of the temperature on the positive and the negative sequence system at fixed slip

The influence of the winding temperature on the positive and the negative sequence system at constant slip s and supply voltage U_{UV} for the example of a 315 kW 4-pole is presented in Figure 3.32.
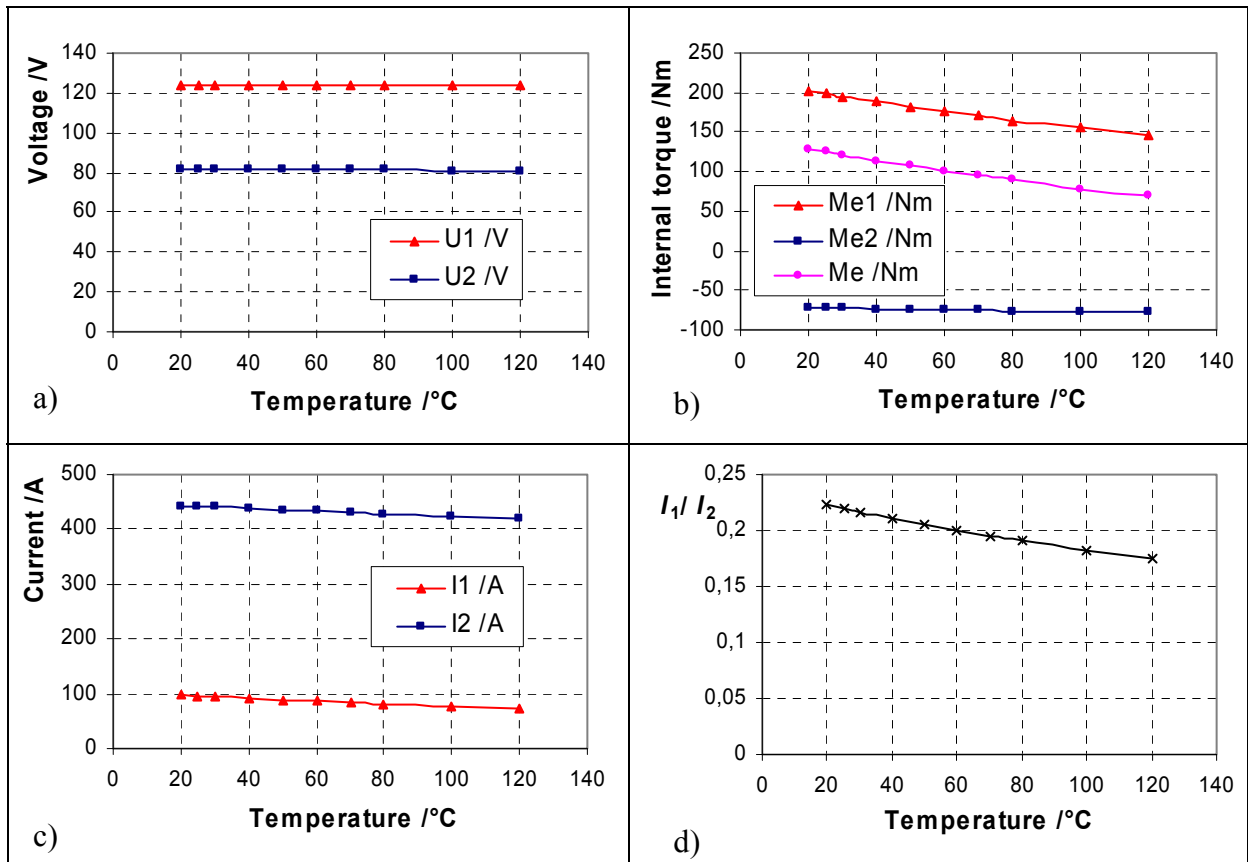
Figure 3.32: Influence of the temperature on the calculated positive and negative sequence
system of a 315 kW 4-pole motor "A317-4" a) Voltage   b) Electromagnetic
internal torque c) Current   d) Ratio of the currents

The Figures show that the influence of the winding temperature on the voltages of the positive U_1 and the negative U_2 sequence system is very small. A 20 K variation of the winding temperature corresponds to about 6 % deviation of the positive I_1 and 1 % of the negative I_2 sequence currents leading to about 7 % deviation of the positive M_{e1} and 2 % of the negative M_{e2} sequence electromagnetic internal torque.

3.5.7 Impact of error in the determination of the winding temperature on the simulated stray load losses

To show the impact of an error in the determination of the winding temperature on the calculated stray load losses, the resulting simulated r.m.s.

values of the asymmetric three phase voltages and currents as well as the terminal power data (output data in Table 3.4) are taken as „measured" values. The evaluation of the stray load losses P_{ad} is done at different assumed temperatures. That means, if the temperature is measured with a certain error.

Figure 3.33a shows the influence of overestimated winding temperature on the simulated stray load losses P_{ad} for a cold machine. The deviation is related to the "true" value $P_{ad,true} = 16.89$ kW at 30°C winding temperature.

Figure 3.33b shows the influence of underestimated winding temperature on the simulated stray load losses P_{ad} for a warm machine. The deviation is related to the "true" value $P_{ad,true} = 10.6$ kW at 100°C winding temperature.
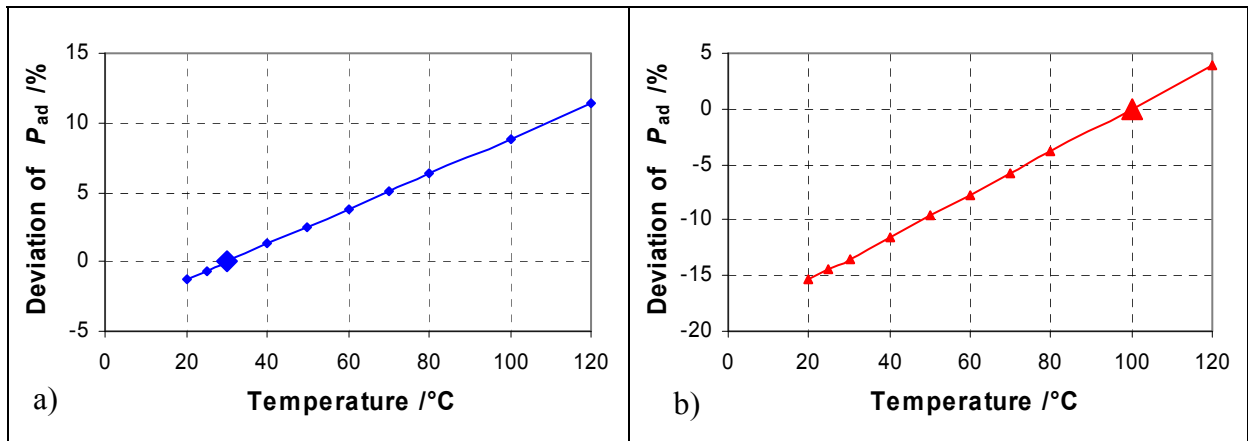
Figure 3.33: Impact of error in the determination of the winding temperature on the calculated stray load losses of a 315 kW 4-pole motor "A317-4"   a) Overestimated temperature $\vartheta_{refer} = 30$°C   b) Underestimated temperature $\vartheta_{refer} = 100$°C

An error of 20 K in the determination of the winding temperature corresponds for the cold machine to 2.5 % and for the warm machine to 3.8 % deviation of the stray load losses P_{ad} from the "true" value $P_{ad,true}$. If the winding temperature is underestimated by 20 K the deviations are the same.

3.6 Comparison of methods A, A1, B and C with a theoretical example

With a theoretical model of a small 11 kW 4-pole motor (TEFC), according to the T-equivalent circuit (Figure 3.22) and the data of Table 3.7, the different

evaluation methods A, A1, B and C will be compared in the following.

The resulting simulated r.m.s. values of the asymmetric three phase voltages and currents as well as the terminal power data (output data in Table 3.7) are taken as „measured" values for the comparison of the evaluation methods A, A1, B and C. The decomposition of the current phasors into real and imaginary part, which is needed for the stray load losses evaluation in the eh-star method, is done by different evaluation methods.

Input data			→ Model →	Output data		
Rated line-to-line voltage	U_N / V	400.0	Line-to-line voltage	U_{UV} /V	151.8
Rated line current	I_N / A	21.62	Line-to-line voltage	U_{VW} /V	168.0
No-load line current	I_0 / A	10.92	Line-to-line voltage	U_{WU} /V	40.25
Number of poles	$2p$	4	Phase current	I_U /A	25.86
Frequency	f /Hz	50	Phase current	I_V /A	30.08
Rated iron losses	P_{FeN} /W	312.4	Phase current	I_W /A	19.07
Rated friction & windage losses	P_{fwN} /W	71.38	Motor input power	$P_{e,in}$ /W	2261
Stator phase resistance	$R_{s,\,20°C}$ / Ω	0.36	input power UV	P_{e,in_UV}/W	3871
Skin-effect_stator	$R_{ad,s}$ / Ω	0	input power WV	P_{e,in_WV}/W	-1610
Stator stray reactance	$X_{s\sigma}$ / Ω	0.85	Eh-resistance	R_{eh} /Ω	2.11
Magnetizing reactance	X_h / Ω	35.9	Eh-reactance	X_{eh} /Ω	0
Rotor resistance ($s = 1$)	$R'_{r,\,20°C,\,s=1}$ /Ω	0.345	Pos. seq. impedance	Z_1 /Ω	10.02
Rotor resistance ($s = 0$)	$R'_{r,\,20°C,\,s=0}$ /Ω	0.215	Neg. seq. impedance	Z_2 /Ω	1.73
Rotor stray reactance	$X'_{r\sigma}$ / Ω	0.92	Pos. seq. current	I_1 /A	6.25
Eh-impedance	Z_{eh} /Ω	2.11	Neg. seq. current	I_2 /A	24.59
Eh-phase angle	φ_{eh} /°	0	Pos. seq. voltage	U_1 /V	61.55
Line-to-line voltage	U_{UV} /V	151.8	Neg. seq. voltage	U_2 /V	40.13
Speed	n /rpm	1466.6	Internal Torque	M_e /Nm	3.77
Winding temperature	ϑ /°C	30.5	Stray load losses	P_{ad} /W	479.6

Table 3.7: Input and output data for theoretical model of an 11 kW 4-pole motor (TEFC)

3.6.1 Influence of the phase angle of the auxiliary impedance on the stray load losses evaluation with methods A and A1

The value of the auxiliary impedance $\underline{Z}_{eh} = Z_{eh} \cdot e^{j\varphi_{eh}}$ does not influence numerically the calculation result in methods B and C (see sections 3.2.2.3 and 3.2.2.4), therefore only the influence of the phase angle φ_{eh} of the impedance $\underline{Z}_{eh}$ on the eh-star evaluation with method A and A1 is presented.

With both evaluation methods A and A1 a resistive auxiliary impedance $R_{eh} = \underline{Z}_{eh}$ is assumed. If the really used impedance $\underline{Z}_{eh} = Z_{eh} \cdot e^{j\varphi_{eh}}$ is either resistive-inductive $\varphi_{eh} > 0°$ or resistive-capacitive $\varphi_{eh} < 0°$, the evaluation methods A and A1 will give slightly wrong results. So we ask: How big is the influence of the phase angle φ_{eh} on the deviation of „evaluated" additional losses from the „true" additional losses P_{ad}, given in Table 3.7 (output data) ? The calculated deviation of stray load losses P_{ad_A}, P_{ad_A1} and of the check input power P_{cont_A}, P_{cont_A1} with methods A and A1 from the „true" values of the stray load losses P_{ad} and the input power $P_{e,in}$ for an assumed phase angle φ_{eh} of the impedance $\underline{Z}_{eh}$ is given for an 11 kW 4-pole motor in Table 3.8 and presented in Figure 3.34.

$Z_{eh} = 2.1\ \Omega$		Resistor-capacitor				*Ohmic*	Resistor-inductor			
Phase angle φ_{eh} /°		-15	-10	-5	-2	0	2	5	10	15
Method A1	$(P_{ad\_A1} - P_{ad})/P_{ad}$ /%	136	87	42	16.5	0.00	-16.1	-40	-77	-114
	$(P_{cont\_A1} - P_{e,in})/P_{e,in}$ /%	-43	-28	-14	-5.3	0.00	5.2	13	24	35
Method A	$(P_{ad\_A} - P_{ad})/P_{ad}$ /%	-4.5	-1.8	-0.43	-0.07	0.00	-0.06	-0.4	-1.4	-3
	$(P_{cont\_A} - P_{e,in})/P_{e,in}$ /%	1.33	0.56	0.13	0.02	0.00	0.02	0.12	0.48	1.04

Table 3.8: Influence of the phase angle φ_{eh} on the evaluated stray load losses with method A and method A1 for an 11 kW 4-pole motor

For purely resistive behaviour $\underline{Z}_{eh} = R_{eh}$, $\varphi_{eh} = 0°$ the evaluated stray load losses determined by the two methods A and A1 are identical with the „true" value $P_{ad} = 479.6$ W (Table 3.7). In case of slightly resistive-capacitive or slightly resistive-inductive behaviour $-10° \leq \varphi_{eh} \leq 10°$ the deviation of the stray

load losses P_{ad_A} from the „true" value P_{ad} is smaller than 2 %. Figure 3.34b shows that the check power P_{cont} is a good indicator for the model and the measurement accuracy in eh-star stray load losses determination. A 2 % deviation of the stray load losses P_{ad_A} from the „true" value P_{ad} corresponds to 0.6 % deviation of the check power P_{cont_A} from the „true" value $P_{e,in}$. In comparison, the deviation of the stray load losses P_{ad_A1} evaluated with the method A1 is with 87 % much bigger and corresponds to about 28 % deviation of the check power P_{cont_A1} from the „true" value $P_{e,in}$. Hence, a big deviation of the check power P_{cont} from the input power $P_{e,in}$ indicates a big difference of the evaluated stray load losses P_{ad} from the „true" value.
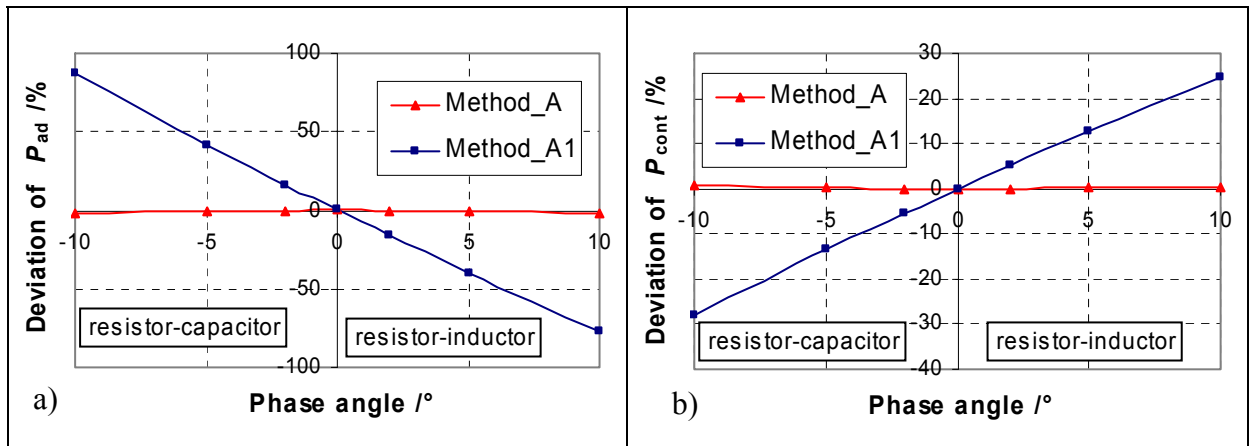
Figure 3.34: Calculated influence of the phase angle φ_{eh} on the evaluation methods A and A1 for an 11 kW 4-pole motor a) Deviation of stray load losses P_{ad} b) Deviation of check input power P_{cont}

3.6.2 Impact of error in the determination of the auxiliary resistance on the eh-star evaluation with methods A and A1

The value of the auxiliary impedance $\underline{Z}_{eh} = Z_{eh} \cdot e^{j\varphi_{eh}}$ does not influence numerically the calculation result with methods B and C (see sections 3.2.2.3 and 3.2.2.4), therefore only the influence of the impedance $\underline{Z}_{eh}$ on the eh-star evaluation with method A and A1 is presented. Even if the impedance $\underline{Z}_{eh}$ is in reality purely resistive, $\underline{Z}_{eh} = R_{eh}$, its absolute value R_{eh} may be influenced by an unknown temperature rise or by a measurement error. We assume a deviation

ΔR_{eh} of the auxiliary resistance R_{eh} from the true value $R_{eh,true} = 2.1\ \Omega$

$$R_{eh} = R_{eh,true} + \Delta R_{eh}\ .\tag{3.121}$$

This calculated influence of varying ΔR_{eh} on the evaluated stray load losses P_{ad_A}, P_{ad_A1} with methods A and A1 at a fixed supply voltage U_{UV} and a fixed slip s and its deviation from the „true" value of the Table 3.7 for $\Delta R_{eh} = 0$ is given in Figure 3.35.
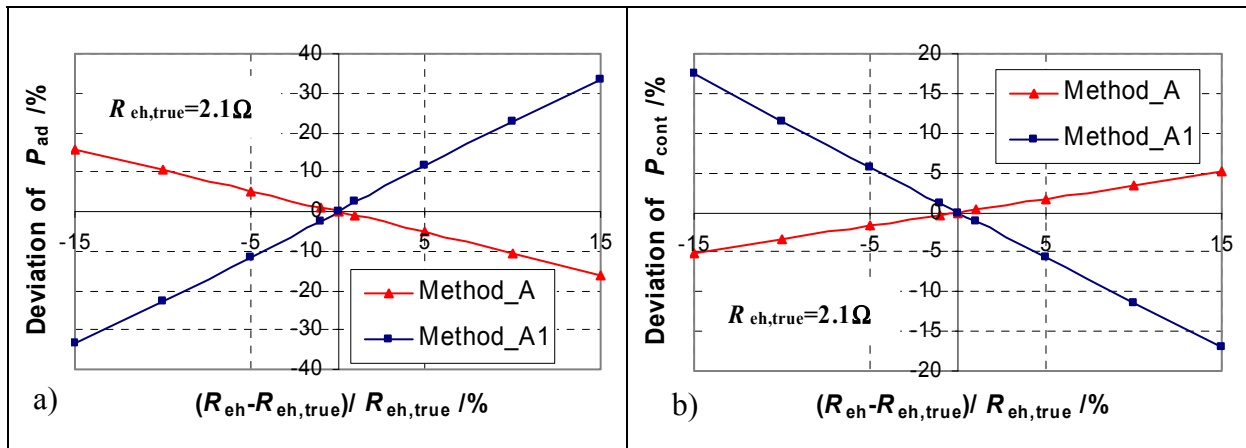
Figure 3.35: Calculated impact of error in the determination of the auxiliary resistance on the evaluation methods A and A1 for a 11 kW 4-pole motor   a) Deviation of stray load losses P_{ad} b) Deviation of check input power P_{cont}

The deviations of evaluated stray load losses with both methods A and A1 from the true P_{ad} vary linearly with the variation of the auxiliary resistance R_{eh}. A 5 % deviation of the auxiliary resistance from the true value $R_{eh,true}$ results in a -5 % deviation of the evaluated stray load losses with method A and 11 % deviation with method A1 from the „true" value P_{ad}. It corresponds to 2 % deviation of the check input power P_{cont_A} and -6 % deviation of P_{cont_A1} from the true value $P_{e,in}$. Figure 3.35 shows that the evaluation method A1 is more sensitive to an error in the determination of the auxiliary resistance R_{eh} than method A.

3.7 Comparison of methods A, A1, B and C for measured motors

The stray load losses of totally enclosed, fan-cooled standard squirrel cage induction motors (TEFC) from different manufacturers (different design) with different frame size 315 mm, 160 mm, 132 mm, 80 mm and different pole count 2, 4, 6 were measured by the eh-star method. The comparison of the evaluated stray load losses with the different methods A, A1, B and C is given for different motors in the following. As the evaluation methods A and A1 are similar and both use an auxiliary *ohmic* respectively purely *ohmic* resistance R_{eh}, these methods will be compared first.

3.7.1 Comparison of the evaluation methods A and A1 for a small and a big motor

The deviation of the measured stray load losses P_{ad_A1} evaluated with the method A1 from the values P_{ad_A} determined with the method A is presented in Table 3.9 for a small 11 kW 4-pole motor "A160-4" and in Table 3.10 for a big 315 kW 4-pole motor "A317-4". The deviation of the checked motor input power P_{cont} from the measured input power $P_{e,in}$ is also given.

In Table 3.9 and Table 3.10 the deviation of the measured stray load losses P_{ad_A1} evaluated with method A1 from the values P_{ad_A} evaluated with method A is big (11 % - 35 %). The check value of the calculated motor input power P_{cont_A1} varies for the method A1 between 2 % - 7 %, with method A only within 0.04 %. This shows clearly that method A should be preferred for the evaluation of the eh-star measurement results.

Test points	1	2	3	4	5	6
$I_2/I_{t,N}$	1.45	1.31	1.14	1.09	0.96	0.71
I_1/I_2	0.22	0.22	0.22	0.22	0.23	0.26
P_{ad_A} /W	293	236	184	167	134	80
$(P_{ad\_A1} - P_{ad\_A})/P_{ad\_A}$ /%	-29	-32	-33	-34	-35	-35
$(P_{cont\_A1} - P_{e,in})/P_{e,in}$ /%	5.53	5.76	5.99	6.10	6.33	6.53
$(P_{cont\_A} - P_{e,in})/P_{e,in}$ /%	0.03	0.04	0.04	0.04	0.04	0.04

Table 3.9: Comparison of the evaluation methods A and A1 for the measured six test points of a small 11 kW 4-pole motor "A160-4"

Test points	1	2	3	4	5	6
$I_2/I_{t,N}$	1.43	1.31	1.20	1.08	0.98	0.79
I_1/I_2	0.16	0.16	0.16	0.16	0.16	0.17
P_{ad_A} /W	3198	2656	2230	1790	1539	881
$(P_{ad\_A1} - P_{ad\_A})/P_{ad\_A}$ /%	-13	-11.3	-10.9	-11.0	-14.6	-18.7
$(P_{cont\_A1} - P_{e,in})/P_{e,in}$ /%	1.30	1.09	1.03	1.02	1.44	1.57
$(P_{cont\_A} - P_{e,in})/P_{e,in}$ /%	0.001	0.001	0.001	0.001	0.001	0.001

Table 3.10: Comparison of the evaluation methods A and A1 for the measured six test points of a big 315 kW 4-pole motor "A317-4"

The comparison of the evaluated stray load losses with the two methods A and A1 is given for different TEFC motors in Table 3.11. The deviation of the evaluated stray load losses P_{ad_A1} with the method A1 from the values determined with the method A varies, for an auxiliary *ohmic* resistance R_{eh}, between 10 % and 60 %. It corresponds to up to 10 % deviation of the check input power P_{cont_A1} from the measured input power $P_{e,in}$. The stray load loss values evaluated with the method A are reliable, as the simulation studies have shown, whereas the method A1 is leading to wrong results and should not be used.

Tested motors	A317-4	A160-4	E160-4	A160-2	C160-2	A132-6	A132-4
	315 kW, 4pole	11 kW, 4pole	11 kW, 4pole	11 kW, 2pole	11 kW, 2pole	5.5 kW, 6pole	5.5 kW, 4pole
P_{ad_A} /W	1578	133	303	188	127	72	136
$(P_{cont\_A} - P_{e,in})/P_{e,in}$ /%	0.001	0.04	0.06	0.2	0.12	0.04	0.05
P_{ad_A1} /W	1419	97	212	140	54	30	73
$(P_{cont\_A1} - P_{e,in})/P_{e,in}$ /%	1.24	6.04	10.6	7.64	8.17	7.74	8.9
$(P_{ad\_A1}-P_{ad\_A})/P_{ad\_A}$ /%	-10	-27	-30	-26	-57	-58	-46

Table 3.11: Evaluation of stray load losses with methods A and A1 for different motors

3.7.2 Influence of the unbalanced auxiliary impedance on the eh-star measurement

To investigate the impact of the phase angle φ_{eh} of the auxiliary impedance $\underline{Z}_{eh}$ on the eh-star measurement and on the evaluation of stray load losses with the two methods A and A1, two measurements with different unbalanced impedances were done:

1) An inductor with an inductance L_{ind} = 0.635 mH and a small resistive component R_{ind} = 0.042 Ohm is used in series with the *ohmic* resistance R_{eh} = 1.95 Ohm. So the influence of the resistive component of the inductance on the impedance $\underline{Z}_{eh}$ is negligible. The phase angle of the resistive-inductive auxiliary impedance is φ_{eh} = 5.6°.

2) A capacitor with the capacitance C_{cap} = 0.169 mF is used in parallel with the *ohmic* resistance R_{eh} = 1.95 Ohm. The phase angle of the resistive-capacitive auxiliary impedance is φ_{eh} = -5.9°.

Table 3.12 shows the impact of the unbalanced impedance on the eh-star measurement. The influence of the slightly resistive-inductive or slightly resistive-capacitive auxiliary impedance on the eh-star measurement is small. The deviations of the stray load losses evaluated with the method C, which is independent from the impedance type, are within 4 %. This small deviation of 4 % is also obtained with method A, where the deviation evaluated with method A1 is very big 109 % respectively 100 %. This shows clearly that method A1

should not be used for the evaluation of the eh-star measurement results.

Auxiliary impedance $\underline{Z}_{eh}$	*Ohmic*	resistor-inductor	Deviation Inductor/*Ohmic*	resistor-capacitor	Deviation Capacitor/*Ohmic*
Phase angle φ_{eh}	0.6°	5.6°		-5.9°	
I_1 / I_2	0.232	0.229	-1.38 %	0.233	0.43 %
P_{ad_A} /W	133	128	-3.56 %	127	-4.31 %
P_{ad_A1} /W	97	-9	-109 %	193	100 %
P_{ad_C} /W	133	131	-1.11 %	128	-3.96 %

Table 3.12: Impact of the unbalanced impedance $\underline{Z}_{eh}$ on the eh-star measurement for an 11 kW 4-pole motor "A160-4"

The impact of the unbalanced impedance on the evaluation of the stray load losses with the methods A and A1, compared with the evaluation method C, is given in Table 3.13 and presented in Figure 3.36. The deviation of the evaluated stray load losses with the method A1 from the method A varies, for a small phase angle φ_{eh}, between 27 % and 107 %. The check value of the calculated motor input power P_{cont_A1} varies for the method A1 between 6 % - 20 %, whereas the value P_{cont_A} evaluated with the method A varies only within 0.5 % from the measured input power $P_{e,in}$.

Auxiliary impedance $\underline{Z}_{eh}$	*Ohmic*	resistor-inductor	resistor-capacitor
Phase angle φ_{eh}	0.6°	5.6°	-5.9°
I_1 / I_2	0.232	0.229	0.233
P_{ad_A} /W	133	128	127
P_{ad_A1} /W	97	-9	193
$(P_{ad\_A1} - P_{ad\_A})/P_{ad\_A}$ /%	-27	-107	52
$(P_{ad\_C} - P_{ad\_A})/P_{ad\_A}$ /%	0.2	2.7	0.6
$(P_{cont\_A} - P_{e,in})/P_{e,in}$ /%	0.04	0.45	0.08
$(P_{cont\_A1} - P_{e,in})/P_{e,in}$ /%	6	20	-9

Table 3.13: Measured influence of the unbalanced impedance $\underline{Z}_{eh}$ on the evaluation of stray load losses with methods A and A1 for an 11 kW 4-pole motor "A160-4"
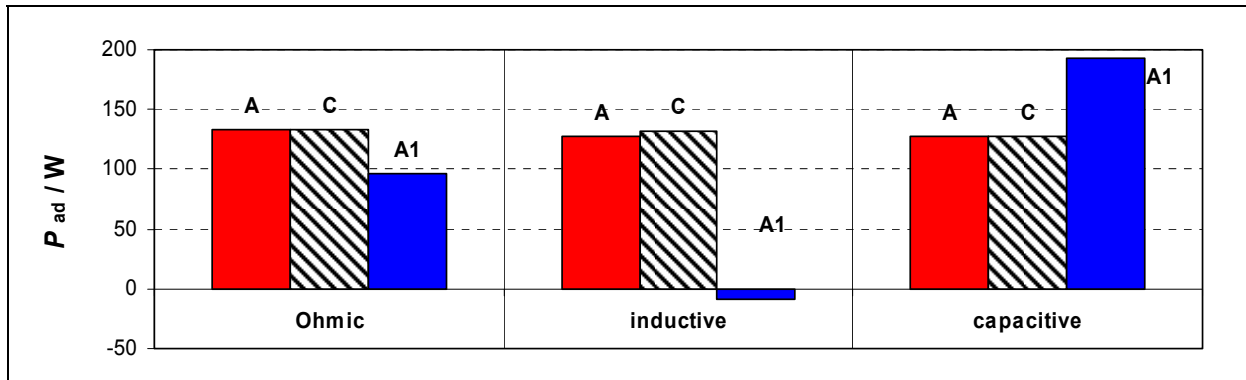
Figure 3.36: Measured impact of the unbalanced impedance $\underline{Z}_{eh}$ on the evaluation of stray load losses with methods A and A1 compared with method C for an 11 kW 4-pole motor "A160-4"

This example shows clearly, that the evaluation method A, if not method C, should be preferred for the evaluation of the eh-star measurement results. Method A1 should not be used !

3.7.3 Impact of the measurement error in electrical quantities on the evaluation methods A, A1, B and C

To show the influence of the measurement error on the evaluation of stray load losses with the different methods A, A1, B and C, an instrument accuracy of 0.2 % for electrical quantities acc. to IEC 61972 is assumed. In Table 3.14 and Table 3.15 each measured parameter is modified separately by +0.2 %. The results are presented for one load point of the eh-star measurement.

+0.2 % error		Input power	Line-to-line voltages			Phase currents		
A160-4	Method	$P_{e,in}$	U_{UV}	U_{VW}	U_{WU}	I_U	I_V	I_W
Deviation of stray load loss in %	A	-1.04	-0.69	1.09	0.34	1.50	2.83	-2.55
	A1	0.00	-10.0	9.43	0.19	-0.63	4.29	-2.69
	B	2.59	-4.22	1.04	0.31	-2.20	3.13	-2.75
	C	-1.05	-0.60	1.03	0.34	1.52	2.83	-2.55

Table 3.14: Influence of the +0.2 % measurement error on evaluated the stray load losses with methods A, A1, B and C for on load point of an 11 kW 4-pole motor "A160-4"

+0.2 % error		Input power	Line-to-line voltages			Phase currents		
A160-4	Method	$P_{e,in}$	U_{UV}	U_{VW}	U_{WU}	I_U	I_V	I_W
Deviation of check input power in %	A	0.03	0.05	0.02	0.03	0.04	0.03	0.03
	A1	5.32	6.76	4.47	5.57	5.87	5.53	5.40
	B	-0.04	0.15	0.05	0.06	0.15	0.05	0.06
	C	0.00	0.00	0.00	0.00	0.00	0.00	0.00

Table 3.15: Influence of the +0.2 % measurement error on the evaluation methods A, A1, B
and C for on load point of an 11 kW 4-pole motor "A160-4"

Table 3.14, Table 3.15 and Figure 3.37 - Figure 3.39 show that in most cases the evaluation method A1 followed by method B are more sensitive to measurement error than methods A and C. This is also given through the deviation of the check input power. The impact of measurement error on the stray load losses evaluation with the methods A and C is the same. The influence of the phase currents I_V and I_W is higher than the influence of the remaining parameters.
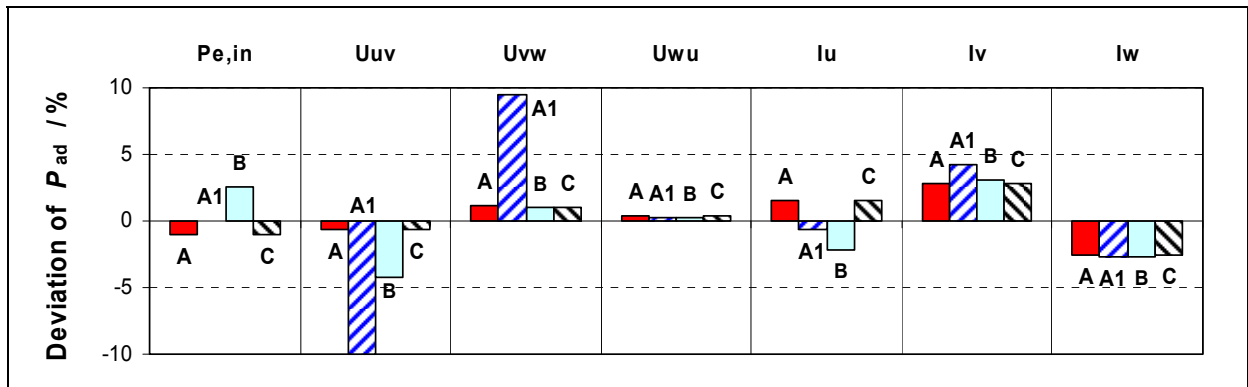
Figure 3.37: Influence of the +0.2 % measurement error on the evaluation methods A, A1, B
and C for one load point of an 11 kW 4-pole motor "A160-4" (Deviation of the
stray load losses P_{ad})
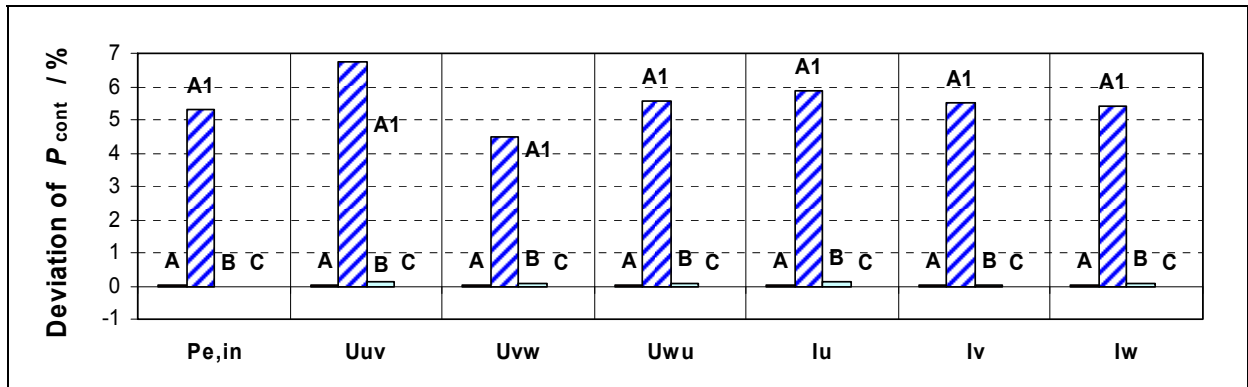
Figure 3.38: Influence of the +0.2 % measurement error on the evaluation methods A, A1, B
and C for one load point of an 11 kW 4-pole motor "A160-4" (Deviation of the
check input power P_{cont})
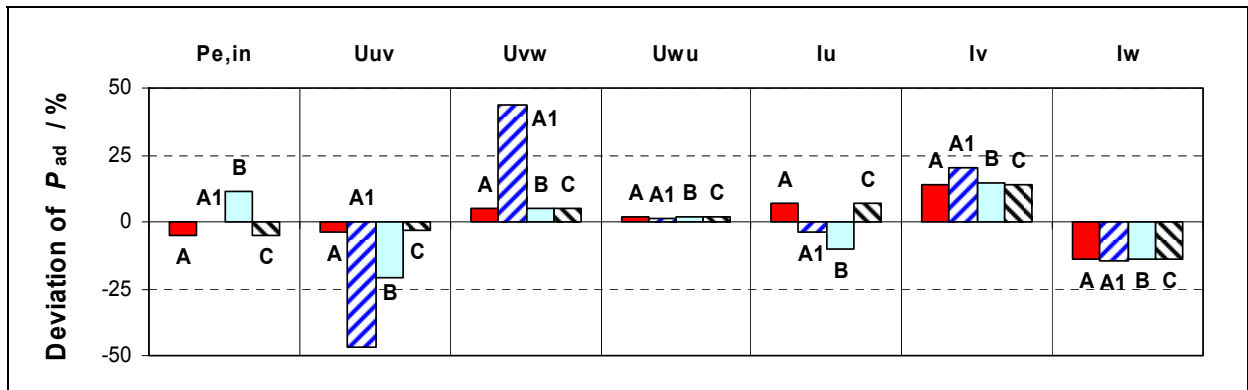
Figure 3.39: Influence of the +1 % measurement error on the stray load losses evaluated with
methods A, A1, B and C for an 11 kW 4-pole motor "A160-4" (Deviation of the
resulting stray load losses over the six test points)

For the resulting stray load losses, over six test points, the impact of +1 %
measurement error is given for different motors (1.1 kW 2-pole, 5.5 kW 6-pole,
11 kW 4-pole and 315 kW 4-pole) in Table 3.16. As the method A1 is more
sensitive to measurement error than other methods, only the methods A, B and C
are presented.

One can see in Table 3.16 that in most cases the evaluation method B is more
sensitive to measurement errors than methods A and C. The impact of the
measurement error on the stray load losses evaluation by methods A and C is the
same, and can be seen from the average values over all the motor ratings,
arranged from higher to lower, where the phase currents $I_W > I_V > I_U$ and the
voltages $U_{UV} > U_{VW} > U_{WU}$.

+1 % error	Motor/Method		$P_{e,in}$	U_{UV}	U_{VW}	U_{WU}	I_U	I_V	I_W
Deviation of the stray load loss in %	B80-2 1.1 kW	A	-0.11	-14.21	6.56	5.73	2.10	11.03	-11.42
		B	6.49	-22.77	6.64	7.43	-3.12	6.48	-7.96
		C	-0.11	-14.19	6.56	5.73	2.10	11.03	-11.42
	A132-6 5.5 kW	A	-6.49	-7.24	8.66	1.86	8.33	15.46	-15.28
		B	13.21	-25.57	8.20	1.28	-13.01	19.96	-18.14
		C	-6.55	-6.32	8.25	1.87	8.47	15.35	-15.25
	A160-4 11 kW	A	-5.25	-4.02	5.14	1.77	6.68	14.12	-14.14
		B	11.61	-20.67	5.05	1.82	-10.22	14.38	-14.19
		C	-5.30	-3.42	4.96	1.78	6.81	14.08	-14.16
	A317-4 315 kW	A	-9.59	-6.39	9.30	3.60	22.49	31.70	-43.98
		B	41.06	-54.69	9.77	1.90	-29.70	38.06	-48.73
		C	-9.59	-5.60	9.84	3.62	22.59	31.69	-43.98

Table 3.16: Influence of the +1 % measurement error on the stray load losses evaluated with methods A, B and C for different motor rating

These examples show clearly that the evaluation methods A1 and B should not be used for the evaluation of the eh-star measurement results !

3.7.4 Comparison of the evaluation methods A, B and C for measured motors

The comparison of the evaluation methods A, B and C for different measured TEFC induction motors is presented in Table 3.17.

Tested motors	A317-4	A160-2	A160-6	A160-4	E160-4	A132-6	A132-4	B80-2
	315 kW, 4pole	11 kW, 2pole	11 kW, 6pole	11 kW, 4pole	11 kW, 4pole	5.5 kW, 6pole	5.5 kW, 4pole	1.1 kW, 2pole
I_1 / I_2	0.16	0.22	0.25	0.22	0.23	0.3	0.26	0.25
P_{ad_A} /W	1578	188	133	133	303	72	136	27
$\Delta P_{cont\_A}/P_{e,in}$ /%	0.001	0.2	0.08	0.04	0.06	0.04	0.05	0.01
P_{ad_B} /W	1606	189	133	131	291	72	132	26
$\Delta P_{cont\_B}/P_{e,in}$ /%	0.01	0.01	0.01	0.06	0.1	0.01	0.09	0.1
P_{ad_C} /W	1578	190	133	133	303	72	137	27
$\Delta P_{cont\_C}/P_{e,in}$ /%	0.00	0.00	0.00	0.00	0.00	0.00	0.00	0.00
$\Delta P_{ad\_B}/P_{ad\_A}$ /%	1.8	0.12	0.08	-1.6	-3.8	-0.5	-3.1	-1.3
$\Delta P_{ad\_C}/P_{ad\_A}$ /%	0.008	0.7	0.5	0.2	0.2	0.4	0.3	0.0

Table 3.17: Evaluation of stray load losses with methods A, B and C for different motors

The deviation of the evaluated stray load losses P_{ad_A} with the simple method A from the values determined with the more accurate method C, for an auxiliary *ohmic* resistance R_{eh}, is smaller than 1 %, whereas the deviation between methods A and B is up to 4 %. This shows clearly that methods C and A should be preferred for the evaluation of the eh-star measurement results.

3.8 Influences of measurement parameters on eh-star results

In this section the influence of the value of the auxiliary resistance R_{eh}, the winding temperature on the measured stray load losses and the repeatability of the eh-star measurement will be shown.

3.8.1 Influence of the auxiliary resistance on measured stray load losses

As mentioned earlier, the value of the auxiliary resistance R_{eh} shall be adjusted, so that the proportion of the positive I_1 to the negative sequence current I_2 stays below 30 %, to get some main flux, and the speed stays typically in the range of rated speed.

The influence of the value of the auxiliary resistance R_{eh} on the measured

stray load losses is presented for different motors in Table 3.18 to Table 3.22. The data are evaluated with the method A and are given for rated load current $I_2/I_{t,N} = 1$. For some motors, especially the small 1.1 kW 2-pole motors and the 11 kW 2-pole motor "A160-2", the measurements were done with a higher value of the auxiliary resistance R_{eh} than the short circuit impedances value Z_{sc} (20 % of rated impedance) of the motors, as the motors break down from synchronous to very low speed and may overheat and the ratio I_1/I_2 increases over 0.3.

The examples in Table 3.18 to Table 3.22 show that with increasing value of the auxiliary resistance R_{eh}, the slip s, the ratio I_1/I_2 and the stray load losses P_{ad} decrease. The exception is the small 1.1 kW 2-pole motor "B80-2", where the stray load losses P_{ad} increase (see Table 3.22).

Measured motors 11 kW	A160-4				E160-4		
R_{eh}/Z_{sc}	0.04	1.0	2.11	5.06	0.04	1.22	5.26
I_1/I_2	0.4	0.23	0.19	0.29	0.34	0.23	0.27
P_{ad} /W	126	130	122	108	316	302	186
Deviation /%	-3.4	0.00	-6.3	-17	4.7	0.00	-38
Speed /rpm	1378	1464	1485	1496	1418	1468	1495
Average winding temp. /°C	35	37	38	38	36	37	36

Table 3.18: Influence of the auxiliary resistance on the measured stray load losses for 11 kW 4-pole motors "A160-4" and "E160-4"

Measured motors 11 kW	A160-2						C160-2		
R_{eh}/Z_{sc}	2.0	2.4	3.0	3.0	3.0	3.0	1.0	2.0	2.9
I_1/I_2	0.28	0.26	0.22	0.23	0.22	0.23	0.27	0.2	0.18
P_{ad} /W	202	198	188	182	184	201	127	128	110
Deviation /%	7	5	0.0	-3.3	-2.2	6.4	0.00	0.53	-14
Speed /rpm	2928	2940	2963	2964	2960	2956	2925	2964	2980
Average winding temp. /°C	66	50	50	50	54	67	47	47	43

Table 3.19: Influence of the auxiliary resistance on the measured stray load losses for 11 kW 2-pole motors "A160-2" and "C160-2"

Measured motors 5.5 kW	A132-6					B132-6		
R_{eh} / Z_{sc}	0.8	1.05	1.36	2.0	3.5	1.0	1.0	2.6
I_1 / I_2	0.36	0.32	0.28	0.26	0.27	0.49	0.52	0.34
P_{ad} /W	75	73	72	66	43.6	178	180	173
Deviation /%	3.3	0.00	-1.2	-9.6	-40	0.00	1.2	-2.9
Speed /rpm	949	961	971	981	990	924	910	979
Average winding temp. /°C	38	39	42	36	39	32	52	34

Table 3.20: Influence of the auxiliary resistance on the measured stray load losses for 5.5 kW 6-pole motors "A132-6" and "B132-6"

Measured motors 5.5 kW	C132-6			
R_{eh} / Z_{sc}	0.7	1.0	1.0	1.8
I_1 / I_2	0.29	0.27	0.27	0.25
P_{ad} /W	60	58	57	43
Deviation /%	4.13	0.00	-2.4	-26
Speed /rpm	960	969	969	979
Average winding temp. /°C	35	37	35	37

Table 3.21: Influence of the auxiliary resistance on the measured stray load losses for 5.5 kW 6-pole motor "C132-6"

Measured motors 1.1 kW	A80-2		B80-2			C80-2		D80-2	
R_{eh} / Z_{sc}	2.08	3.26	2.02	3.02	3.14	1.93	3.81	2.30	3.60
I_1 / I_2	0.23	0.21	0.26	0.25	0.25	0.33	0.26	0.41	0.28
P_{ad} /W	9.9	7.9	24.7	26.8	27.5	36.9	34.4	56.4	49.8
Deviation /%	0.00	-21	0.00	8.6	11	0.00	-7	0.00	-12
Speed /rpm	2907	2954	2910	2950	2955	2833	2950	2714	2870
Average winding temp. /°C	43	42	40	37	39	44	45	36	37

Table 3.22: Influence of the auxiliary resistance on the measured stray load losses for 1.1 kW 2-pole motors

   The influence of the value of the auxiliary resistance R_{eh} on the measured stray load losses at small variation of the auxiliary resistance R_{eh} is not big, as long as the ratio I_1/I_2 is sufficiently small (< 0.3) and the speed stays in the range of the rated speed.

3.8.2 Impact of the winding temperature determination on the eh-star evaluation

Due to the asymmetric operation during the eh-star test, the heating of the three phase resistances is unequal. The maximum current flows in the phase V during the asymmetric eh-star test, in the phase U flows the medium current and in the phase W flows the minimum current. This leads to different heating of the three phase windings. For more accurate evaluation of the stray load losses, one should measure all three phase resistances separately for each test point. As this is too much effort for an economic test procedure, the temperature is measured at the beginning and end of the test. The average value of the hottest phase V and the coldest phase W leads to an "average" temperature rise for calculating the stator winding resistive losses ! So the line-to-line resistance between terminals V and W is used. For the test points between the first load point $I_V/I_N = 1.5$ and the fifth load point $I_V/I_N = 1.0$ the linear interpolation of the temperature is used (see Figure 3.14 and Figure 3.40).

Note:

It is not recommended to determine the winding temperature from the reading of thermocouples, due to the unequal heating of the three phases, if their positions are unknown (see Figure 3.40). Only if the positions of the thermocouples are exactly known, then the use of thermocouples could be recommended.

The determined winding temperature of each phase for the last measured load point (at the end of the test) is exact, due to the extrapolation of the measured resistances to the zero-switch-off time. On the basis of this load point ($I_V/I_N = 0.75$) a comparison of the impact of the winding temperature determination, from the measured resistance of all the three phases separately and of the line-to-line resistance VW (as average value), on the stray load losses is given for an 11 kW 4-pole motor "A160-4" in Table 3.23.

Measured motor A160-4	Winding temperature determined from measured			
	Line-to-line resistance	Phase resistances		
Winding temperature / °C	VW	U	V	W
	46.7	45.8	50.0	43.4
Stray load losses P_{ad_A} /W	78.55	78.35		
Deviation	0.25 %			

Table 3.23: Impact of the winding temperature determination on the eh-star evaluation for an 11 kW 4-pole motor "A160-4" at end of the test ($I_2/I_{tN} = 0.7$)

The influence of the winding temperature determination from the measured resistance of all the three phases separately and of the line-to-line resistance *VW* (as average value) on the resulting stray load losses at rated load current ($I_2/I_{tN} = 1$) is given for an 11 kW 4-pole motor "A160-4" in Table 3.24.

The deviations presented in Table 3.23 and Table 3.24 are identical, so the measurement of the line-to-line resistance *VW* is completely sufficient.

Measured motor A160-4	Winding temperature determined from measured			
	Line-to-line resistance	Phase resistances		
Average winding temperature / °C	VW	U	V	W
	42.1	41.6	43.7	40.4
Stray load losses P_{ad_A} /W	134.95	135.09		
Deviation	-0.106 %			

Table 3.24: Impact of the winding temperature determination on the eh-star evaluation for an 11 kW 4-pole motor "A160-4" at rated load ($I_2/I_{tN} = 1$)

The winding temperature determined from the measured line-to-line resistance *VW* and the reading (average value) of two thermocouples placed in the winding overhang (on the drive and non drive sides), where the exact positions are unknown, is shown for an 11 kW 4-pole motor "D160-4" in Figure 3.40. The deviation of the stray load losses is about 13 %.
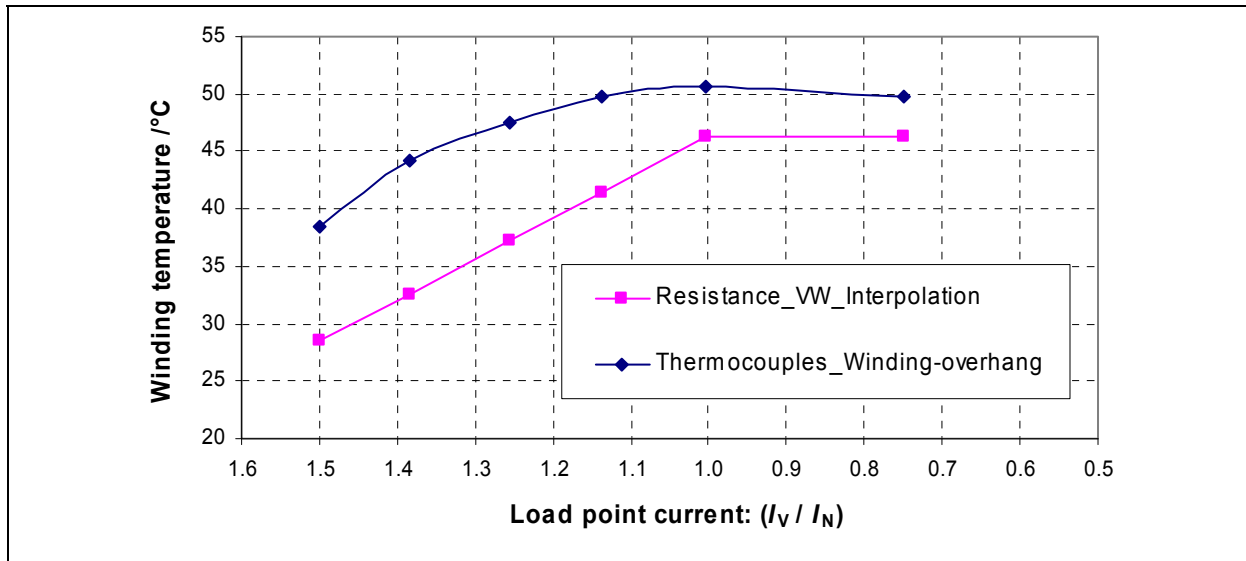
Figure 3.40: Influence of the winding temperature determination on the stray load losses for
an 11 kW 4-pole motor "D160-4"

3.8.3 Impact of the winding temperature on the stray load losses

To show the influence of the winding temperature on the eh-star test, four
measurements at different temperatures were done. The measurement time for
each test is the same, so the temperature difference ϑ_{diff} ($= \vartheta_{\text{end}} - \vartheta_{\text{begin}}$) is
determined only by the current flow during the test.

The influence of the winding temperature on the stray load losses
measurement is given in Table 3.25 and presented in the Figure 3.41. The
deviation of the stray load losses is related to the measurement "warm" as
typical value of the no load test temperature.

A160-4	ϑ_{begin} /°C	ϑ_{end} /°C	ϑ_{av} /°C	ϑ_{diff} /°C	$P_{\text{ad\_A}}$ /W	Offset /W	$\Delta P_{\text{ad\_A}}$/warm
Cold	27.7	40.2	34.0	12.5	129.85	17.13	-2.70 %
Warm	37.9	48.3	43.1	10.4	133.45	9.41	0.00 %
Warm1	46.8	54.4	50.6	7.6	135.16	4.23	1.28%
Warm2	61.9	64.8	63.3	3.0	135.98	-0.59	1.90 %

Table 3.25: Influence of the winding temperature on the stray load losses for an 11 kW 4-pole
motor "A160-4"

Table 3.25 shows that a 20 K variation of the average winding temperature

ϑ_{av} at warm motor corresponds to 2 % deviation of evaluated stray load losses, and a 30 K variation of ϑ_{av} at cold motor leads to about 5 % deviation of evaluated stray load losses. It had to be noted, that there is a dependence between the temperature difference ϑ_{diff} and the offset (the offset is the intercept of the measured curve $P_{ad} = f((I_2/I_{t,N})^2)$ with the ordinate). The smaller the temperature difference ϑ_{diff}, the less the offset.
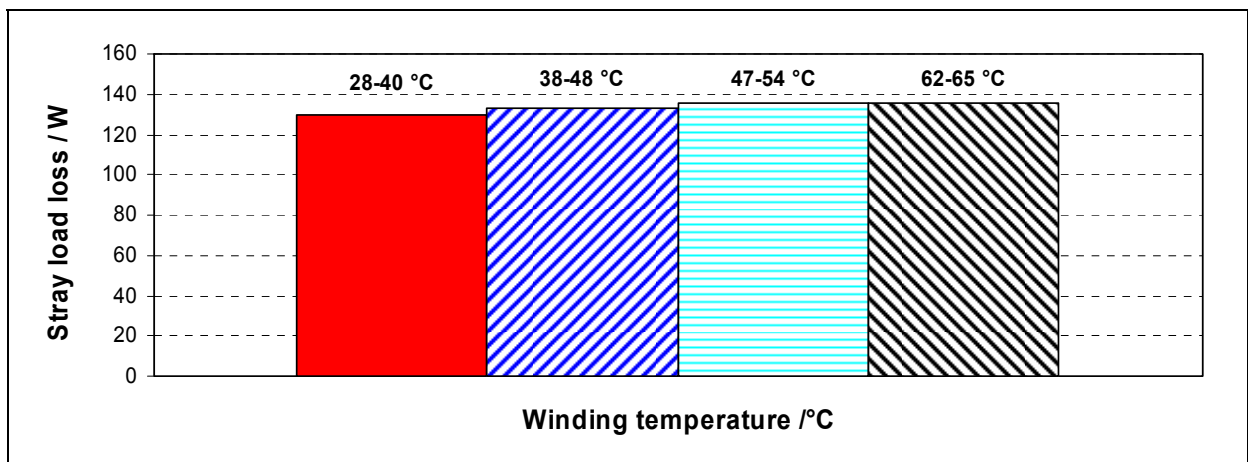
Figure 3.41: Influence of the winding temperature on the stray load losses for an 11 kW 4-pole motor "A160-4"

The impact of the winding temperature on the stray load losses measurement is given for the 11 kW 2-pole motors "A160-2", "B160-2" and the 5.5 kW 6-pole motors "B132-6", "D132-6" in Table 3.26 and for a 55 kW 2-pole motor in Table 3.28 and presented in the Figure 3.42.

Measured motors 11 kW	A160-2				B160-2	
I_1 / I_2	0.22	0.23	0.22	0.23	0.21	0.21
P_{ad} /W	188	182	184	201	102	110
Deviation /%	0.0	-3.3	-2.2	6.4	0.0	7.4
Speed /rpm	2963	2964	2960	2956	2957	2947
Average winding temp. /°C	50	50	54	67	37	52
Begin-End winding temp. /°C	42-58	41-58	41-66	56-78	25-50	42-62

Table 3.26: Influence of the winding temperature on the measured stray load losses for 11 kW 2-pole motors "A160-2" and "B160-2"

Measured motors 5.5 kW	B132-6		D132-6	
I_1 / I_2	0.49	0.52	0.26	0.26
P_{ad} /W	178	181	39	41
Deviation /%	0.0	1.2	0.0	3.7
Speed /rpm	924	910	973	973
Average winding temp. /°C	32	52	34	49
Begin-End winding temp. /°C	25-39	50-54	26-43	44-54

Table 3.27: Influence of the winding temperature on the measured stray load losses for 5.5 kW
6-pole motors "B132-6" and "D132-6"

Measured motor 55 kW 2-pole motor, 60 Hz				
I_1 / I_2	0.26	0.25	0.24	0.25
P_{ad} /W	788	824	843	791
Deviation /%	-6.5	-2.2	0.00	-6.2
Speed /rpm	3574	3577	3580	3575
Average winding temperature /°C	37	25	44	56
Begin-End winding temperature /°C	21-53	23-28	43-45	46-66

Table 3.28: Influence of the winding temperature on the measured stray load losses for a 55
kW 2-pole motor, 60 Hz (Measurement done by P. Angers, LTE-Hydro-Québec,
Institut de recherche Canada, 2007 [Ange 2007])
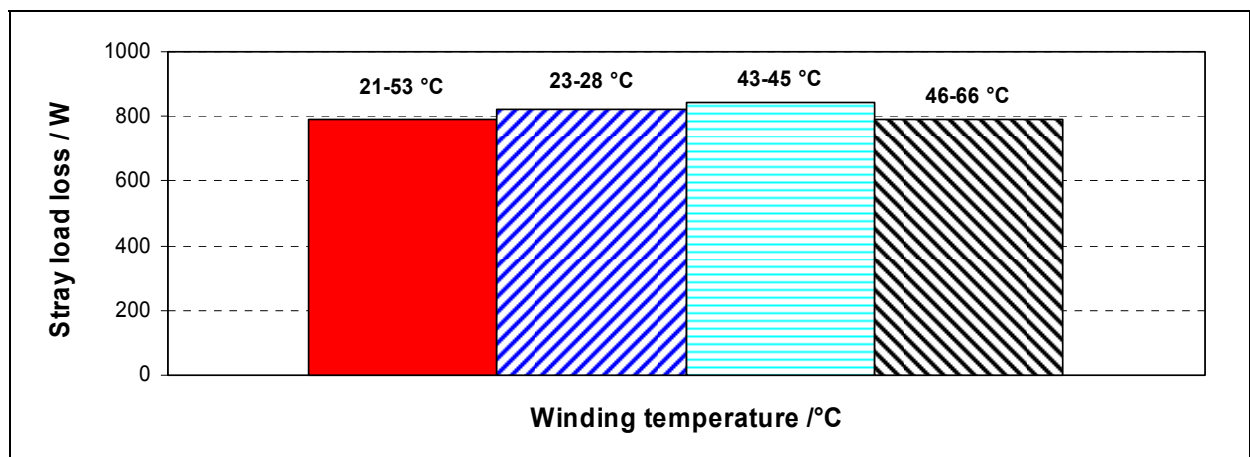
Figure 3.42: Influence of the winding temperature on the stray load losses for a 55 kW 2-pole
motor, 60 Hz (Measurement done by P. Angers, LTE-Hydro-Québec, Institut de
recherche Canada, 2007 [Ange 2007])

3.8.4 Repeatability and the impact of the measurement circuit on the eh-star test

The input power was measured with different circuits to check the repeatability of the results and the impact of the measurement circuit on the eh-star test:

1) in *Aron*-circuit with phase *V* as common phase (Figure 3.13),

2) in *Aron*-circuit with phase *W* as common phase and

3) with the 3-wattmeter-method with a "virtual" star point adapter of the measurement device.

The measurement results are depicted in the Table 3.29, Table 3.30 and Table 3.31 for different motors at different auxiliary resistance R_{eh}. The variation of the stray load losses ΔP_{ad} is related, for each value of the auxiliary resistance R_{eh}, to the result of the measurement in *Aron*-circuit with the phase *V* as common phase (*Aron_V*).

Tested motor	A160-4								
	$R_{eh} / Z_{sc} = 1.0$			$R_{eh} / Z_{sc} = 0.04$			$R_{eh} / Z_{sc} = 5.06$		
	P_{ad} /W	ΔP_{ad} /%	ϑ_{av} /°C	P_{ad} /W	ΔP_{ad} /%	ϑ_{av} /°C	P_{ad} /W	ΔP_{ad} /%	ϑ_{av} /°C
*Aron*_V	132.8	0.0	36	123.4	0.0	35	112.9	0.0	36
*Aron*_W	129.9	-2.2	37	125.5	1.7	35	107.6	-4.7	38
3wattmeter	130.4/129.7	-1.8	35	126.2	2.2	34	112.4	-0.4	37

Table 3.29: Repeatability and the influence of the measurement circuit on the measured stray load losses for 11 kW 4-pole motor "A160-4"

| Tested motor | E160-4 | | | | | | | | |
| | $R_{eh} / Z_{sc} = 1.22$ | | | $R_{eh} / Z_{sc} = 0.04$ | | | $R_{eh} / Z_{sc} = 5.26$ | | |
	P_{ad} /W	ΔP_{ad} /%	ϑ_{av} /°C	P_{ad} /W	ΔP_{ad} /%	ϑ_{av} /°C	P_{ad} /W	ΔP_{ad} /%	ϑ_{av} /°C
*Aron*_V	302.6	0.0	36	305/303	0.0	36	180.6	0.0	37
*Aron*_W	307	1.48	36	316.5	3.9	36			
3wattmeter	302	-0.2	37	316/304	3.8	36	185.9	2.6	36

Table 3.30: Repeatability and the influence of the measurement circuit on the measured stray
load losses for 11 kW 4-pole motor "E160-4"

| Tested motor | A132-6 | | | | | | | | |
| | $R_{eh} / Z_{sc} = 1.05$ | | | $R_{eh} / Z_{sc} = 0.8$ | | | $R_{eh} / Z_{sc} = 3.5$ | | |
	P_{ad} /W	ΔP_{ad} /%	ϑ_{av} /°C	P_{ad} /W	ΔP_{ad} /%	ϑ_{av} /°C	P_{ad} /W	ΔP_{ad} /%	ϑ_{av} /°C
*Aron*_V	72.1	0.0	39	74.1	0.0	40	47.5	0.0	40
*Aron*_W	72.1	-0.05	39	76.3	3.0	40	45.8	-3.6	42
3wattmeter	72.8	0.9	39	75.2	1.5	38			

Table 3.31: Repeatability and the influence of the measurement circuit on the measured stray
load losses for 5.5 kW 6-pole motor "A132-6"

The results of Table 3.29 to Table 3.31 show that the variation of the stray
load losses ΔP_{ad}, especially at $R_{eh} / Z_{sc} = 1$, is small; and is within 5 % for other
values of the auxiliary resistance R_{eh}. So the repeatability of the measurements is
good.

3.9 Measured stray load losses for different motors

The stray load losses measured with the eh-star method at rated load current
($I_2/I_{t,N} = 1$) are presented for different motors in Table 3.32 to Table 3.35. For
some motors the measurement was repeated several times, in the following one
measurement is depicted.

Measured motors	A317-4	90 kW 6-pole, 50 Hz *)	55 kW 2-pole, 60 Hz *)	37 kW 4-pole, 60 Hz *)
I_1 / I_2	0.16	Not specified	0.24	Not specified
Stray load losses /W	1578	1466	843	377
Speed /rpm	1490	Not specified	3580	Not specified
Average winding temp. /°C	102	59	44	36

Table 3.32: Measured stray load losses for 11 kW 4-pole motors at rated load ($I_2/I_{tN} = 1$)

*): Measurement done by P. Angers, LTE-Hydro-Québec, Institut de recherche Canada, 2007 [Ange 2007]

11 kW 4-pole motors	A160-4	B160-4	C160-4	D160-4	E160-4
I_1 / I_2	0.23	0.24	0.24	0.22	0.23
Stray load losses /W	133	104	121	128	302
Speed /rpm	1463	1474	1465	1475	1468
Average winding temp. /°C	43	36	41	37	37

Table 3.33: Measured stray load losses for 11 kW 4-pole motors at rated load ($I_2/I_{tN} = 1$)

11 kW 2- & 6-pole motors	A160-2	B160-2	C160-2	D160-2	A160-6
I_1 / I_2	0.22	0.21	0.27	0.2	0.25
Stray load losses /W	188	102	127	501	127
Speed /rpm	2963	2957	2925	2963	978
Average winding temp. /°C	50	37	47	49	38

Table 3.34: Measured stray load loss for 11 kW 2- and 6-pole motors at rated load ($I_2/I_{tN} = 1$)

5.5 kW 4- & 6-pole motors	A132-6	B132-6	C132-6	D132-6	A132-4
I_1 / I_2	0.28	0.34	0.27	0.26	0.26
Stray load losses /W	72	173	58	41	136
Speed /rpm	971	979	969	973	1433
Average winding temp. /°C	42	34	37	49	40

Table 3.35: Measured stray load loss for 5.5 kW 4- and 6 pole motors at rated load ($I_2/I_{tN} = 1$)

The measured stray load losses for the small motors, 1.1 kW - 0.37 kW, are presented in Table 3.36 to Table 3.38. The measured losses for the 0.55 kW 4-pole and the 0.37 kW 6-pole motor are very small (only some Watt), so the

measurement uncertainty increased. The measurements were repeated several times with other averaging times, with different auxiliary resistance values and for some motors on another day to get a better correlation coefficient. With decreasing power ratings the minimum value of positive vs. negative sequence current, which should stay below 30 %, increases, being about 35 % at 0.55 kW motors and 45 % at 0.37 kW motors. This may lead to too low stray load losses.

1.1 kW, 2-pole motors	A80-2	B80-2	C80-2	D80-2
I_1 / I_2	0.23 / **0.21**	0.26 / **0.25**	0.33 / **0.26**	0.41 / **0.28**
Stray load losses /W	9.9 / **7.9**	24.7 / **27**	36.9 / **34**	56.4 / **50**
Speed /rpm	2907 / 2954	2910 / 2955	2833 / 2950	2714 / 2870
Average winding temp. /°C	43 / 42	40 / 39	44 / 45	36 / 37

Table 3.36: Measured stray load losses for 1.1 kW 2-pole motors at rated load ($I_2/I_{tN} = 1$). Bold letters are results of the measurement at an auxiliary resistance, where the ratio I_1/I_2 is minimum.

0.55 kW 4-pole motors	A80-4	B80-4	C80-4	D80-4
I_1 / I_2	0.49 / **0.36**	**0.35**	0.37 / **0.33**	**0.34**
Stray load losses /W	3.5 / **2.9**	**8.3**	2.2 / **1.5**	**14.8 / 16.5**
Speed /rpm	1331 / 1436	1442	1384 / 1430	1433
Average winding temp. /°C	36	36	39 / 42	37 / 39

Table 3.37: Measured stray load losses for 0.55 kW 4-pole motors at rated load ($I_2/I_{tN} = 1$). Bold letters are results of the measurement at an auxiliary resistance, where the ratio I_1/I_2 is minimum.

0.37 kW 6-pole motors	A80-6	B80-6	C80-6	D80-6
I_1 / I_2	0.45 / **0.42**	**0.39**	0.44 / **0.43**	0.5 / **0.47**
Stray load losses /W	0.8 / **0.8**	**2.2**	0.6 / **0.5**	1 / **0.5**
Speed /rpm	904 / 944	961	932 / 949	898 / 941
Average winding temp. /°C	38	43	39	39

Table 3.38: Measured stray load losses for 0.37 kW 6-pole motors at rated load ($I_2/I_{tN} = 1$). Bold letters are results of the measurement at an auxiliary resistance, where the ratio I_1/I_2 is minimum.

3.10 Harmonic factors during the eh-star test

The quality of the voltage supply influencing the performance of the motors shall comply with the demands of the harmonic voltage factor, defined in IEC 60034-1. The measured harmonic voltage factor of the open circuit voltage of the feeding transformer is $HVF = 0.8\% < 2\%$, which complies with the standard IEC 60034-1.

The measured harmonic voltage factor (HVF) and the harmonic current factor (HCF) acc. to IEC 60034-1, during the eh-star test, are presented in Table 3.39. They are generated mainly due to the induction of the rotor slot harmonics in the stator winding. The increase of the measured additional losses correlates well with an increase of the slot harmonic effects within the machine.

Measured motors	A160-4	C160-4	D160-4	E160-4	A132-4
P_{ad} / P_N /%	1.2	1.1	1.16	2.7	2.5
HVF < 0.02	0.01	0.008	0.011	0.015	0.016
HCF	0.033	0.013	0.044	0.055	0.068

Table 3.39: Measured harmonic factors HVF and HCF for different motors.

For the 4-pole motors 11 kW "E160-4" and 5.5 kW "A132-4" in Table 3.39 the harmonic current factor (HCF) during the eh-star test is higher due to the increased rotor slot harmonic amplitudes.

A comparison of the waveform of the stator currents and the voltages during the eh-star test, at the phase current $I_V = 150\%$ of the rated current I_N, for two 11 kW 4-pole motors "A160-4" and "E160-4" is given in the Figure 3.43 and Figure 3.44. In the shape of the waveform the effect of the slot harmonics is visible.
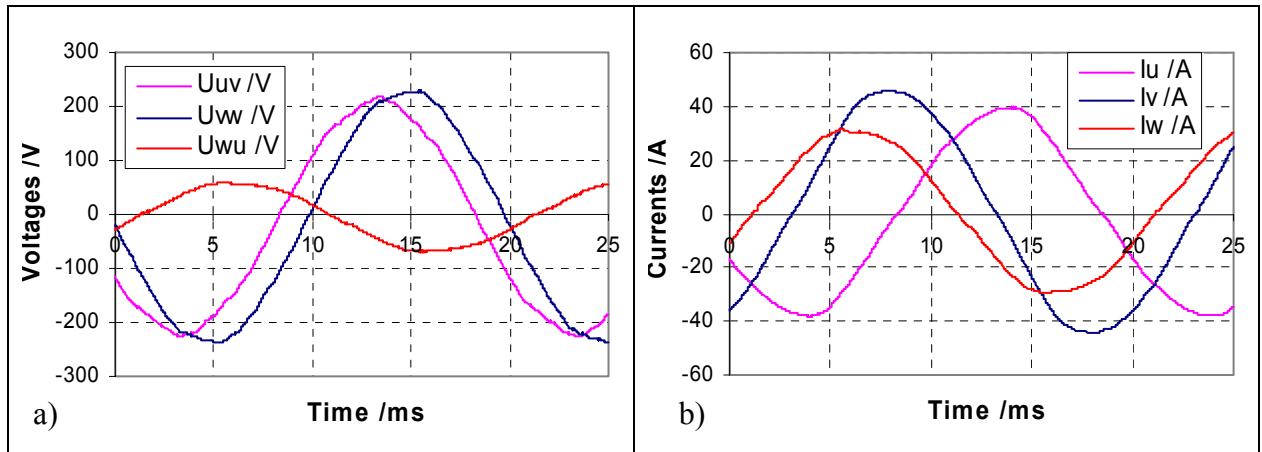
Figure 3.43: Measured waveform of the stator currents and voltages at eh-star test for an 11 kW 4-pole motor "A160-4". The variables are successively measured, thus no information about the phase angle   a) Waveform of the stator line to line voltages b) Waveform of the stator phase current
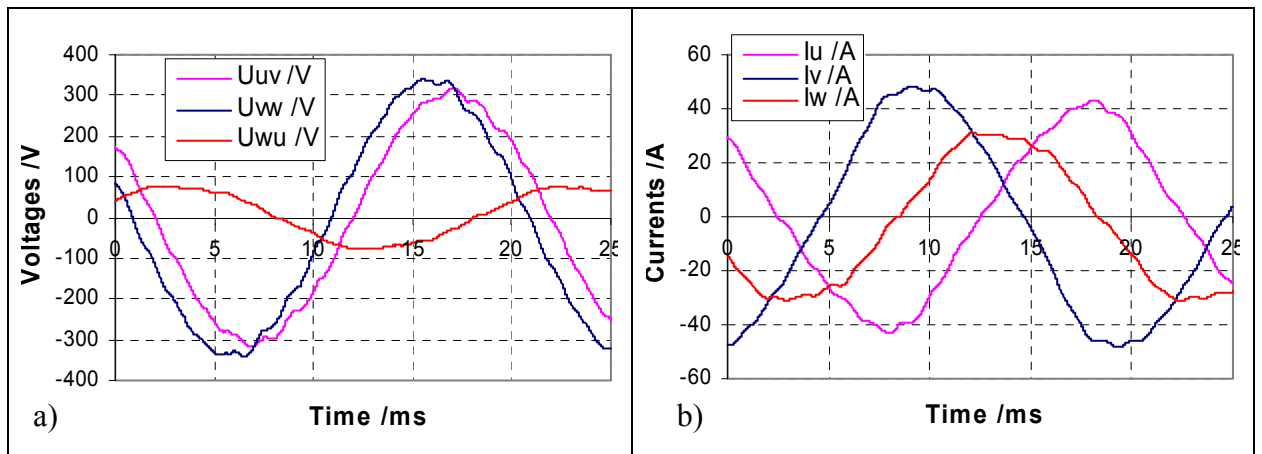
Figure 3.44: Measured waveform of the stator currents and voltages at eh-star test for an 11 kW 4-pole motor "E160-4". The variables are successively measured, thus no information about the phase angle   a) Waveform of the stator line to line voltages b) Waveform of the stator phase current

3.11 Conclusion

The theoretical background and the test procedure of the eh-star method, as an equivalent measurement method to determine the stray load losses, are described in detail. With theoretical and measurement examples a comparison of different evaluation methods A, A1, B and C for the complex current and

voltage phasor determination from the measured r.m.s. current and voltage values is given for the eh-star test post-processing. A checking parameter, the calculated „check" input power P_{cont}, is a good indicator for the accuracy of the calculation-model for the loss balance and of the measurement. The „check" input power P_{cont} should be identical with the measured motor input power $P_{e,in}$ within 1 %.

Method A is useful for an auxiliary *ohmic* resistance R_{eh} and is based, for determination of loss separation, on the measured motor input power $P_{e,in}$. The method A1 needs a purely *ohmic* resistance R_{eh}, whereas the measurement of the input power $P_{e,in}$ is not necessary. In case of using an impedance $\underline{Z}_{eh}$, its resistive component R_{eh} has to be determined as average value of the measured resistances $R_{eh,begin}$ at the beginning and $R_{eh,end}$ at the end $R_{eh,end}$ of the measurement to equalize the temperature influence. In case of slightly resistive-capacitive or slightly resistive-inductive impedance with a phase angle $-10° \leq \varphi_{eh} \leq 10°$ the deviation of evaluated stray load losses with method A from the „true" value is smaller than 2 %. The investigations show that method A1 should not be used for the eh-star measurement evaluation.

For the methods B and C instead of the resistance R_{eh} an impedance $\underline{Z}_{eh}$ (inductor, capacitor or resistor) may be used. The evaluation of stray load losses is independent from the impedance value $\underline{Z}_{eh}$. In method B, which is based on the measured two line-to-line motor input power values P_{e,in_UV} and P_{e,in_WV}, one equation more than unknown parameters exists. This leads either to small deviations in the calculated value of the currents from the measured ones, or the sum of all three calculated phase currents differs slightly from zero. The evaluation method C, where only the measured motor input power $P_{e,in}$ is needed, is the more accurate one.

The influence of different parameters (e.g. the unbalanced auxiliary impedance $\underline{Z}_{eh}$, the value of the impedance, the temperature…) on the stray load losses was shown. Different motor power ratings (315 kW – 0.37 kW) were investigated. For the small motor ratings below 0.55 kW, the eh-star method should not be used for the determination of the stray load losses.

4   COMPARISON OF DIFFERENT MEASUREMENT METHODS FOR EFFICIENCY DETERMINATION

In this chapter the measurement results of different standard TEFC grid-operated cage induction motors (2-, 4- and 6-pole) of current design from six European manufacturers with rated power 0.37 kW, 0.55 kW, 1.1 kW, 5.5 kW and 11 kW will be presented. The stray load losses are determined with the six experimental measurement procedures described in the previous chapter:

1. residual loss method acc. to IEC 60034-2 Ed. 4.0 draft/ IEC 61972,
2. residual loss method acc. to the standard IEEE 112 method B [IEEE 112],
3. reverse rotation test acc. to the standard IEEE 112 and IEC 61972,
4. eh-star method acc. to *Jordan* and *Richter* [Jord 1967, IEC 60034-2 draft],
5. equivalent no-load method acc. to *Bourne* [Bour 1989]
6. and the equivalent no-load method according to *Rawcliffe* and *Menon* [Rawc 1952].

In addition some measurements for one 315 kW four pole standard induction motor and two 1500 kW six pole wind generators are presented.

4.1 Test objects

The set of the tested grid-operated, low voltage squirrel-cage induction machines are:

- Two 1500 kW six pole wind generators. The tests were done in the test field of the manufacturer.

- One 315 kW four pole standard induction motor. The tests were done in the test field of the manufacturer.

- Five 11 kW four pole, four 11 kW two pole and one 11 kW six pole standard induction motors.

- Four 5.5 kW six pole and one 5.5 kW four pole standard induction motors.

- Four 1.1 kW two pole standard induction motors.

- Four 0.55 kW four pole standard induction motors.

- Four 0.37 kW six pole standard induction motors.

The tests of the motors with ratings between 11 kW and 0.37 kW were done in the power lab of the *department of Electrical Energy Conversion at Darmstadt University of Technology*.

To present the test results in anonymous way for the motors supplied by different manufacturers (A, B, C, D and E), a marking of the motor based on the frame size and pole number is given:

11 kW, 4-pole, frame size 160 mm, manufacturer A ... E: e.g. A160-4.
11 kW, 2-pole, frame size 160 mm, manufacturer A ... D: e.g. D160-2.
11 kW, 6-pole, frame size 160 mm, manufacturer A: A160-6.
5.5 kW, 6-pole, frame size 132 mm, manufacturer A ... D: e.g. C132-6.
5.5 kW, 4-pole, frame size 132 mm, manufacturer A: A132-4.
1.1 kW, 2-pole, frame size 80 mm, manufacturer A ... D: e.g. B80-2.
0.55 kW, 4-pole, frame size 80 mm, manufacturer A ... D: e.g. C80-4.
0.37 kW, 6-pole, frame size 80 mm, manufacturer A ... D: e.g. D80-6.

The manufacturer marking (A, B, C, D and E) could be changed between one machine rating to another.

The design data of the 11 kW, 4-pole die-cast motors are summarized in Table 4.1, where Q_s, Q_r are the slot numbers, s_{Qs}, s_{Qr} the slot openings of the stator and the rotor respectively, δ is the air gap, l_{Fe} the iron stack length and D_{si} the diameter of the stator bore.

	A160-4	B160-4	C160-4	D160-4	E160-4
Q_s / Q_r	48 / 40	36 / 28	48 / 40	48 / 36	36 / 28
Ratio: s_{Qs}/δ	6.2	6.6	5.6	7.0	8.6
s_{Qr} /mm	0	0	1.5	0	0
l_{Fe} / D_{si} /mm	200 / 125	180 / 165	194 / 128	135 / 143.5	200 / 130

Table 4.1: Design data of the measured 11 kW, 4-pole motors "X160-4"

4.2 Performed measurements

During this study the following tests were performed:

a) No-load test to determine the no-load losses e.g. acc. to IEC 60034-2 Ed. 4.0 draft [IEC 60034-2 draft].

b) Rated load temperature test to determine the steady state temperature rise e.g. IEC 60034-1, -2 [IEC 60034-1, IEC 60034-2].

c) Indirect measurement of the stray load losses using the "residual loss method" acc. to IEC 60034-2 Ed. 4.0 draft [IEC 60034-2 draft]/ IEC 61972 [IEC 61972] and acc. IEEE 112-method B [IEEE 112].

d) Direct measurement of the stray load losses using the "Reverse Rotation Test" (RRT) acc. to IEEE 112 and acc. to IEC 60034-2 Ed. 4.0 draft [IEC 60034-2 draft]/ IEC 61972 [IEC 61972].

e) Direct measurement of the stray load losses using the "eh-star method" based on the publication of *Jordan* and *Richter* [Jord 1967] and acc. to the guideline [Guid 2005].

f) Direct measurement of the stray load losses using the "equivalent no-load method" acc. to *Bourne* [Bour 1989].

g) Direct measurement of the stray load losses using the "equivalent no-load method" acc. to *Rawcliffe* and *Menon* [Rawc 1952].

Table 4.2 shows the rated power, the pole-count, the number of tested motors and the tests performed.

Power /kW	0.37	0.55	1.1	5.5	5.5	11	11	11
Pole count	6	4	2	6	4	6	4	2
Number of motors	4	4	4	4	1	1	5	4
Input-output test (residual loss method)	√	√	√	√	√	√	√	√
RRT	√	√	√	√	√	√	√	√
Eh-star	√	√	√	√	√	√	√	√
Equivalent no-load of *Bourne*	√	√	(√)	(√)	NM	√	(√)	(√)
Equivalent no-load of *Rawcliffe*	√	(√)	(√)	(√)	√	√	(√)	(√)

Table 4.2: Tested motors and the performed tests
(√): Some of the motors are measured; NM: not measured.

4.2.1 No-load test

The no-load measurement at variable voltage and 50 Hz grid-frequency was performed according to the standards IEC 60034-2 Ed. 4.0 draft/ IEC 61972 and IEEE 112.

Following tables show the rated voltage and the rated current (name plate) for the tested machine, the measured winding resistance as the average value of the three phases for a cold machine at 20°C winding temperature, the terminal connection and the no-load losses segregation (iron, friction and windage losses) according to the standard IEC 61972.

11 kW 4-pole motors	A160-4	B160-4	C160-4	D160-4	E160-4
Rated U /V / I /A, Y	400 / 21.4	690 / 12.1	690 / 12	690 / 12.4	400 / 22.5
Phase resistance @ 20°C /Ω	0.362	0.794	1.145	1.094	0.335
Iron losses /W	327	222	298	341	243
Friction losses /W	70	93	98	62	63

Table 4.3: No-load loss segregation acc. to IEC 61972 for 11 kW, 4-pole motors

11 kW 2- & 6-pole motors	A160-2	B160-2	C160-2	D160-2	A160-**6**
Rated U/V / I/A, Y	690 / 11.5	400 / 21.7	690 / 12.5	400 / 21.2	690 / 13.6
Phase resistance @ 20°C /Ω	0.9117	0.3247	1.088	0.3614	1.1528
Iron losses /W	320	367	380	196	399
Friction losses /W	311	168	264	287	27

Table 4.4: No-load loss segregation acc. to IEC 61972 for 11 kW, 2-pole and 6-pole motors

5.5 kW 6- & 4-pole motors	A132-6	B132-6	C132-6	D132-6	A132-**4**
Rated U/V / I/A, Y	690 / 7	400 / 13.8	690 / 7.7	400 / 13.4	690 / 8.6
Phase resistance @ 20°C /Ω	2.5454	0.6296	2.5058	0.6568	2.765
Iron losses /W	311	321	274	208	182
Friction losses /W	49	26	14	36	49

Table 4.5: No-load loss segregation acc. to IEC 61972 for 5.5 kW, 6-pole and 4-pole motors

1.1 kW 2-pole motors	A80-2	B80-2	C80-2	D80-2
Rated U/V / I/A, Δ	231 / 4.43	231 / 4.27	231 / 4.32	231 / 4.9
Phase resistance @ 20°C /Ω	6.518	6.109	6.193	7.034
Iron losses /W	98	87	101	136
Friction losses /W	14	15	14	16

Table 4.6: No-load loss segregation acc. to IEC 61972 for 1.1 kW, 2-pole motors

0.55 kW 4-pole motors	A80-4	B80-4	C80-4	D80-4
Rated U/V / I/A, Δ	231 / 2.89	231 / 2.76	231 / 2.65	231 / 2.67
Phase resistance @ 20°C /Ω	13.876	14.38	19.328	13.866
Iron losses /W	75	57	65	49
Friction losses /W	8	3	4	6

Table 4.7: No-load loss segregation acc. to IEC 61972 for 0.55 kW, 4-pole motors

0.37 kW 6-pole motors	A80-6	B80-6	C80-6	D80-6
Rated U/V / I/A, Δ	231 / 2.14	231 / 2.2	231 / 2.22	231 / 2.16
Phase resistance @ 20°C /Ω	25.92	25.412	27.929	23.097
Iron losses /W	50	47	46	43
Friction losses /W	3	3	2	4

Table 4.8: No-load loss segregation acc. to IEC 61972 for 0.37 kW, 6-pole motors

4.2.2 Rated load temperature test

The rated load temperature test is performed to determine the steady state temperature rise according to the standards IEC 61972 and IEEE 112 where a rated load (rated output power) is applied with a dynamometer until thermally stable condition is reached (e.g. see Figure 4.1).
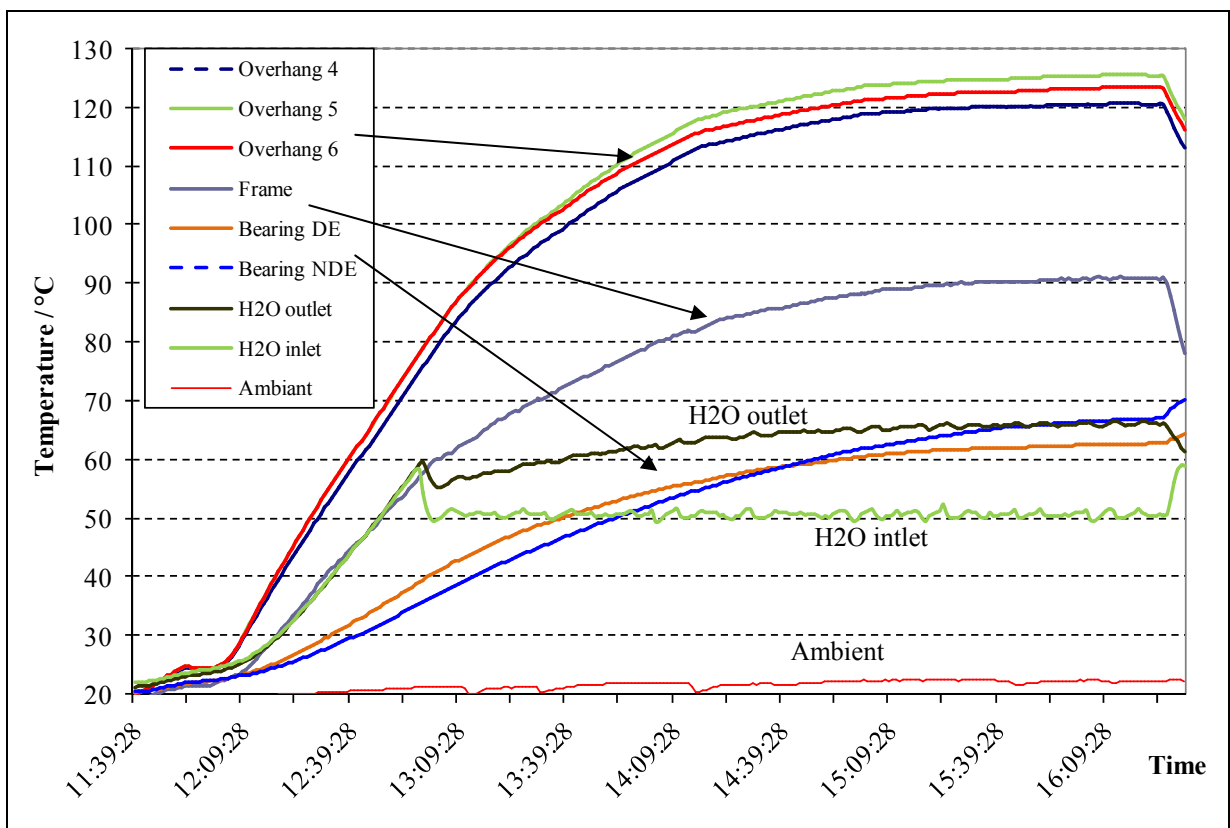
Figure 4.1: Thermally stable condition and the temperature distribution during the heat run at rated load for the water cooled 6-poles, 1.5 MW cage wind generator "A550-6L"

Following tables show the results obtained where the steady state temperature rise was measured via the stator resistance, which is extrapolated to the switch off-time (zero second) acc. to IEC 60034-1.

To improve the measurement accuracy and therefore to get better correlation coefficient R, the reading of the measured data should be recorded over an averaging time e.g. of about 10 s, depending on the rating of the motor (thermal time constant), for each load point, especially in the input-output test with the torque and the speed measurement. An averaging time of about 1 s was found to

be too low in some cases, see Table 4.15.

11 kW 4-pole motors	A160-4	B160-4	C160-4	D160-4	E160-4
Averaging time /s	1.1	1.1	1.1	1.1	10
Speed /rpm	1456.1	1466.7	1453.1	1453.4	1435.7
Corrected torque /Nm	72.1	71.6	72.3	72.3	73.37
Winding temper. rise /K	65.8	49.3	76.8	78.2	82.8

Table 4.9: Results of the rated load temperature test for 11 kW, 4-pole motors

11 kW 2- & 6-pole motors	A160-2	B160-2	C160-2	D160-2	A160-**6**
Speed /rpm	2899.1	2939.4	2930.6	2877.6	967.5
Corrected torque /Nm	36.4	35.9	35.9	36.8	107.9
Winding temper. rise /K	93.2	76.4	80.4	79.4	68

Table 4.10: Results of the rated load temperature test for 11 kW, 2-pole and 6-pole motors

5.5 kW 6- & 4-pole motors	A132-6	B132-6	C132-6	D132-6	A132-**4**
Speed /rpm	962.4	958.5	950.9	964.3	1394.5
Corrected torque /Nm	54.8	55	55.5	54.7	37.8
Winding temper. rise /K	71.6	78.7	87.3	57.1	86.6

Table 4.11: Results of the rated load temperature test for 5.5 kW, 6-pole and 4-pole motors

1.1 kW 2-pole motors	A80-2	B80-2	C80-2	D80-2
Speed /rpm	2832.6	2845.3	2842.8	2711.2
Corrected torque /Nm	3.72	3.71	3.70	3.90
Winding temperature rise /K	81.7	73	81.1	86.3

Table 4.12: Results of the rated load temperature test for 1.1 kW, 2-pole motors

0.55 kW 4-pole motors	A80-4	B80-4	C80-4	D80-4
Speed /rpm	1408.1	1409.2	1387.8	1378.1
Corrected torque /Nm	3.73	3.72	3.79	3.82
Winding temperature rise /K	73.8	76	84.1	53.7

Table 4.13: Results of the rated load temperature test for 0.55 kW, 4-pole motors

0.37 kW 6-pole motors	A80-6	B80-6	C80-6	D80-6
Speed /rpm	916.9	949.9	918.5	912.2
Corrected torque /Nm	3.85	3.74	3.86	3.87
Winding temperature rise /K	68.2	71.3	71.2	49.5

Table 4.14: Results of the rated load temperature test for 0.37 kW, 6-pole motors

4.2.3 Indirect measurement of the stray load losses using the "residual loss method" acc. to IEC 61972

The *Ohmic* losses, the stray load losses, the directly measured efficiency ($\eta_{\text{dir}} = P_{\text{out}}/P_{\text{e,in}}$), the indirectly measured efficiency ($\eta_{\text{indir,c}} = P_{\text{out,c}}/P_{\text{e,in}}$) determined with the residual losses and the corrected output power obtained from the input-output method acc. to IEC 61972 are presented in the following tables. The correlation coefficient R for each test is indicated. Note that for each case a value higher than 0.95 has been obtained. The measured stray load losses compared to the input power (Stray load losses/$P_{\text{e,in}}$) are also given, which are for all cases bigger than those obtained from the assigned value 0.5 % stated in IEC 60034-2. The differences between the directly measured efficiency η_{dir} from the input and the output powers and the indirectly measured efficiency $\eta_{\text{indir,c}}$ are also depicted, which are small than 1 %. A comparison to the assumption acc. to IEC 60034-2 is presented in Figure 4.2 for 11 kW motor "B160-4".

Figure 4.2: Comparison of the efficiencies from the measurement acc. to IEC 61972 and the assumptions acc. to IEC 60034-2, for 11 kW, 4-pole motor "B160-4"

11 kW 4-pole motors	A160-4	B160-4[*)]	C160-4	D160-4	E160-4
Winding temperature rise /K	65.9	49.0	76.7	78.2	82.8
Electrical input power /W	12463	12150	12528	12631	12737
Corrected mechanical output power /W	10959	10991	10915	11020	11027
Corrected stator copper losses @ 25°C /W	647	433	709	704	654
Corrected rotor cage losses @ 25°C /W	346	275	370	389	524
Stray load losses /W	139	148	170	150	241
Stray load losses/$P_{e,in}$ /%	1.11	1.22	1.4	1.18	1.89
$\eta_{indir,c} = P_{out,c}/P_{e,in}$ /%	87.93	90.46[*)]	87.12	87.25	86.57
$\eta_{dir} = P_{out}/P_{e,in}$ /%	88.23	90.42	87.90	86.98	86.25
$\eta_{dir} - \eta_{indir,c}$	0.30	-0.04	0.78	-0.27	-0.32
Correlation coefficient R	0.988	0.978	0.96	0.968	0.996

Table 4.15: Stray load losses and the efficiencies for 11 kW, 4-pole motors acc. to IEC 61972
[*)]: Eff1, the remaining motors are classified as Eff2.

11 kW 2- & 6-pole motors	A160-2	B160-2	C160-2	D160-2	A160-6
Winding temperature rise /K	93.2	76.4	80.4	79.4	68
Electrical input power /W	12832	12549	12665	13366	12743
Corrected mechanical output power /W	11004	11019	10981	11089	11009
Corrected stator copper losses @ 25°C /W	552	607	682	654	829
Corrected rotor cage losses @ 25°C /W	415	234	277	524	382
Stray load losses /W	261	184	139	643	134
Stray load losses/$P_{e,in}$ /%	2.03	1.47	1.1	4.81	1.05
$\eta_{indir,c} = P_{out,c}/P_{e,in}$ /%	85.76	87.82	86.7	82.97	86.39
$\eta_{dir} = P_{out}/P_{e,in}$ /%	85.50	87.72	86.78	82.11	86.36
$\eta_{dir} - \eta_{indir,c}$	-0.26	-0.1	0.08	-0.86	-0.03
Correlation coefficient R	0.9992	0.9973	0.9955	0.9992	0.9971

Table 4.16: Stray load losses and efficiencies for 11 kW, 2- and 6-pole motors acc. to IEC 61972

5.5 kW 6- & 4-pole motors	A132-6	B132-6	C132-6	D132-6	A132-4
Winding temperature rise /K	71.6	78.7	87.3	57.1	86.6
Electrical input power /W	6609	6763	6759	6474	6754
Corrected mechanical output power /W	5515	5541	5529	5530	5470
Corrected stator copper losses @ 25°C /W	495	480	612	445	458
Corrected rotor cage losses @ 25°C /W	223	252	298	214	465
Stray load losses /W	66	171	80	56	151
Stray load losses/$P_{e,in}$ /%	1.00	2.53	1.19	0.86	2.75
$\eta_{indir,c} = P_{out,c}/P_{e,in}$ /%	83.45	81.93	81.81	85.42	80.99
$\eta_{dir} = P_{out}/P_{e,in}$ /%	83.32	81.35	81.02	85.25	81.19
η_{dir} - $\eta_{indir,c}$	-0.13	-0.58	-0.79	-0.17	0.2
Correlation coefficient R	0.9857	0.9994	0.9995	0.9935	0.993

Table 4.17: Stray load losses and efficiencies for 5.5 kW, 6- and 4-pole motors acc. to IEC 61972

1.1 kW 2-pole motors	A80-2	B80-2	C80-2	D80-2
Winding temperature rise /K	81.4	73.2	80.4	86.2
Electrical input power /W	1433	1431	1468	1626
Corrected mechanical output power /W	1097	1110	1098	1088
Corrected stator copper losses @ 25°C /W	171	146	155	227
Corrected rotor cage losses @ 25°C /W	70	64	67	136
Stray load losses /W	16.8	29.7	50.5	96.9
Stray load losses/$P_{e,in}$ /%	1.17	2.07	3.44	5.96
$\eta_{indir,c} = P_{out,c}/P_{e,in}$ /%	76.56	77.53	74.80	66.88
$\eta_{dir} = P_{out}/P_{e,in}$ /%	76.83	77.30	74.94	67.24
η_{dir} - $\eta_{indir,c}$	0.27	-0.23	0.14	0.36
Correlation coefficient R	0.986	0.996	0.998	0.996

Table 4.18: Stray load losses and efficiencies for 1.1 kW, 2-pole motors acc. to IEC 61972

0.55 kW 4-pole motors	A80-4	B80-4	C80-4	D80-4
Winding temperature rise /K	73.6	75.8	84.2	52.7
Electrical input power /W	800	793	833	780
Corrected mechanical output power /W	548	550	543	544
Corrected stator copper losses @ 25°C /W	151	143	183	121
Corrected rotor cage losses @ 25°C /W	38	37	46	51
Stray load losses /W	11.2	17.7	17	22
Stray load losses/$P_{e,in}$ /%	1.41	2.23	2	2.82
$\eta_{indir,c} = P_{out,c}/P_{e,in}$ /%	68.47	69.33	65.19	69.70
$\eta_{dir} = P_{out}/P_{e,in}$ /%	68.99	69.18	66.09	70.46
$\eta_{dir} - \eta_{indir,c}$	0.52	-0.15	0.9	0.76
Correlation coefficient R	0.997	0.996	0.991	0.994

Table 4.19: Stray load losses and efficiencies for 0.55 kW, 4-pole motors acc. to IEC 61972

0.37 kW 6-pole motors	A80-6	B80-6	C80-6	D80-6
Winding temperature rise /K	68.2	71.3	71	49.3
Electrical input power /W	599	602	619	578
Corrected mechanical output power /W	372	373	369	371
Corrected stator copper losses @ 25°C /W	153	160	179	131
Corrected rotor cage losses @ 25°C /W	36	21	35	37
Stray load losses /W	7.9	12.8	9.6	4.0
Stray load losses/$P_{e,in}$ /%	1.31	2.13	1.55	0.69
$\eta_{indir,c} = P_{out,c}/P_{e,in}$ /%	62.12	61.91	59.59	64.17
$\eta_{dir} = P_{out}/P_{e,in}$ /%	62.18	61.62	59.89	64.08
$\eta_{dir} - \eta_{indir,c}$	0.06	-0.29	0.3	-0.09
Correlation coefficient R	0.994	0.995	0.998	0.996

Table 4.20: Stray load losses and efficiencies for 0.37 kW, 6-pole motors acc. to IEC 61972

4.2.3.1 Comparison of the efficiency from the measurement and the assumptions

The directly measured efficiency ($\eta_{dir} = P_{out}/P_{e,in}$) and the indirectly measured efficiency ($\eta_{indir,c} = P_{out,c}/P_{e,in}$) determined with the residual losses and the corrected output power obtained from the input-output method acc. to IEC 61972 for the 11 kW and the 5.5 kW motor are compared in the following Tables with the values determined from the assumptions:

a) 0.5 % of the electrical input $P_{e,in}$ acc. IEC 60034-2 [IEC 60034-2],

b) the assumed value of the stray load losses given in (4.1) for ratings 1 kW $< P_{out} <$ 10000 kW acc. IEC 61972 -2 [IEC 61972] and

$$P_{ad} = \left(0.025 - 0.005 \cdot \log_{10}\left(P_{out}/1\mathrm{kW}\right)\right) \cdot P_{e,in} \tag{4.1}$$

c) the assumed value of 1.8 % of the rated output power for ratings smaller than 90 kW acc. IEEE 112-method E1 [IEEE 112].

11 kW motors	A160-4	E160-4	A160-**6**	C160-2	D160-2
$\eta_{indir,c} = P_{out,c}/P_{e,in}$ /%	87.93	86.57	86.39	86.70	82.97
$\eta_{dir} = P_{out}/P_{e,in}$ /%	88.23	86.25	86.36	86.78	82.11
$\eta_{indir,IEC60034-2}$ /%	88.57	88.07	86.97	87.34	87.28
$\eta_{indir,IEC61972-2}$ /%	87.11	86.57	85.49	85.87	85.80
$\eta_{indir,IEEE112-E1}$ /%	87.49	87.00	85.91	86.28	86.29

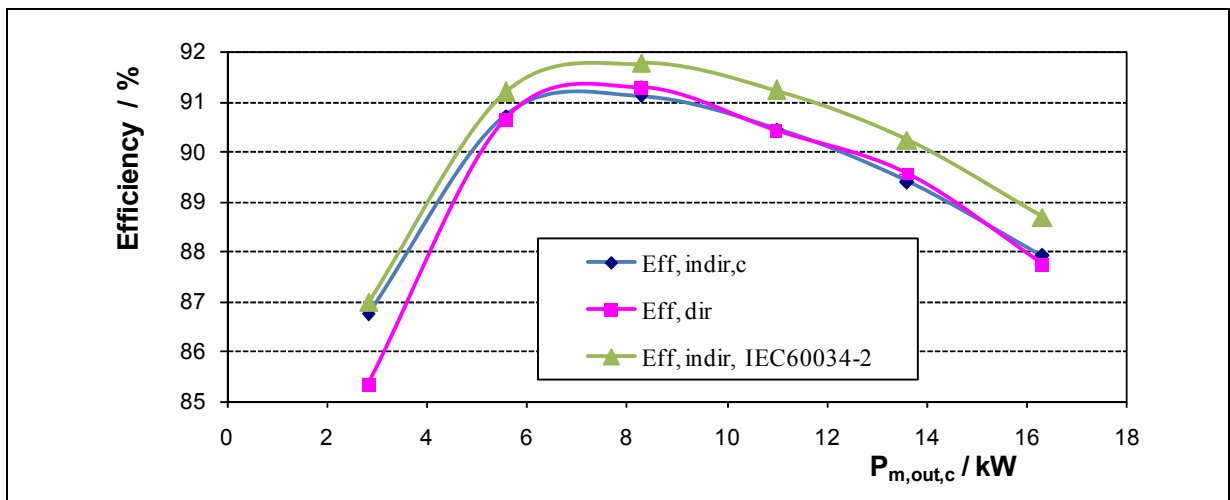Table 4.21: Comparison of the efficiencies from the measurement acc. to IEC 61972 and the assumptions acc. to IEC 60034-2, acc. to IEC 61972-2 and acc. to IEEE 112-E1 for 11 kW, 4-, 6- and 2-pole motors

For the 11 kW and the 5.5 kW motor it can be seen, in Table 4.21 and Table 4.22, respectively, that the efficiency values obtained from different testing standards can differ by several percent. Depending on the method applied the efficiency can vary from -1.5 % to 5 %. The measured efficiency varies only between -1 % and 0.3 %.

5.5 kW motors	A132-6	B132-6	D132-6	A132-**4**
$\eta_{\text{indir,c}} = P_{\text{out,c}}/P_{\text{e,in}}$ /%	83.45	81.93	85.42	80.99
$\eta_{\text{dir}} = P_{\text{out}}/P_{\text{e,in}}$ /%	83.32	81.35	85.25	81.19
$\eta_{\text{indir,IEC60034-2}}$ /%	84.03	84.02	85.83	82.88
$\eta_{\text{indir,IEC61972-2}}$ /%	82.40	82.40	84.20	81.24
$\eta_{\text{indir,IEEE112-E1}}$ /%	83.03	83.06	84.79	81.90

Table 4.22: Comparison of the efficiencies from the measurement acc. to IEC 61972 and the assumptions acc. to IEC 60034-2, acc. to IEC 61972-2 and acc. to IEEE 112-E1 for 5.5 kW 6- and 4-pole motors

The efficiency variations of the cited methods related to the indirectly measured efficiency ($\eta_{\text{indir,c}} = P_{\text{out,c}}/P_{\text{e,in}}$) determined with the residual losses and the corrected output power obtained from the input-output method acc. to IEC 61972 are presented in Figure 4.3 for 11 kW and 5.5 kW motors.
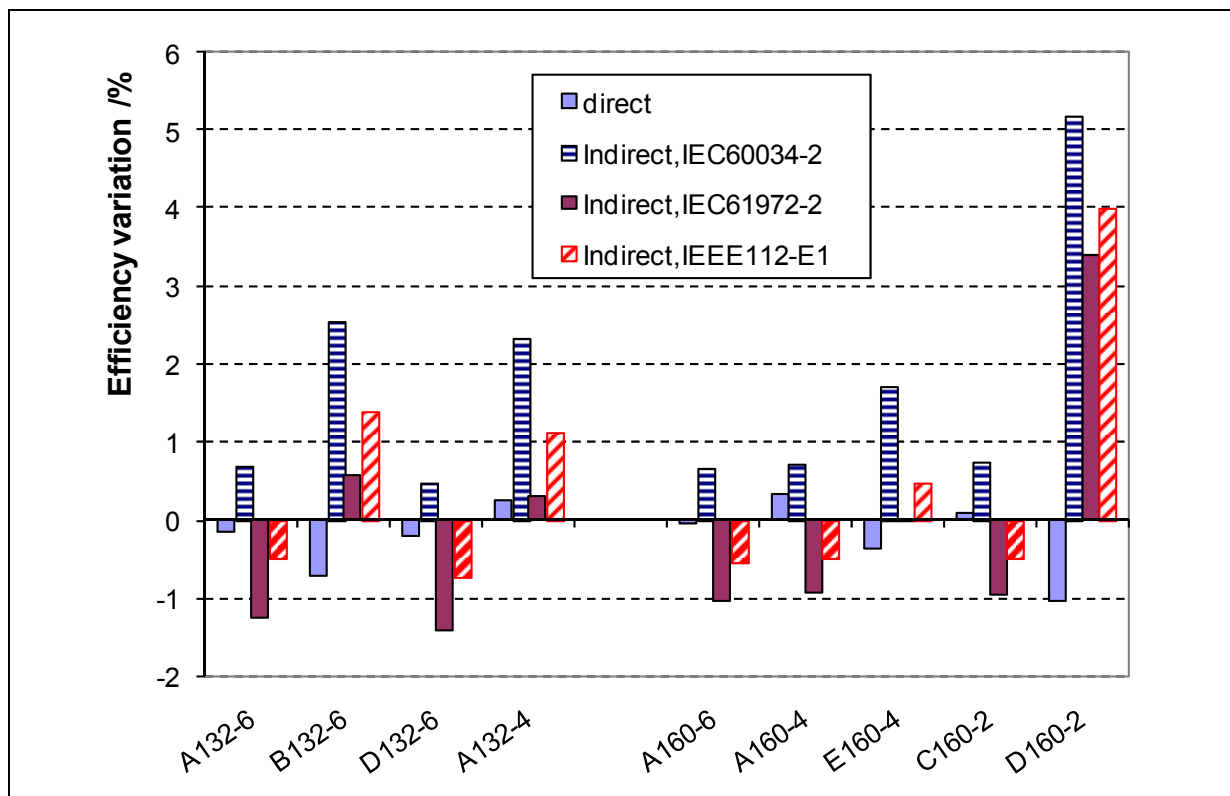
Figure 4.3: Efficiency variation related to the indirectly measured efficiency from the measurement acc. to IEC 61972 and the assumptions acc. to IEC 60034-2, acc. to IEC 61972-2 and acc. to IEEE 112-E1 for 5.5 kW and 11 kW motors

4.2.3.2 Influence of the friction and windage losses on the stray load losses calculation

Under load the speed n and the friction and windage losses P_{fw}, due to the dominating fan in TEFC induction motors, vary between overload and partial load test as presented in Figure 4.4. To investigate the influence of the smaller friction and windage losses P_{fw} under load due to the reduced speed n on the determined stray load losses P_{ad}, the evaluation is done in slightly different ways according to IEC 61972:

a) Constant friction and windage losses P_{fw} at no-load and under load acc. to IEC 61972 and

b) the friction and windage losses P_{fw} are considered to be load-dependent, varying with the speed n by an exponent of 2.5 ($\sim n^{2.5}$).
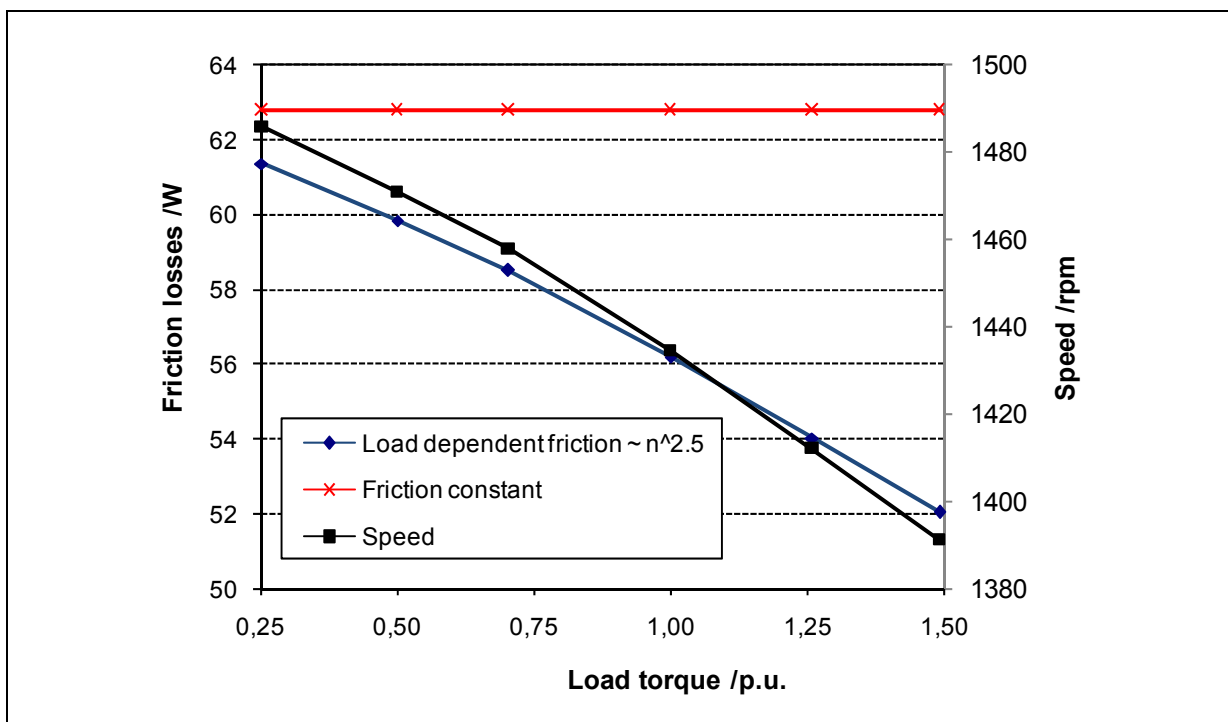
Figure 4.4: The consideration of the friction and windage losses as function of the speed variation during the load for an 11 kW, 4-pole motor "E160-4"

The slip s and the speed n change during the load test and therefore also the friction and windage losses P_{fw} (see Figure 4.4), so for more accurate

determination of the stray load losses P_{ad} this influence should be taken into account ! Also, with which exponent the friction and windage losses P_{fw} should be considered ? This needs further investigation, which is not task of this work. In our example in Figure 4.4 the exponent 2.5 ($\sim n^{2.5}$) fits well.

11 kW 4- & 6-pole motors	A160-4		E160-4		A160-**6**	
	a) Friction constant	b) Friction $\sim n^{2.5}$	a) Friction constant	b) Friction $\sim n^{2.5}$	a) Friction constant	b) Friction $\sim n^{2.5}$
Friction losses /W	70.1	65.0	62.8	56.2	27.2	25.0
Electrical input /W	12463	12463	12737	12737	12743	12743
Corrected mechanical output /W	10959	10961	11027	11030	11009	11010
Stray load losses /W	139	142	241	245	134	135
Variation relating to a) /%	0.00	2.18	0.00	1.74	0.00	1.10
$\eta_{indir,c} = P_{out,c}/P_{e,in}$ /%	87.93	87.95	86.57	86.59	86.39	86.40
Correlation coeff. R	0.988	0.989	0.996	0.996	0.997	0.997

Table 4.23: Influence of the friction and windage losses on the stray load losses and efficiency determination for 11 kW, 4- and 6-pole motors acc. to IEC 61972

11 kW 2-pole motors	A160-2		C160-2		D160-2	
	a) Friction constant	b) Friction $\sim n^{2.5}$	a) Friction constant	b) Friction $\sim n^{2.5}$	a) Friction constant	b) Friction $\sim n^{2.5}$
Friction losses /W	311	285	264	244	287	258
Stray load losses /W	261	277	139	144	643	654
Variation relating to a) /%	0.00	5.57	0.00	3.87	0.00	1.54
$\eta_{indir,c} = P_{out,c}/P_{e,in}$ /%	85.76	85.84	86.7	86.81	82.97	83.17
Correlation coeff. R	0.999	0.999	0.9955	0.9956	0.999	0.999

Table 4.24: Influence of the friction and windage losses on the stray load losses and efficiency determination for 11 kW, 2-pole motors acc. to IEC 61972

As shown in Table 4.23 and Table 4.24 and in the Figure 4.5 the influence of the friction and windage losses P_{fw} on the determination of the stray load losses P_{ad} can be significant, especially at high speed motors. For the 2- pole motors

the variation is in the range between 2 % and 5 %.
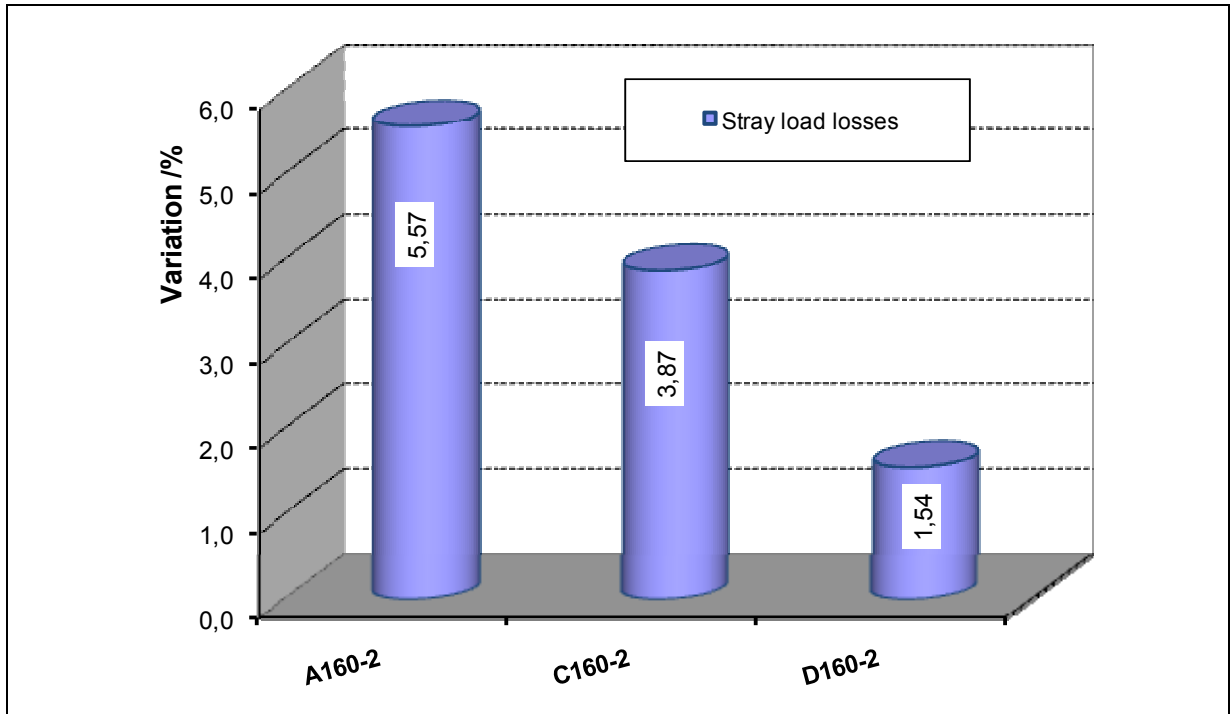
Figure 4.5: The variation of the stray load losses determined with the load dependent friction and windage losses for 11 kW, 2-pole motors acc. to IEC 61972

4.2.4 Indirect measurement of the stray load losses using the "residual loss method" acc. to IEEE 112-method B

The *Ohmic* losses, the stray load losses P_{ad}, the indirectly measured efficiency ($\eta_{indir,c} = P_{out,c}/P_{e,in}$) determined with the residual losses and the corrected output power obtained from the input-output method acc. to IEEE 112-method B are presented in the following tables. For comparison the directly measured efficiency ($\eta_{dir} = P_{out}/P_{e,in}$) is also given. The correlation coefficient R for each test is indicated. Note that for each case a value higher than 0.90 has been obtained. The measured stray load losses compared to the input power (Stray load losses/$P_{e,in}$) are also given, which are for all cases bigger than those obtained from the assumed value of 0.5 % of the electrical input power as stated in IEC 60034-2.

11 kW 2- & 6-pole motors	A160-2	B160-2	C160-2	D160-2	A160-**6**
Winding temper. rise /K	93.2	76.4	80.4	79.4	68
Electrical input power /W	12832	12549	12665	13366	12743
Corrected mechanical output power /W	11009	11039	11023	11089	11016
Corrected stator copper losses @ 25°C /W	552	607	682	654	829
Corrected rotor cage losses @ 25°C /W	400	220	267	512	373
Stray load losses /W	239	148	96	628	98
Stray load losses/$P_{e,in}$ /%	1.86	1.18	0.76	4.7	0.77
$\eta_{indir,c} = P_{out,c}/P_{e,in}$ /%	85.8	87.97	87.04	82.96	86.45
$\eta_{dir} = P_{out}/P_{e,in}$ /%	85.50	87.72	86.78	82.11	86.36
Correlation coefficient R	0.998	0.9973	0.9812	0.9989	0.9875

Table 4.25: Stray load losses and the efficiencies for 11 kW, 2- and 6-pole motors acc. to IEEE 112-B

5.5 kW 6-pole motors	A132-6	B132-6	C132-6	D132-6
Winding temper. rise /K	71.6	78.7	87.3	57.1
Electrical input power /W	6609	6763	6759	6474
Corrected mechanical output power /W	5489	5537	5519	5530
Corrected stator copper losses @ 25°C /W	495	480	612	445
Corrected rotor cage losses @ 25°C /W	216	246	289	210
Stray load losses /W	50	152	39	44
Stray load losses/$P_{e,in}$ /%	0.75	2.25	0.58	0.68
$\eta_{indir,c} = P_{out,c}/P_{e,in}$ /%	83.06	81.87	81.66	85.42
$\eta_{dir} = P_{out}/P_{e,in}$ /%	83.32	81.35	81.02	85.25
Correlation coefficient R	0.964	0.9993	0.9833	0.9745

Table 4.26: Stray load losses and the efficiencies for 5.5 kW, 6-pole motors according to IEEE 112-B

1.1 kW 2-pole motors	A80-2[*)]	B80-2	C80-2	D80-2
Winding temper. rise /K	92.4	81.9	92.6	101
Electrical input power /W	1433	1431	1468	1626
Corrected mechanical output power /W	1087	1102	1096	1066
Corrected stator copper losses @ 25°C /W	170	146	155	227
Corrected rotor cage losses @ 25°C /W	66	62	64	124
Stray load losses /W	-1.12	20.3	39.2	60.1
Stray load losses/$P_{e,in}$ /%	-0.08	1.42	2.67	3.7
$\eta_{indir,c} = P_{out,c}/P_{e,in}$ /%	75.85	76.97	74.64	65.52
$\eta_{dir} = P_{out}/P_{e,in}$ /%	76.83	77.30	74.94	67.24
Correlation coefficient R with IEEE 112-B	-0.139	0.983	0.991	0.957
Correlation coefficient R with IEC 61972	0.986	0.996	0.998	0.996

Table 4.27: Stray load losses and efficiencies for 1.1 kW, 2-pole motors acc. to IEEE 112-B

[*)]: For the "motor A80-2" the measurement could not be evaluated according to IEEE 112-method B [IEEE 112], because negative stray load losses are derived and bad correlation coefficient $R < 0.9$ compared to IEC 61972 [IEC 61972], as load-independent iron losses are assumed.

For one small motor 1.1 kW, 2-pole "A80-2", two small motors 0.55 kW, 4-pole "A80-4" and "C80-4" and three small motors 0.37 kW, 6-pole "A80-6", "C80-6" and "D80-6" the test - results - could not be evaluated according to IEEE 112-method B. For each rating only one example is given to show the limit of this method. The p.u. value of the stator phase resistance increases with decreasing power rating. The resistive voltage drop reduces significantly the inner voltage U_i. Therefore under load the iron losses P_{Fe} decrease. The standards IEC 60034-2 Ed. 4.0 draft [60034-2 draft] and IEC 61972 [IEC 61972] consider this fact, so always positive stray load losses P_{ad} are measured. The standard IEEE 112-B [IEEE 112] considers the iron losses P_{Fe} to be independent of the load, leading in some cases to negative stray load losses P_{ad} and a bad correlation coefficient $R < 0.9$, especially for small power rating 0.37 kW.

Measured motors	0.55 kW 4-pole			0.37 kW 6-pole	
	B80-4	C80-4[*)]	D80-4	B80-**6**	D80-**6**[*)]
Winding temper. rise /K	87.4	96.8	58.9	77.5	53.6
Electrical input power /W	793	833	780	602	578
Corrected mechanical output power /W	548	540	541	369	369
Corrected stator copper losses @ 25°C /W	143	183	121	160	131
Corrected rotor cage losses @ 25°C /W	35	43	49	20	35
Stray load losses /W	10.5	2.3	14.9	6.0	-1.7
Stray load losses/$P_{e,in}$ /%	1.32	0.28	1.92	0.99	-0.3
$\eta_{indir,c} = P_{out,c}/P_{e,in}$ /%	69.03	64.77	69.3	61.23	63.73
$\eta_{dir} = P_{out}/P_{e,in}$ /%	69.18	66.09	70.46	61.62	64.08
Correlation coefficient R with IEEE 112-B	0.974	0.39	0.986	0.978	-0.66
Correlation coefficient R with IEC 61972	0.996	0.991	0.994	0.995	0.996

Table 4.28: Stray load losses and the efficiencies for 0.55 kW, 4-pole and for 0.37 kW, 6-pole motors acc. to IEEE 112-B

[*)]: The measurement could not be evaluated according to IEEE 112-method B (see the note under Table 4.27).

4.2.4.1   Influence of the determination of the resistive losses on the stray load losses calculation

To show the influence of the stator winding temperature $\vartheta_{Cu,s}$ determination on the stray load losses P_{ad} calculation, the test data of the measured points are used with an averaging time of 10 s to determine the stray load losses P_{ad} for an 11 kW, 4-pole motor "E160-4". For fair comparison the evaluation is done acc. to IEEE 112-method B, where the iron losses P_{Fe} are taken as load independent. The stator winding temperature $\vartheta_{Cu,s}$ is determined in slightly different ways:

a) Resistance test at each load point: The winding temperature $\vartheta_{Cu,s}$ is determined via the measured resistance R_s at each load point (extrapolated to 0 seconds after switching off the motor).

b) Thermocouples: The winding temperature $\vartheta_{Cu,s}$ is determined as average reading of thermocouples installed on the overhang winding in DE- and NDE-side acc. to IEEE 112-method B.

c) Thermocouples related: The winding temperature $\vartheta_{Cu,s}$ is determined as average reading of thermocouples installed on the overhang winding in DE- and NDE-side. The resistance R_s for each load point is determined from the temperature $\vartheta_{Cu,s}$ of the winding at that point in relation to the resistance R_s and the temperature $\vartheta_{Cu,s}$ measured at rated load temperature test acc. to IEC 60034-2 Ed. 4.0 draft/ IEC 61972.

d) Interpolation acc. to IEC 60034-2 Ed. 4.0 draft: The temperature $\vartheta_{Cu,s}$ for 100% load and higher loads is the value determined before 150% load. The temperature $\vartheta_{Cu,s}$ for loads less than 100% is taken as varying linearly with the load, using the reading before the test for 100% load and after the lowest reading for 25% load (IEC 60034-2 Ed. 4.0 draft and IEC 61972).

e) Average value: The winding temperature $\vartheta_{Cu,s}$ is determined as the average value of the resistances R_s measured at the beginning and the end of the test (extrapolated to 0 seconds after switching off the motor).

The traces of the winding temperature $\vartheta_{Cu,s}$ for compared methods are presented as function of the load in Figure 4.6 for an 11 kW, 4-pole motor "E160-4" with an averaging time of 10 s and in Figure 4.7 for 1.1 kW, 2-pole motor "C80-2" with an averaging time of 2 s. As shown in the first example the traces, except for the curve of the average method, are near to each other in the range under 100 % load, whereas in the range over 100 % load the curve of the interpolation method is lower. Of course this finding could change from one sample machine to another depending on the positions and the number of the embedded thermocouples as given in Figure 4.7.
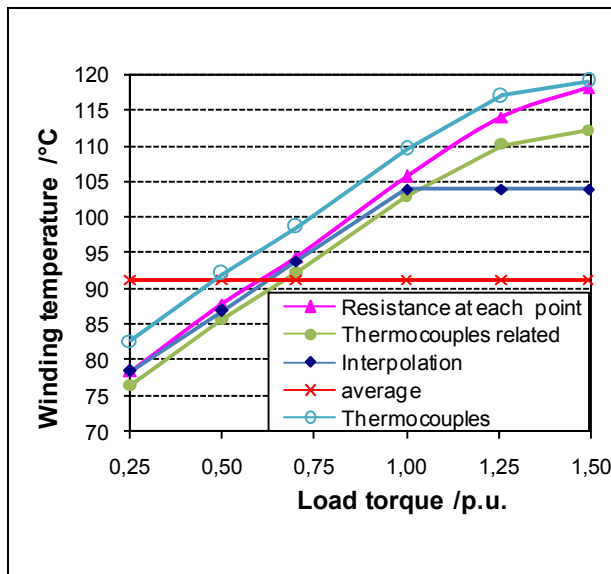
Figure 4.6: The winding temperatures as function of the load for 11 kW, 4-pole motor "E160-4"
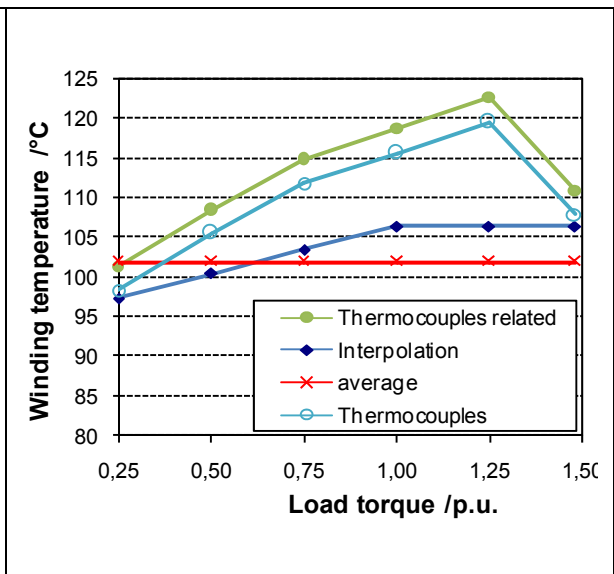
Figure 4.7: The winding temperatures as function of the load for 1.1 kW, 2-pole motor "C80-2"

In Table 4.29 and in the Figure 4.8 for an 11 kW motor the sensitivity of the stray load losses P_{ad}, is shown related to the evaluation with the resistance R_s measured at each load point, which is the accurate and therefore the more expensive method. For this example the stray load losses P_{ad} vary between 0.5 % and 25 % and the efficiency varies between 0.1 % and 0.6 %. Of course this influence should be smaller for larger motors with higher thermal time constant, and should vary also with the position and the number of the thermocouples. The value of the stray load losses P_{ad} evaluated with the hottest thermocouple as suggested in the standard IEEE 112 deviates by -3.3 % whereas the evaluation with the coldest one deviates by +2.2 % from the value obtained with the resistance R_s measured at each load point. It has to be noted that in the comparison in this example, due to the resistance measurement at each load point, the interpolation methods and the averaging methods are disadvantaged as for this method the test should be taken quickly (as recommended in the standards).

For a small motor of 1.1 kW the variation of the stray load losses P_{ad} and the efficiency determined with different temperature methods (related to the interpolation method) are depicted in the Figure 4.9.

E160-4	a) Resistance at each point	b) Thermocoupl average	c) Thermocoupl related	d) Interpolation	e) Average value
Mechan. output /W	11051	11058	11036	11022	10974
Correct. rotor loss /W	520	514	525	523	544
Stray losses /W	206	205	217	232	259
Variation to a)	0.0 %	-0.49 %	4.98 %	12.54 %	25.66 %
$P_{ad}/P_{e,in}$ /%	1.62	1.61	1.7	1.82	2.03
Efficiency /%	86.76	86.82	86.64	86.53	86.16
Offset /W	49	46	47	39	32
Correlat. coeff. R	0.9961	0.9952	0.9956	0.9948	0.9964

Table 4.29: Influence of the stator winding temperature on the stray load losses and the efficiency determination for an 11 kW, 4-pole motor "E160-4" acc. to IEEE 112-B
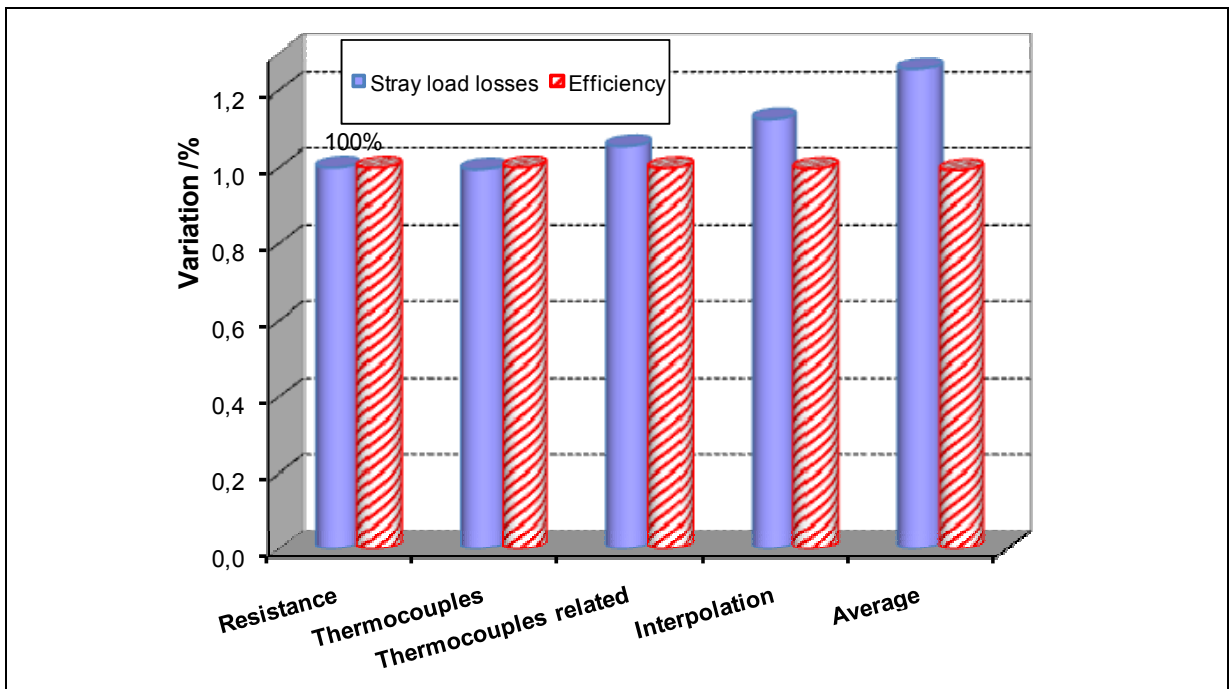
Figure 4.8: The variation of the stray load losses and the efficiency determined with different temperature methods (related to the resistance method) for an 11 kW, 4-pole motor "E160-4" acc. to IEEE 112-B
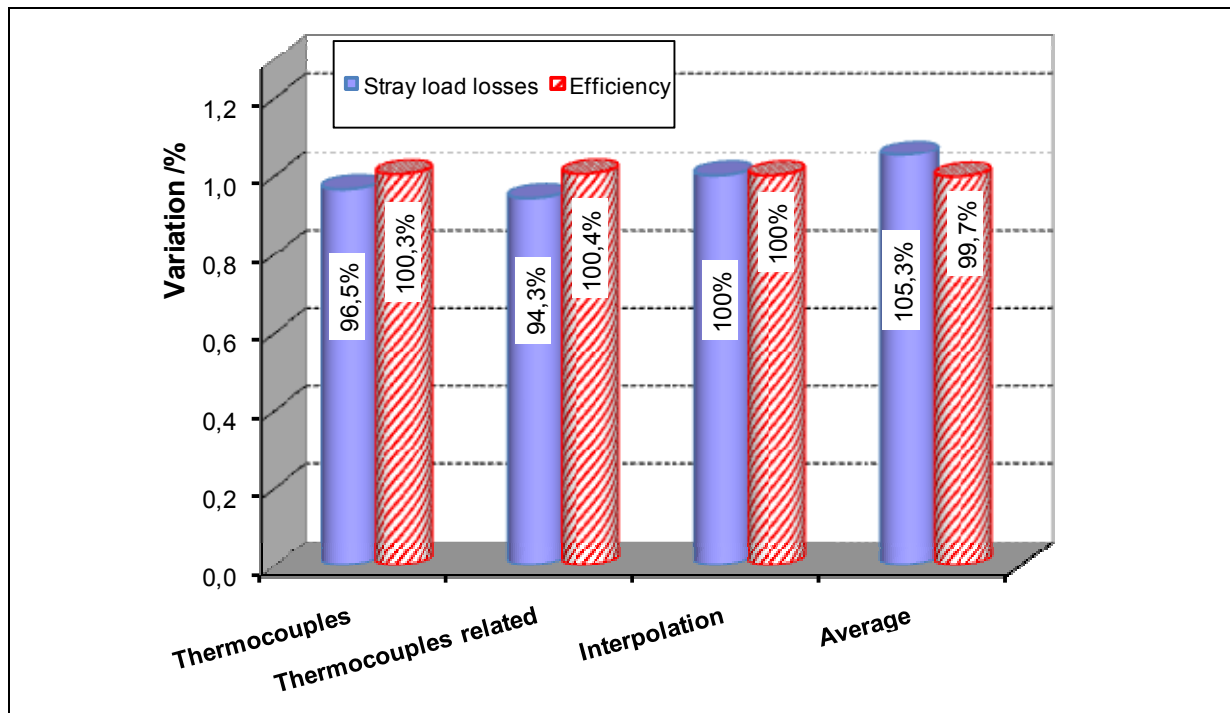
Figure 4.9: The variation of the stray load losses and efficiency determined with different temperature methods (related to the interpolation method) for an 1.1 kW, 2-pole motor "C80-2" acc. to IEEE 112-B

4.2.5 Direct measurement of the stray load losses using the reverse rotation test

The stray load losses P_{ad} directly measured with the reverse rotation test acc. to IEEE 112 [IEEE 112], where the winding temperature $\vartheta_{Cu,s}$ is determined acc. to IEC 60034-2 Ed. 4.0 draft/ IEC 61972 (Interpolation method), are presented in the following tables. The smoothened data of the measured stray load losses in the stator $P_{ad,s,c}$ during the removed rotor test and in the rotor $P_{ad,r,c}$ during the reverse rotation test and the resulting stray load losses $P_{ad,c}$ are depicted.

11 kW 4-pole motors	A160-4	B160-4	C160-4	D160-4	E160-4
Removed rotor test /W	32	22.6	38	42	43
Reverse rotation test /W	180	139	168	265	373
Stray load losses /W	212	162	206	307	416

Table 4.30: The measured stray load losses in the stator and in the rotor with the reverse rotation test for 11 kW, 4-pole motors

11 kW 2- & 6-pole motors	A160-2	B160-2	C160-2	D160-2	A160-6
Removed rotor test /W	25	31	29	40	23
Reverse rotation test /W	283	150	123	714	203
Stray load losses /W	308	181	152	754	226

Table 4.31: The measured stray load losses in the stator and in the rotor with the reverse rotation test for 11 kW, 2- and 6-pole motors

5.5 kW 6- & 4-pole motors	A132-6	B132-6	C132-6	D132-6	A132-4
Removed rotor test /W	14	12	13	10	35
Reverse rotation test /W	116	238	111	57	200
Stray load losses /W	130	250	124	67	235

Table 4.32: The measured stray load losses in the stator and in the rotor with the reverse rotation test for 5.5 kW, 6- and 4-pole motors

1.1 kW 2-pole motors	A80-2	B80-2	C80-2	D80-2
Removed rotor test /W	1	2	3	3
Reverse rotation test /W	14	25	47	78
Stray load losses /W	15	27	50	81

Table 4.33: The measured stray load losses in the stator and in the rotor with the reverse rotation test for 1.1 kW, 2-pole motors

0.55 kW 4-pole motors	A80-4	B80-4	C80-4	D80-4
Removed rotor test /W	0.5	0.8	0.8	1
Reverse rotation test /W	4.5	7.2	5.2	16
Stray load losses /W	5	8	6	17

Table 4.34: The measured stray load losses in the stator and in the rotor with the reverse rotation test for 0.55 kW, 4-pole motors

0.37 kW 6-pole motors	A80-6	B80-6	C80-6	D80-6
Removed rotor test /W	0.4	1	0.3	0.3
Reverse rotation test /W	2.6	2	1.7	1.7
Stray load losses /W	3	3	2	2

Table 4.35: The measured stray load losses in the stator and in the rotor with the reverse rotation test for 0.37 kW, 6-pole motors

4.2.5.1 Influence of the determination of the resistive losses on the stray load losses calculation

The measured stray load losses in the stator during the removed rotor test and in the rotor during the reverse rotation test are determined in different way:

a) Average value: The winding temperature is determined as the average value of the measured resistances at the beginning and the end of the test (extrapolated to 0 seconds after switching off the motor).

b) Interpolation acc. to IEC 60034-2 Ed. 4.0 draft: The temperature for 100% load and higher loads is the value determined before applying 150% load. The temperature for loads less than 100% is taken as varying linearly with the load, using the reading before the test for 100% load and after the lowest reading for 25% load (IEC 60034-2 Ed. 4.0 draft and IEC 61972).

c) Thermocouples related: The winding temperature is determined as average reading of thermocouples installed on the overhang winding in DE- and NDE-side. The resistance for each load point is determined from the temperature of the winding at that point in relation to the resistance and the temperatures measured at test begin.

The smoothened data for the stray load losses of different motors were compared in the Figure 4.10 for a 1.1 kW motor and in the Table 4.36 and Table 4.37 for 11 kW motors to show the sensitivity of the calculation method itself on the results.

a) Average/ b) Interpol.	A160-4	B160-4	C160-4	D160-4	E160-4
Removed rotor test /W	41 / 32	23.5 / 22.6	45 / 38	53 / 42	54 / 43
Reverse rotation test /W	189 / 180	135 / 139	165 / 168	266 / 265	378 / 373
Stray load losses /W	230 / 212	159 / 162	210 / 206	319 / 307	432 / 416
Variation relating to b)	8.5 %	-1.8 %	1.9 %	3.9 %	3.8 %

Table 4.36: The influence of stator winding temperature determination on stray load losses in the stator and in the rotor with the reverse rotation test for 11 kW, 4-pole motors

As shown in the Table 4.36 and Table 4.37 and in the Figure 4.10 the sensitivity of the stray load losses on the winding temperature determination varies for these examples between -2 % and 8 %.
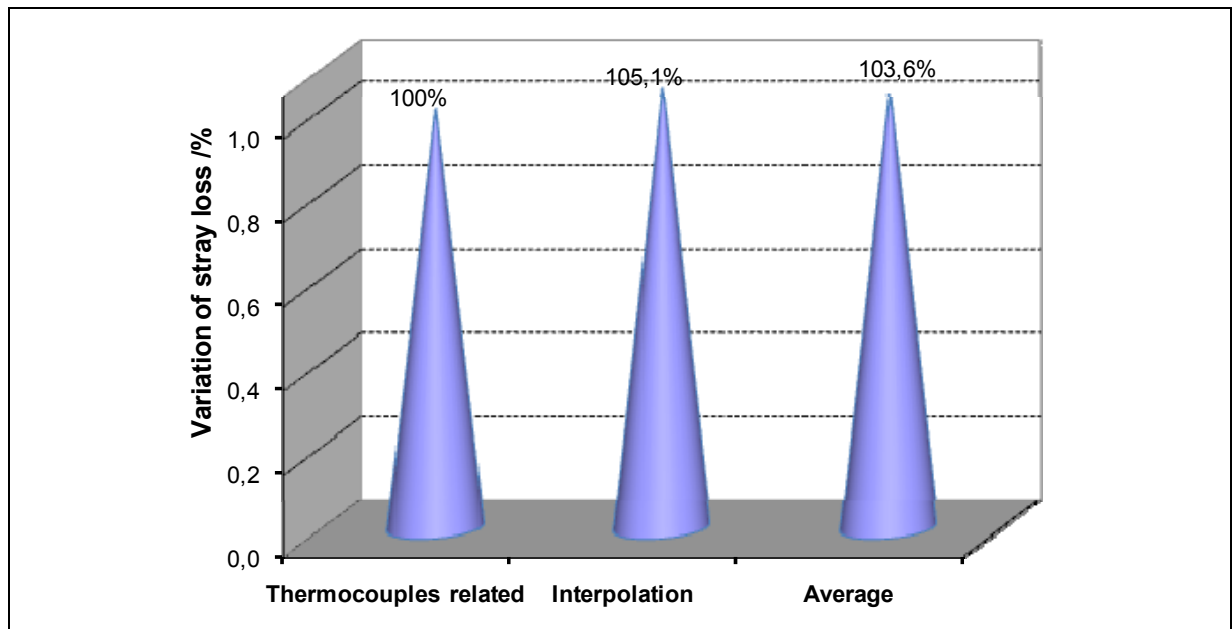
Figure 4.10: The variation of the stray load losses measured in the reverse rotation test determined with different temperature methods (related to the thermocouples related method) for a 1.1 kW, 2-pole motor "C80-2"

11 kW, A160-2	a) Average	b) Interpolation	c) Thermocouples related
Removed rotor test /W	24	25	12
Reverse rotation test /W	276	283	294
Stray load losses /W	300	308	306
Variation relating to c)	-1.9 %	-0.6 %	0.0 %

Table 4.37: The influence of stator winding temperature determination on stray load losses in the stator and in the rotor with the reverse rotation test for 11 kW, 2-pole motor

4.2.6 Direct measurement of the stray load losses with eh-star method

The directly measured stray load losses for uncoupled motor operated under unbalanced condition acc. to the eh-star method [Jord 1967, Guid 2005] and the standard IEC 60034-2 Ed. 4.0 draft [IEC 60034-2 draft] are depicted in Table 3.35 - 3.38 of the previous chapter (chapter 3).

4.2.7 Direct measurement of the stray load losses using the equivalent no-load method of *Bourne*

The stray load losses measured directly with the equivalent no-load method acc. to *Bourne* [Bour 1989] using the no-load current I_0 and the rated current I_N are presented for some measured motors in the following Tables where the resistance is determined by measuring the stator winding temperature using two thermocouples installed on the winding overhang. The resistance for each voltage point is determined from the temperature of the winding at that point in relation to the resistance and temperature measured before the start of the test. To measure the loss component due to circulating current in delta-connected winding of 3-times stator frequency f_s, caused by the saturation harmonic, the test was done in delta-connection for all motors. The influence of the resistive losses and the terminal connection on the results of the stray load losses is presented in the next sections.

11 kW 4-pole motors	A160-4	D160-4	E160-4
Rated / no-load current /A	37 / 19	22 / 10	37 / 13
Stray losses at no-load current /W	48	18	-4
Stray load losses /W	225	194	98
Correlation coefficient R	0.9934	0.9967	0.994

Table 4.38: The measured stray load losses with the equivalent no-load method of *Bourne* for 11 kW, 4-pole motors

11 kW 2- & 6-pole motors	A160-2	C160-2	A160-**6**
Rated / no-load current /A	21 / 7	21.7 / 11	23 / 13
Stray losses at no-load current /W	45	50	8
Stray load losses /W	885	352	115
Correlation coefficient R	0.9993	0.9998	0.9993

Table 4.39: The measured stray load losses with the equivalent no-load method of *Bourne* for 11 kW, 2- and 6-pole motors

5.5 kW 6- & 4-pole motors	A132-6	B132-6	C132-6
Rated / no-load current /A	12.2 / 7	24 / 15	13 / 9
Stray losses at no-load current /W	51	74	66
Stray load losses /W	336	189	196
Correlation coefficient R	0.9998	0.9993	0.9995

Table 4.40: The measured stray load losses with the equivalent no-load method of *Bourne* for 5.5 kW, 6-pole motors

1.1 kW 2-pole motors	A80-2	B80-2	C80-2	D80-2
Rated / no-load current /A	4.43 / 3.1	4.27 / 2.47	4.32 / 2.69	4.9 / 3.32
Stray losses at no-load current /W	43	8	7	74
Stray load losses /W	65	30	23	105
Correlation coefficient R	0.9983	0.9938	0.9999	0.9996

Table 4.41: The measured stray load losses with the equivalent no-load method of *Bourne* for 1.1 kW, 2-pole motors

0.55 kW 4-pole motors	A80-4	B80-4	C80-4	D80-4
Rated / no-load current /A	2.89 / 2.59	2.76 / 2.23	2.65 / 2.32	2.67 / 1.92
Stray losses at no-load current /W	29	6	3	8
Stray load losses /W	12	7	2.5	9
Correlation coefficient R	0.9983	0.9665	0.9959	0.9997

Table 4.42: The measured stray load losses with the equivalent no-load method of *Bourne* for 0.55 kW, 4-pole motors

0.37 kW 6-pole motors	A80-6	B80-6	C80-6	D80-6
Rated / no-load current /A	2.14 / 1.95	2.2 / 1.93	2.22 / 2.07	2.16 / 2.03
Stray losses at no-load current /W	13	5	7	3
Stray load losses /W	7	5	3	1
Correlation coefficient R	0.9988	0.9808	0.9985	0.9984

Table 4.43: The measured stray load losses with the equivalent no-load method of *Bourne* for 0.37 kW, 6-pole motors

4.2.7.1 Influence of the determination of the resistive losses on the stray load losses calculation

The measurement data are used to determine the stray load losses in two different ways to show the sensitivity of the resistive losses on the results:

a) The resistive losses are determined with the thermocouples method described above and with

b) Interpolation method acc. to IEC 60034-2 Ed. 4.0 draft: The temperature for 100 % rated voltage and higher is the value determined before the test. The temperature for voltages less than 100 % is taken as linear with the voltage, using the reading before the test for 100 % rated voltage and after the lowest reading for 20 % rated voltage.

The variations (5 % to 240 %) depicted in the Table 4.44 to Table 4.46 are high, especially for the smallest motors and show that the resistive losses must be measured accurately. It has to be noted that the Interpolation method acc. to

IEC 60034-2 Ed. 4.0 draft is inaccurate for the equivalent no-load method of *Bourne* as more test point over 100 % rated voltage are needed than in the standardized no-load test.

1.1 kW 2-pole motors	A80-2	B80-2	C80-2	D80-2
Stray load loss with thermocouples /W	65	30	23	105
Stray load loss with Interpolation /W	69	31	26	110
Variation rel. to thermocouples /%	6.1	4.9	14.8	4.8

Table 4.44: Influence of the winding temperature determination on measured stray load losses with the equivalent no-load method of *Bourne* for 1.1 kW, 2-pole motors

0.55 kW 4-pole motors	A80-4	B80-4	C80-4	D80-4
Stray load loss with thermocouples /W	12	7	2.5	9
Stray load loss with Interpolation /W	14	8	8.4	13
Variation rel. to thermocouples /%	23.2	14.9	240	40.8

Table 4.45: Influence of the winding temperature determination on measured stray load losses with the equivalent no-load method of *Bourne* for 0.55 kW, 4-pole motors

0.37 kW 6-pole motors	A80-6	B80-6	C80-6	D80-6
Stray load loss with thermocouples /W	7	5	3	1
Stray load loss with Interpolation /W	9	7	8	3
Variation rel. to thermocouples /%	30.1	51.8	164	190

Table 4.46: Influence of the winding temperature determination on measured stray load losses with the equivalent no-load method of *Bourne* for 0.37 kW, 6-pole motors

4.2.7.2   Comparison of the stray load losses in star and delta connection

To show the influence of the terminal connection on the results of the directly measured stray load losses with the equivalent no-load method acc. to *Bourne* [Bour 1989], the test was done for one 11 kW, 4-pole motor in delta- and in star-connection. The difference of the stray load losses was negligible as presented in Table 4.47 and in Figure 4.11.

11 kW 4-pole motor	E160-4	
Terminal connection	Delta	Star
Stray load losses /W	97.9	100.5
Correlation coefficient R	0.994	0.995
Variation relating to delta /%	0.0 %	2.6 %

Table 4.47: Influence of the terminal connection on the measured stray load losses with the equivalent no-load method of *Bourne* for 11 kW, 4-pole motor "E160-4"
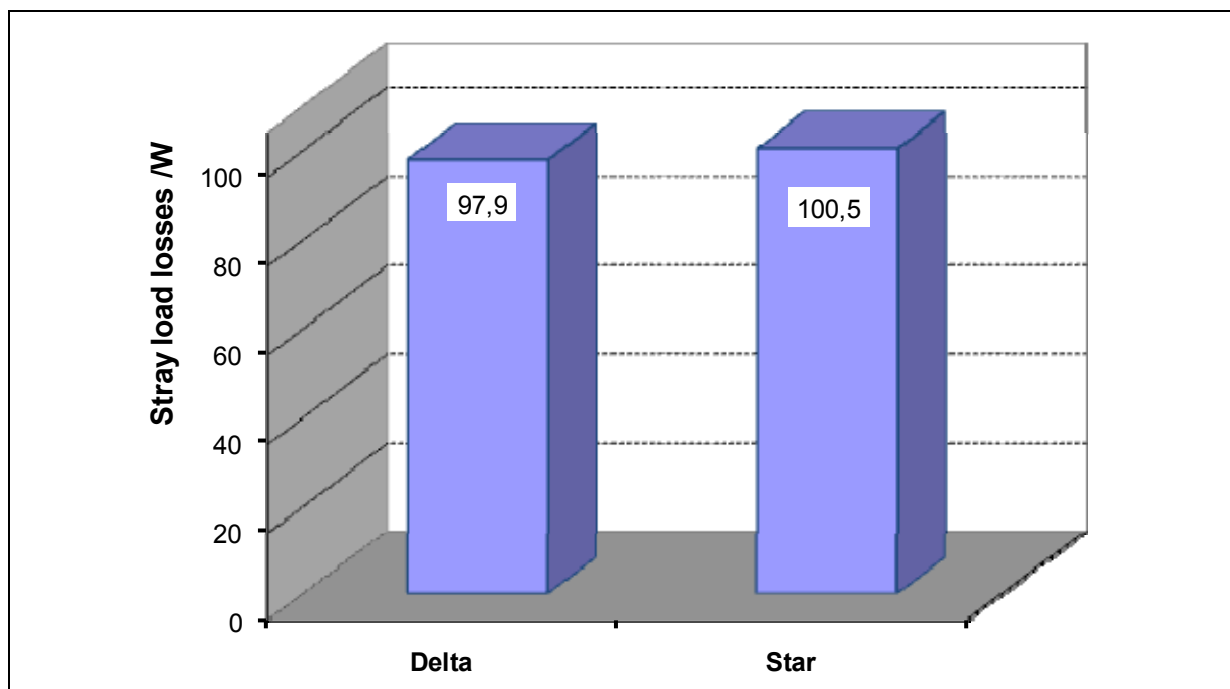
Figure 4.11: The measured stray load losses in delta- and in star-connection with the equivalent no-load method of *Bourne* for 11 kW, 4-pole motor "E160-4"

4.2.8 Direct measurement of the stray load losses using the equivalent no-load method of *Rawcliffe*

For some motors measured with standardized no-load test, the tests results are evaluated acc. to the *Rawcliffe*'s method [Rawc 1952] without calculation of the secondary hysteresis losses $P_{Fe.hy.r.calcul}$ as the measured harmonic-frequency losses $P_{hf.measure}$ were higher than with e.g. IEC 61972, or the evaluation was not possible as the slip s of the machine is zero or the values are erratic (e.g. see

Table 4.54 - Table 4.59). For the method acc. to *Rawcliffe* and *Menon*, with stray load losses directly measured with equivalent no-load, the slip *s* and the friction and windage losses P_{fw} at rated voltage U_N are presented for some tested motors in the following Tables.

11 kW 4-pole motors	A160-4	B160-4	C160-4	E160-4
Friction loss /W	70	93	98	63
Slip /%	0.007	0.087	0.013	0.000
Stray load losses /W	Not possible [2]	624	Not possible [2]	-63

Table 4.48: The measured stray load losses with the equivalent no-load method of *Rawcliffe* for 11 kW, 4-pole motors

[2]: The measurement could not be evaluated as the slip is zero or the values are erratic.

11 kW 2- & 6-pole motors	A160-2	C160-2	D160-2	A160-**6**
Friction loss /W	311	264	287	27
Slip /%	0.11	0.11	0.02	0.03
Stray load losses /W	319	537	-167	297

Table 4.49: The measured stray load losses with the equivalent no-load method of *Rawcliffe* for 11 kW, 2-pole and 6-pole motors

5.5 kW 6- & 4-pole motors	A132-6	B132-6	D132-6	A132-**4**
Friction loss /W	49	26	36	49
Slip /%	0.107	0.076	0.00	0.093
Stray load losses /W	223	230	-36	95

Table 4.50: The measured stray load losses with the equivalent no-load method of *Rawcliffe* for 5.5 kW, 6-pole and 4-pole motors

1.1 kW 2-pole motors	A80-2	C80-2	D80-2
Friction loss /W	14	14	16
Slip /%	0.117	0.16	0.13
Stray load losses /W	21	44	17

Table 4.51: The measured stray load losses with the equivalent no-load method of *Rawcliffe* for 1.1 kW, 2-pole motors

0.55 kW 4-pole motors	B80-4	C80-4	D80-4
Friction loss /W	3	4	6
Slip /%	0.12	0.187	0.207
Stray load losses /W	Not possible [2]	28	43

Table 4.52: The measured stray load losses with the equivalent no-load method of *Rawcliffe* for 0.55 kW, 4-pole motors

[2]: The measurement could not be evaluated as the slip is zero or the values are erratic.

0.37 kW 6-pole motors	A80-6	B80-6	C80-6	D80-6
Friction loss /W	3	3	2	4
Slip /%	0.20	0.056	0.101	0.120
Stray load losses /W	13	Not possible [2]	8	7

Table 4.53: The measured stray load losses with the equivalent no-load method of *Rawcliffe* for 0.37 kW, 6-pole motors

[2]: The measurement could not be evaluated as the slip is zero or the values are erratic.

4.3 Comparison of different measurement methods for stray load losses in cage induction machines

The stray load loss measurements were performed by different methods with the same equipment for the same motor size in the power lab of the *Department of Electrical Energy Conversion, Darmstadt University of Technology*. The comparison of the measured stray load losses for the investigated methods related to the value obtained from the residual loss method acc. to IEC 61972 / IEC 60034-2 Ed. 4.0 draft is presented in the following Tables and is shown in Figure 4.12 for the 5.5 kW and 11 kW motors. The results from the equivalent no-load method of *Rawcliffe* are not presented as no good correlation was obtained.

Ratio of stray loss for 11 kW, 4-pole motors	A160-4	B160-4	C160-4	D160-4	E160-4
IEEE 112-method B /IEC 61972	_ [1]	_ [1]	_ [1]	_ [1]	0.9
RRT /IEC 61972	1.53	1.09	1.21	2.03	1.72
Eh-star /IEC 61972	0.96	0.7	0.71	0.85	1.2
No-load of *Bourne* /IEC 61972	1.63	Not measured	Not measured	1.29	0.4
No-load of *Rawcliffe* /IEC 61972	Not possible [2]	4.22	Not possible [2]	Not evaluated	-0.27

Table 4.54: Measured stray load losses from different methods related to the results of the residual loss method acc. to IEC 61972 for four 11 kW, 4-pole motors, five different manufacturers

[1]: The measurement could not be evaluated according to IEEE 112-method B because the thermocouples were not supplied in the winding of the machine.

[2]: The measurement could not be evaluated as the slip is zero or the values are erratic.

Ratio of stray loss for 11 kW 2- & 6-pole motors	A160-2	B160-2	C160-2	D160-2	A160-**6**
IEEE 112-method B /IEC 61972	0.92	0.8	0.69	0.98	0.73
RRT /IEC 61972	1.17	0.98	1.09	1.17	1.69
Eh-star /IEC 61972	0.72	0.56	0.91	0.78	0.95
No-load of *Bourne* /IEC 61972	3.38	Not measured	2.53	Not measured	0.86
No-load of *Rawcliffe* /IEC 61972	1.22	Not evaluated	1.9	-0.26	2.22

Table 4.55: Measured stray load losses from different methods related to the results of the residual loss method acc. to IEC 61972 for four 11 kW, 2- and 6-pole motors, four different manufacturers

Ratio of stray loss for 5.5 kW 6- & 4-pole motors	A132-6	B132-6	C132-6	D132-6	A132-**4**
IEEE 112-method B /IEC 61972	0.74	0.89	0.5	0.78	
RRT /IEC 61972	1.96	1.46	1.53	1.22	1.54
Eh-star /IEC 61972	0.99	1.01	0.72	0.72	0.89
No-load of *Bourne* /IEC 61972	5.1	1.1	2.42	Not measured	Not measured
No-load of *Rawcliffe* /IEC 61972	3.38	1.35	Not evaluated	-0.67	0.63

Table 4.56: Measured stray load losses from different methods related to the results of the residual loss method acc. to IEC 61972 for four 5.5 kW, 6- and 4-pole motors, five different manufacturers

Figure 4.12 summarize a comparison of the measured stray load losses, the assigned value of 0.5 % ($P_{ad} = 0.005 \cdot P_{e,in}$) acc. to IEC 60034-2 [IEC 60034-2] and the assigned value depending on the rated power acc. to IEC 61972-2 [IEC 61972] for the 11 kW and 5.5 kW motors.

Ratio of stray load losses for 1.1 kW 2-pole motors	A80-2	B80-2	C80-2	D80-2
IEEE 112-method B /IEC 61972	-[*)]	0.68	0.78	0.62
RRT /IEC 61972	0.92	0.92	1.0	0.84
Eh-star /IEC 61972	0.59	0.84	0.73	0.58
No-load of *Bourne* /IEC 61972	3.89	1.02	0.45	1.08
No-load of *Rawcliffe* /IEC 61972	1.26	Not evaluated	0.87	0.18

Table 4.57: Measured stray load losses from different methods related to the results of the residual loss method acc. to IEC 61972 for four 1.1 kW, 2-pole motors, four different manufacturers

[*)]: The measurement could not be evaluated according to IEEE 112-method B (see the note under Table 4.27).

Ratio of stray load losses for 0.55 kW, 4-pole motors	A80-4	B80-4	C80-4	D80-4
IEEE 112-method B /IEC 61972	-[*)]	0.59	-[*)]	0.68
RRT /IEC 61972	0.44	0.46	0.38	0.78
Eh-star /IEC 61972	0.31	0.47	0.13	0.68
No-load of *Bourne* /IEC 61972	1.07	0.39	0.15	0.41
No-load of *Rawcliffe* /IEC 61972	Not evaluated	Not possible [2)]	1.66	1.96

Table 4.58: Measured stray load losses from different methods related to the results of the residual loss method acc. to IEC 61972 for four 0.55 kW, 4-pole motors, four different manufacturers

[2)]: The measurement could not be evaluated as the slip is zero or the values are erratic.

Ratio of stray load losses for 0.37 kW, 6-pole motors	A80-6	B80-6	C80-6	D80-6
IEEE 112-method B /IEC 61972	-[*)]	0.46	-[*)]	-[*)]
RRT /IEC 61972	0.35	0.26	0.17	0.39
Eh-star /IEC 61972	0.12	0.17	0.06	0.25
No-load of *Bourne* /IEC 61972	0.91	0.39	0.31	0.25
No-load of *Rawcliffe* /IEC 61972	1.69	Not possible [2)]	0.84	1.75

Table 4.59: Measured stray load losses from different methods related to the results of the residual loss method acc. to IEC 61972 for four 0.37 kW, 6-pole motors, four different manufacturers

Figure 4.12 gives a comparison of the measured stray load losses P_{ad} acc. to the residual loss method, the RRT, the eh-star test, some results from the equivalent no-load method of *Bourne*, the assigned value of 0.5 % acc. to IEC 60034-2 ($P_{ad} = 0.005 \cdot P_{e,in}$) and the assigned value depending on the rated power acc. to IEC 61972-2 for the 11 kW and 5.5 kW motors. The results from the equivalent no-load method of *Rawcliffe* are not presented as no good correlation was found. The 15 motors are arranged in order of increasing stray load losses acc. to the residual loss method from number 1 to 15. The RRT method yields too high stray load losses, whereas the residual loss (input-output) method and the eh-star results correlate quite well. The results showed that the assigned

value of 0.5% acc. to IEC 60034-2 yields often too low stray load losses. The results of the equivalent no-load method of *Bourne* can be either too big or too low and only in few cases they are fitting quite well, so no good overall correlation is given.
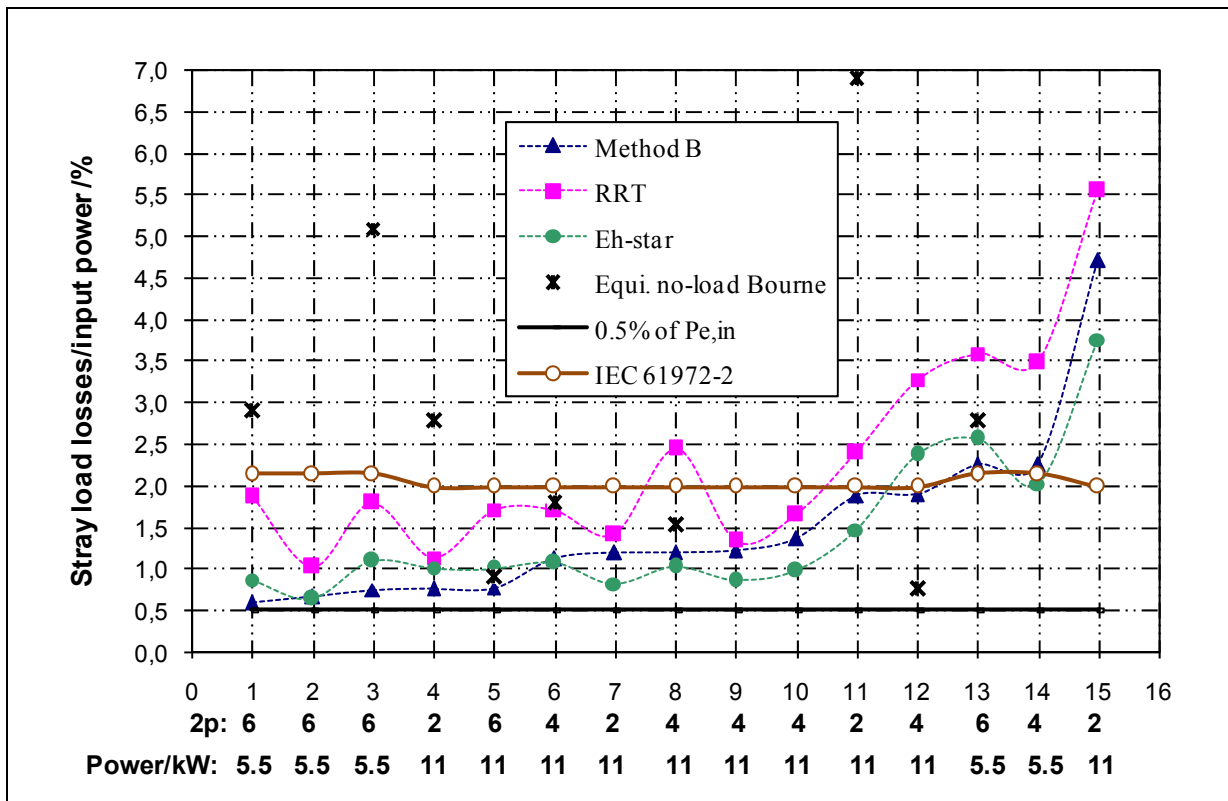
Figure 4.12: Measured stray load losses as percentage of the input power, evaluated from 4 different test methods, the assigned value of 0.5 % of the electrical input power acc. to IEC 60034-2 and the assigned value depending on the rated output power acc. to IEC 61972-2 for 15 different motors of 5.5 kW and 11 kW of six manufacturers

In Figure 4.13 a comparison of the measured stray load losses for the 1.1 kW, 0.55 kW and 0.37 kW motors is shown. Also the assigned value of 0.5% acc. to IEC 60034-2 can be seen, and the assigned values acc. to IEC 61972-2 are depicted. The results from the equivalent no-load method of *Rawcliffe* are not presented as no good correlation was found. The motors are arranged for each rating and in order of increasing stray load losses acc. to the residual loss method.
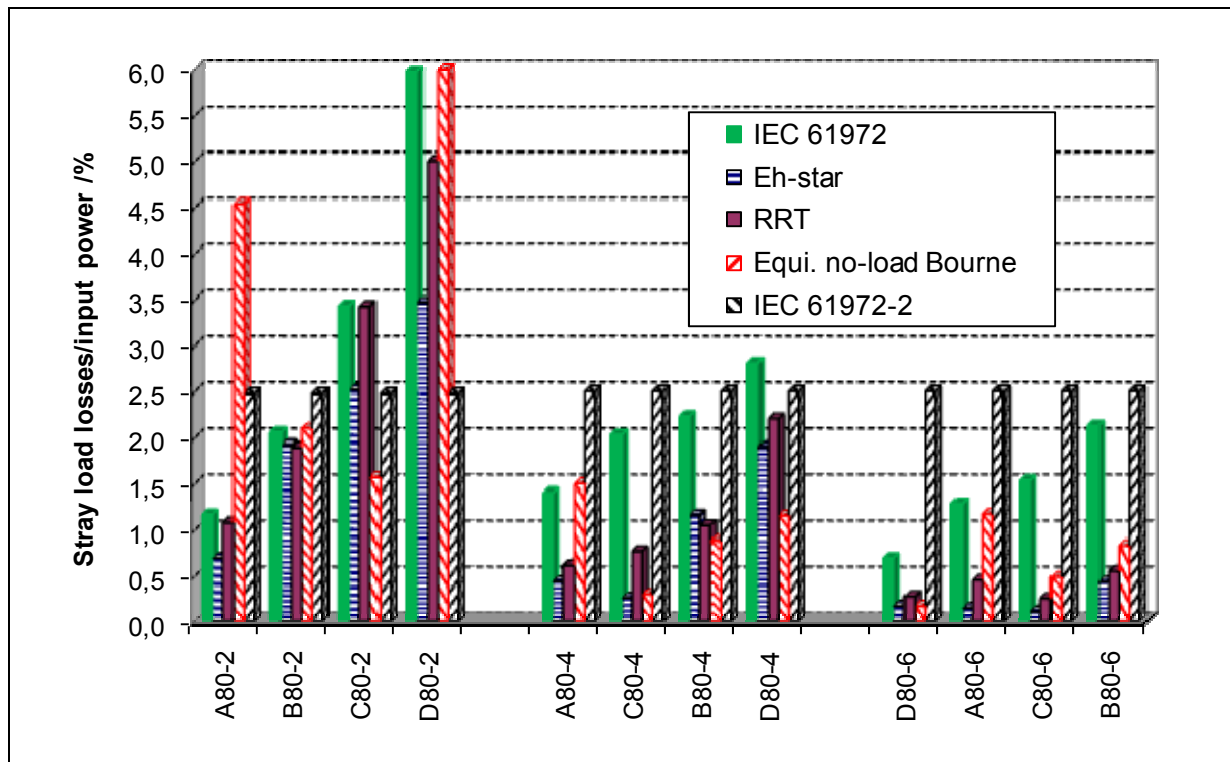
Figure 4.13: Measured stray load losses as percentage of the input power, evaluated from 4 different test methods, the assigned value depending on the rated output power acc. to IEC 61972-2 for 12 different motors of 1.1 kW, 0.55 kW and 0.37 kW of four manufacturers

4.4 Measurement of 315 kW cage induction machine

The tests of the 315 kW four pole standard induction motor (TEFC) were done in the test field of the manufacturer. The test results at 50 Hz grid-operation are presented in the following Tables.

315 kW 4-pole motor "A317-4"			
Rated U /V / I /A, Δ	Phase resistance @ 20°C /Ω	Iron losses /kW	Friction loss /kW
400 / 540	0.0103	1.303	2.673

Table 4.60: No load loss segregation acc. to IEC 61972 for 315 kW, 4-pole motor "A317-4"

315 kW 4-pole motor "A317-4"	
Winding temperature rise /K	86.7
Speed /rpm	1486.5
Torque / kNm	2.026
Electrical input power /kW	327.55
Corrected mechanical output power /kW	314.05
Corrected stator copper losses @ 25°C /kW	4.35
Corrected rotor cage losses @ 25°C /kW	2.893
Stray load losses /kW	2.358
Stray load losses/$P_{e,in}$ /%	0.72
Correlation coefficient R	0.977
Indirect Efficiency $P_{out,c}/P_{e,in}$ /%	95.88
Indirect Efficiency acc. IEC 60034-2 /%	96.10
Indirect Efficiency acc. IEC 61972-2 /%	95.35
Direct Efficiency $P_{out}/P_{e,in}$ /%	96.28

Table 4.61: Stray load losses and efficiency acc. to IEC 61972 compared with the efficiencies acc. to IEC 60034-2 and IEC 61972-2 for 315 kW, 4-pole motor "A317-4"

The stray load losses are determined in this example using the winding temperature of the rated load temperature test for the five load points as the temperature was not available for the load test. The torque was measured by a torque-meter of range 10 kNm. At 125 % rated load only 25 % of full scale is utilised. The difference between the directly measured efficiency η_{dir} from the input and the output powers (input-output test) and the indirectly measured efficiency $\eta_{indir,c}$ (residual loss method) is 0.4 %.

Ratio of the stray load loss for 315 kW 4-pole motor "A317-4"	
IEC 61972 / Eh-star	1.49
IEC 60034-2 / Eh-star	1.03

Table 4.62: Measured stray load losses with input-output acc. to IEC 61972 related to the results of the eh-star method compared with the assumed value of 0.5 % of the electrical input power acc. to IEC 60034-2 for 315 kW, 4-pole motor "A317-4"

4.5 Measurement of 1500 kW cage wind generators

Two different grid-operated low voltage six poles, squirrel-cage rotor asynchronous generators for 1500 kW wind turbines with different types of the stator winding were tested:

1) generator with Round wire winding "A550-6R" and

2) generator with Litz wire (braid) winding "A550-6L".

Some data of the generators are given Table 4.63.

1500 kW 6-pole generators, 600 V Δ, 60 Hz	A550-6R	A550-6L
Winding type	Round wire	Litz wire
Slot fill factor /%	37.4	79
Slot number in stator / rotor	72 / 86	72 / 86
Iron stack length /mm	980	900
Stator bore diameter / Air gap /mm	540 / 1.75	540 / 1.75
Rotor Cu-cross-section /mm²	169	190
Wedge (stator slot)	non magnetic	magnetic

Table 4.63: Data of the measured 1500 kW, 6-pole generators

A calibrated dc-motor with known losses is used to drive the induction generators. For the round wire winding generator "A550-6R" with higher stray load losses (see Table 4.66) the heat run test (input-output) is done only at partial load of ca. 80 % of the rated output power due to the thermal limit of the winding insulation. For this generator the mechanical power is also measured by a 10 kNm-torque-meter. The experience showed that the measurements with the torque-meter were more accurate than with the calibrated dc-motor with known losses and is therefore used further.

The tests on the water cooled wind generators were done in the test field of the manufacturer. The test results at 60 Hz grid-operation are presented in the following Tables.

1500 kW 6-pole generators	Rated U /V / I /A, Δ	Phase resistance @ 20°C /Ω	Iron losses /kW	Friction loss /kW
A550-6R	600 / 1580	0.00295	8.84	2.49
A550-6L	600 / 1580	0.00287	8.93	1.92

Table 4.64: No load losses segregation acc. to IEEE 112 for 1500 kW, 6-pole generators

4.5.1 Direct measurement of the stray load losses using the reverse rotation test

The smoothened data of the measured stray load losses in the stator during the removed rotor test and in the rotor during the reverse rotation test acc. to IEEE 112, where the mechanical power is measured with a 2 kNm-torque-meter, are presented in Table 4.65.

1500 kW 6-pole generators	A550-6R	A550-6L
Removed rotor test /kW	11.5	1.4
Removed rotor test /rated power /%	0.76 %	0.09 %
Reverse rotation test /kW	18	11.1
Reverse rotation test /rated power /%	1.2 %	0.74 %
Stray load losses /kW	29.5	12.5
Stray load losses /rated power /%	1.96 %	0.83 %

Table 4.65: The measured stray load losses at rated current in the stator and in the rotor with the reverse rotation test acc. to IEEE 112 for 1500 kW, 6-pole generators

The fundamental-frequency stray load losses $P_{ad,s}$ in the stator of the round wire winding generator "A550-6R" are excessively high, about 0.76 % of rated power, due to the skin effect, especially the circulating current (first order eddy current losses). With increasing the resistance due to the skin effect the inductance decreases and consequently the "filter" effect of the winding decreases also which leads to higher high-frequency stray load losses. Also the higher-frequency stray load losses $P_{ad,r}$ in the rotor are high in comparison with the litz wire winding generator "A550-6L".

4.5.2 Indirect measurement of the stray load losses using the "residual loss method" acc. to IEEE 112-method B

This test is only applied on the round wire winding generator "A550-6R", where the mechanical power is also measured by a 10 kNm-torque-meter at partial load of ca. 80 % of the rated output power. The results of the input-output test acc. to IEEE 112-method B (residual losses) compared with the stray load losses and the efficiency acc. to IEEE 112-method E (stray load losses from the reverse rotation test) are presented in Table 4.66 and Figure 4.14.

As depicted in Table 4.66 the stray load losses determined indirectly with the residual loss method acc. to IEEE 112-method B, which suffers from inaccuracy at high efficiency (see Table 4.70), deviate by 63 % from the stray load losses determined directly with the reverse rotation test acc. to IEEE 112-method E. The difference in the efficiency between both methods is above 0.5 % for this example.

1500 kW 6-pole generator "A550-6R" at 80 % rated output power		
Method	IEEE 112-B	IEEE 112-E
Winding temper. rise over 50°C inlet water /K	80.5	80.5
Speed /rpm	1212.9	1212.9
Torque / kNm	10.02	10.075
Electrical output /kW	1228.94	1228.94
Corrected mechanical input /kW	1272.36	1279.65
Stray load losses /kW	11.52	18.81
Stray load losses/Rated output /%	0.77	1.25
Correlation coefficient R	0.992	Not applicable
Indirect Efficiency $P_{e,out}/P_{m,c,in}$ /%	96.587	96.037
Indirect Efficiency acc. IEC 60034-2 /%	97.082	97.082
Indirect Efficiency acc. IEC 61972-2 /%	96.902	96.902
Direct Efficiency $P_{e,out}/P_{m,in}$ /%	96.590	Not applicable

Table 4.66: Stray load losses and efficiency acc. to IEEE 112-method B and IEEE 112-method E compared with the efficiencies acc. to IEC 60034-2 and IEC 61972-2 for 1500 kW, 6-pole generator "A550-6R" at 80 % of the rated output power
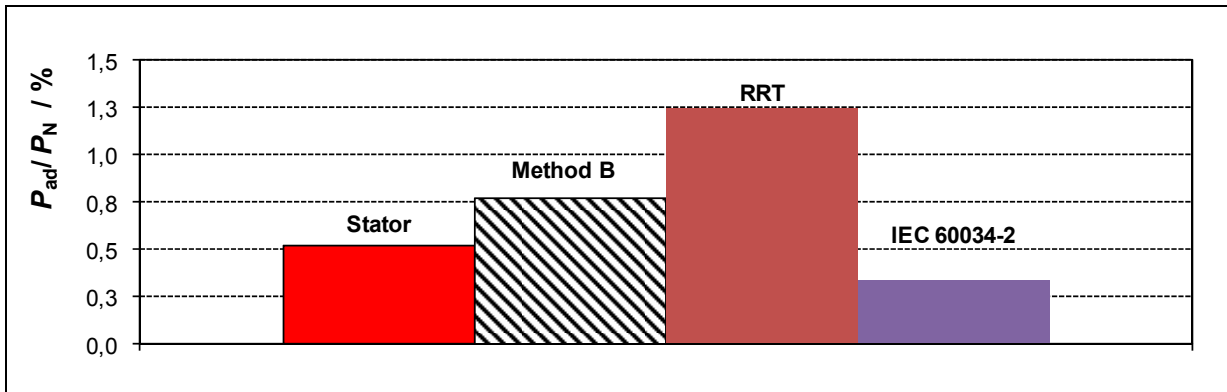
Figure 4.14: The stator and the total stray load losses acc. to IEEE 112-method B and IEEE 112-method E compared with the value acc. to IEC 60034-2 for 1500 kW, 6-pole generator "A550-6R" at 80 % of the rated output power

Due to the heating problem the generator could not run continuously at full load, otherwise the insulation life time will be strongly reduced. To avoid destruction due to overheating the practical consequence of this effect is the derating! It has to be noted that, only by direct measurement of the stray load losses - separately in the stator and in the rotor - the source of the heating could be identified. With the residual loss method (input-output test) e.g. acc. to IEEE 112-method B it would not be possible.

To estimate the winding temperature rise $\Delta\vartheta_{Cu,s}$, the slip s and therefore the efficiency η at rated load the equivalent heat losses P_{eq}, which are heating the stator winding, should be determined.

4.5.2.1 Equivalent heat losses in the stator winding

The equivalent heat losses P_{eq}, which are heating the stator winding, include all losses dissipated in the stator and the rotor with different weight as assumed in the expression

$$P_{eq} = P_{Cu,s} + P_{ad,s} + 0.5 \cdot P_{Fe} + 0.2 \cdot \left(P_{Cu,r} + P_{ad,r}\right).$$ (4.2)

Due to the cooling system with water-jacket in the housing and inner air-fan-cooling of the rotor, only 20 % of the rotor losses ($P_{Cu,r} + P_{ad,r}$) and 50 % of the

iron losses P_{Fe} are are taken into account heating the stator winding. The fundamental-frequency stray load losses $P_{ad,s}$ in the stator and the higher-frequency stray load losses $P_{ad,r}$ in the rotor are taken from the reverse rotation test.

1500 kW 6-pole generator "A550-6R"	Load		80 % (measured)	100 % (calculated)
Line current	I_s	A	1300	1580
Stator copper losses	$P_{Cu,s}$	W	7143	12191
Stator stray load losses	$P_{ad,s}$	W	7787	11500
Iron losses	P_{Fe}	W	8842	8842
Rotor copper losses	$P_{Cu,r}$	W	13466	23238
Rotor stray load losses	$P_{ad,r}$	W	12189	18003
Equivalent heat losses	P_{eq}	W	24481	36361
Winding temper. rise over 50°C inlet water	$\Delta\vartheta_{Cu,s}$	K	80.5	137.3
Heat transfer capability	$P_{eq}/\Delta\vartheta_{Cu,s}$	W/K	304	265

Table 4.67: Heat transfer capability for 1500 kW, 6-pole generator "A550-6R"

As shown in the Table 4.67 the calculated winding temperature rise $\Delta\vartheta_{Cu,s}$ of 137 K at full-load exceeds the limit of the specified insulation class "F".

4.5.2.2 Determination of the efficiency at full-load

With the determined values of the winding temperature rise $\Delta\vartheta_{Cu,s}$ and the slip s from the equivalent heat losses P_{eq}, the indirectly determined efficiency η at rated load is calculated for the generator "A550-6R" acc. to IEEE 112-method E and presented in the following table. A comparison of the efficiency determined acc. to IEEE 112-method E1, where the stray load losses are assumed to be 1.2 % of the rated output, is also given. The efficiencies determined acc. to IEEE 112-method E/E1 for both generators are compared in Table 4.69.

1500 kW 6-pole generator "A550-6R"		
IEEE 112-method E/E1	80 % (measured)	100 % (calculated)
Winding temper. rise over 50°C inlet water /K	80.5	137.3
Speed /rpm	1212.9	1218.2
Torque / kNm	10.075	12.346
Electrical output /kW	1228.94	1500
Corrected mechanical input /kW	1279.65	1574.99
Stray load losses /kW	18.81	28.34
Stray load losses/Rated output /%	1.25	1.89
Indirect Efficiency $P_{e,out}/P_{m,c,in}$ /%	96.037	95.239
Indirect Efficiency acc. IEEE 112-E1 /%	96.555	96.240

Table 4.68: Determination of the efficiency at full-load acc. to IEEE 112-method E compared with the efficiency acc. to IEEE 112-method E1 for 1500 kW, 6-pole generator "A550-6R"

As given in Table 4.69 the efficiency-difference determined acc. to IEEE 112-method E between both generators is above 1 %. For the generator "A550-6L" the values of the winding temperature rise $\Delta\vartheta_{Cu,s}$ and the slip s are measured values.

1500 kW 6-pole generators		
IEEE 112-method E/E1	A550-6R	A550-6L
Winding temper. rise over 50°C inlet water /K	137.3	83.8
Speed /rpm	1218.2	1219.1
Torque / kNm	12.346	12.239
Electrical output /kW	1500	1504.9
Corrected mechanical input /kW	1574.99	1562.66
Stray load losses /kW	28.34	12.02
Stray load losses/Rated output /%	1.89	0.80
Indirect Efficiency $P_{e,out}/P_{m,c,in}$ /%	95.239	96.304
Indirect Efficiency acc. IEEE 112-E1 /%	96.240	95.938

Table 4.69: Stray load losses and efficiency at full-load acc. to IEEE 112-method E compared with the efficiency acc. to IEEE 112-method E1 for 1500 kW, 6-pole generators "A550-6R" and "A550-6L"

4.5.3 Impact of the measurement error on the stray load losses

To show the influence of the measurement error on the stray load losses measured directly with the RRT acc. IEEE 112 and indirectly with the residual loss method (input-output test) acc. IEEE 112-method B, an instrument accuracy class of 0.2 % acc. to IEEE 112 is assumed. In Table 4.70 and Figure 4.15 each measured parameter is modified separately by +0.2 %. The results are presented as the measured P_{ad} and the corrected (smoothed) $P_{ad,c}$ stray load losses.

1500 kW 6-pole generator "A550-6R"		Deviation of stray load losses			
	Method	*Residual loss*		*RRT*	
Assumed measurement error		ΔP_{ad} /%	$\Delta P_{ad,c}$ /%	ΔP_{ad} /%	$\Delta P_{ad,c}$ /%
+0.2 %	$P_{e,out}$	-21.5	-16.4	-0.32	-0.33
+0.2 %	$P_{m,in}$	22.1	16.7	0.29	0.30
+0.5 %	$P_{m,in}$	55.2	41.9	0.73	0.74

Table 4.70: Influence of the measurement error on directly and indirectly measured stray load losses for 1500 kW, 6-pole generator "A550-6R"
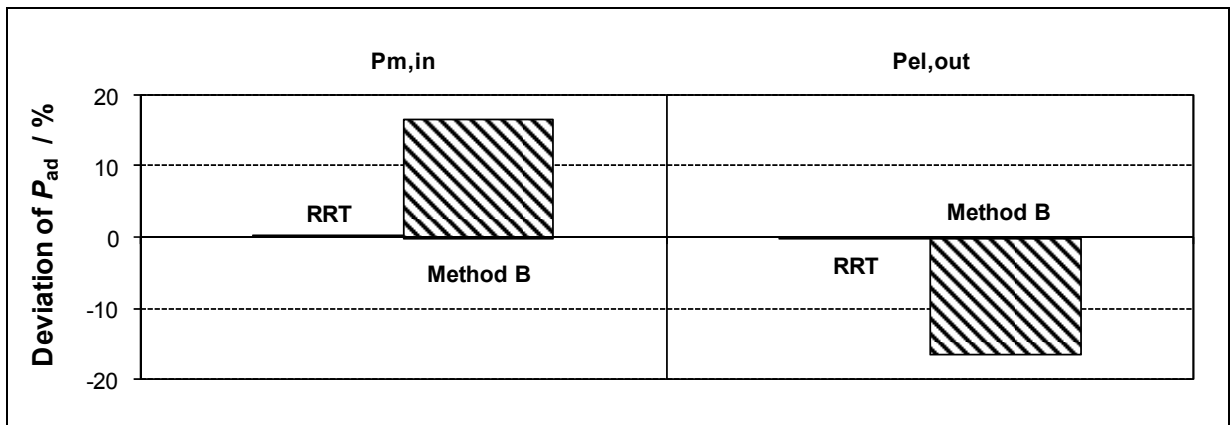
Figure 4.15: Influence of the +0.2 % measurement error on directly (RRT) and indirectly (method B) measured stray load losses for 1500 kW, 6-pole generator "A550-6R"

Table 4.70 and Figure 4.15 shows that the stray load losses measured indirectly with the residual loss method acc. IEEE 112-method B are more sensitive to measurement error than the directly measured stray load losses from the RRT acc. IEEE 112. The impact of the measurement error on the RRT

results is the same for the measured and the smoothed values, whereas the influence on the measured values with method B is higher than on the corrected values.

4.6 Conclusion

The stray load losses were measured with the residual loss method acc. to IEEE 112-method B and acc. to IEC 61972/ IEC 60034-2 Ed. 4.0 draft, with the reverse rotation test acc. to the standard IEEE 112 and IEC 61972, with the eh-star method acc. to *Jordan* and *Richter* [Jord 1967] and acc. to the new proposed standard IEC 60034-2 Ed. 4, 2nd CDV, with the equivalent no-load method acc. to *Bourne* [Bour 1989] and with the equivalent no-load method acc. to *Rawcliffe* and *Menon* [Rawc 1952]. The measured values were compared with different assumptions acc. to the standards.

- The experimental evaluation of the 5.5 kW and 11 kW motors with pole count 2, 4 and 6 showed good coincidence between the residual loss methods (input-output methods) and the eh-star method, whereas the RRT method gives bigger stray load losses.

- The power rating 1.1 kW proved to be still good measurable, whereas for the power ratings 550 W and 370 W the stray load losses are very small (only some Watt), so the measurement uncertainty increases.

- With decreasing power rating the p.u. stator resistance per phase value increases. The resistive voltage drop significantly reduces the inner voltage. Therefore the iron losses decrease under load. This fact is considered in the standard IEC 60034-2 Ed. 4.0 draft so always positive stray load losses were measured, whereas the standard IEEE 112-B considers the iron losses to be load independent leading in some cases to negative stray load losses, especially at small power rating 370 W.

- For the power rating less than 1.1 kW the RRT method yields – unlike in case of bigger motors – the same or less stray load losses than the residual loss methods (input-output methods) for the investigated motors.

- For the small power rating the eh-star method yields lower stray load losses than the residual loss methods. With decreasing power ratings the minimum value of the positive vs. the negative sequence current, which

should stay below 30 %, increases – being about 35 % at 550 W and 45 % at 370 W. This may lead to too low stray load losses.

- The results of the equivalent no-load method of *Bourne* can be either too big or too low and only in few cases are fitting quite well, so no good overall correlation was found.

- The results of the equivalent no-load method of *Rawcliffe*, which were sometimes not possible to be evaluated, can be either too big or too low and only in few cases are fitting quite well, so no good correlation was found.

- The measured stray load losses are for all cases bigger than those obtained from the assigned value of 0.5 % of the electrical input power stated in IEC 60034-2.

To improve the measurement accuracy and therefore to get better correlation coefficient R, the reading of the measured data should be taken over an averaging time e.g. of about 10 s, depending on the rating of the motor (thermal time constant), for each load point especially in the input-output test with the torque measurement.

In addition, the influence of the temperature, the resistive losses, the iron losses and the friction and windage losses on the determination of the stray load losses and the efficiency was shown.

The stray load losses must be measured and cannot be replaced by any kind of fixed assumption.

The efficiency values obtained from different testing standards can differ by several percent. For big machines with high efficiency the direct measurement of the "small" stray load losses could be useful. Another advantage of this method is the separate identification of the stray load losses in the stator and in the rotor, which is helpful for purposeful optimizing of the machine design. In comparison, the residual loss methods e.g. acc. to IEEE 112-method B and the calorimetric method determine the stray load losses as a sum.

The stray load losses have a considerable impact on the performance of the machine. By a measured example it was shown that, due to the stray load losses, the generator could not run continuously at full load. To avoid insulation destruction the practical consequence of this effect, due to the overheating, is the derating !

5   INVESTIGATION OF STRAY LOAD LOSS COMPONENTS

Three main issues form the objective of this chapter: the basics of eddy current losses in conductors, analytical calculation of the stray load losses in the stator winding due to skin effect and a comparison of the measurement on a 1500 kW low-voltage grid-operated cage induction generators with profile, litz and round wire winding. Some measures to suppress the stray load losses in the stator winding due to circulating currents will be given. In addition the cause for overheating of the highly utilised round wire winding will be shown. The chapter will be closed with an overview on main stray load loss components in 11 kW cage induction motors and a comparison between measurement and analytical calculation.

5.1 Losses in induction machines

Generally the losses in induction machines can be subdivided into the conventional losses (*Ohmic* losses, iron losses, friction and windage losses) and the stray load losses, namely in the stator and in the rotor, at no-load and under load as summarised in Table 5.1. These losses can be reduced by using quality materials, as well as by optimising the design.

Losses	At No-load	At Load
Stator	Copper losses in winding Iron losses in active iron stack, in housing and bearing brackets Stray no-load losses	Copper losses in winding Iron losses in active iron stack, in housing and bearing brackets Stray load losses
Rotor	Friction and windage losses Stray no-load losses	*Ohmic* (copper) losses in winding Iron losses in active iron stack, in shaft and metallic fan Stray load losses

Table 5.1: Simplified distribution of the losses in induction machines

5.1.1 Conventional losses

The losses called conventional are

1. *Ohmic* losses in the conductors expressed by I^2R, they increase rapidly with the load current and can be decreased e.g. by increasing the cross section of the stator and the rotor conductors, and by using copper instead aluminium,

2. Iron losses mainly in the steel laminations of the stator and the rotor due to hysteresis and eddy currents, varying with flux density and frequency. They can be reduced e.g. by using thinner laminations, sharp punching tools and improved magnetic materials,

3. and the mechanical losses due to friction in the bearings and – in case of slip ring machines – brush friction losses, the ventilation and windage losses. They can be decreased e.g. by using low friction bearings, improved and optimized ventilation and fan design.

5.1.2 Stray load losses

The stray load losses are due to e.g. the stray flux, the step-like (non sinus) distribution of the air gap flux density due to the arrangement of the winding and the cage in the slots, inter-bar currents and mechanical imperfections in the air

gap, also the eccentricity fields induce voltages in the parallel paths of the stator windings and give rise to equalizing currents [Kett 1984]. They can be reduced by optimal design and careful manufacturing (see also e.g. [Ober 1969]).

The main components of stray load losses in squirrel-cage induction motors can be subdivided as follows [Bind 1988, Bind 2006m]:

a) Fundamental-frequency stray load losses in the stator which consist of

- skin effect (first and second order) in the stator winding,

- stray load losses in the end region due to axial flux components [Taeg 1987]

- eddy current losses especially at high saturation in the stator housing and in metallic parts e.g. the bearing brackets.

b) Higher-frequency stray load losses in the rotor and stator which include

- skin effect in the rotor cage, harmonic rotor currents due to the third space harmonic caused by iron saturation

- losses due to inter-bar currents in cages with skewed rotor slots [Kron 1969]

- tooth pulsation losses in the rotor and the stator caused by the distortion of the air gap flux density distribution due to the slot openings

- surface losses in the rotor and the stator

- losses in the stator winding due to harmonic currents [Kron 1969] and circulating currents in delta connected stator windings due to the third space harmonic caused by iron saturation.

- iron losses in the stator core due to the third space harmonic caused by the distortion of the field distribution due to iron saturation.

5.2 Basics of eddy currents in conductors located in the slot

The conductor e.g. a deep bar in the slot is exposed to AC pulsating slot stray flux density B_Q, which is excited by the current in the conductor itself I_{bar}

[Bind 2006m]. The slot flux density B_Q induces, according to *Faraday*'s law $u_i = -d\Phi_Q / dt$, an additional voltage in the bar, which causes eddy current I_{Ft} (Ft: *Foucault*-current) to flow in the bar. Due to the negative sign in *Faraday*'s law the field of eddy current B_{QFt} opposes the original slot flux density B_Q (*Lenz*'s rule) and weakens it as presented in Figure 5.1 and Figure 5.3. The superposition of the bar current I_{bar} and eddy current I_{Ft} yields increased current density in the upper bar region and reduced current density J in the bottom of the bar ("current displacement or skin effect", see Figure 5.3). Hence the bar current I_{bar} flows mainly in upper half of the bar, thereby using only part of the bar cross section, which leads to an increase of the effective bar resistance and reduces the inductance as shown in the principle equivalent circuit in Figure 5.2.
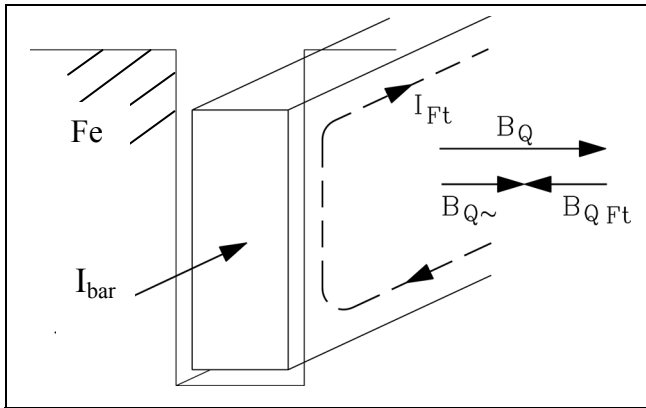
Figure 5.1: Eddy current I_{Ft} in deep bar [Bind 2006m]
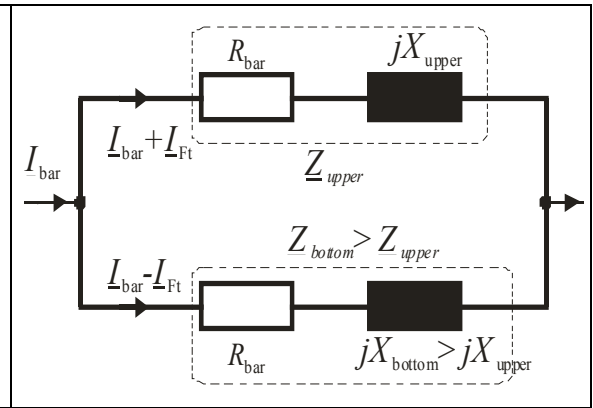
Figure 5.2: Asymmetrical current distribution due to eddy current

With *Ampere*'s law we get for the stray flux density - simplified - a linear rise along the bar and constant value above the bar (see Figure 5.3) [Bind 2006m]

$$\oint_C \vec{H} \cdot d\vec{s} = H_Q(x) \cdot b_Q = J \cdot x \cdot b_{bar}$$

$$B_Q(x) = \mu_0 \cdot H(x)$$

$$= \mu_0 \cdot J \cdot x \cdot \frac{b_{bar}}{b_Q} = \mu_0 \cdot \frac{I_{bar}}{b_Q} \cdot \frac{x}{h_{bar}} \qquad\qquad 0 \le x \le h_{bar} \tag{5.1}$$

$$B_Q = \mu_0 \cdot I_{bar} / b_Q \qquad\qquad h_{bar} \le x \le h_Q$$
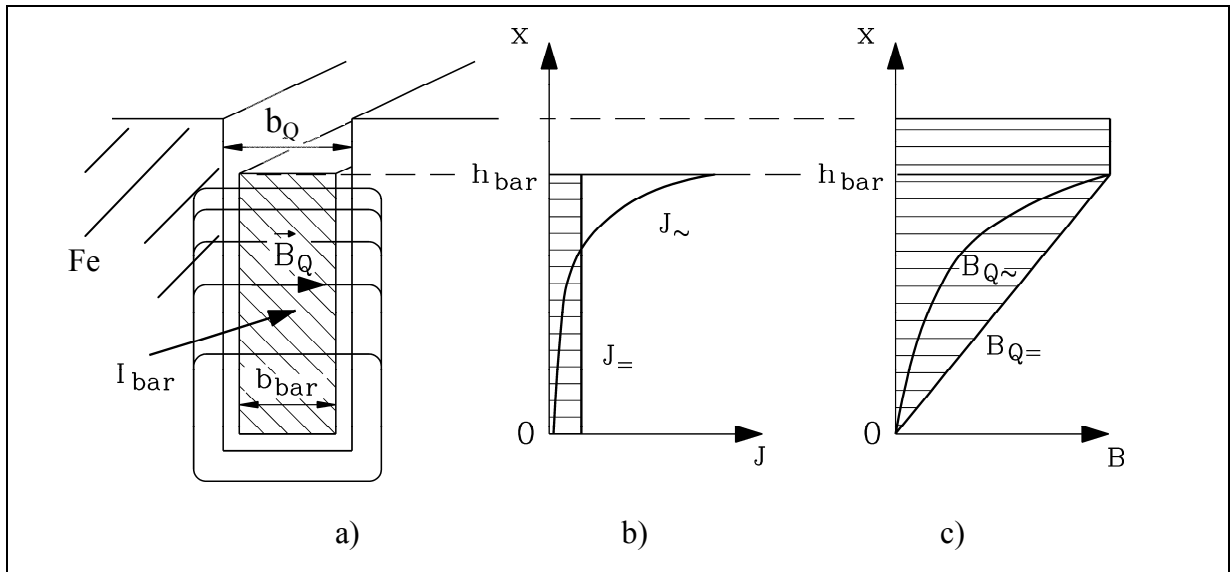
Figure 5.3: Current displacement in deep bar in comparison to DC current situation.
  a) Slot and bar cross section with slot stray flux lines,
  b) Bar current density distribution with/without skin effect,
  c) Slot flux density distribution with/without skin effect [Bind 2006m]

The skin effect causes an increase of the effective conductor resistance compared to the DC resistance R_{DC}

$$k_r = \frac{R_{AC}}{R_{DC}} = \varphi(\xi) + c \cdot \psi(\xi) \text{ , for special case of one conductor } c = 0 \qquad (5.2)$$

For more details about the functions $\varphi(\xi)$, $\psi(\xi)$ and the reduced conductor height ξ see section 5.3.3.

The skin effect depends mainly on:

- Frequency f

- Conductor height h_{TL}

- Conductor conductivity κ taking the temperature into account

- Conductor permeability μ.

5.3 Calculation of the stray load losses in the stator winding

One of the main origins of the stator component of the stray load losses in the analyzed, low voltage wind generators are the losses $P_{ad,s,1.O}$ due to first and $P_{ad,s,2.O}$ due to second order skin effect in the stator winding, mainly in the slots along the stack length l_{Fe}:

a) First order eddy currents (1.O), or circulating currents, flow in loops composed of insulated, parallel partial conductors or wires which are connected at the ends of the conductors or the coil (see Figure 5.4).

b) Second order eddy currents (2.O) are displacement currents within the conductors or the wires themselves (see Figure 5.4 and Figure 5.1).
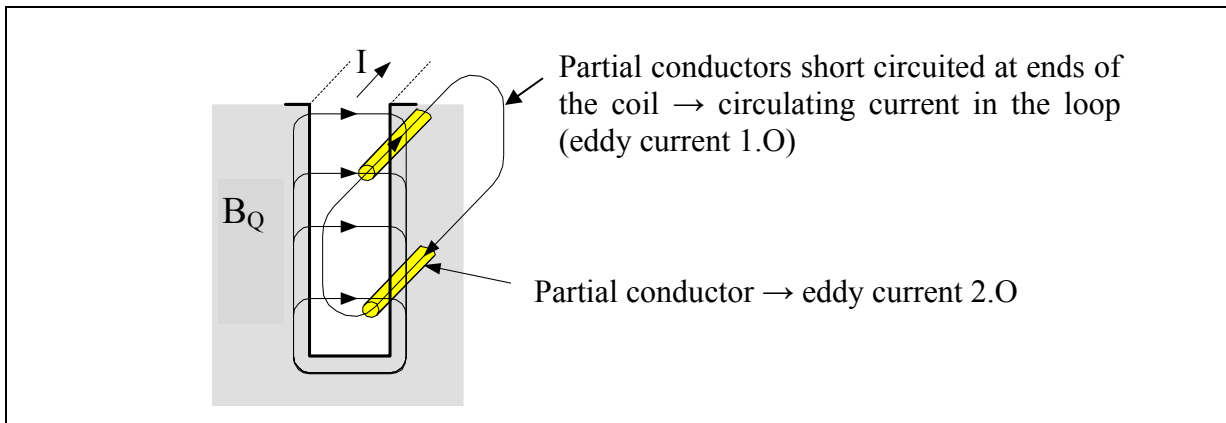
Figure 5.4: Principle sketch of the first order and second order skin effect

This uneven distribution of the current in the conductors and in the short-circuited conductor-loops may be regarded as increasing the stator DC resistance $R_{s,dc}$ by the resistance coefficients $k_{r1.O}$ (first order skin effect) and $k_{r2.O}$ (second order skin effect). Analytical formulas – *Field's* and *Emde's* formulas [Vogt 1974] – exist only for rectangular profiled conductors, with distinguished placement of the conductors in the slot. Therefore, calculation of the eddy current losses for the round wire winding with arbitrarily – randomly, undefined – distributed conductors can be only approximated by an equivalent rectangular slot approximation for the real oval-shaped stator slot (Figure 5.18).

5.3.1 Calculation model

The analytical model [Vogt 1974] is based on the following assumptions:

1) The stray flux lines in the slot are perpendicular to the slot wall (see also [Lamm 1966])

2) The radial stray flux lines through the slot opening are neglected

3) The conductors in the slot are parallel

4) The permeability of the iron stack is assumed to be infinite.

In the analytical model the following is considered:

1) Eddy current losses in conductors located in the slot region

2) Eddy current losses in the straight part of the winding overhang

3) Eddy current losses in the curved part of the winding overhang

4) First order skin effect

5) Second order skin effect

6) Dependence on temperature, which is assumed to be constant for all conductors.

7) Pitching of coils

8) Transposition of conductors, which is usual for two-layer windings with profile copper conductors.

5.3.2 Definition of winding parameters

Some winding parameters for the round wire winding in the equivalent rectangular slot, for the profiled winding and for the coil dimensions are presented in the Figure 5.5 with

b_{TL} :   width of partial conductor
h_{TL} :   height of partial conductor

n_n :   number of partial conductors side by side (horizontal) per slot
$n_ü$:   number of partial conductors one above the other per slot
h_w :   height of the turn per coil
b_Q :   slot width
h_Q :   slot height
$w_ü$:   number of turns one above the other per slot
a_p :   number of parallel partial conductors per turn
W :   coil width
l_m :   length of the conductor ($l_m = l_{Fe} + l_{b1} + l_{b2}$)
l_{Fe} :   length of the iron stack
l_{b1} :   length of the conductor in the straight part of the winding overhang
l_{b2} :   length of the conductor in the curved part of the winding overhang.
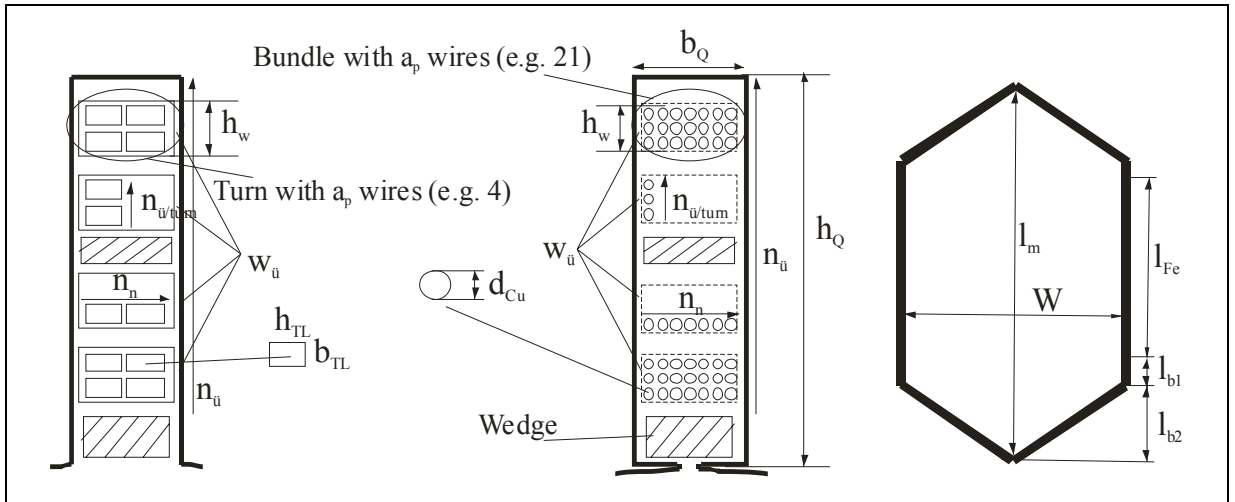
Figure 5.5: The winding parameters for the profiled winding and the round wire winding in the equivalent slot and the coil dimensions

5.3.3 Eddy current losses in conductors located in slot region

The eddy current losses in the slot region along the stack length l_{Fe} are the important part of the eddy current losses in the stator winding.

For the calculation of the eddy current losses and the resistance coefficient k_r the functions $\varphi(\xi)$, $\psi(\xi)$ will be used where ξ is the reduced conductor height. The functions $\varphi(\xi)$, $\psi(\xi)$ are plotted vs. ξ in Figure 5.6. The function $\varphi(\xi)$ considers the influence of the field induced from the conductor itself whereas the

proximity factor $\psi(\xi)$ considers the influence of the field induced from other conductors in the slot. The dimensionless parameter ξ of a conductor is the ratio of its height h_{TL} to the penetration depth d_E which is determined by solution of the *Maxwell's* equations.

$$\varphi(\xi) = \xi \cdot \frac{\sinh(2\xi) + \sin(2\xi)}{\cosh(2\xi) - \cos(2\xi)} \tag{5.3}$$

$$\psi(\xi) = 2\xi \cdot \frac{\sinh(\xi) - \sin(\xi)}{\cosh(\xi) + \cos(\xi)} \tag{5.4}$$

$$\xi = h_{TL} / d_E = h_{TL} \cdot \sqrt{\pi \cdot f \cdot \mu_{TL} \cdot \kappa_{TL} \cdot b_{TL} / b_Q} \tag{5.5}$$

The parameter ξ in (5.5) depends on the frequency f, the conductor height h_{TL}, the conductor conductivity κ at test temperature, the conductor permeability μ ($\mu_{Cu} = \mu_{Al} = \mu_0$) and the ratio of the conductor width b_{TL} to the slot width b_Q. For each case i.e. the first and second order skin effect the parameters $\xi_{1.O}$ and $\xi_{2.O}$ respectively will be calculated in the next section.
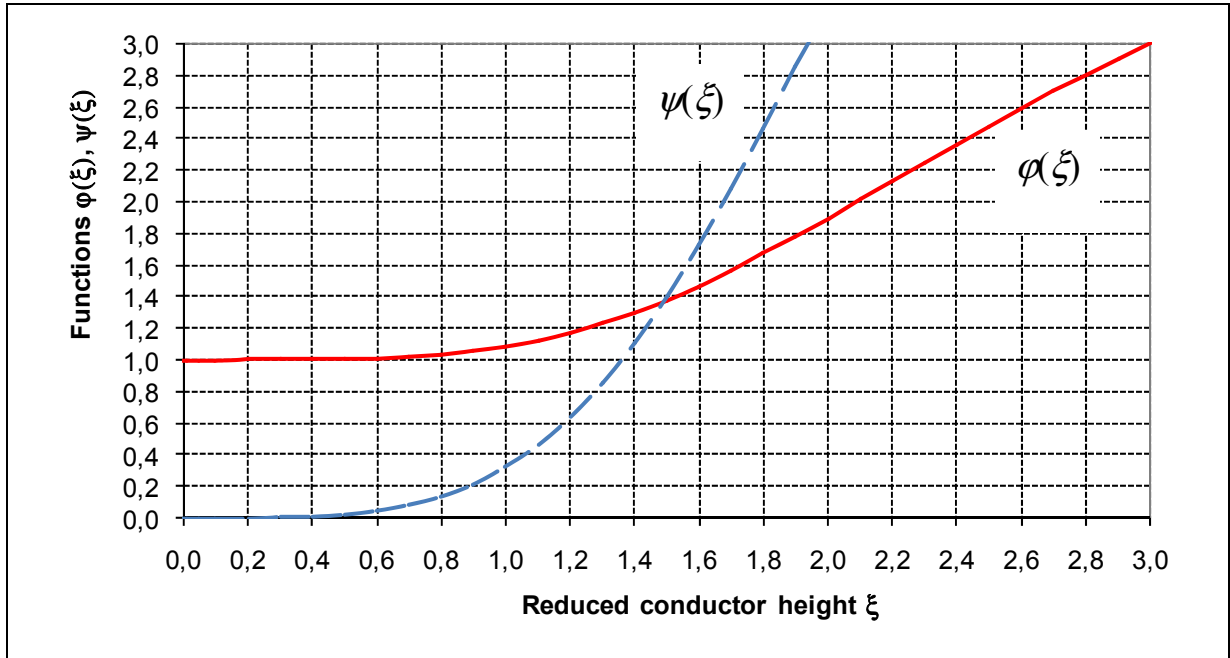
Figure 5.6: The functions $\varphi(\xi)$, $\psi(\xi)$ vs. ξ

The resistance coefficient k_r can be given in general as (5.6) where the factor c is to be determined for each case dependent on the type of winding: single-layer winding, transposed two-layer winding, pitching of the winding etc.

$$k_r = \varphi(\xi) + c \cdot \psi(\xi) \ . \tag{5.6}$$

5.3.4 Eddy current losses in winding overhang

Due to the small stray flux the eddy current losses in winding overhangs are negligible in comparison with the eddy current losses in the slot region especially for small motors and wind generators of some MW. To determine this component of the losses in end windings a 2D field calculation [Bind 1988] is used. The air is substituted by an "equivalent slot width" $b_{Q,e}$.

5.3.4.1   Eddy current losses in straight part of winding overhang

According to [Bind 1988] the tangential field of the end winding, formed by a rectangular shaped bundle of conductors (height h_c, width b_c) which leaves the slot, carrying the total current per coil I_c , is

$$B_t = \frac{\mu_0 \cdot I_c}{4 \cdot \pi \cdot h_c} \cdot \left[\ln(1+r^2) + 2 \cdot r \cdot \mathrm{arctg}(\frac{1}{r}) \right] = \frac{\mu_0 \cdot I_c}{2 \cdot b_{Q,e1}}, \quad r = \frac{2 \cdot h_c}{b_c} \tag{5.7}$$

The "equivalent slot width" $b_{Q,e1}$ of the straight part of the winding overhang along the axial length l_{b1} is then

$$b_{Q,e1} = \frac{2 \cdot \pi \cdot h_c}{\ln\left(1 + \left(\frac{2h_c}{b_c} \right)^2 \right) + \frac{4h_c}{b_c} \cdot \mathrm{arctg}\left(\frac{b_c}{2h_c} \right)} \ . \tag{5.8}$$

In this "equivalent slot width" $b_{Q,e1}$ a half coil height $h_c/2$ according to *Pohl* [Rich 1967] may be introduced to calculate the resistance coefficient $k_{r1.O}$ of the first and $k_{r2.O}$ of the second order skin effect.

5.3.4.2   Eddy current losses in curved part of winding overhang

Analogue to the "equivalent slot width" $b_{Q,e1}$ for the straight part of the winding overhang an "equivalent slot width" $b_{Q,e2}$ for the curved part of the winding overhang along the circumference length l_{b2} is derived using the half coil height $h_c/2$

$$b_{Q,e2} = \frac{2 \cdot \pi \cdot h_{c2}}{\ln\left(1 + \left(\frac{2h_{c2}}{b_c}\right)^2\right) + \frac{4h_{c2}}{b_c} \cdot \operatorname{arctg}\left(\frac{b_c}{2h_{c2}}\right)}, \quad h_{c2} = \frac{h_c}{2}. \tag{5.9}$$

According to *Pohl* a half coil height $h_{c2}/2$ may be introduced for calculating the resistance coefficient $k_{r1.O}$ of the first and $k_{r2.O}$ of the second order skin effect.

5.3.5   Consideration of the pitching of the winding

The pitching of the winding W/τ_p reduces the eddy current losses due to the smaller total amount of the slot ampere-turns amplitude. It affects only the part regarding the function $\psi(\xi)$, which considers the influence of the field induced from other conductors in the slot, whereas $\varphi(\xi)$ considers the influence of the field induced from the conductor itself (see equation (5.6), (5.10) … (5.20)).

A comparison of the influence of the pitching on the eddy current losses between *Binder* formula [Bind 2006c] and *Vogt* [Vogt 1974] is given.

5.3.5.1   Influence of the pitching on the second order skin effect

With the functions $\varphi(\xi_{2.O})$ and $\psi(\xi_{2.O})$ given in (5.3) and (5.4) the average value of the resistance coefficient $k_{r2.O}$ for the second order eddy current of pitched and usually transposed two-layer winding over the conductors per slot can be calculated as

$$k_{r2.O} = \varphi(\xi_{2.O}) + \left(\frac{n_{\ddot{u}}^2 - 1}{3} \cdot k_{Bind}\right) \cdot \psi(\xi_{2.O}) \qquad (5.10)$$

$n_{\ddot{u}}$:   number of partial conductors one above the other per slot
k_{Bind} : simplified pitching coefficient.

The influence of the pitching on the eddy current losses $P_{Ft,2.O}$ acc. to [Bind 2006c] will be compared with the consideration acc. to [Vogt 1974]. The pitching coefficient k_{Bind} acc. to [Bind 2006c] is

$$k_{Bind} = \frac{7}{16} + \frac{9}{16} \cdot \frac{W}{\tau_p} \qquad (5.11)$$

W :   coil width
τ_p :   pole pitch.

The resistance coefficient $k_{r2.O}$ for the second order eddy current of pitched and usual transposed two-layer winding can be calculated acc. to [Vogt 1974] as

$$k_{r2.O} = \varphi(\xi_{2.O}) + \left(\frac{5 \cdot n_{\ddot{u}}^2 - 8}{24} + \frac{n_{\ddot{u}}^2}{8} \cdot \cos\varphi\right) \cdot \psi(\xi_{2.O}) \qquad (5.12)$$

$n_{\ddot{u}}$:   number of partial conductors one above the other per slot
φ :   phase angle between the currents in the upper and lower layer conductor.

For the slots $(q - s_w)$ where the conductors carry the same currents in the upper and lower layer ($\varphi = 0°$) the equation (5.12) can be written as

$$k_{r2.O} = \frac{(q - s_w)}{q} \cdot \left[\varphi(\xi_{2.O}) + \frac{n_{\ddot{u}}^2 - 1}{3} \cdot \psi(\xi_{2.O})\right] \qquad (5.13)$$

q :   number of the slots per pole and phase
s_w :   number of the mixed slots (different phases in upper and lower layer).

For the mixed slots (s_w), where the conductors carry different currents in the upper and lower layer e.g. ($\varphi = 60°$) the equation (5.12) can be written as

$$k_{r2.O} = \frac{s_w}{q} \cdot \left[\varphi(\xi_{2.O}) + \left(\frac{5 \cdot n_{ü}^2 - 8}{24} + \frac{n_{ü}^2}{8} \cdot \cos(60°) \right) \cdot \psi(\xi_{2.O}) \right] \qquad (5.14)$$

With (5.13) and (5.14) the average value of the resistance coefficient $k_{r2.O}$ can be calculated as

$$k_{r2.O} = \varphi(\xi_{2.O}) + \left(\frac{n_{ü}^2 - 1}{3} - \frac{s_w \cdot n_{ü}^2}{q \cdot 16} \right) \cdot \psi(\xi_{2.O}). \qquad (5.15)$$

In Table 5.2 the influence of the pitching on the eddy current losses $P_{Ft,2.O}$ acc. to [Bind 2006c] is compared to the consideration acc. to [Vogt 1974].

Winding data	Pitching acc. [Bind 2006c]		Pitching acc. [Vogt 1974]	
	$W/\tau_p = 10/12$; $q = 4$; $s_w = 2$; $n_{ü} = 20$			
Pitching influence $W/\tau_p = 10/12$	$\left(\frac{n_{ü}^2 - 1}{3} \right) \cdot \left(\frac{7}{16} + \frac{9}{16} \cdot \frac{W}{\tau_p} \right)$	120.531	$\left(\frac{n_{ü}^2 - 1}{3} - \frac{s_w \cdot n_{ü}^2}{q \cdot 16} \right)$	120.500
Pitching influence $W/\tau_p = 11/12$	$\left(\frac{n_{ü}^2 - 1}{3} \right) \cdot \left(\frac{7}{16} + \frac{9}{16} \cdot \frac{W}{\tau_p} \right)$	126.75	$\left(\frac{n_{ü}^2 - 1}{3} - \frac{s_w \cdot n_{ü}^2}{q \cdot 16} \right)$	126.766
Without pitching $W/\tau_p = 12/12$	$(n_{ü}^2 - 1)/3$	133.0	$(n_{ü}^2 - 1)/3$	133.0

Table 5.2: Comparison of different pitching consideration and the influence of the pitching

Table 5.2 shows that both considerations of the pitching are identical. In addition the pitching of the winding ($W/\tau_p = 10/12$) reduces the eddy current losses $P_{Ft,2.O}$ by 10 %, in this case compared to unpitched windings.

5.3.5.2 Influence of the pitching on the first order skin effect

As stated in [Vogt 1974, Müll 1956] the pitching of the winding does not influence the first order eddy current losses $P_{Ft,1.O}$ in usual transposed two-layer windings with profile conductors.

For the two-layer round wire winding, which is inserted in the slots usually without transposition, the influence of the pitching on the first order eddy

current losses $P_{\text{Ft},1.\text{O}}$ can be estimated, depending on the sequence of the conductors in the slot acc. to [Müll 1956].

The resistance coefficient $k_{\text{r1.O}}$ for the pitched winding with $W > (\tau_{\text{p}} - q)$ can be calculated as

$$k_{\text{r1.O}} = \varphi(\xi_{1.\text{O}}) + (c_{\text{Mü}} - k_{\text{Mü}}) \cdot \psi(\xi_{1.\text{O}}) ; \quad (c_{\text{Mü}} - k_{\text{Mü}}) = d_{\text{Mü}} \tag{5.18}$$

$$c_{\text{Mü}} = \eta_{\text{Mü}} \cdot (\eta_{\text{Mü}} + 1); \quad \eta_{\text{Mü}} = (\textstyle\sum (v_{\text{Mü}} - 1) - \sum \rho_{\text{Mü}}) / p_{\text{slot}} \tag{5.19}$$

$$k_{\text{Mü}} = \left[(p_{\text{pu}} - \frac{w_{\text{ü}}}{4}) \cdot \left(2 \cdot \eta_{\text{Mü}} - 2 \cdot (p_{\text{pu}} - \frac{w_{\text{ü}}}{4}) + 1 \right) \cdot \frac{s_{\text{w}}}{2 \cdot q} \right] \tag{5.20}$$

p_{pu} :   number of the positive passes in the upper layer
$w_{\text{ü}}$:   number of turns one above the other per slot
q :   number of the slots per pole and phase
$v_{\text{Mü}}$:   positive sequences of the partial conductor
$\rho_{\text{Mü}}$:   negative sequences of the partial conductor (transposed or twisted)
p_{slot} :   number of passes through the slot ($p_{\text{slot}} = w_{\text{ü}}$: number of turns per slot for two-layer and $p_{\text{slot}} = 2 \cdot w_{\text{ü}}$ for single-layer winding).

Independent of the pitching, the value of the term $k_{\text{Mü}}$ in (5.20) is zero for the usual transposed two-layer winding as presented in the example of the Table 5.3. In this case the term $d_{\text{Mü}}$ in (5.18) is in agreement with the well known equation $(w_{\text{ü}}^2 - 4)/16$ (see (5.25)).

For the unpitched two-layer winding ($s_{\text{w}} = 0$) without transposition the term $d_{\text{Mü}}$ in (5.18) is in agreement with the well known equation $(w_{\text{ü}}^2 - 1)/4$ (see (5.21)).

In Table 5.3 the influence of the pitching on the first eddy current losses for the usual transposed, non transposed, pitched and unpitched two-layer winding is summarized.

Winding data		$W/\tau_p = 10/12$; $q = 4$; $s_w = 2$; $w_{\ddot{u}} = 4$ ($= p_{slot}$)						
Parameter		$\Sigma(v_{M\ddot{u}}-1)$	$\Sigma\rho_{M\ddot{u}}$	$\eta_{M\ddot{u}}$	$c_{M\ddot{u}}$	p_{pu}	$k_{M\ddot{u}}$	$d_{M\ddot{u}}$
Usually transposed two-layer winding	Pitched / Unpitched winding	1	7	-1.5	0.75	0	0	0.75
Not transposed two-layer winding	Pitched winding	6	0	1.5	3.75	2	0.5	3.25
	Unpitched winding	6	0	1.5	3.75	2	0	3.75

Table 5.3: Influence of the pitching on the first eddy current losses

For the example given in Table 5.3 the pitching of the winding $W/\tau_p = 10/12$ reduces the eddy current losses only by 15 % in the non transposed winding, whereas the transposition is more effective.

As *Müller*'s method [Müll 1956] described in (5.18), depending on the sequence of the conductors in the slot, is complicated, the influence of the pitching on the first order eddy current losses $P_{Ft,1.O}$ of the two-layer round wire winding can be estimated by the developed equation (5.22).

$$k_{r1.O} = \varphi(\xi_{1.O}) + \frac{w_{\ddot{u}}^2 - 1}{4} \cdot \psi(\xi_{1.O}) \tag{5.21}$$

$$k_{r1.O} = \varphi(\xi_{1.O}) + \left(\frac{w_{\ddot{u}}^2 - 1}{4} - \frac{s_w \cdot w_{\ddot{u}}^2}{q \cdot 16} \right) \cdot \psi(\xi_{1.O}) \tag{5.22}$$

For the unpitched two-layer round wire winding ($s_w = 0$) without transposition the equation (5.22) is in agreement with the well known equation (5.21).

A comparison of the pitching consideration in (5.18) acc. to [Müll 1956] with the estimation in (5.22) and the influence of the pitching on the first order eddy current losses for the non transposed round wire winding are presented in Table 5.4. As can be seen in Table 5.4 the results of both considerations are identical. Therefore the developed equation (5.22) is used in the calculation model.

Winding data	Pitching acc. [Müll 1956] (5.18)		Pitching acc. estimation (5.22)	
	$W/\tau_p = 10/12$; $q = 4$; $s_w = 2$; $w_ü = 4$ ($= p_{slot}$)			
Pitching influence $W/\tau_p = 10/12$	$d_{Mü}$	3.25	$\left(\dfrac{w_ü^2 - 1}{4} - \dfrac{s_w \cdot w_ü^2}{q \cdot 16}\right)$	3.25
Pitching influence $W/\tau_p = 11/12$	$d_{Mü}$	3.5	$\left(\dfrac{w_ü^2 - 1}{4} - \dfrac{s_w \cdot w_ü^2}{q \cdot 16}\right)$	3.5
Without pitching $W/\tau_p = 12/12$	$d_{Mü}$	3.75	$\left(\dfrac{w_ü^2 - 1}{4} - \dfrac{s_w \cdot w_ü^2}{q \cdot 16}\right)$	3.75

Table 5.4: Comparison of different pitching consideration and the influence of the pitching on the first eddy current losses for the non transposed round wire winding

5.4 Model for profile conductor winding

The pitched two-layer winding with profile copper conductors is inserted in the slots with the usual transposition of the partial conductors. That means the sequence of the partial conductors, which are short circuited SC at the beginning and the end of the turn, changes in the next slot (see Figure 5.7). Due to the usual transposition and suitable connection of the coils the first order eddy current losses $P_{ad,s,1.O}$ can be reduced as shown in Table 5.3.
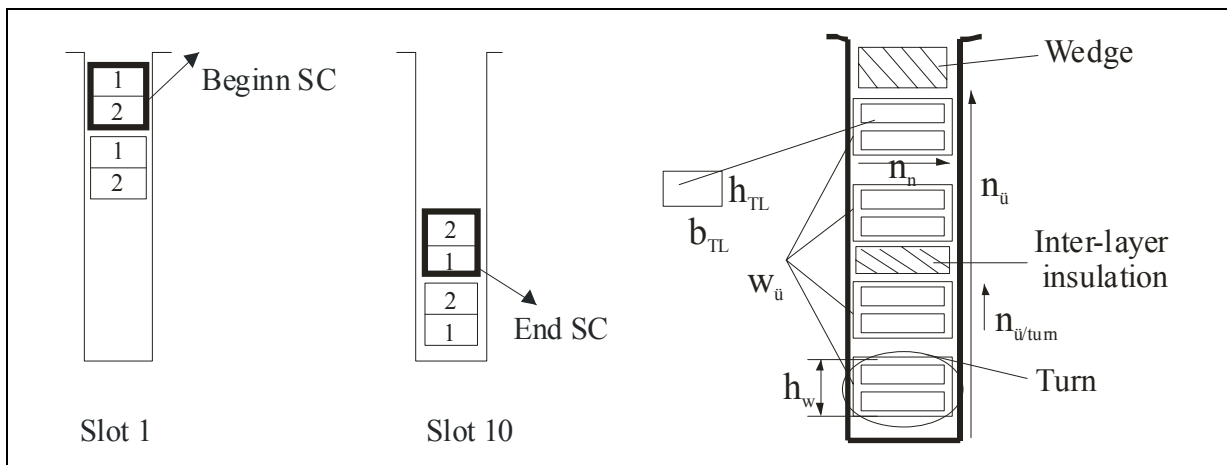
Figure 5.7: Transposed two-layer profile winding with two parallel partial conductors

5.4.1 First order skin effect

The first order eddy current losses $P_{ad,s,1.O}$ due to circulating currents are proportional to the height of the turn h_w.

The reduced conductor height $\xi_{1.O}$ for the first order eddy current is

$$\xi_{1.O} = h_w \cdot \sqrt{\pi \cdot f \cdot \mu_0 \cdot \kappa_{warm} \cdot b_{TL} \cdot n_n / b_{Q,e}} \cdot \sqrt{l_i / l_m} \tag{5.23}$$

f: frequency
κ_{warm} : conductor conductivity at test temperature
μ_0 : magnetic permeability of empty space ($\mu_{Cu} = \mu_0 = 4\pi \cdot 10^{-7}$ Vs/(Am))
b_{TL} : width of partial conductor
n_n : number of partial conductors side by side (horizontal) per slot
$b_{Q,e}$: equivalent slot width (see Table 5.5)
l_i : length of the conductor in the regions (see Table 5.5)
l_m : length of the conductor ($l_m = l_{Fe} + l_{b1} + l_{b2}$).

For the calculation of $\xi_{1.O}$ for different parts of the winding, the equivalent slot width $b_{Q,e}$ and the length l_i should be substituted accordingly (see Table 5.5).

	Slot region along the iron stack	Straight part of the winding overhang	Curved part of the winding overhang
Red. Cond. height $\xi_{1.O}$	$\xi_{1.O,Q}$	$\xi_{1.O,b1}$	$\xi_{1.O,b2}$
Resistance coeff. $k_{r1.O}$	$k_{r1.O,Q}$	$k_{r1.O,b1}$	$k_{r1.O,b2}$
Eddy current loss /W	$P_{Ft,1.O,Q}$	$P_{Ft,1.O,b1}$	$P_{Ft,1.O,b2}$
Equiv. slot width $b_{Q,e}$ /mm	b_Q	$b_{Q,e1}$	$b_{Q,e2}$
Length l_i /mm	l_{Fe}	l_{b1}	l_{b2}
Turns per slot $w_ü$	$w_ü$	$w_ü/2$	$w_ü/4$

Table 5.5: First order skin effect parameters for different sections of the winding

The height of the turn per coil h_w is

$$h_w = \frac{a_P}{n_n} \cdot (h_{TL} + d_{insl,TL}) - d_{insl,TL} \tag{5.24}$$

a_p : number of parallel partial conductors per turn
n_n : number of partial conductors side by side (horizontal) per slot
h_{TL} : partial conductor height (without insulation)

$d_{insl,TL}$:   insulation thickness of the partial conductor (both sides).

With the functions $\varphi(\xi_{1.O})$ and $\psi(\xi_{1.O})$ given in (5.3) and (5.4) the average value of the resistance coefficient $k_{r1.O}$ for the first order eddy current of transposed two-layer winding over the conductors per slot can be calculated as

$$k_{r1.O} = \varphi(\xi_{1.O}) + \frac{w_{\ddot{u}}^2 - 4}{16} \cdot \psi(\xi_{1.O}) \tag{5.25}$$

$w_{\ddot{u}}$:   number of turns one above the other per slot (see Table 5.5).

For the calculation of $k_{r1.O}$ for different sections of the winding, the number of turns $w_{\ddot{u}}$ one above the other per slot should be substituted accordingly (see Table 5.5).

As investigated in the section before, the pitching of the winding does not influence the first order eddy current losses for usual transposed two-layer winding, see also [Vogt 1974, Müll 1956]. So the first order eddy current losses $P_{Ft,1.O}$ in different sections of the winding (see Table 5.5) can be calculated as

$$P_{Ft,1.O} = (k_{r1.O} - 1) \cdot P_{Cu,s,dc} = (k_{r1.O} - 1) \cdot 3 \cdot R_{s,dc} \cdot I_s^2 \tag{5.26}$$

$P_{Cu,s,dc}$:   DC copper losses (without skin effect)
$R_{s,dc}$:   DC resistance (without skin effect)
I_s :   Stator current.

The stray load losses due to the circulating current $P_{ad,s,1.O}$ in the stator winding are

$$P_{ad,s,1.O} = P_{Ft,1.O,Q} + P_{Ft,1.O,b1} + P_{Ft,1.O,b2} \quad . \tag{5.27}$$

5.4.2 Second order skin effect

The second order eddy current losses $P_{ad,s,2.O}$ in the partial conductors are proportional to the height of the partial conductor h_{TL}.
The reduced conductor height $\xi_{2.O}$ for the second order eddy current is

$$\xi_{2.\mathrm{O}} = h_{\mathrm{TL}} \cdot \sqrt{\pi \cdot f \cdot \mu_0 \cdot \kappa_{\mathrm{warm}} \cdot b_{\mathrm{TL}} \cdot n_{\mathrm{n}} / b_{\mathrm{Q,e}}} \qquad (5.28)$$

f :   frequency
κ_{warm} : conductor conductivity at test temperature
μ_0 :   magnetic permeability of empty space ($\mu_{\mathrm{Cu}} = \mu_0 = 4\pi \cdot 10^{-7}$ Vs/(Am))
b_{TL} :   width of partial conductor
n_{n} :   number of partial conductors side by side (horizontal) per slot
$b_{\mathrm{Q,e}}$:   equivalent slot width (see Table 5.6).

For the calculation of $\xi_{2.\mathrm{O}}$ for different parts of the winding, the equivalent slot width $b_{\mathrm{Q,e}}$ should be substituted accordingly (see Table 5.6).

	Slot region along the iron stack	Straight part of the winding overhang	Curved part of the winding overhang
Red. Cond. height $\xi_{2.\mathrm{O}}$	$\xi_{2.\mathrm{O,Q}}$	$\xi_{2.\mathrm{O,b1}}$	$\xi_{2.\mathrm{O,b2}}$
Resistance coeff. $k_{\mathrm{r2.O}}$	$k_{\mathrm{r2.O,Q}}$	$k_{\mathrm{r2.O,b1}}$	$k_{\mathrm{r2.O,b2}}$
Eddy current loss /W	$P_{\mathrm{Ft,2.O,Q}}$	$P_{\mathrm{Ft,2.O,b1}}$	$P_{\mathrm{Ft,2.O,b2}}$
Equiv. slot width $b_{\mathrm{Q,e}}$ /mm	b_{Q}	$b_{\mathrm{Q,e1}}$	$b_{\mathrm{Q,e2}}$
Length l_{i} /mm	l_{Fe}	l_{b1}	l_{b2}
Partial conductors one above the other per slot $n_{\mathrm{ü}}$	$n_{\mathrm{ü}}$	$n_{\mathrm{ü}}/2$	$n_{\mathrm{ü}}/4$

Table 5.6: Second order skin effect parameters for different sections of the winding

With the functions $\varphi(\xi_{2.\mathrm{O}})$ and $\psi(\xi_{2.\mathrm{O}})$ given in (5.3) and (5.4) the average value of the resistance coefficient $k_{\mathrm{r2.O}}$ for the second order eddy current of pitched and usual transposed two-layer winding over the conductors per slot can be calculated as

$$k_{\mathrm{r2.O}} = \varphi(\xi_{2.\mathrm{O}}) + \left(\frac{n_{\mathrm{ü}}^2 - 1}{3} - \frac{s_{\mathrm{w}} \cdot n_{\mathrm{ü}}^2}{q \cdot 16} \right) \cdot \psi(\xi_{2.\mathrm{O}}) \qquad (5.29)$$

$n_{\mathrm{ü}}$:   number of partial conductors one above the other per slot (see Table 5.6)
s_{w} :   number of the mixed slots (different phases in upper and lower layer)
q :   number of slots per pole and phase.

For the calculation of $k_{\mathrm{r2.O}}$ for different sections of the winding the number of partial conductors one above the other per slot $n_{\mathrm{ü}}$ should be substituted

accordingly (see Table 5.6).

The second eddy current losses $P_{\text{Ft,2.O}}$ in different sections of the winding (see Table 5.6) can be calculated as

$$P_{\text{Ft,2.O}} = P_{\text{Cu,s,dc}} \cdot (k_{\text{r2.O}} - 1) \cdot l_{\text{i}} / l_{\text{m}} \qquad (5.30)$$

$P_{\text{Cu,s,dc}}$:   DC copper losses (without skin effect)
l_{i} :   length of the conductor in the regions (see Table 5.6)
l_{m} :   length of the conductor ($l_{\text{m}} = l_{\text{Fe}} + l_{\text{b1}} + l_{\text{b2}}$).

The stray load losses due to the second order eddy current $P_{\text{ad,s,2.O}}$ in the stator winding are

$$P_{\text{ad,s,2.O}} = P_{\text{Ft,2.O,Q}} + P_{\text{Ft,2.O,b1}} + P_{\text{Ft,2.O,b2}} \quad . \qquad (5.31)$$

The stray load losses $P_{\text{ad,s}}$ in the stator winding due to the skin effect are the sum of $P_{\text{ad,s,1.O}}$ and $P_{\text{ad,s,2.O}}$, the first and the second order eddy current losses:

$$P_{\text{ad,s}} = P_{\text{ad,s,1.O}} + P_{\text{ad,s,2.O}} \quad . \qquad (5.32)$$

5.4.3 Example

In the following an example for the calculation model is given for the pitched two-layer winding with profile copper conductors for the 1500 kW, 6-pole generator "A550-6P" at 60 Hz grid feeding.

The needed data of the profiled conductor winding for the calculation model are given in Table 5.7, some calculated data in Table 5.8, the calculated first order eddy current losses $P_{\text{ad,s,1.O}}$ in Table 5.9, the calculated second order eddy current losses $P_{\text{ad,s,2.O}}$ in Table 5.10 and a comparison of both in Table 5.11.

Width of partial conductor	b_{TL} /mm	5.6
Height of partial conductor	h_{TL} /mm	3.35
Insulation thickness of the partial conductor	$d_{insl,TL}$ /mm	0.35
Number of parallel partial conductors per turn	a_p	4
Number of partial conductors side by side per slot	n_n	2
Number of turns one above the other per slot	$w_{ü}$	10
Conductor length	l_m /mm	1449.2
Length of the iron stack	l_{Fe} /mm	900
Length of the straight part of the winding overhang	l_{b1} /mm	40
Length of the curved part of the winding overhang	l_{b2} /mm	469.2
Pitching of the winding	W/τ_p	10/12
Slot width	b_Q /mm	13
Winding temperature	$\vartheta_{Cu,s}$ /°C	35.9

Table 5.7: Data of the profiled conductor winding "A550-6P"

Number of partial conductors one above the other per slot	$n_{ü}$	20
Coil height (under- and upper layer)	h_c /mm	74
Coil width	b_c /mm	11.9
Height of the turn per coil	h_w /mm	7.05
DC copper losses	$P_{Cu,s,dc}$ /W	6570

Table 5.8: Some calculated data for the profiled conductor winding "A550-6P"

First order skin effect			Slot region	Winding overhang	
Parameter		Equation		Straight	Curved
Equivalent slot width	$b_{Q,e}$ /mm	(5.8), (5.9)	13	66.01	41.05
Reduced cond. height	$\xi_{1,O}$	(5.23)	0.581356	0.076918	0.236226
Functions	$\varphi(\xi_{1,O})$	(5.3)	1.010110	1.000003	1.000277
	$\psi(\xi_{1,O})$	(5.4)	0.037900	0.000012	0.001038
Resistance coeff.	$k_{r1,O}$	(5.25)	1.237512	1.000018	1.000423
Eddy current losses	$P_{Ft,1,O}$ /W	(5.26)	1560.44	0.12	2.78
Ratio of losses	$P_{Ft,1,O}/P_{Cu,s,dc}$		23.75 %	0.002 %	0.042 %
Stray load losses	$P_{ad,s,1,O}$ /W	(5.27)	1563.34		

Table 5.9: Calculated first order eddy current losses at 60 Hz for the profiled conductor winding "A550-6P"

Second order skin effect			Slot region	Winding overhang	
Parameter		Equation		Straight	Curved
Equivalent slot width	$b_{Q,e}$ /mm	(5.8), (5.9)	13	66.01	41.05
Reduced cond. height	$\xi_{2.O}$	(5.28)	0.350542	0.155561	0.197273
Functions	$\varphi(\xi_{2.O})$	(5.3)	1.001341	1.000052	1.000135
	$\psi(\xi_{2.O})$	(5.4)	0.005030	0.000195	0.000505
Resistance coeff.	$k_{r2.O}$	(5.29)	1.60747	1.00588	1.00378
Eddy current losses	$P_{Ft,2.O}$ /W	(5.30)	2478.6	2.13	8.04
Ratio of losses	$P_{Ft,1.O}$ /$P_{Cu,s,dc}$		37.73 %	0.03 %	0.12 %
Stray load losses	$P_{ad,s,2.O}$ /W	(5.31)	2488.74		

Table 5.10: Calculated second order eddy current losses at 60 Hz for the profiled conductor winding "A550-6P"

Table 5.9 and Table 5.10 show that the determined eddy current losses in the winding overhang are negligibly small < 1 % for this example.

Stray load losses	$P_{ad,s,1.O}$ /W	$P_{ad,s,2.O}$ /W	$P_{ad,s}$ /W	$P_{ad,s}$ /$P_{Cu,s,dc}$
	1563.34	2488.74	4052.1	62 %

Table 5.11: Comparison of calculated first and second order eddy current losses at 60 Hz for the profiled conductor winding "A550-6P"

As can be seen for this example in Table 5.11, due to lower number of parallel partial conductors per turn a_p the first order eddy current losses $P_{ad,s,1.O}$ are by 39 % of the stray load losses $P_{ad,s}$ smaller compared to the second order eddy current losses $P_{ad,s,2.O}$ amounting to 61 % of $P_{ad,s}$ in the stator winding. The losses $P_{ad,s,2.O}$ are high due to the relatively high partial conductor height h_{TL}.

5.4.4 Influence of winding parameters on calculated stray load losses

The influence of the pitching on the second order skin effect is investigated in the previous section. The calculated impact of other parameters like conductor height h_{TL}, number of parallel partial conductors a_p, turn number per slot $w_ü$, winding temperature and supply frequency will be investigated in following.

5.4.4.1 Influence of the conductor height

The influence of the conductor height h_{TL} on the second order skin effect of a two-layer profile winding with two parallel partial conductors $a_p = n_{\ddot{u}} = 2$ and $w_{\ddot{u}} = 10$ turns per slot at 60 Hz is shown in Figure 5.8 and Table 5.12.
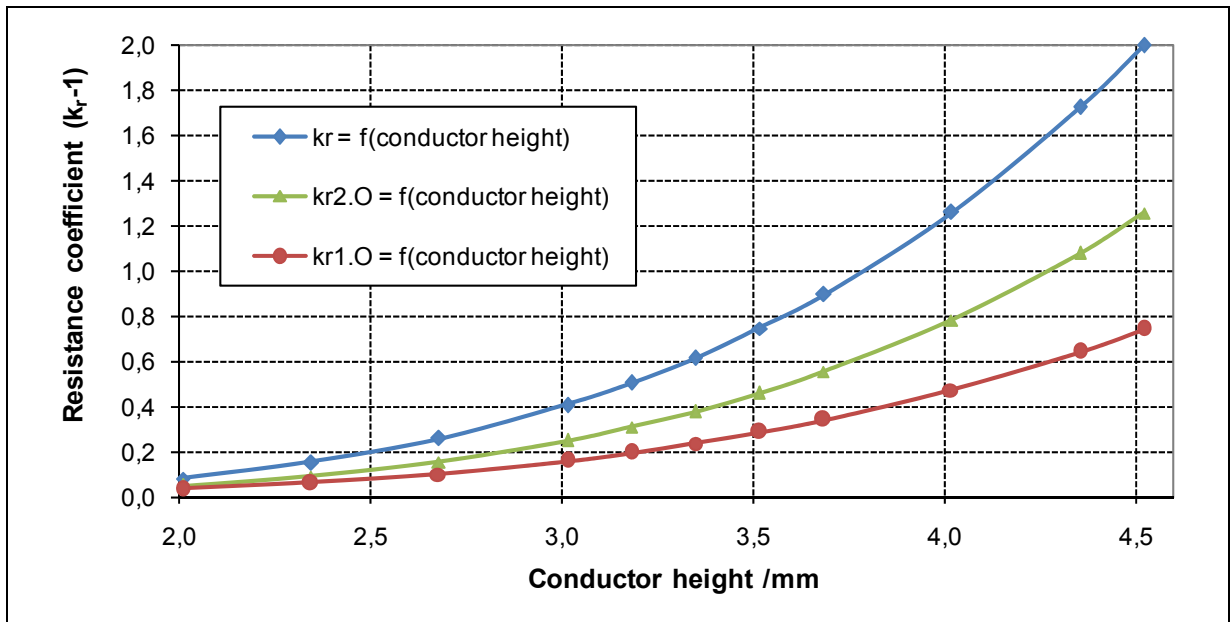
Figure 5.8: Influence of the conductor height on the calculated first and second order skin effect of two-layer profile winding "A550-6P" with two parallel partial conductors

Increasing of h_{TL} / %	0	17	33	**50**	58	67	83	100	Deviation for 50 %
h_{TL} /mm	2.01	2.34	2.68	3.01	3.18	3.35	3.68	4.02	50 %
h_w /mm	4.37	5.04	5.71	6.38	6.715	7.05	7.72	8.39	46 %
$\xi_{2.O}$	0.210	0.245	0.280	0.315	0.333	0.351	0.386	0.421	50 %
$(k_{r2.O} - 1)$	0.049	0.091	0.155	0.249	0.309	0.379	0.554	0.784	405 %
$\xi_{1.O}$	0.360	0.416	0.471	0.526	0.554	0.581	0.637	0.692	46 %
$(k_{r1.O} - 1)$	0.035	0.062	0.103	0.160	0.196	0.238	0.341	0.475	353 %
$(k_r - 1)$	0.085	0.154	0.258	0.409	0.505	0.617	0.896	1.259	383 %
Dev. of (k_r-1)/%	**0**	82	205	383	497	629	959	1389	

Table 5.12: Influence of the conductor height on the calculated first and second order skin effect for the profiled conductor two-layer winding "A550-6P"

If the conductor height h_{TL} is increased by 50 % the resistance coefficient $(k_{r2.O} - 1)$ will increase by 405 % , and due to increasing of the turn height h_w by 46 % the resistance coefficient $(k_{r1.O} - 1)$ increases by 353 % and therefore the $(k_r - 1)$ deviates by 353 %.

The resistance coefficients $(k_{r2.O} - 1)$ and $(k_{r1.O} - 1)$ are plotted vs. the reduced conductor height $\xi_{2.O}$ and $\xi_{1.O}$ for different conductor height h_{TL} in Figure 5.9.

Figure 5.9: The calculated first and second order skin effect as function of the reduced
conductor height when the conductor height is changed for two-layer profile
winding "A550-6P"

5.4.4.2   Influence of the number of the parallel conductors

The influence of the parallel partial conductors $a_p = n_{\ddot{u}}$ (one above the other) on the first and on the second order skin effect of the two-layer profile winding with $w_{\ddot{u}} = 10$ turns per slot at 60 Hz is presented in Figure 5.10 and Table 5.13 for a conductor height $h_{TL} = 3.35$ mm.

As can be seen the number of parallel partial conductors a_p affects the first order eddy current losses stronger than that of the second order. At constant

conductor height h_{TL} = 3.35 mm the resistance coefficient ($k_{r1.O}$ - 1) will increase by 429 % whereas the resistance coefficient ($k_{r2.O}$ - 1) increases by 125 % and therefore the resulting (k_r - 1) deviates by 242 % if the number of the parallel partial conductors a_p (one above the other) is increased by 50 %.

Figure 5.10: Influence of the number of parallel partial conductors on the calculated first and second order skin effect of two-layer profile winding "A550-6P"

Increasing of a_p / %	-50	0.00	**50**	100	200	300	400	Deviation for 50 %
a_p	1	2	3	4	6	8	10	50 %
h_w /mm	3.35	7.05	10.75	14.45	21.85	29.25	36.65	52 %
$\xi_{2.O}$	0.351	0.351	0.351	0.351	0.351	0.351	0.351	0 %
($k_{r2.O}$ - 1)	0.095	0.379	0.851	1.512	3.400	6.043	9.440	125 %
$\xi_{1.O}$	0.276	0.581	0.886	1.192	1.802	2.412	3.022	52 %
($k_{r1.O}$ - 1)	0.012	0.238	1.260	3.898	15.48	30.27	41.55	429 %
(k_r - 1)	0.107	0.617	2.111	5.410	18.88	36.32	50.99	242 %
Dev. of (k_r-1)/%	-83	**0**	242	777	2962	5788	8167	

Table 5.13: Influence of the number of parallel partial conductors on the calculated first and second order skin effect for the profiled conductor two-layer winding "A550-6P"

The resistance coefficients of the first and the second order skin effect ($k_{r1.O}$ - 1) and ($k_{r2.O}$ - 1) are plotted vs. the reduced conductor height $\xi_{1.O}$ and $\xi_{2.O}$ for different parallel partial conductor numbers in Figure 5.11.
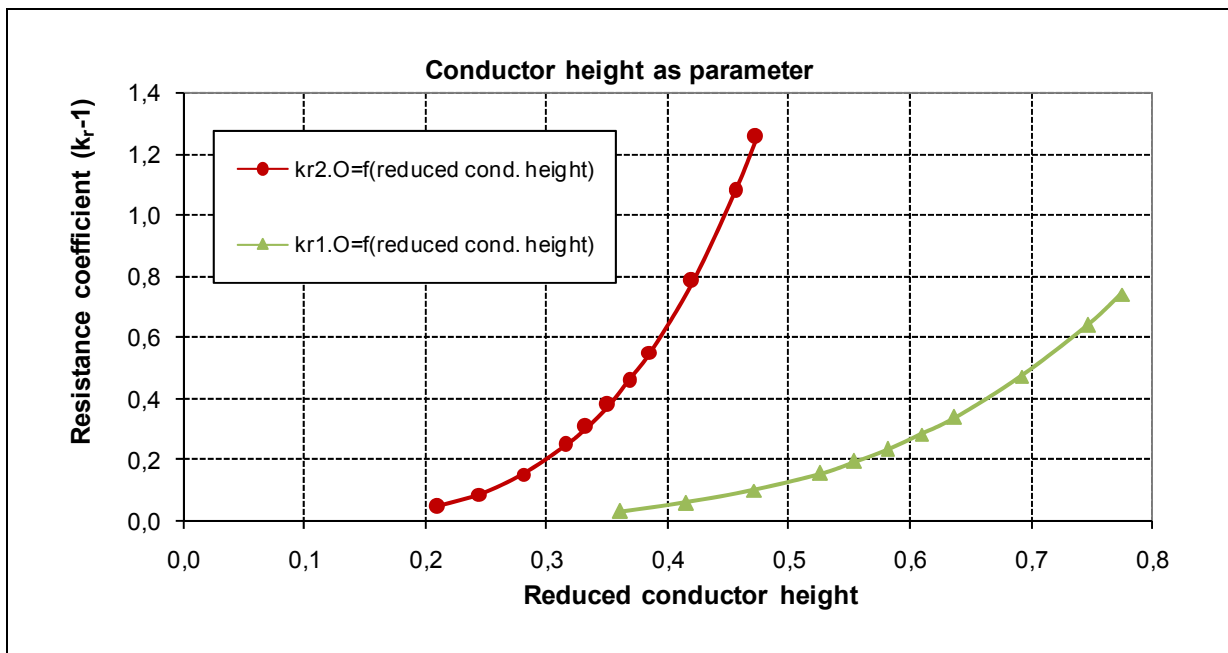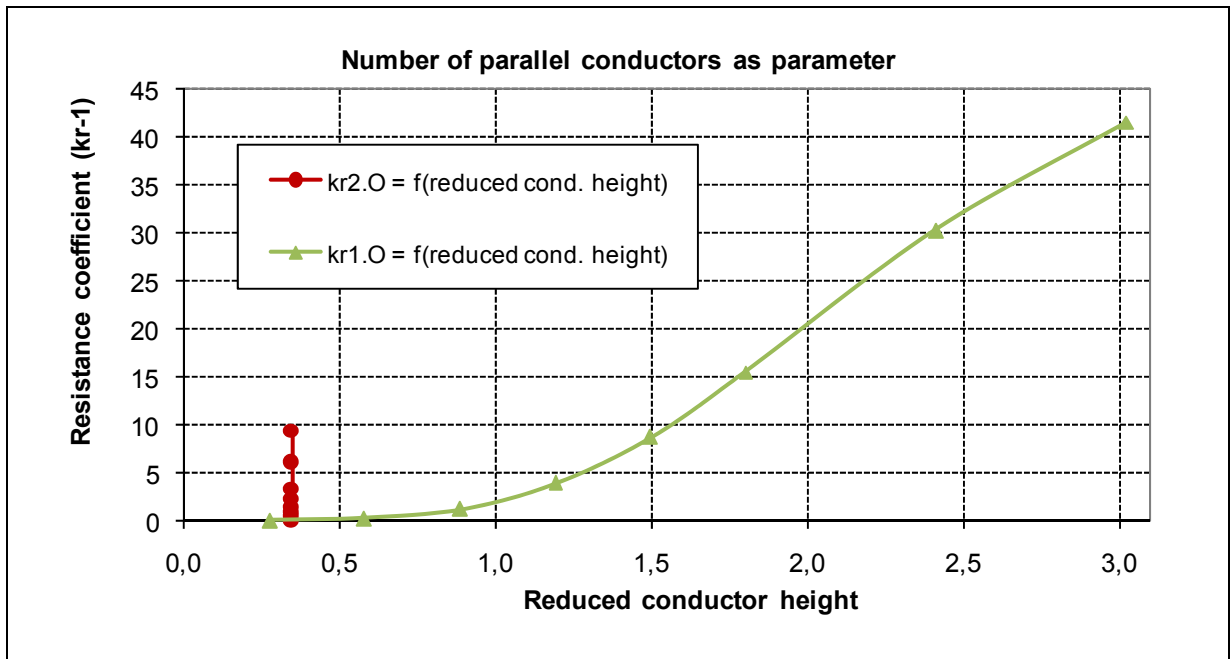

Figure 5.11: The calculated first and second order skin effect as function of the reduced conductor height when the number of the parallel partial conductors is changed for two-layer profile winding "A550-6P"

5.4.4.3   Influence of the turn number

In Figure 5.12 the influence of the number $w_{ü}$ of the turns per slot (one above the other) on the first and second order skin effect ($k_{r1.O}$ - 1) and ($k_{r2.O}$ - 1) of the two-layer profile winding of machine "A550-6P" at 60 Hz for two parallel partial conductors $a_p = n_ü = 2$ with a conductor height $h_{TL} = 3.35$ mm is shown. As only two parallel partial conductors $a_p = n_ü = 2$ per turn are used for this example, the increase of the first order skin effect ($k_{r1.O}$ - 1) is lower than that of the second order ($k_{r2.O}$ - 1). With higher turn number per slot $w_{ü}$ the skin effect becomes higher.

The impact of the variation of the turn number per slot $w_{ü}$ on the first and on the second order skin effect and the deviations for 100 % increase of the turn number per slot $w_{ü}$ are depicted in Table 5.14.
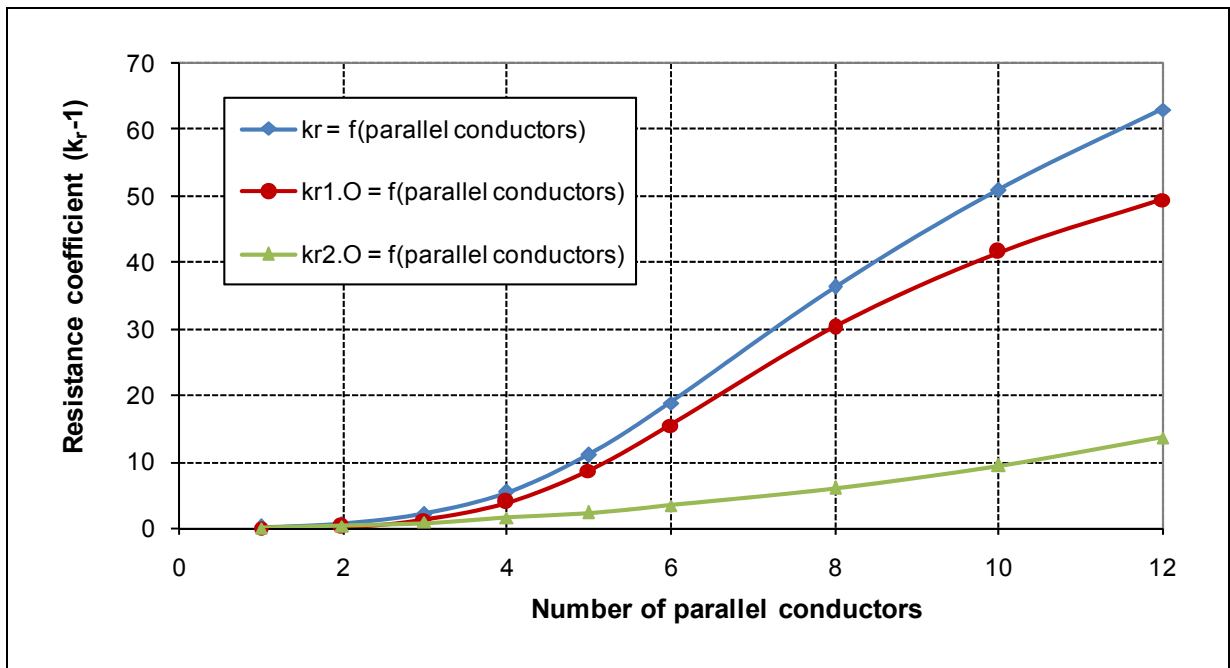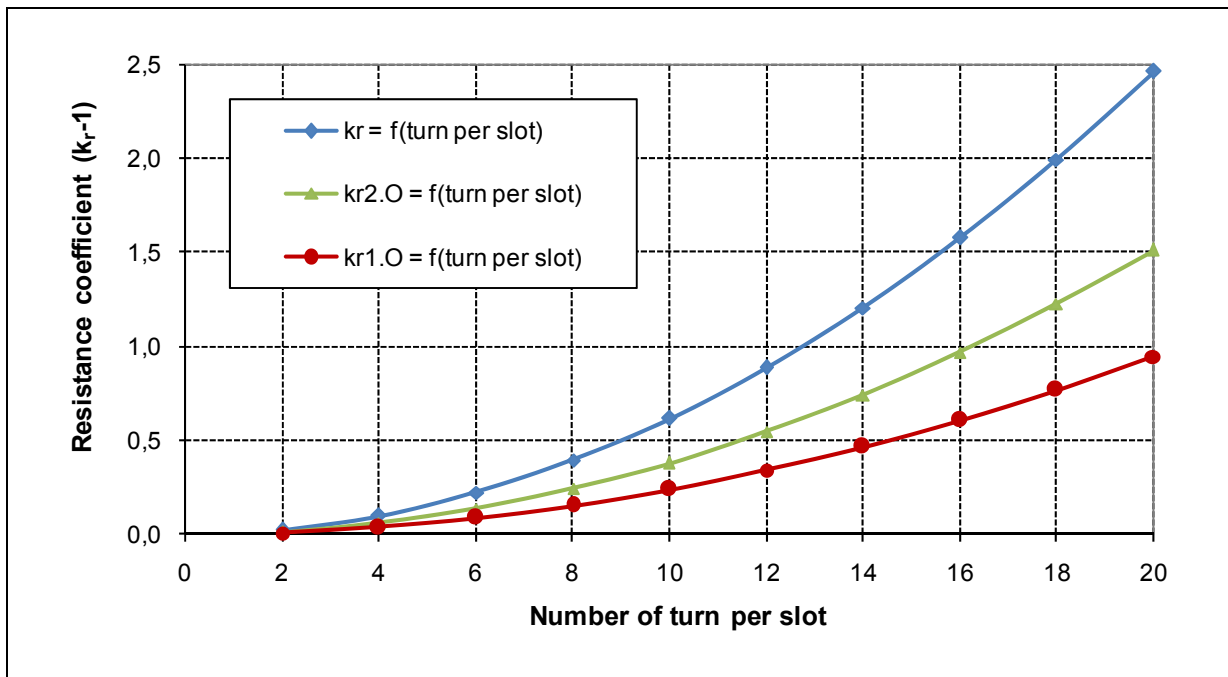
Figure 5.12: Influence of the number of turns per slot on the calculated first and second order skin effect of two-layer profile winding "A550-6P"

Increasing of $w_{ü}$ / %	-50	0.00	50	100	150	200	300	400	Deviation for 100 %
$w_{ü}$ per slot	2	4	6	**8**	10	12	**16**	20	100 %
h_w /mm	7.05	7.05	7.05	7.05	7.05	7.05	7.05	7.05	0 %
$\xi_{2.O}$	0.351	0.351	0.351	0.351	0.351	0.351	0.351	0.351	0 %
$(k_{r2.O} - 1)$	0.015	0.061	0.137	0.243	0.379	0.545	0.968	1.512	299 %
$\xi_{1.O}$	0.581	0.581	0.581	0.581	0.581	0.581	0.581	0.581	0 %
$(k_{r1.O} - 1)$	0.010	0.039	0.086	0.153	0.238	0.342	0.608	0.949	298 %
$(k_r - 1)$	0.026	0.100	0.223	0.395	0.617	0.887	1.576	2.461	299 %
Dev. of (k_r-1)/%	-74	**0**	124	296	519	790	1480	2368	

Table 5.14: Influence of the number of turns per slot on the calculated first and second order skin effect for the profiled conductor two-layer winding "A550-6P"

As can be seen the number of turns per slot affects the second order eddy current losses stronger than that of the first order. If the number of the turns per slot is increased from 8 to 16 the resistance coefficient ($k_{r2.O}$ - 1) will increase by 299 % whereas the resistance coefficient ($k_{r1.O}$ - 1) increases by 298 % and therefore the (k_r - 1) deviates by 299 %.

5.4.4.4   Influence of the temperature

In Figure 5.13 the influence of the temperature on the first and on the second order skin effect of the two-layer profile winding "A550-6P" at 60 Hz for two parallel partial conductors $a_p = n_{\ddot{u}} = 2$ with a conductor height $h_{TL} = 3.35$ mm and $w_{\ddot{u}} = 10$ turns per slot (one above the other) is shown. Also the values of the stray load losses and the copper losses related to the values at 20 °C winding temperature are presented. The calculated values for varying temperatures and the deviations are depicted in Table 5.15 and Table 5.16.

Figure 5.13: Influence of the temperature on the calculated first and second order skin effect of two-layer profile winding "A550-6P"

The temperature influences the first and the second order eddy current losses in the same amount. If the temperature increases e.g. from 60 °C to 120 °C the resistance coefficients $(k_{r2.O} - 1)$, $(k_{r1.O} - 1)$ and $(k_r - 1)$ will be reduced by 31 % as shown in Table 5.15.

Temperature /°C	10	20	40	**60**	100	**120**	140	160	Dev. for 100 %
$\xi_{2.O}$	0.369	0.361	0.348	0.336	0.315	0.306	0.298	0.290	-9 %
$(k_{r2.O} - 1)$	0.463	0.428	0.368	0.319	0.248	0.221	0.198	0.178	-31 %
$\xi_{1.O}$	0.611	0.599	0.577	0.557	0.523	0.508	0.494	0.481	-9 %
$(k_{r1.O} - 1)$	0.291	0.268	0.231	0.201	0.156	0.139	0.124	0.112	-31 %
$(k_r - 1)$	0.754	0.696	0.599	0.520	0.404	0.359	0.322	0.290	-31 %
Dev. of (k_r-1)/%	8	**0**	-14	-25	-42	-48	-54	-58	

Table 5.15: Influence of the temperature on the calculated first and second order skin effect for the profiled conductor two-layer winding "A550-6P"

With increasing winding temperature the stray load losses $P_{ad,s}$ decrease, the DC copper losses $P_{Cu,s}$ increase and the resulting copper losses $(P_{ad,s} + P_{Cu,s})$ increase as presented in Table 5.16.

Temperature /°C	10	20	40	**60**	100	**120**	140	160	Dev. for 100 %
$P_{ad,s}/ P_{ad,s20°C}$	1.04	1.00	0.93	0.86	0.76	0.72	0.68	0.65	-16.9 %
$P_{Cu,s}/ P_{Cu,s20°C}$	0.96	1.00	1.08	1.16	1.31	1.39	1.47	1.55	20.3 %
$P_{sum}/ P_{sum20°C}$	0.99	1.00	1.02	1.04	1.09	1.12	1.15	1.18	7.6 %

Table 5.16: Influence of the temperature on the calculated skin effect and copper losses for the profiled conductor two-layer winding "A550-6P"

5.4.4.5   Influence of the frequency

The influence of the frequency on the first and on the second order skin effect of the two-layer profile winding "A550-6P" with two parallel partial conductors $a_p = n_ü = 2$, a conductor height $h_{TL} = 3.35$ mm and $w_ü = 10$ turns per slot is presented in Figure 5.14. The calculated values when the frequency changes and the deviations are given in Table 5.17.
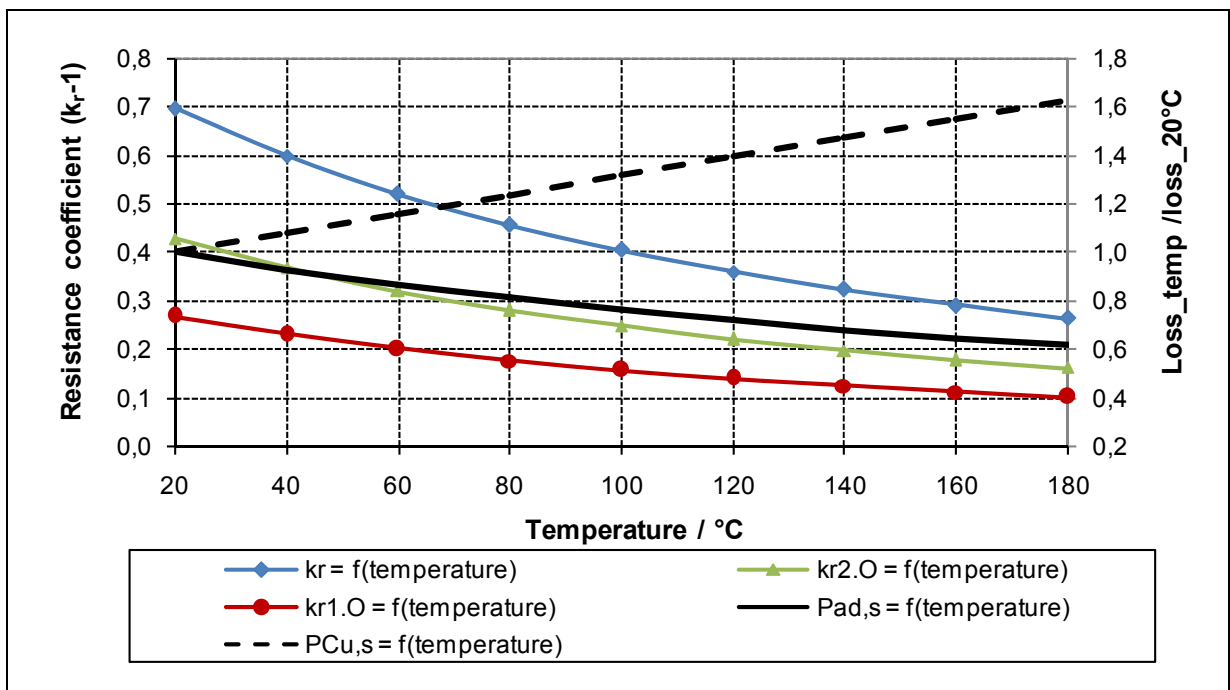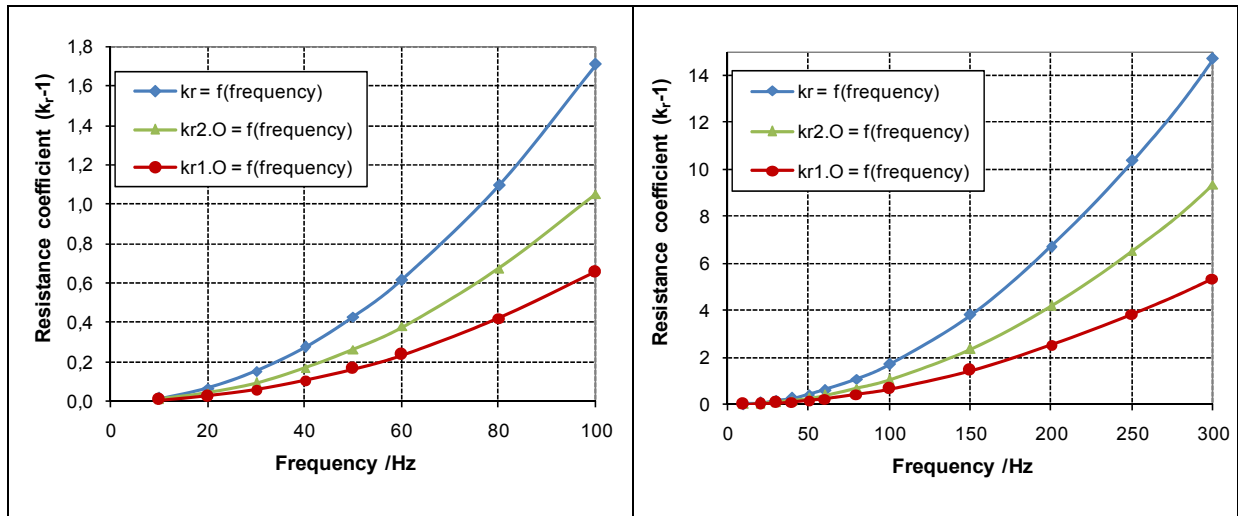
Figure 5.14: Influence of the frequency on the calculated first and second order skin effect of two-layer profile winding "A550-6P"

Frequency /°C	10	40	**50**	60	80	**100**	200	300	400	Dev. for 100 %
$\xi_{2.O}$	0.143	0.286	0.320	0.351	0.405	0.453	0.64	0.78	0.91	41 %
$(k_{r2.O} - 1)$	0.011	0.168	0.263	0.379	0.673	1.051	4.18	9.33	16.40	299 %
$\xi_{1.O}$	0.237	0.475	0.531	0.581	0.671	0.751	1.06	1.30	1.50	41 %
$(k_{r1.O} - 1)$	0.007	0.106	0.165	0.238	0.422	0.656	2.53	5.36	8.83	296 %
$(k_r - 1)$	0.017	0.274	0.429	0.617	1.095	1.707	6.71	14.70	25.23	298 %
Dev. of (k_r-1)/%	-96	-36	**0**	44	155	298	1466	3329	5786	

Table 5.17: Influence of the frequency on the calculated first and second order skin effect for the profiled conductor two-layer winding "A550-6P"

As can be seen in Table 5.17 the frequency influences the first and the second order eddy current losses nearly by the same amount. If the frequency increases e.g. from 50 Hz to 60 Hz the resistance coefficients $(k_{r2.O} - 1)$, $(k_{r1.O} - 1)$ and $(k_r - 1)$ will increase by 44 % and by 300 % at 100 Hz, respectively.

5.4.5 Measured example

The measured and the smoothed stray load losses in the stator $P_{ad,s}$ of the profiled conductor winding "A550-6P" at 60 Hz as function of the stator currents and in dependency of the frequency at constant rated current are

depicted in Figure 5.15 and compared to the calculation in the Table 5.18. As can be seen the calculation fits well with the measurement for this example, and the influence of the frequency on the stray load losses is also given for the calculation model.

1500 kW 6-pole generator	A550-6P		
Stray load losses at removed rotor test	Calculated	Measured	Deviation
First order eddy current loss $P_{ad,s,1.O}$ /kW	1.56	--	
Second order eddy current loss $P_{ad,s,2.O}$ /kW	2.49	--	
Stator stray load losses $P_{ad,s}$ /kW	4.05	4.24	- 4.4 %
Resistance coefficient $P_{ad,s}/P_{Cu,s,dc}$	0.62	0.65	- 4.4 %

Table 5.18: Comparison of calculated and measured stray load losses in the stator at 60 Hz for the profiled conductor winding "A550-6P"
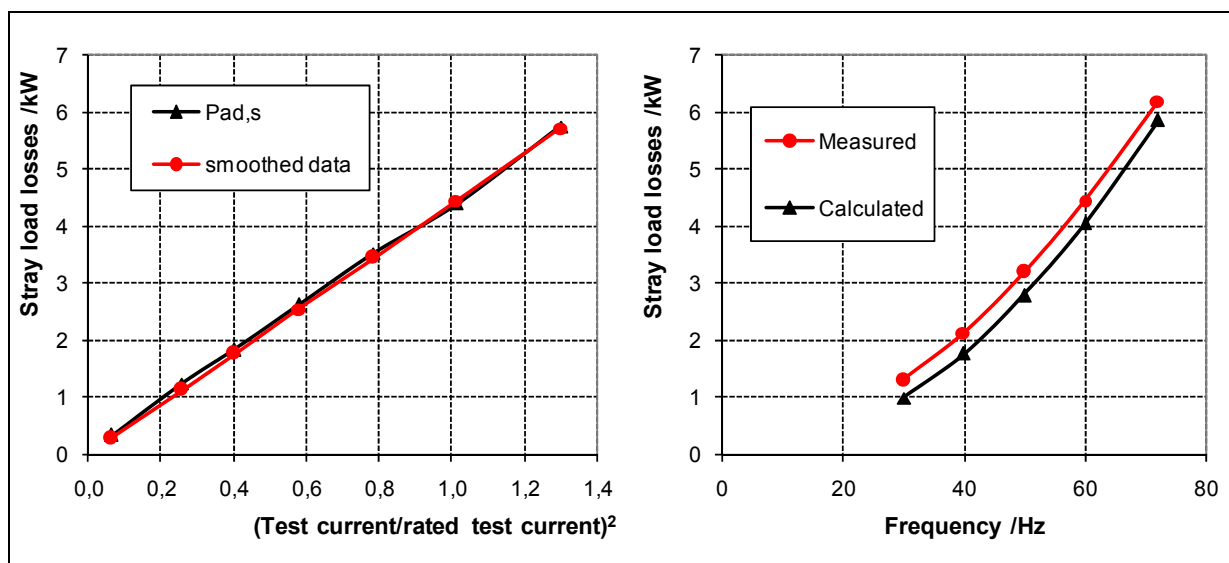
Figure 5.15: The measured stray load losses in the stator at 60 Hz as function of the stator current and a comparison to the calculation at different frequency and rated current for the profiled conductor winding "A550-6P"

5.5 Model for litz wire winding

The pitched two-layer winding with litz (braid) wires is inserted in the slots with transposition of the partial conductors. The partial conductors composed of

twisted uninsulated thin wires are pressed and formed as profile copper conductors (see Figure 5.16). The twisting here should not influence the eddy current losses as the wires are uninsulated. Due to the usual transposition and suitable connection of the coils the first order eddy current losses could be reduced.
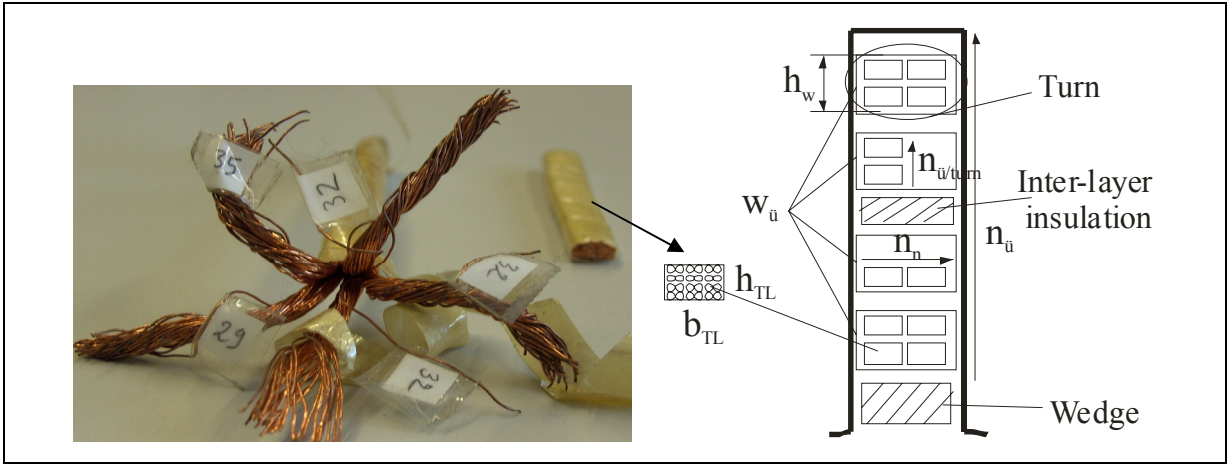
Figure 5.16: The twisted thin wires and the formed profile conductor of the litz wire winding

For the calculation model the partial conductors, composed of twisted thin wires, are considered as solid profiled partial conductor with an equivalent conductivity. Due to the twisting of the thin wires the copper cross section is smaller than of the solid profiled copper. This can be considered by a "litz fill factor" k_{LF}, which is determined according to (5.33). It represents the ratio of the calculated winding resistance $R_{s,cal}$ for the solid conductor and the measured winding resistance $R_{s,meas}$. The value obtained for this example is $k_{LF} = 0.75$, which correlates with the values between 0.75 and 0.85 acc. to *Hillebrand* [Hill 1914].

$$k_{LF} = \frac{R_{s,cal}}{R_{s,meas}} = \frac{w \cdot 2 \cdot l_m}{\kappa \cdot a \cdot a_p \cdot A_{Cu,solid} \cdot R_{s,meas}} \quad (5.33)$$

w :   number of turns per phase
l_m :   length of the conductor ($l_m = l_{Fe} + l_{b1} + l_{b2}$)
κ :   conductor conductivity at test temperature
a :   number of parallel winding branches
a_p :   number of parallel partial conductors

$A_{\text{Cu,solid}}$:   copper cross section of the solid profiled partial conductor.

The resistance of the litz wire winding R_s can be estimated as

$$R_s = \frac{w \cdot 2 \cdot l_m}{\kappa \cdot a \cdot a_p \cdot A_{\text{Cu,solid}} \cdot \pi / 4} \quad .$$

(5.34)

5.5.1 First order skin effect

The first order eddy current losses $P_{\text{ad,s,1.O}}$ due the circulating currents between the parallel partial conductors are proportional to the height of the turn h_w. All the equations in the preceding section for profiled conductor windings also hold for the litz wire winding if we change the conductivity to ($\kappa_{\text{warm}} \cdot k_{\text{LF}}$). The reduced conductor height $\xi_{1.O}$ for the first order eddy current is

$$\xi_{1.O} = h_w \cdot \sqrt{\pi \cdot f \cdot \mu_0 \cdot \kappa_{\text{warm}} \cdot k_{\text{LF}} \cdot b_{\text{TL}} \cdot n_n / b_{\text{Q,e}}} \cdot \sqrt{l_i / l_m}$$

(5.35)

f :   frequency
μ_0 :   magnetic permeability of empty space ($\mu_{\text{Cu}} = \mu_0 = 4\pi \cdot 10^{-7}$ Vs/(Am))
κ_{warm} : conductor conductivity at test temperature
k_{LF} :   litz fill factor
b_{TL} :   width of partial conductor
n_n :   number of partial conductors side by side (horizontal) per slot
$b_{\text{Q,e}}$:   equivalent slot width (see Table 5.5)
l_i :   length of the conductor in the regions (see Table 5.5)
l_m :   length of the conductor ($l_m = l_{\text{Fe}} + l_{\text{b1}} + l_{\text{b2}}$).

For the calculation of $\xi_{1,O}$ for different parts of the winding, the equivalent slot width $b_{\text{Q,e}}$ and the length l_i should be substituted accordingly (see Table 5.5).

The equations (5.25), (5.26) and (5.27) to calculate the resistance coefficient $k_{\text{r1.O}}$, the first order eddy current losses $P_{\text{Ft,1.O}}$ and for the stray load losses $P_{\text{ad,s,1.O}}$ for the profiled conductor are valid for the litz wire winding, respectively . For the calculation of $k_{\text{r1.O}}$ for different sections of the winding, the number of turns $w_{\text{ü}}$ one above the other per slot should be substituted accordingly (see Table 5.5).

5.5.2 Second order skin effect

The reduced conductor height $\xi_{2.O}$ for the second order eddy current losses $P_{ad,s,2.O}$ is proportional to the height of the partial conductor h_{TL}.

$$\xi_{2.O} = h_{TL} \cdot \sqrt{\pi \cdot f \cdot \mu_0 \cdot \kappa_{warm} \cdot k_{LF} \cdot b_{TL} \cdot n_n / b_{Q,e}} \qquad (5.36)$$

For the calculation of $\xi_{2.O}$ and $k_{r2.O}$ for different sections of the winding, the equivalent slot width $b_{Q,e}$ and the number of partial conductors one above the other per slot $n_{ü}$ should be substituted accordingly (see Table 5.6).

The equations (5.29)…(5.31) to calculate the resistance coefficient $k_{r2.O}$, the second order eddy current losses $P_{Ft,2.O}$ and the stray load losses $P_{ad,s,2.O}$ for the profiled conductor are also valid for the litz wire winding.

5.5.3 Measured example

The measured and the smoothed stray load losses in the stator of the litz wire winding "A550-6L" at 60 Hz are depicted in Figure 5.17 and compared to the calculation in the Table 5.19. As can be seen the calculation fits well with the measurement for this example. It has to be noted that the winding of this generator is connected in a way to compensate the eddy current losses, therefore the losses are low.

1500 kW 6-pole generator	A550-6L		
Stray load losses at removed rotor test	Calculated	Measured	Deviation
First order eddy current loss $P_{ad,s,1.O}$ /kW	0.88	--	
Second order eddy current loss $P_{ad,s,2.O}$ /kW	0.63	--	
Stator stray load losses $P_{ad,s}$ /kW	1.505	1.419	6 %
Resistance coefficient $P_{ad,s}/P_{Cu,s,dc}$	0.15	0.14	6 %

Table 5.19: Comparison of calculated and measured stray load losses in the stator at 60 Hz for the litz wire winding "A550-6L"
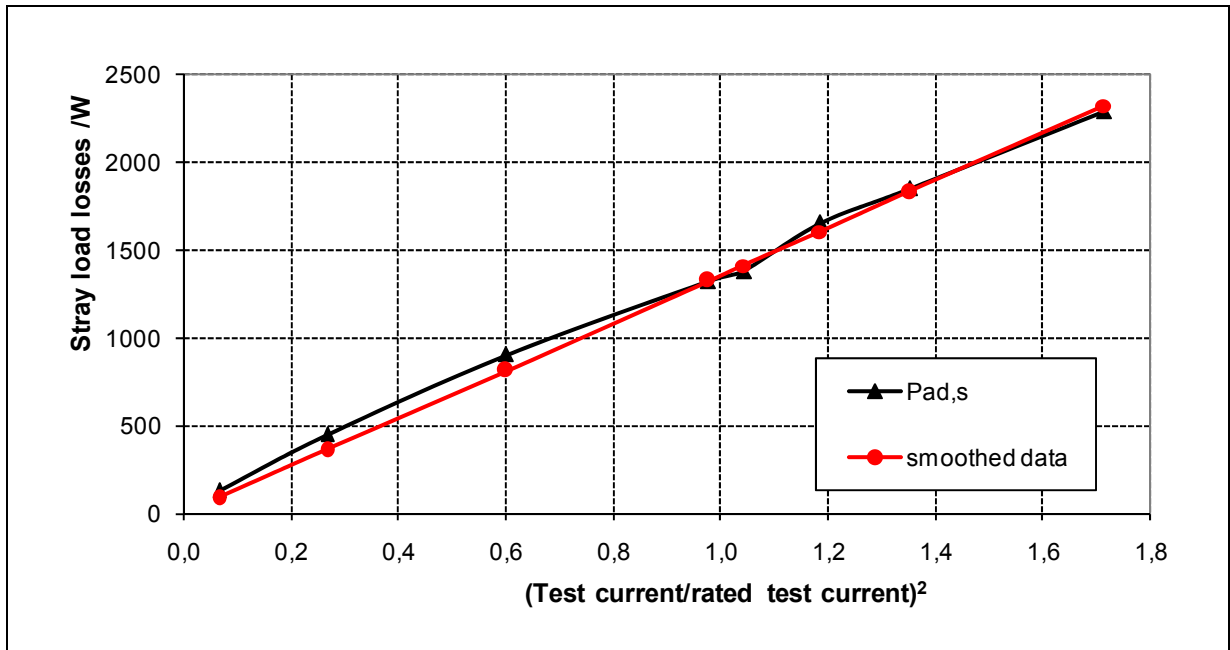
Figure 5.17: The measured and the smoothed stray load losses in the stator at 60 Hz for the litz wire winding "A550-6L"

5.6 Model for round wire winding

The coil of the two-layer winding is composed of many insulated round wires (bundle) as shown in Figure 5.18. At the ends of the coil the bundles are conductively connected. The winding is inserted in the slots without transposition of the coil sides, like it is done for the profiled two-layer winding see Figure 5.7. So the slot stray flux in both coil sides is calculated without changing the direction of the slot stray flux penetration, which yields higher eddy current losses than with the change which is usual for the transposed two-layer winding with profile copper conductors.

Analytical formulas – *Field´*s and *Emde´*s formulas [Vogt 1974] – exist only for conductors arranged in a slot like profiled conductors in a rectangular shaped slot. Therefore the calculation of the eddy current losses for round wire winding with arbitrarily distributed wires can be only an approximation. The real oval-shaped stator slot (Figure 5.18) is substituted by a rectangular slot of an equivalent slot width $b_{Q,e}$ and the randomly distributed conductors and turns are

substituted by an equivalent ideal or best case and bad case arrangement as shown in Figure 5.18.

$$b_{Q,e} = (b_{top} + b_{bot})/2 \tag{5.37}$$

b_{top} :   slot width of the oval-shaped slot at the top edge (see Figure 5.18)
b_{bot} :   slot width of the oval-shaped slot at the bottom edge.
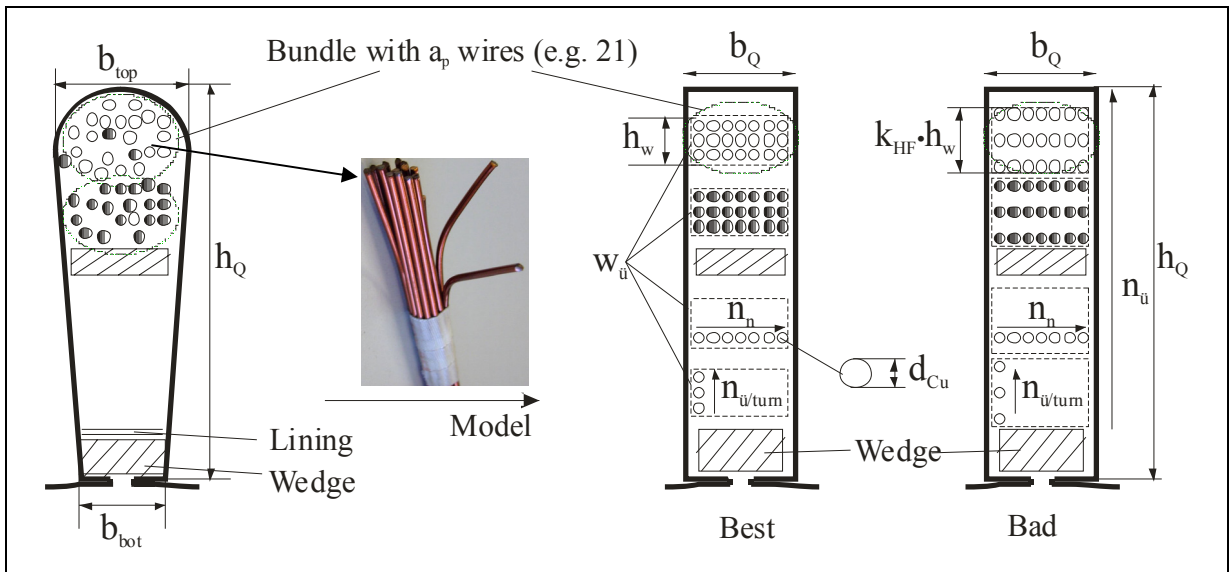
Figure 5.18: The real geometry with randomly wire distribution and the equivalent slot for the calculation model best and bad case for the round wire winding

Due to the low slot fill factor and the undefined arrangement of the turns in the slot an extension factor k_{HF} is introduced to consider the height of the turn referred to the coil in the bad case as presented in Figure 5.18. So two extremely different conductor arrangements in the slot are assumed and other distributions are not considered.

$$k_{HF} = (h_Q - h_{wedge} - \sum h_{insl})/h_c \tag{5.38}$$

h_Q :   slot height
h_{wedge} : wedge height
Σh_{insl} : sum of the height of the insulation materials in the slot (e.g. lining, inter-layer insulation, inter-turns insulation …)
h_c :   coil height.

The coil height h_c of the lower and upper layer is calculated as

$$h_c = w_ü \cdot d_{\text{Cu,insl}} \cdot a_p / n_n = n_{\text{ü/turn}} \cdot w_ü \cdot d_{\text{Cu,insl}} = n_ü \cdot d_{\text{Cu,insl}} \qquad (5.39)$$

a_p :   number of parallel wires in a bundle (partial conductors) per turn
n_n :   number of wires or partial conductors side by side (horizontal) per slot
$w_ü$:   number of turns one above the other per slot (see Table 5.5)
$d_{\text{Cu,insl}}$:   diameter of the insulated wire (partial conductor height)
$n_{\text{ü/turn}}$:   number of wires (partial conductors) one above the other per turn
$n_ü$:   number of partial conductors one above the other per slot (see Table 5.5).

The ratio of the equivalent slot width $b_{\text{Q,e}}$ to the diameter of the insulated wire $d_{\text{Cu,insl}}$ gives the assumed number of the wires side by side (horizontal) per slot n_n

$$n_n = (b_{\text{Q,e}} - 2 \cdot d_{\text{lin,insl}}) / d_{\text{Cu,insl}} \qquad (5.40)$$

$d_{\text{lin,insl}}$: thickness of the slot lining (insulation at slot walls)

The assumed number of wires one above the other per turn $n_{\text{ü/turn}}$ is

$$n_{\text{ü/turn}} = a_p / n_n \qquad (5.41)$$

and the assumed number of partial conductors one above the other per slot $n_ü$

$$n_ü = a_p \cdot w_ü / n_n = n_{\text{ü/turn}} \cdot w_ü. \qquad (5.42)$$

5.6.1 Winding for One speed

The eddy current losses for one speed generators e.g. 6 poles 1500 kW "A550-6R" where only one winding exists in the slot will be handled in this section. The two speeds generator e.g. 4/6 poles 900/200 kW "A445-46R" where two windings exist in the slot follows in the next section.

5.6.1.1   First order skin effect

As the first order eddy currents are proportional to the height of the turn per coil h_w, the extension factor k_{HF} of the turn height referred to the coil height in the low filled slot is introduced to determine the reduced conductor height $\xi_{1.O}$

for the first order eddy current

$$\xi_{1.O} = h_w \cdot k_{HF} \cdot \sqrt{\pi \cdot f \cdot \mu_0 \cdot \kappa_{warm} \cdot d_{Cu} \cdot n_n / b_{Q,e}} \cdot \sqrt{l_i / l_m} \qquad (5.43)$$

$$h_w = n_{\ddot{u}/turn} \cdot (d_{Cu} + d_{insl,TL}) - d_{insl,TL} \qquad (5.44)$$

f :   frequency
μ_0 :   magnetic permeability of empty space ($\mu_{Cu} = \mu_0 = 4\pi \cdot 10^{-7}$ Vs/(Am))
κ_{warm} : conductor conductivity at test temperature
k_{HF} :   turn height extension factor $k_{HF} = 1$ for best case and $k_{HF} > 1$ for bad case
d_{Cu} :   diameter of the wire (without insulation)
n_n :   number of wires side by side (horizontal) per slot
$b_{Q,e}$:   equivalent slot width (see Table 5.5)
l_i :   length of the conductor in the regions (see Table 5.5)
l_m :   length of the conductor ($l_m = l_{Fe} + l_{b1} + l_{b2}$)
$d_{insl,TL}$:   insulation thickness of the wire (both sides).

For the calculation of $\xi_{1.O}$ for different parts of the winding, the equivalent slot width $b_{Q,e}$ and the length l_i should be substituted accordingly (see Table 5.5).

With the functions $\varphi(\xi_{1.O})$ and $\psi(\xi_{1.O})$ given in (5.3) and (5.4) the average value of the resistance coefficient $k_{r1.O}$ over the whole conductors per slot for the first order eddy currents of pitched and non transposed two-layer winding can be calculated as

$$k_{r1.O} = \varphi(\xi_{1.O}) + \left(\frac{w_{\ddot{u}}^2 - 1}{4} - \frac{s_w \cdot w_{\ddot{u}}^2}{q \cdot 16} \right) \cdot \psi(\xi_{1.O}) \qquad (5.45)$$

$w_{\ddot{u}}$:   number of turns one above the other per slot (see Table 5.5)
s_w :   number of the mixed slots (different phases in upper and lower layer)
q :   number of the slots per pole and phase.

The first order eddy current losses $P_{Ft,1.O}$ and the stray load losses $P_{ad,s,1.O}$ are calculated by the equations (5.26) and (5.27), respectively. For the calculation of $k_{r1.O}$ for different sections of the winding the number of turns one above the other per slot $w_{\ddot{u}}$ should be substituted accordingly (see Table 5.5).

5.6.1.2   Second order skin effect

The reduced conductor height $\xi_{2.\mathrm{O}}$ for the second order eddy current losses $P_{\mathrm{ad,s,2.O}}$ is proportional to the wire height d_{Cu}

$$\xi_{2.\mathrm{O}} = d_{\mathrm{Cu}} \cdot \sqrt{\pi \cdot f \cdot \mu_0 \cdot \kappa_{\mathrm{warm}} \cdot d_{\mathrm{Cu}} \cdot n_{\mathrm{n}} / b_{\mathrm{Q,e}}} \tag{5.46}$$

For the calculation of $\xi_{2.\mathrm{O}}$ and $k_{\mathrm{r2.O}}$ for different sections of the winding, the equivalent slot width $b_{\mathrm{Q,e}}$ and the number of partial conductors one above the other per slot $n_{\mathrm{ü}}$ should be substituted accordingly (see Table 5.6).

With the functions $\varphi(\xi_{2.\mathrm{O}})$ and $\psi(\xi_{2.\mathrm{O}})$ given in (5.3) and (5.4) the average value of the resistance coefficient $k_{\mathrm{r2.O}}$ for the second order eddy current of pitched and non transposed two-layer winding over the whole conductors per slot can be calculated as

$$k_{\mathrm{r2.O}} = \varphi(\xi_{2.\mathrm{O}}) + \left(\frac{n_{\mathrm{ü}}^2 - 1}{3} - \frac{s_{\mathrm{w}} \cdot n_{\mathrm{ü}}^2}{q \cdot 16} \right) \cdot \psi(\xi_{2.\mathrm{O}}) \tag{5.47}$$

$n_{\mathrm{ü}}$:   number of partial conductors one above the other per slot (see Table 5.6)
s_{w} :   number of the mixed slots (different phases in upper and lower layer)
q :   number of the slots per pole and phase.

The second eddy current losses $P_{\mathrm{Ft,2.O}}$ and the stray load losses $P_{\mathrm{ad,s,2.O}}$ are calculated by the equations (5.30) and (5.31), respectively.

5.6.1.3   Measured example

The measured stray load losses in the stator compared with the smoothed values of the round wire winding "A550-6R" at 60 Hz are depicted in Figure 5.19 and compared to the calculation in the Table 5.20. For this machine, with higher stray load losses in the stator winding, the calculation model also in the bad case deviates by 60 %. It seems that the wires of the turns are vertically arranged (worst case) due to the lower slot fill factor. This generator can be seen as worst case example for the stray load losses in round wire stator winding. The variation of the measured stray load losses at 50 Hz within two identical series

for 130 generators is presented in Figure 5.20. Also there are some samples with higher stray load losses in the stator winding.

1500 kW 6-pole generator	A550-6R		
Stray load losses at removed rotor test	Calculated best	Calculated bad	Measured
First order eddy current loss $P_{ad,s,1.O}$ /kW	1.60	4.17	--
Second order eddy current loss $P_{ad,s,2.O}$ /kW	0.356	0.356	--
Stator stray load losses $P_{ad,s}$ /kW	1.95	4.53	11.35
Resistance coefficient $P_{ad,s}$ /$P_{Cu,s,dc}$	0.18	0.42	1.05
Deviation /%	- 83	- 60	--

Table 5.20: Comparison of calculated and measured stray load losses in the stator at 60 Hz for the round wire winding "A550-6R"
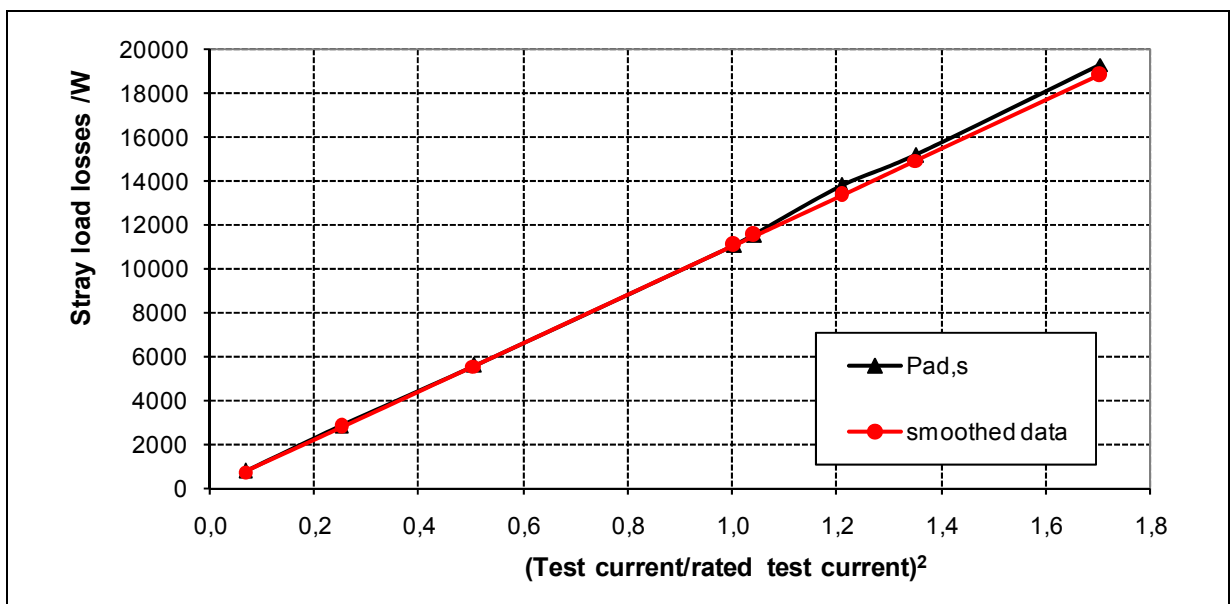
Figure 5.19: The measured and smoothed stray load losses in the stator, acc. to the standard IEEE112, at 60 Hz for the round wire winding "A550-6R"

With this high amount of stray load losses, about 0.76 % of rated power, localised only in the stator winding and mainly due to the circulating current, this round wire winding was overheated and could be not run continuously at full load, otherwise the insulation life time will be strongly reduced. The practical consequence of this effect to avoid destruction due to overheating is the derating ! Further investigations confirm this finding. In addition, with increasing resistance due to the skin effect the inductance decreases and

consequently the "filter" effect of the winding decreases also which leads to higher high-frequency stray load losses.

The comparison of the calculated and measured stray load losses in the stator for two different 6-pole round wire windings "A550-6R0x" and "A550-6R1x" is given in Table 5.21. For some machines the measured value of the stray load losses is between the best and bad case calculation and for others is out of this range due to randomly distribution of the wires in the slot (see Figure 5.20). For the generator "A550-6R03" with low losses it seems that the wires are "unintentionally" twisted, which reduces the eddy current losses. For the generator "A550-6R14" with high losses it seems that the wires of the turns are vertically arranged (worst case) due to the lower slot fill factor. It has to be noted that the measurements are done only at one load point and not acc. to the standards, i.e. the measurement inaccuracy increases !

1500 kW 6-pole generator		A550-6Rx		
Stray load losses at removed rotor test		Calculated best	Calculated bad	Measured
Resistance coef. $P_{ad,s}/P_{Cu,s,dc}$ (Deviation / %)	A550-6R01	0.14 (-51)	0.32 (11)	0.28
Resistance coef. $P_{ad,s}/P_{Cu,s,dc}$ (Deviation / %)	A550-6R02	0.14 (-46)	0.32 (21)	0.26
Resistance coef. $P_{ad,s}/P_{Cu,s,dc}$ (Deviation / %)	A550-6R03	0.14 (66)	0.32 (273)	0.08
Resistance coef. $P_{ad,s}/P_{Cu,s,dc}$ (Deviation / %)	A550-6R14	0.11 (-68)	0.21 (-36)	0.33
Resistance coef. $P_{ad,s}/P_{Cu,s,dc}$ (Deviation / %)	A550-6R15	0.11 (-32)	0.21 (36)	0.16

Table 5.21: Comparison of calculated and measured stray load losses in the stator for the round wire winding "A550-6Rx"

5.6.1.4   Impact of wire distribution on measured stray load losses

The influence of the wire distribution in the slots on the measured stray load losses in the stator of the 4-pole winding at 50 Hz grid frequency, for the two speeds round wire winding "A550-46R" is presented for two series over 130

samples in Figure 5.20. It has to be noted that the measurements are done only at one load point and not acc. to the standards, i.e. the measurement inaccuracy increases !
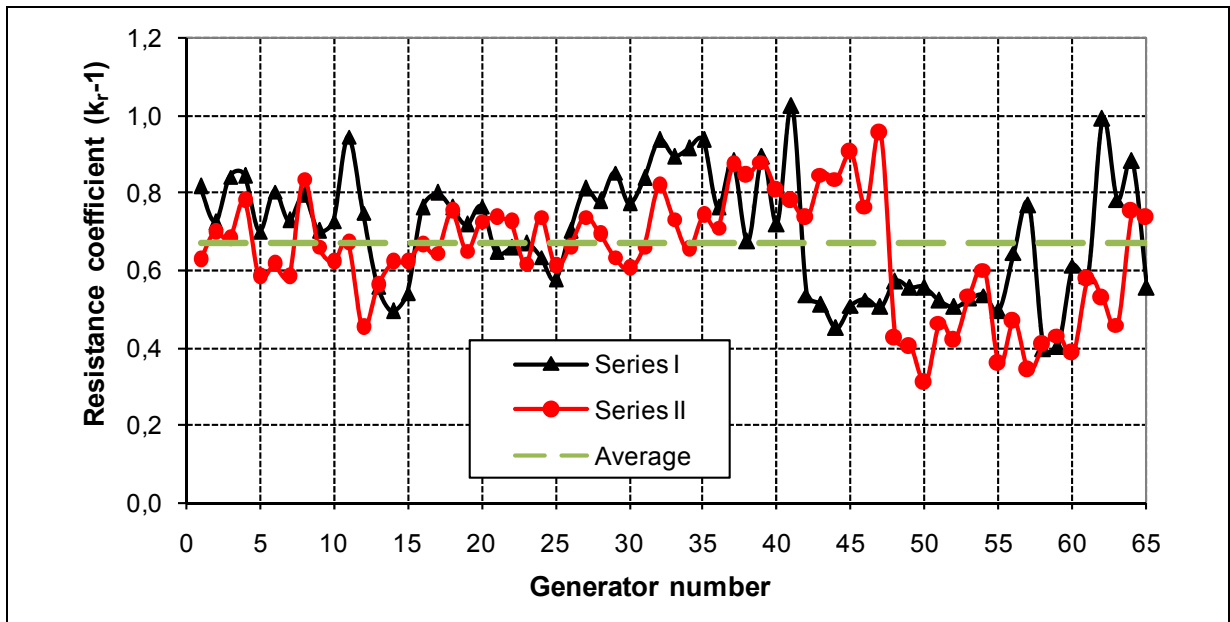
Figure 5.20: The measured stray load losses in the stator at 50 Hz for the two speed round wire winding "A550-**4**6R"

Due to the randomly distributed wires in the slot, the measured resistance coefficient for this generator varies between 0.3 and 1.0 with an average value of 0.67.

5.6.1.5   Impact of wire insertion on measured stray load losses

The influence of mechanical and manual insertion of the wires in the slots on the measured stray load losses in the stator of the 4-pole winding at 50 Hz grid frequency for the two speeds round wire winding generator "A445-**4**6R" is presented in Figure 5.21. With carefully manual "Hand" (H1, H2, H3) insertion of the wires in the slot the measured resistance coefficient is lower and varies between 0.4 and 0.6, whereas the measured values with mechanical (M1, M2, M3) insertion are about 1.0 and higher. So a reduction of about 50 % of stray load losses in the winding can be realized by careful hand insertion. Of course

the hand insertion is more expensive than the mechanical method, but if there are heating or efficiency problems it should be done.
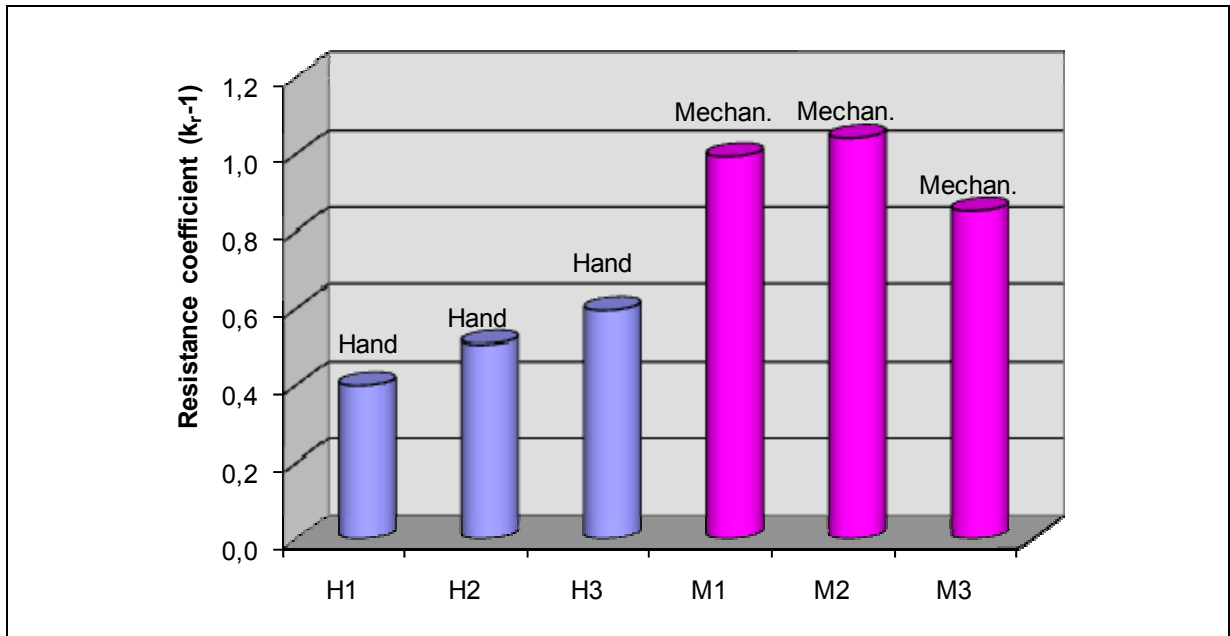
Figure 5.21: Impact of wire insertion on measured stray load losses in the stator of the 4-pole winding at 50 Hz for the two speeds round wire winding "A445-**4**6R"

5.6.1.6   Impact of wire number on measured stray load losses

The influence of the number of wires per turn on the measured stray load losses in the stator for the 4-pole winding of the two speeds round wire winding "A550-**4**6R1" is presented in Table 5.23 and in Figure 5.22. The compared three generators are of identical design and manufacture, but with different wire numbers per turn. We assume that the insertion of the wires in the slots is also - nearly - identical.

1500 kW 4/6-pole generator A550-46R1	Stray load losses at removed rotor test		
Increasing of wire number per turn / %	100	103	113
Resistance coefficient $P_{ad,s}/P_{Cu,s,dc}$	0.74	0.92	1.23
Deviation / %	--	25	66

Table 5.22: Influence of the wire number per turn on measured stray load losses in the stator at rated current and 50 Hz for the two speeds round wire winding "A550-**4**6R1"

With higher wire number per turn the stray load losses become high, especially with higher frequency. A 3 % increase of the wire number leads to 25 % increase of the stray load losses at rated frequency 50 Hz, and 13 % more wires result in 66 % stray load losses, respectively, as shown in Table 5.23.
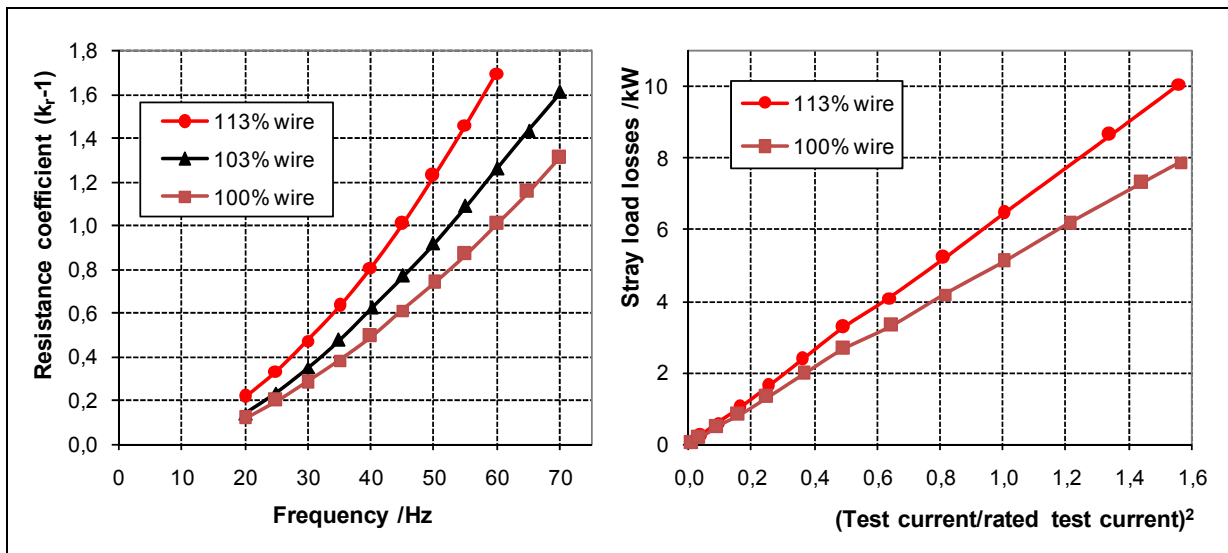
Figure 5.22: The influence of the number of wires per turn on the measured stray load losses in the stator at different frequency rated current and at 50 Hz different currents for the two speeds round wire winding "A550-**46**R1"

1500 kW 4/6-pole generator A550-**46**R1	Stray load losses at removed rotor test		
Increasing of wire number per turn / %	100	103	113
Resistance coefficient $P_{ad,s}/P_{Cu,s,dc}$	0.74	0.92	1.23
Deviation / %	--	25	66

Table 5.23: The influence of the number of wires per turn on the measured stray load losses in the stator at rated current and 50 Hz for the two speeds round wire winding "A550-**46**R1"

5.6.2 Winding for Two speeds

The two speeds generator e.g. 4/6 poles 900/200 kW "A445-46R", contains different windings for each speed. The windings are inserted in the slot with different fill factors. The fill factors of the windings, k_{f1} and k_{f2}, are utilised to determine the cross section A_1 occupied by the high power winding "winding 1"

in the slot e.g. 4-poles 900 kW. This oval-shaped slot cross section is substituted by a rectangular slot of an equivalent slot width $b_{Q,e}$ and slot height $h_{Q,1}$ (see Figure 5.23). For this "new" slot the same arrangements and the formulas given in the preceding section for on speed generator are applied.
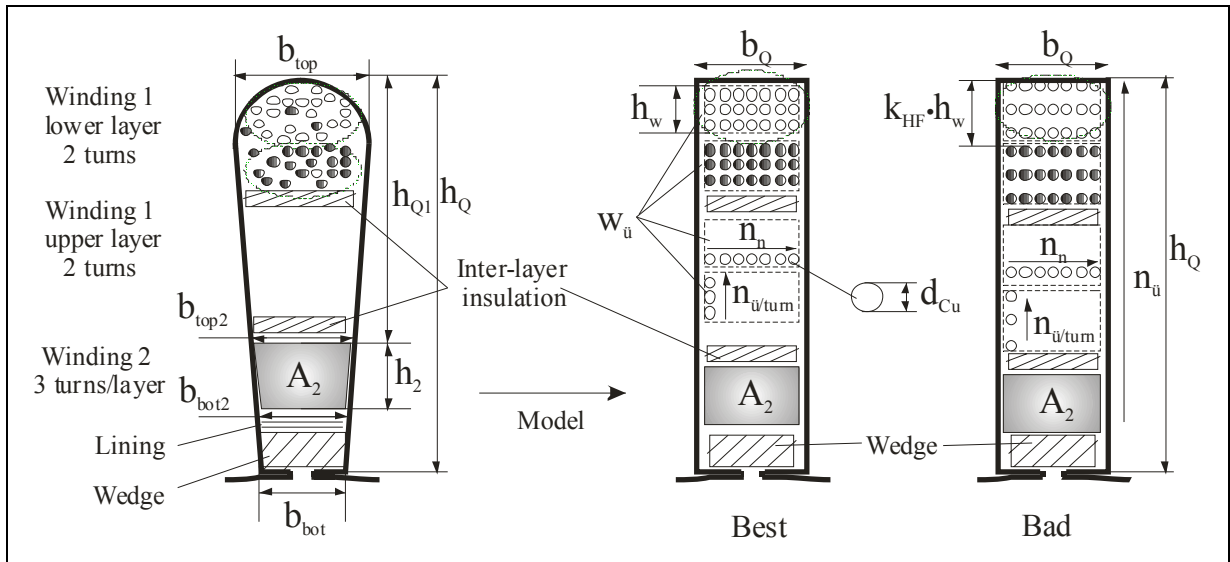
Figure 5.23: The real geometry with randomly wire distribution and the equivalent slot for the calculation model for the two speeds round wire winding

The cross section A_2 occupied by the low power winding "winding 2" in the slot can be calculated on the one hand with the fill factors k_{f1} and k_{f2} as

$$A_2 = \frac{k_{f2}}{k_{f1} + k_{f2}} \cdot A_Q \tag{5.48}$$

k_{f1} :   fill factor of the high power winding "winding 1"
k_{f2} :   fill factor of the low power winding "winding 2"
A_Q :   slot cross section.

and on the other hand from the slot geometry (trapezoid, see Figure 5.23) as

$$A_2 = (b_{bot2} + b_{top2}) \cdot h_2 / 2 \tag{5.49}$$

$$b_{bot2} = (b_{bot} + 2 \cdot x_{bot2}); \qquad b_{top2} = (b_{bot} + 2 \cdot x_{top2}) \tag{5.50}$$

b_{bot} :   slot width of the oval-shaped slot at the bottom edge
b_{bot2} :   slot width at the bottom of the "winding 2"

b_{top2} : slot width at the top edge of the "winding 2"
h_2 :   height of (trapezoid) the cross section of the "winding 2".

With the set of equations (5.51)…(5.53) the height h_2 of the "winding 2" can be determined as given in (5.54).

$$x_{bot2} = (b_{top} - b_{bot}) \cdot (h_{wedge} + 2 \cdot d_{lin,insl}) / (2 \cdot h_Q) \tag{5.51}$$

$$x_{top2} = (b_{top} - b_{bot}) \cdot (h_2 + h_{wedge} + 2 \cdot d_{lin,insl}) / (2 \cdot h_Q) \tag{5.52}$$

$$c = x_{bot2} / (h_{wedge} + 2 \cdot d_{lin,insl}) = (b_{top} - b_{bot}) / (2 \cdot h_Q) \tag{5.53}$$

$$h_2 = -\frac{(b_{bot} + 2 \cdot x_{bot2})}{2 \cdot c} + \sqrt{\left(\frac{b_{bot} + 2 \cdot x_{bot2}}{2 \cdot c}\right)^2 + \frac{A_2}{c}} \tag{5.54}$$

$d_{lin,insl}$:thickness of the slot lining.

Finally the slot height $h_{Q,1}$ and the equivalent slot width $b_{Q,e}$ of the high power winding "winding 1" is

$$h_{Q,1} = h_Q - h_2 - (h_{wedge} + 3 \cdot d_{lin,insl}) \tag{5.55}$$

$$b_{Q,e} = (b_{top} + b_{bot} + 2 \cdot x_{top2}) / 2 \tag{5.56}$$

For this "new" slot the same arrangements and the same formulas and calculation procedure given in the preceding section for on speed generator are applied.

5.6.2.1   Measured example

The comparison of calculated and measured stray load losses in the stator of the high power winding for some two speeds round wire winding generators is given in Table 5.24. For some machines the measured value of the stray load

losses is between the best and bad case calculation, and for others is out of this range due to randomly distributed wires in the slot (see Figure 5.20) and due to the sensitivity of the calculation model on the winding and the slot parameters, which sometimes are not known. For the generator "A550-**4**6R02.2" with lower measured losses as in best case calculated in best case it seems that the wires are "unintentionally" twisted, which reduces the eddy current losses. It has to be noted that the measurements are done only at one load point and not acc. to the standards i.e. the measurement inaccuracy increases!

	Power /kW		Calculated best	Calculated bad	Measured
A445-46R2	900/200	$P_{ad,s}/P_{Cu,s,dc}$ (Deviation / %)	0.46 (-5)	0.97 (99)	0.49
A445-46R3	900/200	$P_{ad,s}/P_{Cu,s,dc}$ (Deviation / %)	0.46 (-52)	0.97 (0.4)	0.97
A550-46R02.1	1500/400	$P_{ad,s}/P_{Cu,s,dc}$ (Deviation / %)	1.08 (8)	2.63 (161)	1.01
A550-46R02.2	1500/400	$P_{ad,s}/P_{Cu,s,dc}$ (Deviation / %)	1.08 (41)	2.53 (232)	0.76
A556-68R67.1	1500/900	$P_{ad,s}/P_{Cu,s,dc}$ (Deviation / %)	0.29 (-22)	0.46 (24)	0.37
A556-68R97.1	1500/900	$P_{ad,s}/P_{Cu,s,dc}$ (Deviation / %)	0.18 (-25)	0.30 (29)	0.23

Table 5.24: Comparison of calculated and measured stray load losses in the stator for the two speeds round wire winding at 50 Hz

5.6.2.2   Influence of stator stray load losses on temperature rise

Of course all loss components contribute to the heating and the temperature rise of the winding, and any reduction of these losses, e.g. the stray load losses in the winding due the skin effect, will lead to a reduction of the temperature level in the winding without improving the cooling effectiveness. The correlation between the stray load losses in the winding due skin effect, expressed by the resistance coefficient $(k_r - 1)$, and the winding temperature rise

during the heat run at full load is presented in Figure 5.24 for the 4-pole winding of the two speeds round wire winding generator "A445-**4**6R". It can be seen that at lower values of the resistance coefficient (k_r - 1) the temperature rise is about 10 K lower and the winding is cooler.
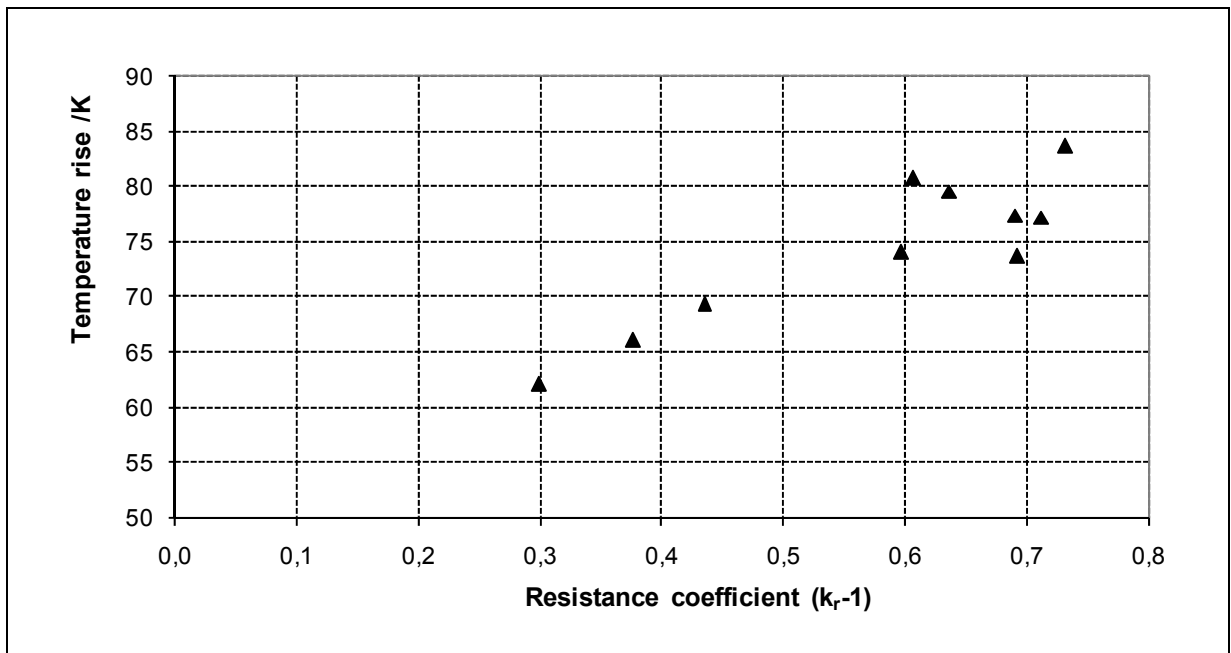
Figure 5.24: Measured temperature rise as function of measured stator stray load losses in the 4-pole winding for the two speeds round wire winding "A445-**4**6R"

5.7 Eddy current losses in stator press plates

The winding overhang stray flux causes eddy current losses in the winding overhang conductors, in the end sheets of the iron stack (press plates) and in the massive conductive end-shields. The magnetic flux densities were measured by Hall probes at different positions to estimate the losses in the massive conductive iron parts in the end region.

5.7.1 Measurement of the magnetic flux density in end region

The stray flux in the end region penetrates the stator iron stack end sheets

(press plate) as well as the massive conductive iron parts of the stator housing (frame) and the end shields. In dependence of the value of this flux and the material properties of the "conductive" parts the eddy current losses could be high, as known from large synchronous generators, where special measures should be taken to reduce them [Trax 2003, Klau 2005]. For the investigated highly utilised 1500 kW 6-pole wind generators the measured flux is small.

The magnetic flux densities were measured at different positions in the end region and under different test conditions at 60 Hz grid-operation:

- Removed rotor test

- Load test

- No-load test

- Reverse rotation test

- Locked rotor test.

The positions of the Hall probes in the end region are presented in the Figure 5.25 and described in Table 5.25.
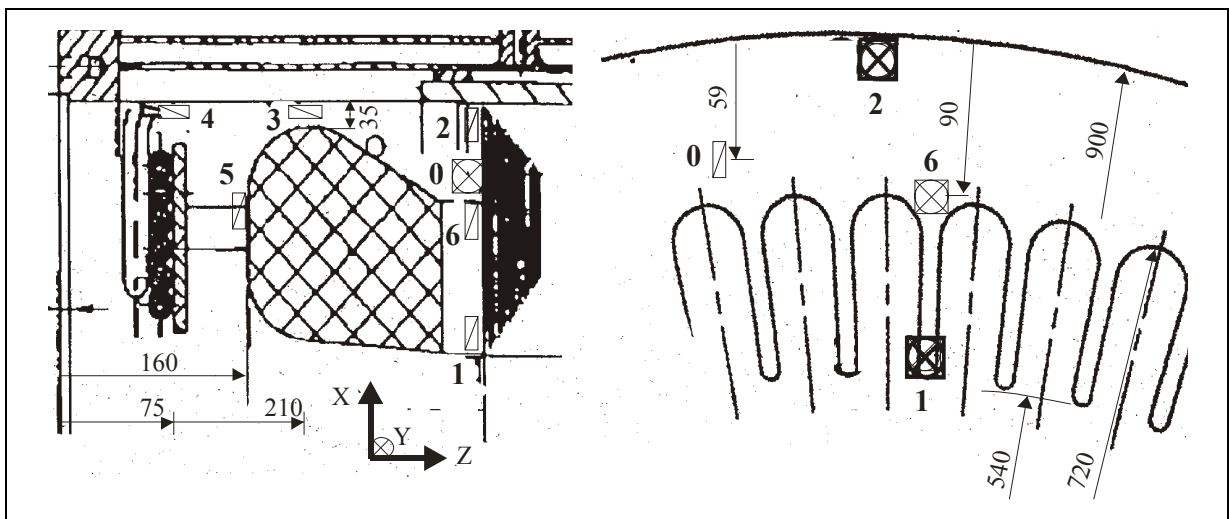
Figure 5.25: Position of the Hall probes in the end region (Z: axial; Y: tangential; X: radial) for 1500 kW, 6-pole generator "A550-6R" [ELIN EBG-Motoren GmbH]

Hall probes nr.	Symbol	Description
1	B_{Z1}	axial flux density in the press finger at tooth tip
6	B_{Z2}	axial flux density in the press finger at tooth bottom
2	B_{Z3}	axial flux density in the edge of the press plate
5	B_{Z4}	axial flux density in winding overhang
3	B_{X1}	radial flux density in frame part over the winding overhang
4	B_{X2}	radial flux density in frame part near to the end shield (bearing)
0	B_{Y1}	tangential flux density in the press plate

Table 5.25: The distribution of the Hall probes in the end region for 1500 kW, 6-pole
generators with round wire "A550-6R" and litz wire "A550-6L"

The measured magnetic flux densities as function of the stator current during
the load test at rated voltage and 60 Hz grid-operation are presented for some
positions (points) in the Figure 5.26 for the round wire 1500 kW, 6-pole
generator "A550-6R".

Figure 5.26: The measured axial flux density distribution in the end region, on the press finger
at tooth tip B_{Z1}, on the press finger at tooth bottom B_{Z2} and on the winding
overhang B_{Z4} as function of the stator current during the load test for 1500 kW, 6-
pole generator "A550-6R"

The comparison of the measured magnetic flux densities at different points
under different test conditions at rated current 1580 A are given in Table 5.26
and presented in Figure 5.27 and Figure 5.28. As can be seen the field
distribution in the end region is complex. The field distribution in the end region

during the reverse rotation test and the locked rotor test are in the same range and lower than the values measured during the load test and the removed rotor test. The effect of the rotor current can be seen when the results of the reverse rotation test will be compared with the results of the removed rotor test, where the voltage is reduced. Of course the rotor current reduces the field excited by the stator current.

1500 kW 6-pole generators,	Measured flux density / mT						
"A550-6R"	B_{Y1}	B_{Z1}	B_{Z2}	B_{Z3}	B_{Z4}	B_{X1}	B_{X2}
Removed rotor test	7.90	122.32	-[1]	0.80	20.94	1.91	0.83
Load test [2]	6.93	104.39	31.40	0.56	20.64	1.80	0.75
Locked rotor test	6.98	50.87	30.34	0.56	19.56	2.17	0.69
Reverse rotation test	7.21	49.01	30.28	0.61	21.10	2.18	0.81

Table 5.26: The measured flux density distribution in the end region, on the press plate B_{Y1}, on the press finger at tooth tip B_{Z1}, on the press finger at tooth bottom B_{Z2}, on the edge of the press plate B_{Z3}, on the winding overhang B_{Z4}, on the frame part over the winding overhang B_{X1} and on the frame part near to the end shield B_{X2} at rated current 1580 A during different tests for 1500 kW, 6-pole generator "A550-6R"
[1]: Not measured. [2]: Extrapolated from the curve in Figure 5.26, as the generator could not be loaded with 100 % load due to the heating problem.

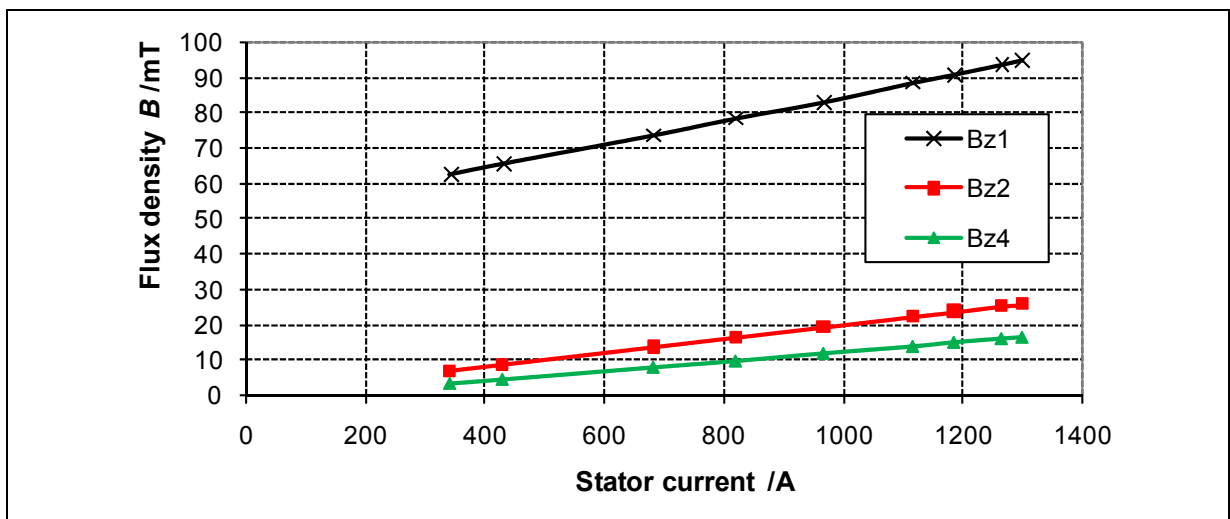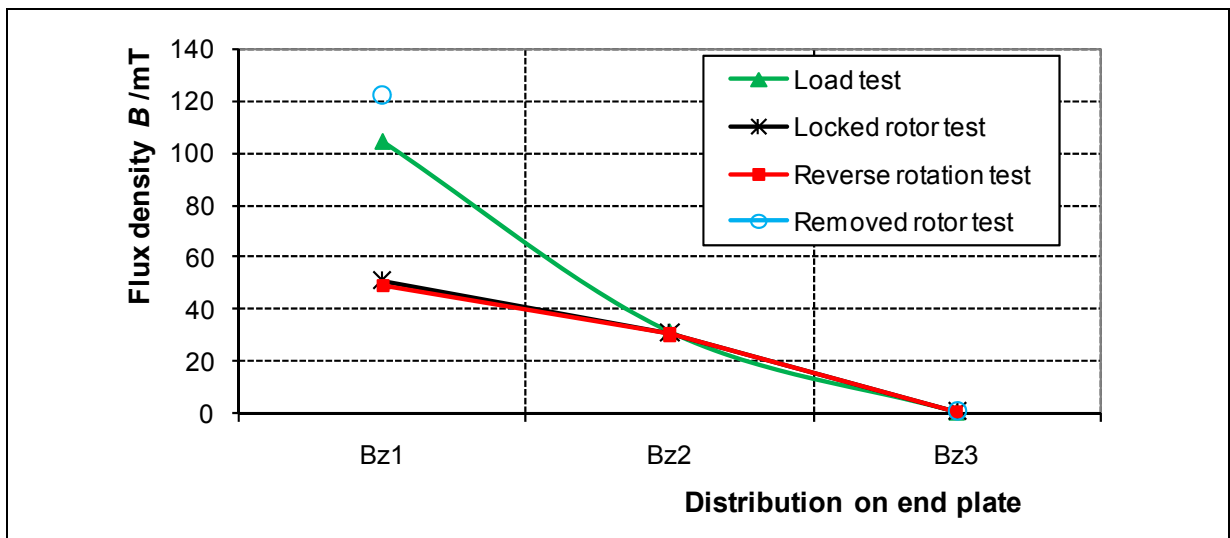Figure 5.27: The axial flux density distribution in the end plate, on the press finger at tooth tip B_{Z1}, on the press finger at tooth bottom B_{Z2} and on the edge of the press plate B_{Z3} at rated current during different tests for 1500 kW, 6-pole generator "A550-6R"

As shown in Figure 5.27 the measured axial flux density at the end plate varies strongly from the tooth tip B_{Z1} to the outer stator diameter B_{Z3}, especially in the load test and the removed rotor test. Also the radial flux density at the stator housing (frame) diminishes with the distance from the iron stack to the end shield, as can be seen in Figure 5.28.
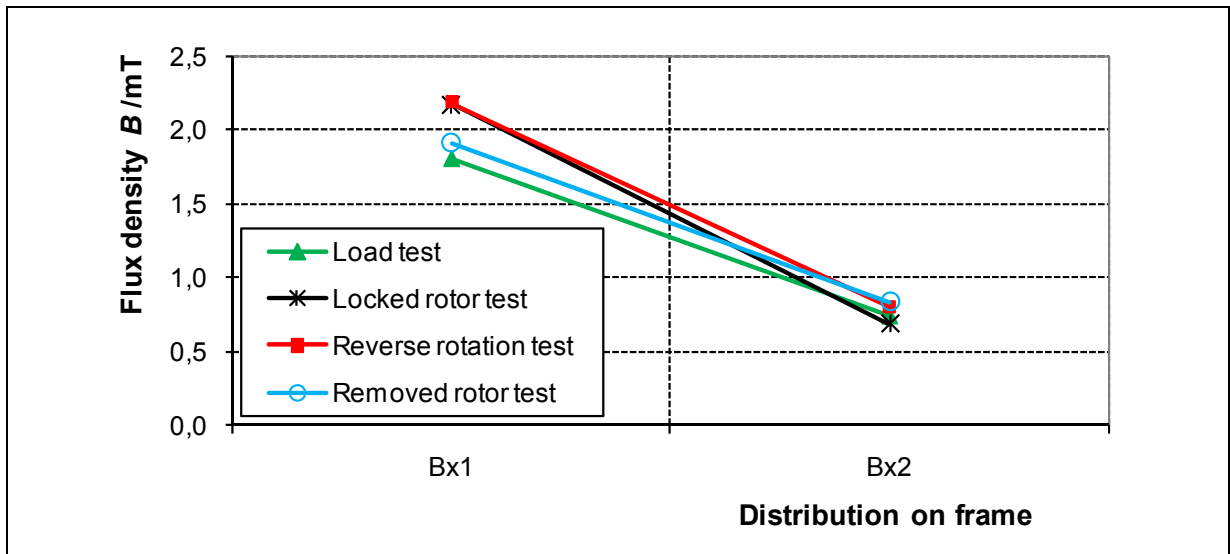
Figure 5.28: The radial flux density distribution in the end region, on the frame part over the winding overhang B_{X1} and on the frame part near to the end shield B_{X2} at rated current during different tests for 1500 kW, 6-pole generator "A550-6R"

The measured magnetic flux densities at rated voltage 600 V and no-load current 315 A during the no-load test compared with the load test at different currents are given in Table 5.27 where the measured values are in the same range for the same current values.

From the comparison of the measured magnetic flux densities at rated voltage 600 V, no-load current 315 A and full load current 1580 A it can be seen that the measured iron losses at the standardized no-load test for the efficiency determination are smaller than the real iron losses at full load. That means that this part of the iron losses will be charged to the stray load losses by the indirect measurement of the stray load losses (input-output test with segregation of the losses) acc. to IEC 61972 [IEC 61972] and IEEE 112-method B [IEEE 112], whereas it is lost by allowance of the stray load losses acc. to e.g. IEC 61972-2 and IEEE 112-method E1 for the efficiency determination!

1500 kW 6-pole generators. "A550-6R"	Measured flux density / mT				
	B_{Y1}	B_{Z1}	B_{Z2}	B_{Z3}	B_{Z4}
No-load test at 315 A	4.97	61.77	6.64	0.20	2.78
Load test at 315 A	4.58	57.59	6.66	0.18	2.94
Load test at 1580 A	6.93	104.39	31.40	0.56	20.64

Table 5.27: Comparison of the measured flux density distribution in the end region at no-load current during the no-load and load tests, on the press plate B_{Y1}, on the press finger at tooth tip B_{Z1}, on the press finger at tooth bottom B_{Z2}, on the edge of the press plate B_{Z3} and on the winding overhang B_{Z4} for 1500 kW, 6-pole generator "A550-6R"

Figure 5.29 and Table 5.28 give a comparison of the measured flux densities for the round wire "A550-6R" and litz wire "A550-6L" generator at rated current 1580 A during the removed rotor test and the load test.

1500 kW 6-pole generators. at 1580 A		Measured flux density / mT				
		B_{Z1}	B_{Z2}	B_{Z3}	B_{X1}	B_{X2}
Removed rotor test	Round wire	122.32	-[1]	0.80	1.91 (135mm)[*]	0.83 (270mm)[*]
	Litz wire	121.14	-[1]	0.80	9.02 (122mm)[*]	0.52 (282mm)[*]
Load test	Round wire	104.39	31.40	0.56	1.80	0.75
	Litz wire	104.14	22.37	0.61	7.82	0.64

Table 5.28: The measured flux density distribution in the end region for 1500 kW, 6-pole generators with round wire "A550-6R" compared to litz wire "A550-6L" at rated current 1580 A during different tests, on the press finger at tooth tip B_{Z1}, on the press finger at tooth bottom B_{Z2}, on the edge of the press plate B_{Z3}, on the frame part over the winding overhang B_{X1} and on the frame near to the end shield B_{X2}
[1]: Not measured. [*]: Position of the Hall probes measured from the iron stack end.

As can be seen on the press finger at tooth tip B_{Z1} the measured flux densities are identical for the both machines, whereas on the press finger at tooth bottom B_{Z2} of the round wire generator "A550-6R" the value is higher due to the smaller tooth width of 11.7 mm (rectangular shape) at this point compared with the litz

wire generator "A550-6L" with tooth width of 17.6 mm and triangular tooth shape. On the stator housing inside over the winding overhang B_{X1} and on the frame part near to the end shield B_{X2} the measured values for both generators are different due to the different localization of the hall probes and different configuration of the winding overhang.
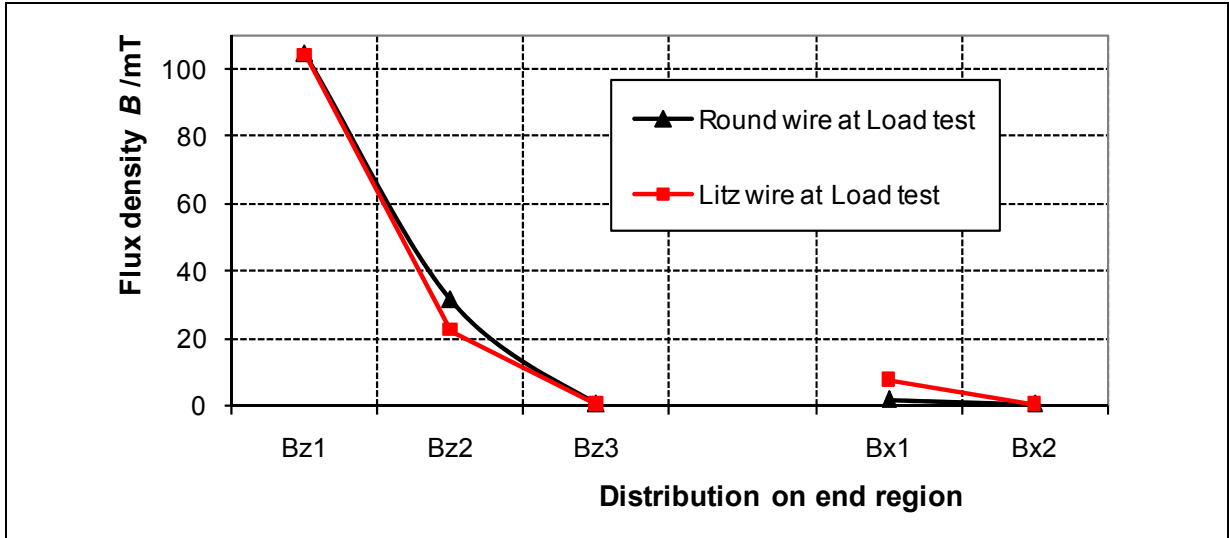
Figure 5.29: Comparison of the measured flux density distribution in the end region for 1500 kW, 6-pole generators with round wire "A550-6R" and litz wire "A550-6L" at load test by rated current 1580 A, on the press finger at tooth tip B_{Z1}, on the press finger at tooth bottom B_{Z2}, on the edge of the press plate B_{Z3}, on the frame part over the winding overhang B_{X1} and on the frame near to the end shield B_{X2}.

5.7.2 Analytical calculation of the eddy current losses in press plates

On the basis of a 2D-model for massive conductive half space, for thick plate [Bind 2000] and the measured axial flux density by Hall probes at load test the eddy current losses in the stator iron stack end sheets (press plate) are calculated. With the abbreviations u, v, $\tilde{a}$ and $\tilde{b}$ the analytical equation for the surface eddy current loss density in the press plates p_{plat} ($= P_{plat}/A_{plat}$) is

$$p_{plat} = \frac{\kappa_{Fe} \cdot \tau_p}{4 \cdot \pi \cdot \tilde{a}} \cdot \frac{(\mu_0 \cdot \hat{a}_e \cdot 2 \cdot f \cdot \tau_p)^2}{u^2 + v^2} \qquad (5.57)$$

$$u = \sinh(\frac{\pi \cdot d_e}{\tau_p}) + \frac{\tilde{a} \cdot \mu_0}{\mu_{Fe}} \cdot \cosh(\frac{\pi \cdot d_e}{\tau_p}); \quad v = \frac{\tilde{b} \cdot \mu_0}{\mu_{Fe}} \cdot \cosh(\frac{\pi \cdot d_e}{\tau_p}) \qquad (5.58)$$

$$\tilde{a} = \sqrt{\frac{1 + \sqrt{1 + R_m^2}}{2}}; \quad \tilde{b} = \sqrt{\frac{-1 + \sqrt{1 + R_m^2}}{2}} \qquad (5.59)$$

$$R_m = \frac{\mu_{Fe} \cdot \kappa_{Fe}}{\pi / \tau_p} \cdot \frac{2 \cdot \pi \cdot f}{\pi / \tau_p} = \mu_{Fe} \cdot \kappa_{Fe} \cdot 2 \cdot f \cdot \tau_p^2 / \pi \qquad (5.60)$$

κ_{Fe} :   conductivity of the iron sheet ($= 8 \cdot 10^6$ S/m)
τ_p :   pole pitch of the field wave
μ_0 :   magnetic permeability of empty space ($\mu_0 = 4\pi \cdot 10^{-7}$ Vs/(Am))
$\hat{a}_e$:   exciting current loading
f :   frequency ($= 60$ Hz)
d_e :   air gap between excitation and massive body ($= 0.1$ m)
μ_{Fe} :   relative magnetic permeability of the iron sheet ($= 500$)
R_m :   magnetic *Reynolds* number.

The exciting current loading $\hat{a}_e$ is derived from the measured axial flux density $B_z(d_e)$ as

$$\hat{a}_e = \frac{B_Z(z = d_e)}{\mu_0} \cdot \left(\sinh(\frac{\pi \cdot d_e}{\tau_p}) + \frac{\mu_0}{\mu_{Fe}} \cdot \cosh(\frac{\pi \cdot d_e}{\tau_p}) \right). \qquad (5.61)$$

To calculate the eddy current losses on the press plates the surface of the yoke is divided into 3 rings, and an exponential curve of the measured flux density between the positions on the press finger at tooth bottom B_{Z2} and on the edge of the press plate B_{Z3} is assumed. As shown in Table 5.29 the surface eddy current losses in the press plates are small for this machine rating.

Parameter	τ_p	A_{ring}	B_z	$\hat{a}_e$	P_{ring}/A_{ring}	P_{ring}	R_m	$\tilde{a}$	$\tilde{b}$
Unit	m	m²	mT	A/m	W/m²	W	--	--	--
Ring 1	0.393	0.0707	17.23	12212	680.61	96.22	29609	121.68	121.67
Ring 2	0.424	0.0763	5.19	3357	66.04	10.08	34536	131.41	131.41
Ring 3	0.456	0.0820	1.56	930.4	6.31	1.04	39842	141.14	141.14
Surface eddy current losses in the press plates						107.3			

Table 5.29: Surface eddy current losses in the press plates at rated load for 1500 kW, 6-pole generator "A550-6R"

5.8 Stator phase inductances at removed rotor test

During the removed rotor test four kinds of flux are acting [Sche 1909]:

- stray flux in the slot,

- stray flux between the teeth edges (through the slot opening),

- stray flux in the winding overhang and

- the stator bore flux.

Through this distribution the equivalent circuit of the induction machine with removed rotor is given in Figure 5.30. Beside the stator phase winding resistance R_s including the stray load losses due to the skin effect $R_{ad,s}$, three different stator inductances are part of this equivalent circuit:

- the slot inductance $L_{s\sigma Q}$ (stray flux in the slot and between the teeth edges),

- the stator winding overhang inductance $L_{s\sigma b}$ and

- the stator main - bore inductance L_{bore}.

With assembled rotor all cited stray fluxes – on the stator side – are acting, plus the flux of the harmonics of the air gap field. Instead of the stator bore flux the main flux is acting. The value of the stator stray reactance with assembled rotor is different from that without rotor [Jord 1970, Rich 1953]. Acc. to *Schenkel* the estimation of the stray flux in the slot and in the winding overhang

from the removed rotor test is accurate enough [Sche 1909].

In Figure 5.31 the principle hyperbolic curves of the flux lines for a 4-pole induction machine during the removed rotor test are presented [Jord 1970, Sche 1909].
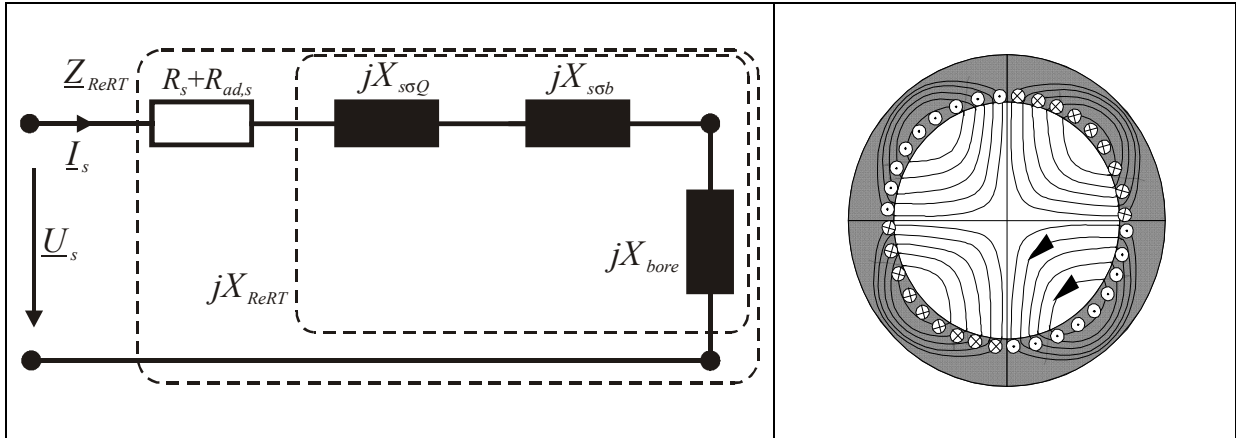
Figure 5.30: Equivalent circuit of the induction machine with removed rotor without consideration of the small iron losses

Figure 5.31: Flux lines at ReRT for 4-pole motor

During the removed rotor test (ReRT) the stator stray reactances of the slot $X_{s\sigma Q}$ and of the winding overhang $X_{s\sigma b}$ are measured together with the - main - bore reactance X_{bore}

$$X_{\text{ReRT}} = X_{s\sigma Q} + X_{s\sigma b} + X_{bore} = \sqrt{Z_{\text{ReRT}}^2 - (R_{s,dc} + R_{ad,s})^2} \tag{5.62}$$

$$\underline{Z}_{\text{ReRT}} = \underline{U}_s / \underline{I}_s; \qquad (R_{s,dc} + R_{ad,s}) = R_{s,dc} \cdot k_r \tag{5.63}$$

$R_{s,dc}$: stator phase DC-resistance
$R_{ad,s}$: stator phase AC-resistance considering the stray load losses in the stator winding due to the skin effect
k_r : resistance coefficient.

The stator stray reactances in the slot $X_{s\sigma Q}$ and in the winding overhang $X_{s\sigma b}$ can be estimated from the measured stator reactance X_{ReRT} and from the measured or calculated bore reactance X_{bore} as

$$X_{s\sigma \text{ReRT}} = X_{s\sigma Q} + X_{s\sigma b} = X_{\text{ReRT}} - X_{bore} = \sqrt{Z_{\text{ReRT}}^2 - (R_{s,dc} \cdot k_r)^2} - X_{bore} \tag{5.64}$$

5.8.1 Calculation of the stator bore reactance

For the calculation of the stator bore reactance X_{bore}, an empirical formula is used in the following expression. The corrected length of the iron stack l'_{Fe} should consider the stray flux at the machine axial ends, e.g. 10 % [Böde 1962, Bind 2006c] or acc. to (5.67) as suggested in Clause A40 of [IEC 60034-4]. The stator stray reactances of the slot $X_{\text{s}\sigma Q}$ and of the winding overhang $X_{\text{s}\sigma b}$ are calculated in well-known manner [Bind 2006c, Vogt 1974].

$$X_{\text{bore}} = 2 \cdot 2 \cdot \mu_0 \cdot m \cdot w^2 \cdot k_{\text{w}}^2 \cdot f \cdot l'_{\text{Fe}} \cdot (1 + \sigma_{\text{s}}) / p \tag{5.65}$$

$$l'_{\text{Fe}} = 1.1 \cdot l_{\text{Fe}} \tag{5.66}$$

$$l'_{\text{Fe}} = L_{\text{Fe}} + \tau_{\text{p}} / 6 - n_{\text{k}} . l_{\text{k}} / 2 \tag{5.67}$$

μ_0 : magnetic permeability of empty space ($\mu_0 = 4\pi \cdot 10^{-7}$ Vs/(Am))
m : number of phase ($m = 3$)
w : number of turns per phase
k_{w} : winding factor
f : supply frequency
p : number of pole pairs
σ_{s} : *Blondel'*s stray coefficient (estimated value for 1500 kW generator 0.07)
l'_{Fe} : corrected length of the iron stack
l_{Fe} : length of the iron stack (without radial ventilation ducts)
L_{Fe} : total length of the iron stack (with radial ventilation ducts)
τ_{p} : pole pitch
n_{k} : number of the radial ventilation ducts
l_{k} : length (thickness) of the radial ventilation ducts.

A comparison of the analytically calculated stator stray reactances $(X_{\text{s}\sigma Q} + X_{\text{s}\sigma b})_{\text{cal}}$ with the estimated value $(X_{\text{s}\sigma Q} + X_{\text{s}\sigma b})$ from ReRT at rated current is presented in Table 5.30 for the 1500 kW, 6-pole generator "A550-6R" and in Table 5.31 for the 5.5 kW, 4-pole motor "A132-4".

As can be seen in Table 5.30 the calculated stator stray reactances $(X_{\text{s}\sigma Q} + X_{\text{s}\sigma b})_{\text{cal}}$ deviate from the estimated value $(X_{\text{s}\sigma Q} + X_{\text{s}\sigma b})$ from ReRT within 6 %. It has to be noted that the stator stray reactances $(X_{\text{s}\sigma Q} + X_{\text{s}\sigma b})$ are in the

range of the calculated bore reactance X_{bore} for this example of the "big" 6-pole generator "A550-6R".

1500 kW, 6-pole generator	Equation		"A550-6R"	
Stator phase current /A		I_s	912.5	ReRT
Stator phase voltage /V		U_s	168.9	
Stator phase resistance warm /Ω		$R_{s,dc}$	0.00432	
Resistance coefficient		k_r	2.07	
Measured stator reactance /Ω	(5.63)	X_{ReRT}	0.1849	Corresponding stator stray reactances acc. (5.64) /Ω
Number of turns per phase		w	18	
Winding factor		k_w	0.925	
Length of the iron stack /m		l_{Fe}	0.98	
Blondel's stray coefficient		σ_s	0.07	$(X_{s\sigma Q} + X_{s\sigma b})$
Calculated bore reactance /Ω	(5.65)	$X_{bore, cal}$	0.0877	0.0972
Calculated bore reactance with corrected iron length /Ω	(5.66)	$X_{bore, cal\_10\%}$	0.0964	0.0885
Calculated bore reactance with corrected iron length_IEC /Ω	(5.67)	X_{bore, cal_IEC}	0.0919	0.093
Calculated stator stray reactances /Ω	Analytic	$(X_{s\sigma Q} + X_{s\sigma b})_{cal}$	0.0935	

Table 5.30: The calculated stator reactances during the removed rotor test at 60 Hz and rated current for 1500 kW, 6-pole generator "A550-6R"

5.8.2 Measurement of the stator bore reactance

The method - described in (5.64) - is not accurate enough as the bore reactance X_{bore} might be calculated with an assumption of additional flux at the machine axial ends, e.g. of 10 %. This calculation can lead to high stator stray reactances $(X_{s\sigma Q} + X_{s\sigma b})$, especially for short machines and low-pole machines [Böde 1962, Bonf 1962, Rich 1953]. To increase the accuracy of the estimated stator stray reactances $(X_{s\sigma Q} + X_{s\sigma b})$ in (5.64) the bore reactance X_{bore} should be measured with an extra bore-coil [Sche 1909, IEC 60034-4].

The bore-coil is shown in Figure 5.32. The length of the bore-coil should be equal to the length of the iron stack l_{Fe}, and the width is equal to the pole pitch

τ_p. The bore-coil with w_{coil} turns is placed in the bore during the ReRT. At the terminals of the bore-coil the induced voltage U_{coil} can be measured, which is proportional to the bore flux Φ_{ReRT}

$$U_{coil} = \sqrt{2} \cdot \pi \cdot f \cdot w_{coil} \cdot k_{w,coil} \cdot \Phi_{ReRT}; \quad k_{w,coil} = 1 \tag{5.68}$$

w_{coil} : number of turns of the bore-coil
$k_{w,coil}$: winding factor of the bore-coil ($k_{w.coil} = 1$).

With the stator data the bore reactance X_{bore} is given as

$$X_{bore} = \frac{\sqrt{2} \cdot \pi \cdot f \cdot w \cdot k_w \cdot \Phi_{ReRT}}{I_s} = \frac{w \cdot k_w}{w_{coil} \cdot k_{w,coil}} \cdot \frac{U_{coil}}{I_s} = \ddot{u}_U \cdot \frac{U_{coil}}{I_s} \tag{5.69}$$

I_s : stator phase current during the ReRT
$\ddot{u}_U$: voltage transformation ratio between the stator winding and the bore-coil.
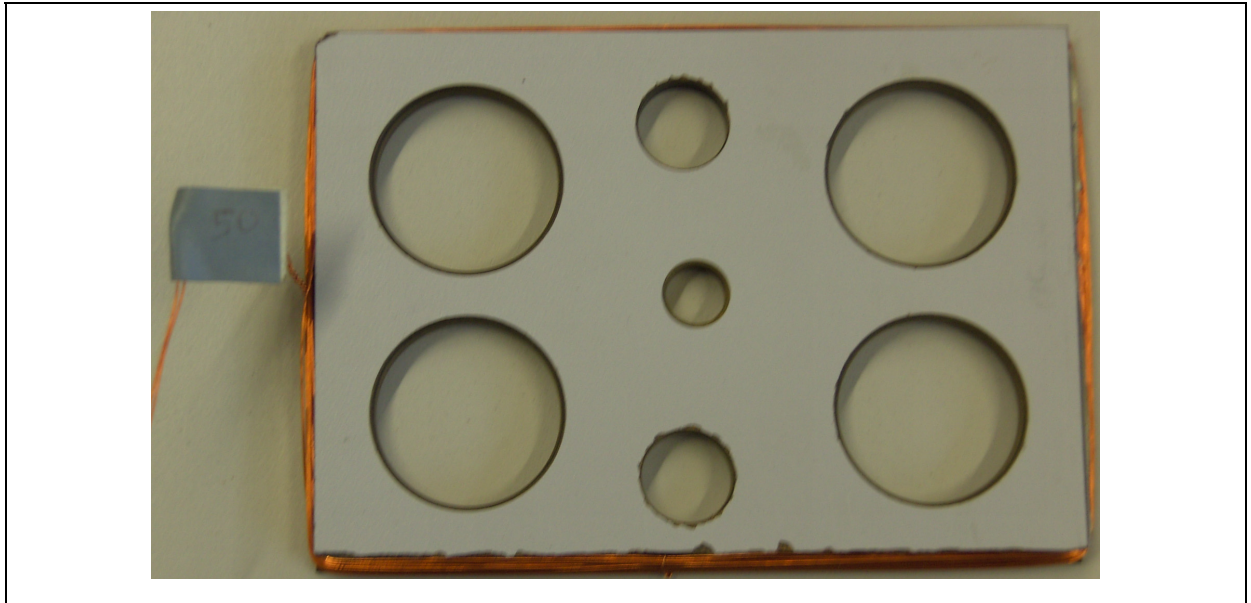
Figure 5.32: The bore-coil with 50 turns a 0.38 mm insulated wire diameter for the measurement of the bore reactance during the removed rotor test for 5.5 kW, 4-pole motor "A132-4".

The bore flux Φ_{ReRT} – measured with the bore-coil – as function of the stator current I_s and the stator voltage U_s during the removed rotor test is depicted in Figure 5.33 for the 5.5 kW, 4-pole motor "A132-4". The bore flux Φ_{ReRT} is

proportional to the stator current I_s and to the stator voltage U_s.
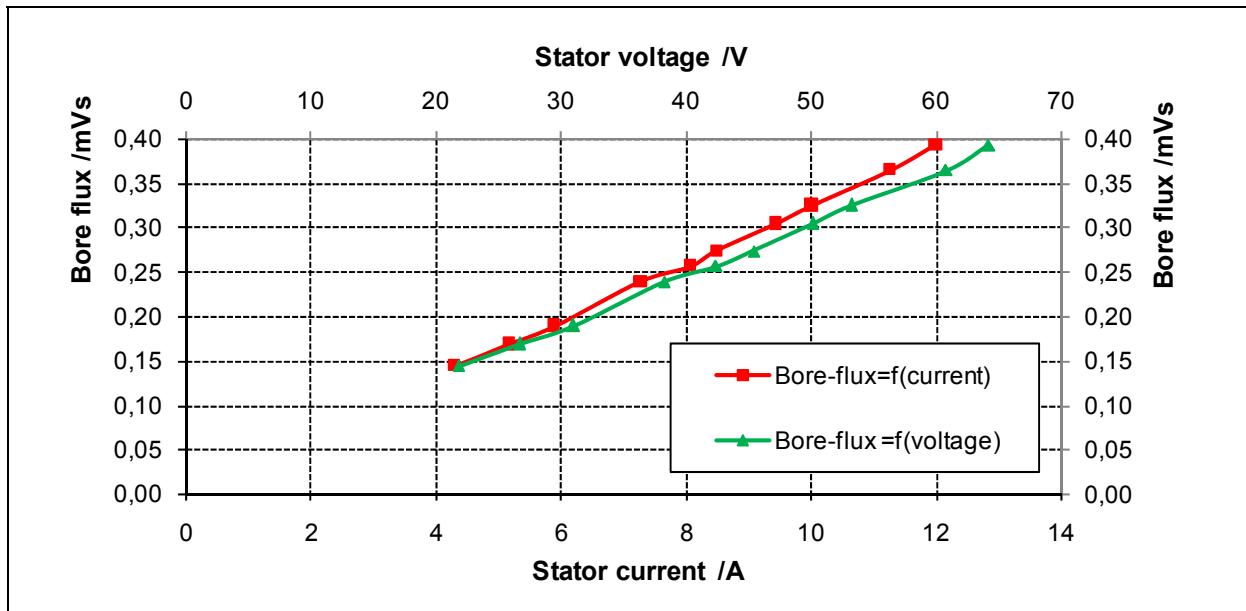
Figure 5.33: Measured bore flux as function of the stator current and stator voltage during the removed rotor test for 5.5 kW, 4-pole motor "A132-4"

As can be seen in Table 5.31 the calculated bore reactance $X_{\text{bore, cal\_IEC}}$ acc. to (5.67) deviates from the value X_{bore} measured with the bore-coil acc. to (5.69) within 8 %; the stator stray reactances $(X_{s\sigma Q} + X_{s\sigma b})$ determined with the calculated bore reactance X_{bore} deviate from the measured value within 4 %. For this example of the "short" 4-pole motor "A132-4" the analytically calculated stator stray reactances $(X_{s\sigma Q} + X_{s\sigma b})_{\text{cal}}$ are smaller than the measured value and deviate by 51 %. This finding correlates with the observation of *Richter* [Rich 1953, p. 432]. The ratio of the stray reactances $(X_{s\sigma Q} + X_{s\sigma b})$ and the bore reactance X_{bore} is 1.8. In comparison the stator stray reactances $(X_{s\sigma Q} + X_{s\sigma b})$ are in the range of the calculated bore reactance X_{bore} for the example of the "big" 6-pole generator "A550-6R".

5.5 kW 4-pole motor "A132-4"	Equation		
Number of turns of the bore-coil; Winding factor		w_{coil}; $k_{\text{w,coil}}$	50; 1
Measured induced voltage in the bore-coil /V		U_{coil}	4.05
Measured bore flux /mVs	(5.68)	Φ_{ReRT}	0.3646
Measured bore reactance /Ω	(5.69)	X_{bore}	3.012
Stator phase current /A; phase voltage /V		I_{s}; U_{s}	6.5; 61.7
Stator phase resistance warm /Ω		$R_{\text{s,dc}}$	3.509
Resistance coefficient		k_{r}	1.094
Measured stator reactance /Ω	(5.63)	X_{ReRT}	8.67
Measured stator stray reactances /Ω	(5.64)	$(X_{\text{s}\sigma\text{Q}} + X_{\text{s}\sigma\text{b}})$	5.658
Number of turns per phase; Winding factor		w; k_{w}	252; 0.96
Length of the iron stack /m		l_{Fe}	0.1253
Blondel's stray coefficient		σ_{s}	0.04
Calculated bore reactance /Ω	(5.65)	$X_{\text{bore, cal}}$	2.874
Calc. bore reactance with corrected iron length /Ω	(5.66)	$X_{\text{bore, cal\_10\%}}$	3.161
Calc. bore reactance with correct. iron length_IEC /Ω	(5.67)	$X_{\text{bore, cal\_IEC}}$	3.249
Calculated stator stray reactances /Ω	Analytic	$(X_{\text{s}\sigma\text{Q}} + X_{\text{s}\sigma\text{b}})_{\text{cal}}$	2.765

Table 5.31: Measured reactances with the bore-coil during the removed rotor test at 50 Hz and rated current compared to the calculated on for 5.5 kW, 4-pole motor "A132-4"

Note: The manufacturer data for this motor were not available. Some dimensions were measured where possible. The number of turns per phase w was derived from the measured phase resistance R_{s}. This increases the uncertainties in the calculated parameters.

5.9 Iron losses at removed rotor test

The iron losses in the stator core $P_{\text{Fe,ReRT}}$ during the removed rotor test (ReRT) are small and can be neglected due to the reduced voltage ($P_{\text{Fe}} \sim B^2$, $B \sim U$). But for a more accurate estimation of the resistance coefficient k_{r} due to the skin effect the iron losses in the stator core $P_{\text{Fe,ReRT}}$ can be derived from the ratio of the fluxes as

$$P_{\text{Fe,ReRT}} = P_{\text{Fe,N}} \cdot \left(\Phi_{\text{ReRT}} / \Phi_{\delta 1} \right)^2 \tag{5.70}$$

$P_{\text{Fe,ReRT}}$: iron losses in the stator core during the removed rotor test
Φ_{ReRT} : flux during the removed rotor test at reduced voltage
$P_{\text{Fe,N}}$: iron losses in the stator core at rated voltage
$\Phi_{\delta 1}$: rated air gap flux (fundamental) of the IM (with rotor) at rated voltage.

The ratio of the flux during the removed rotor test Φ_{ReRT} at reduced voltage and the rated flux $\Phi_{\delta 1}$ of the IM (with rotor) at rated voltage is given by [Jord 1970]

$$\frac{\Phi_{\text{ReRT}}}{\Phi_{\delta 1}} = \sqrt{2} \cdot \mu_0 \cdot k_{\text{w}} \cdot \frac{A_s}{B_{\delta 1}} \tag{5.71}$$

μ_0 : magnetic permeability of empty space ($\mu_0 = 4\pi \cdot 10^{-7}$ Vs/(Am))
k_{w} : winding factor
A_s : stator current loading
$B_{\delta 1}$: air gap flux density (fundamental) of the IM (with rotor) at rated voltage.

With the number of the phases m and the stator current I_s the stator current loading A_s can be determined as

$$A_s = \frac{2 \cdot m \cdot w \cdot I_s}{2 \cdot p \cdot \tau_{\text{p}}} \tag{5.72}$$

w : number of turns per phase
τ_{p} : pole pitch.

The air gap flux density (fundamental) $B_{\delta 1}$ of the IM (with rotor) at rated voltage $U_{\text{s,N}}$ (assuming the terminal voltage $U_{\text{s,N}} \approx U_{\text{h}}$) is

$$B_{\delta 1} = \frac{U_{\text{s,N}} / (1 + \sigma_s)}{2 \cdot \sqrt{2} \cdot w \cdot k_{\text{w}} \cdot \tau_{\text{p}} \cdot f \cdot l_{\text{Fe}}} \tag{5.73}$$

l_{Fe} : length of the iron stack
f : supply frequency
σ_s : *Blondel*'s stray coefficient which considers the voltage drop on the stator stray reactance (estimated value 0.07).

With the equations (5.72) and (5.73) the equation (5.71) can be rewritten as

$$\frac{\Phi_{\text{ReRT}}}{\Phi_{\delta 1}} = \frac{X_{\text{bore}} \cdot I_s \cdot}{U_{s,N}} = \frac{2 \cdot 2 \cdot \mu_0 \cdot m \cdot w^2 \cdot k_w^2 \cdot f \cdot l_{\text{Fe}} \cdot I_s}{p \cdot U_{s,N} / (1 + \sigma_s)} \tag{5.74}$$

The fundamental-frequency stray load losses $P_{\text{ad,s}}$ in the stator including the small amount of the iron losses during the removed rotor test, the stray load losses in the winding due to the skin effect considering the iron losses at reduced voltage and the ratio of the flux during the removed rotor test and the rated flux are compared in Table 5.32 for the round wire winding generator "A550-6R", the litz wire winding generator "A550-6L" and the profiled conductor winding generator "A550-6P". The amount of the iron losses during the removed rotor test is about 2 % of the iron losses at rated voltage. This leads – depending of the value of the stray load losses in the stator – to a deviation of 1 %...15 % of the determined stray load losses in the winding due to the skin effect.

1500 kW 6-pole generators	A550-6R	A550-6L	A550-6P
Rated voltage / voltage at removed rotor test	600 V / 169 V	600 V / 182 V	600 V / 181 V
Measured iron loss at rated voltage /kW	8.842	8.927	9.06 (calcul.)
Calcul. iron loss at removed rotor /kW	0.157	0.204	0.209
Stator stray load loss (incl. iron loss) /kW	11.543	1.383	4.61
Stator winding stray load losses /kW	11.386	1.179	4.4
Deviation in stray load losses	-1.36 %	-14.7 %	-4.5 %
Ratio of the fluxes: $\Phi_{\text{ReRT}} / \Phi_{\delta 1}$	13 %	15 %	15 %
Ratio of the iron losses: $P_{\text{Fe,ReRT}}/P_{\text{Fe,N}}$	1.78 %	2.28 %	2.31 %

Table 5.32: The measured stray load losses at rated current in the stator with and without consideration of the iron losses for 1500 kW, 6-pole generators

During the short circuit test or locked rotor test (SCT) the voltage (main flux) is also reduced, like during the removed rotor test (ReRT). Except for some differences like the reduced stray inductances due to increased saturation of the tooth tips through the zig-zag stray flux at higher slip s (SCT), we ask if the estimation of the iron losses during both tests is comparable.

Richter [Rich 1936] estimates the iron losses in the stator core $P_{\text{Fe,SC}}$ during

the SCT acc. to the equation (5.75). Is this estimation also valid for the iron losses $P_{Fe,ReRT}$ in the stator core during the ReRT ? The iron losses estimated by the equations (5.70) and (5.75) are compared in Table 5.33. It can be seen that the estimated iron losses during the removed rotor test acc. to *Richter* can differ by 1 % to 11 % for these examples.

$$P_{Fe,SC} = \left(U_{ReRT}/U_{s,N}\right)^2 \cdot P_{Fe,N}/4 \overset{!}{\approx} P_{Fe,ReRT} \tag{5.75}$$

U_{ReRT} : reduced voltage during the removed rotor test
$U_{s,N}$:   rated voltage
$P_{Fe,N}$: iron losses in the stator core at rated voltage.

1500 kW 6-pole generators	A550-6R	A550-6L	A550-6P
Rated voltage / voltage at removed rotor test	600 V / 169 V	600 V / 182 V	600 V / 181 V
Measured iron losses at rated voltage /kW	8.842	8.927	9.06 (calcul.)
Calcul. iron loss at ReRT acc. (5.70) /kW	0.157	0.204	0.209
Estimated iron losses at removed rotor from short circuit relation acc. (5.75) /kW	0.175	0.205	0.206
Deviation in iron losses	11.4 %	0.6 %	1.6 %

Table 5.33: Comparison of the estimated iron losses during the ReRT at 60 Hz for 1500 kW, 6-pole generators

5.10 Measures to reduce the eddy current losses in the winding

Due to the AC current of stator frequency the AC slot leakage flux will induce eddy currents in the conductors, leading to additional losses in the conductors and uneven current density distribution. Therefore the height of the single conductor should be reduced beyond the critical value and /or segmented into many parallel insulated strands, which are twisted and arranged in a suitable way to reduce the eddy currents like the *Roebel* [Bind 2006g] bars. The twists may be made in various combinations as to the number and the place, e.g. only in the back, front or all end connections, after each or several turns... Besides the twist the height of the turn should be reduced, might it be through the insulation

material between the turns in the slot or through careful manual inserting instead of mechanical inserting.

5.10.1 Modelling

To reduce the first order eddy current losses due to the circulating currents, in loops composed of insulated partial conductor wires connected at the ends, a simplified model is given in Figure 5.34.
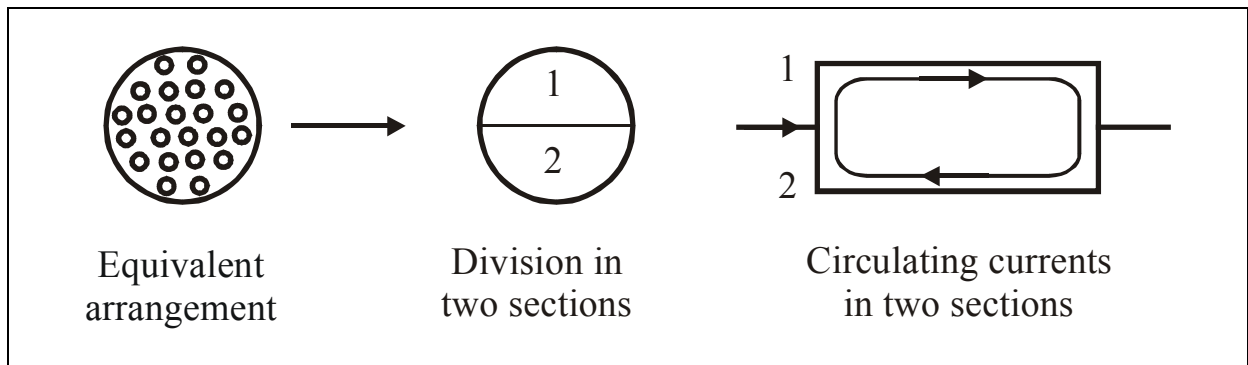
Figure 5.34: Simplified model showing the circulating currents between two sections for the round wire winding

The simplified model can be described as:

1) The real – random – distribution of the wires will be substituted by an equivalent arrangement.

2) The coil consisting of many insulated round wires (bundle) will be divided vertically into two sections. Each section (section 1 and section 2) is composed of a number of wires. Horizontally the potential differences due to the radial stray flux are small and can be neglected.

3) Each section should change successively its position in the slot so that each one comes to every position. Then all sections have the same impedance and carry the same current.

4) In all the slots flows the same current (unpitched winding).

5) The transverse magnetic field in the slot will be divided into few levels or positions depending on the number of the turns per slot $w_{\ddot{u}}$ (Figure 5.35).

To estimate the effectiveness of the measures to reduce the first order skin effect, the method described by *Lammeraner* [Lamm 1966] is choosen as it is simple. Also the works of *Müller* [Müll 1956] and *Kučera* [Kuče 1956] deal with this topic.

Example 1

As presented in Figure 5.35 the coil of the two-layer winding is composed of many insulated round wires (bundle). At the ends of the coil the bundle are conductively short circuited (SC). The winding is inserted in the slots without transposition of the coil sides, like it is done for the single layer winding. So the slot stray flux in both coil sides is calculated without changed direction of the slot stray flux penetration, which yields higher eddy current losses than with this change, which is usual for the transposed two-layer winding with profile copper conductors. The winding consists of $w_{\ddot{u}} = 4$ turns per slot and passes through 4 slots ($q = 2$).

Figure 5.35: The coil of the two-layer round wire winding with four turns per slot passing through four slots without transposition, without twists and the magnetic field level

As can be seen in the Figure 5.35 each section remains in the same position – magnetic field level – in the slots.

The expanded view for the coil is presented in Figure 5.36.
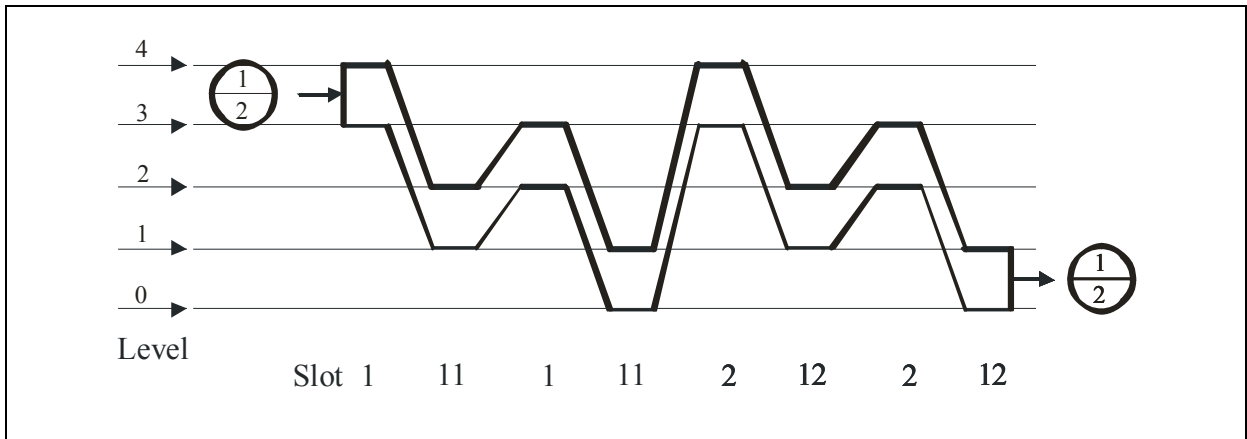
Figure 5.36: Expanded view for the coil of the two-layer round wire winding with four turns per slot passing through four slots without transposition, without twists and the magnetic field level

The resistance coefficient can be written as

$$k_{r1.O} = \varphi(\xi_{1.O}) + c_1 \cdot c_2 \cdot \psi(\xi_{1.O}) \tag{5.76}$$

c_1 : average value of the "potential" of section 1
c_2 : average value of the "potential" of section 2.

The values c_1 and c_2 will be determined from the expanded view in Figure 5.36. We are to follow the course of each section from one short-circuited end to the other short-circuited end, add the level values and take the average as:

$$c_1 = \frac{(4+2+3+1)\big|_{slot\,1\to11} + (4+2+3+1)\big|_{slot\,2\to12}}{8} = \frac{5}{2} = 2.5 \tag{5.77}$$

$$c_2 = \frac{(3+1+2+0)\big|_{slot\,1\to11} + (3+1+2+0)\big|_{slot\,2\to12}}{8} = \frac{3}{2} = 1.5 \tag{5.78}$$

For this example, the coil of the two-layer winding with four turns per slot

passing through four slots (1-11-2-12) without transposition and without twists, the product of c_1 and c_2 is 3.75. This result is identical with the value calculated acc. to the equation (5.45), where $w_{\ddot{u}} = 4$.

5.10.2 Twisting in winding overhang

The practicable twisting, for the round wire winding, is done in the winding overhang between two equal coils (in the middle of the winding). Several twists might be possible but not practicable !

To reduce the circulating currents in the coil of example 1, a twist (11/2) will be made in the winding overhang between the slot 11 and the slot 2 as shown in Figure 5.37 and Figure 5.38.
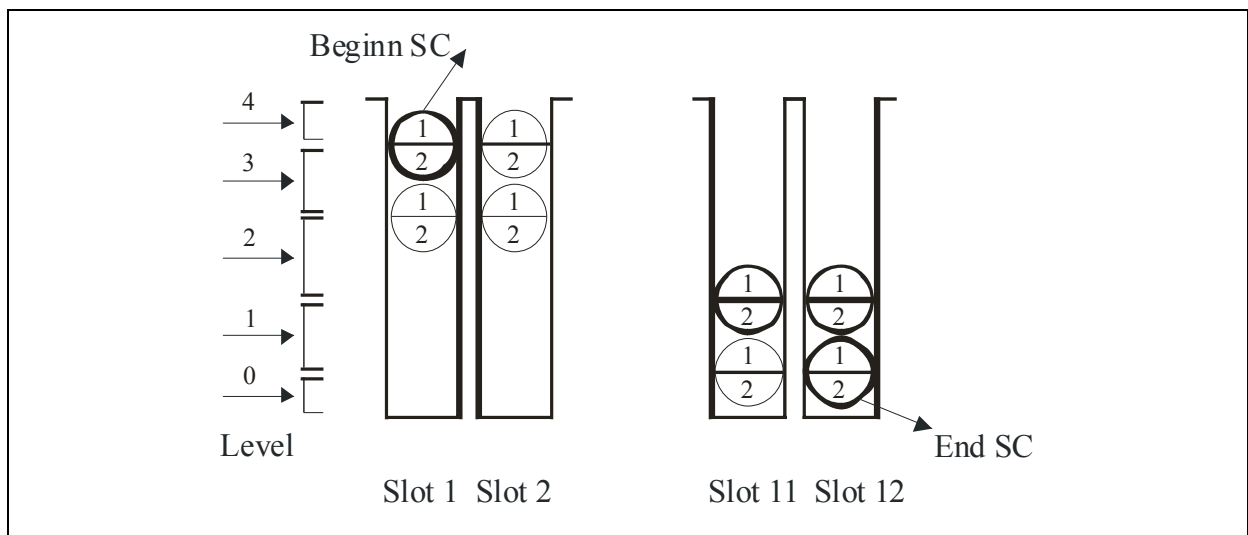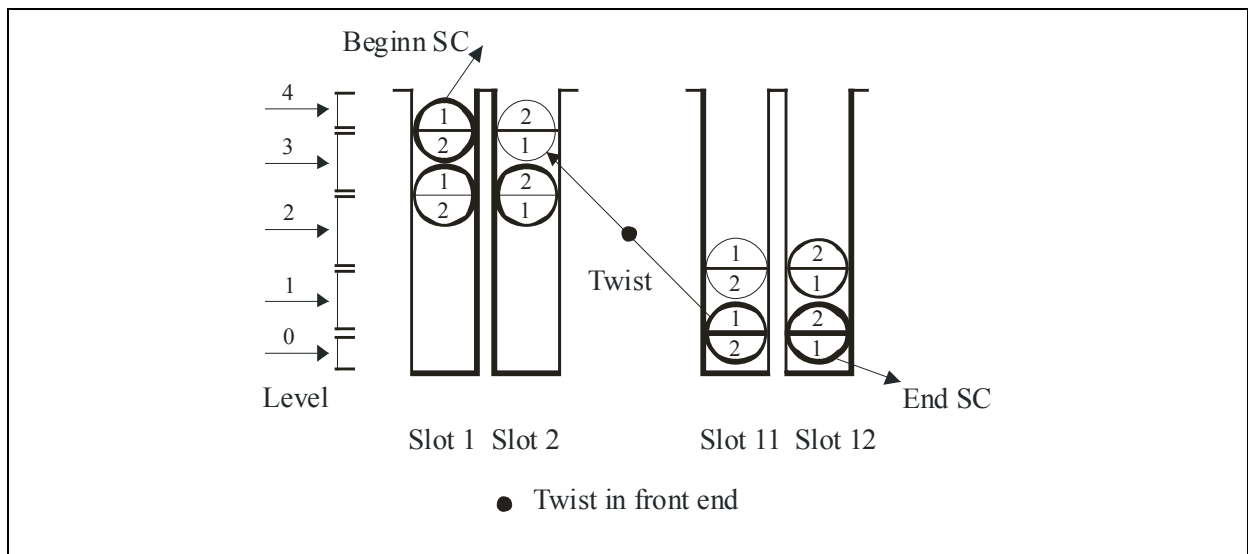

Figure 5.37: Twist in winding overhang in the middle of the two-layer round wire winding
with four turns per slot passing through four slots without transposition

As can be seen in the Figure 5.37 each section changes successively its position in the slot, so that each one comes to every position.
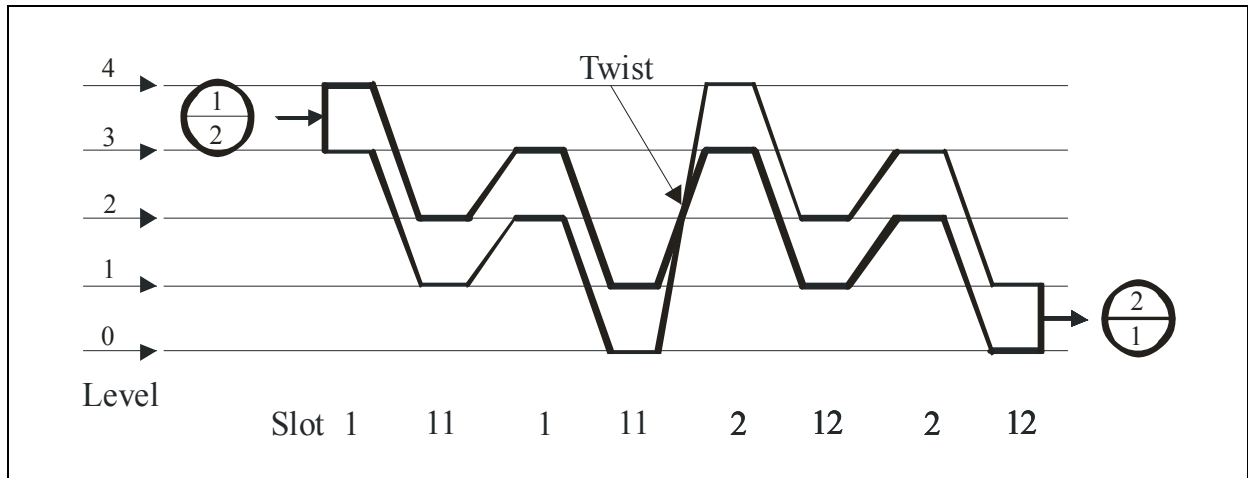
Figure 5.38: Expanded view for the twist in winding overhang in the middle of the two-layer winding with four turns per slot passing through four slots without transposition

From the expanded view in Figure 5.38 the values c_1 and c_2 will be determined, like in former example, but with changing the sign after the twist as:

$$c_1 = \frac{(4+2+3+1)\big|_{\text{slot }1\to11} + (-3-1-2-0)\big|_{\text{slot }2\to12}}{8} = \frac{1}{2} = 0.5 \qquad (5.79)$$

$$c_2 = \frac{(3+1+2+0)\big|_{\text{slot }1\to11} + (-4-2-3-1)\big|_{\text{slot }2\to12}}{8} = -\frac{1}{2} = -0.5 \qquad (5.80)$$

With a twist in the winding overhang in the middle of the coil (11/2) the product of c_1 and c_2 for this example is -0.25.

5.10.3 Transposition

The coil of example 1 will be inserted in the slots with "transposition" of the coil sides, like in the usual two-layer winding with profile copper conductors. This can be realised with 6 twists after each half turn in the winding overhang but not in the middle of the coil (11-2); 3 twists between slot 1 and slot 11 in (1/11), (11/1), (1/11) and 3 twists between slot 2 and slot 12 in (2/12), (12/2), (2/12).
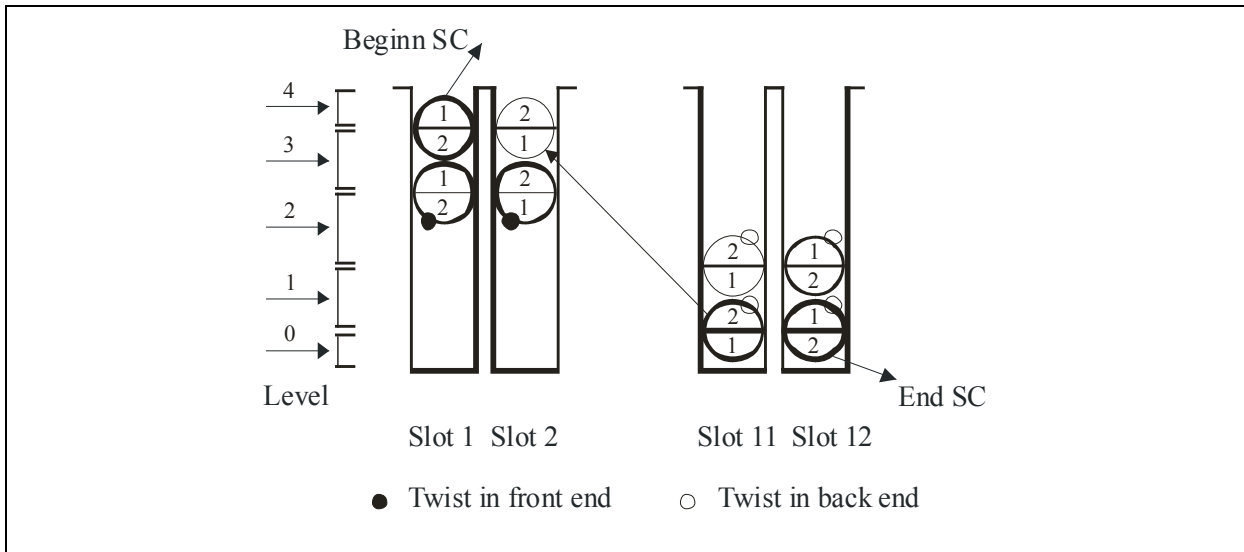
Figure 5.39: "Transposition" of the two-layer round wire winding with four turns per slot passing through four slots

As can be seen in the Figure 5.39 the winding is compensated as each section changes successively its position in the slot, so that each section comes to every position.

For this configuration the product of c_1 and c_2 is -0.25. This value is the same as obtained with only one twist as presented in the Figure 5.37.

$$c_1 = \frac{(4-1+3-0)\big|_{slot\,1\rightarrow11} + (-3+2-2+1)\big|_{slot\,2\rightarrow12}}{8} = \frac{4}{8} = 0.5 \qquad (5.81)$$

$$c_2 = \frac{(3-2+2-1)\big|_{slot\,1\rightarrow11} + (-4+1-3+0)\big|_{slot\,2\rightarrow12}}{8} = -\frac{4}{8} = -0.5 \qquad (5.82)$$

If we made a twist in the middle of the winding (11/2) in addition to the 6 twists after each half turn the compensation will be affected and the product of c_1 and c_2 will be 0.75.

An example of transposition is given in Figure 5.40 for a profiled conductor winding with four turns per slot and four partial conductors per turn.
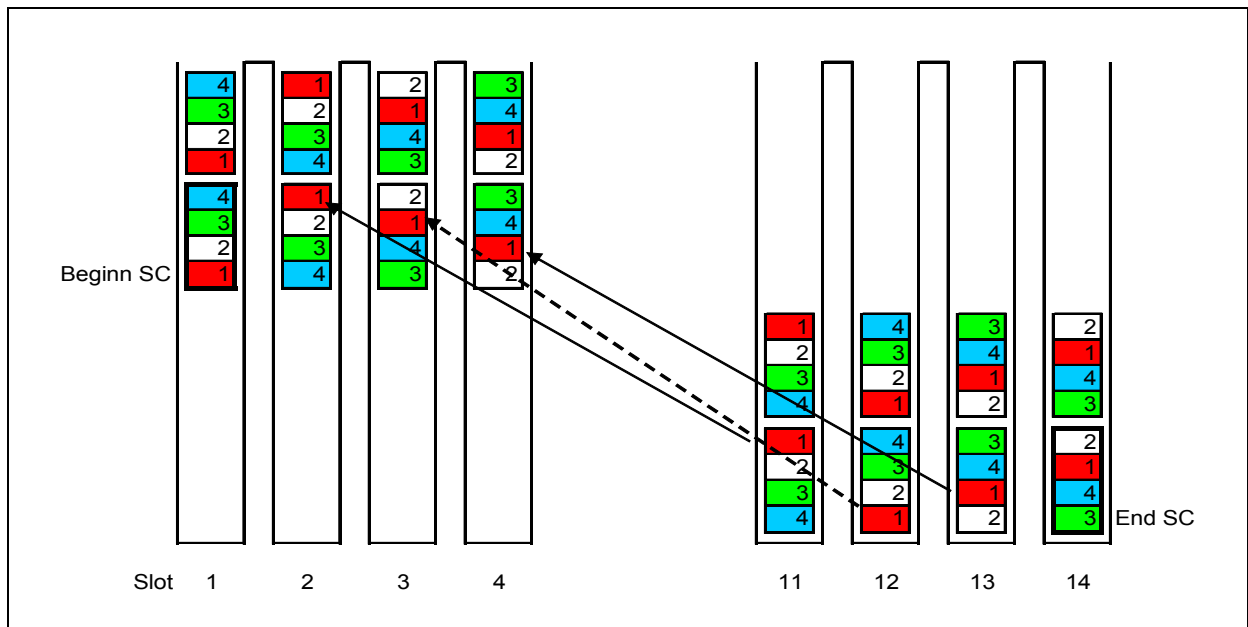
Figure 5.40: Transposition of the two-layer profiled conductor winding with four turns per slot passing through eight slots

The winding is fully compensated as each partial conductor comes to every position in the slot. For this distribution the number of the slots should be divisible by the number of the partial conductors. It is expensive but the circulating current losses are effectively suppressed !

5.10.4 Twisting in the slot region

The most effective measure to reduce the circulating current losses is the compensation along the slot (each coil side) like by the expensive *Roebel* bar.

To achieve full compensation the twist should be done in the middle of the slots for each turn as presented in Figure 5.41 and Figure 5.42. With the twist in the middle of the slots it is difficult to insert the coils of the round wire winding in the slots, and so this measure is expensive and not practicable !
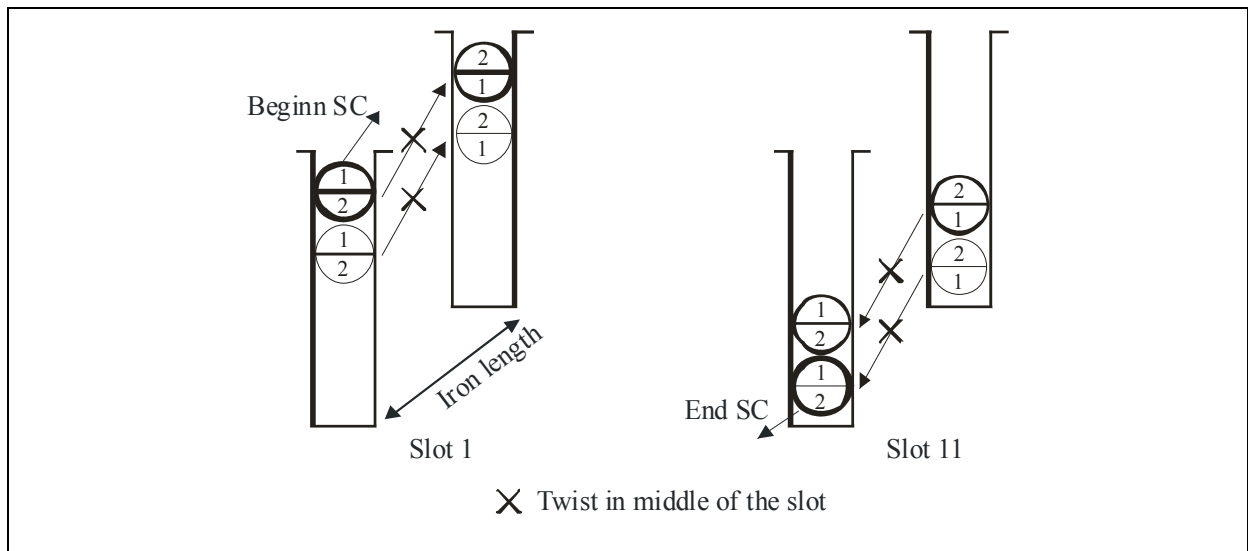
Figure 5.41: Twist in the middle of the slot for the two-layer round wire winding with four turns per slot passing through two slots
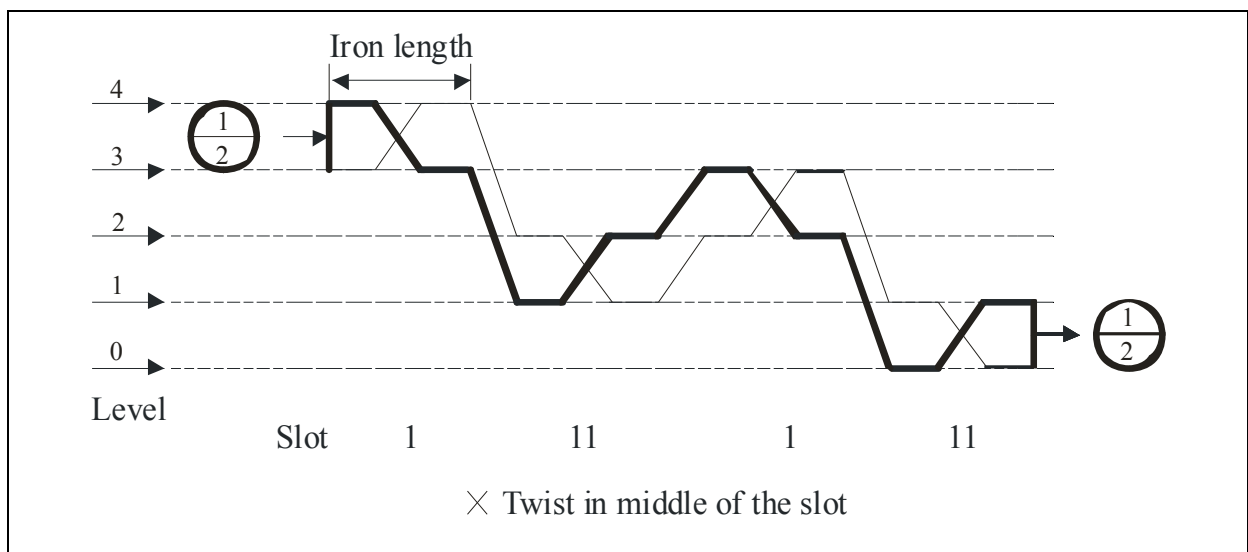
Figure 5.42: Expanded view for the twist in the middle of the slot for the two-layer round wire winding with four turns per slot passing through two slots

5.11 Tested measures reducing eddy current losses in the winding

The simplest measure to reduce the eddy current losses in round wire windings is careful hand insertion (H1, H2, H3) of the winding in the slot

instead of mechanical insertion (M1, M2, M3). A reduction of about 50 % of the stator stray load losses in the winding can be achieved as shown in Figure 5.43 for the two speeds round wire winding generator "A445-**4**6R". Sometime this is not enough, in case of heating or efficiency problems, and then the twisting in the winding overhang in the middle of the coil should be done.
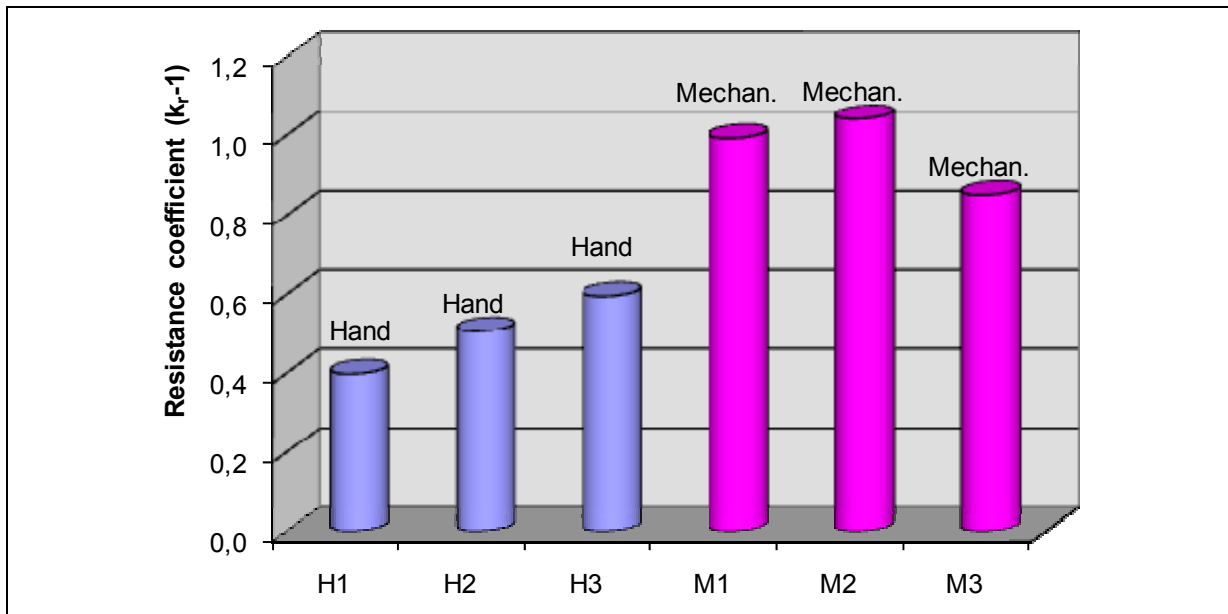
Figure 5.43: Reduction of stray load losses with hand compared to mechanically insertion for the two speeds round wire winding "A445-**4**6R" at 50 Hz

As presented in Figure 5.44 for the two speeds round wire winding generator "A445-**4**6R" with twist in the middle of the coil (T1, T2), a reduction of about 46 % of the stator stray load losses can be realized compared to the hand inserted untwisted winding (R1, R2, R3).

For on speed round wire winding generator "A550-6R5" with twist in the middle of the coil (T1, T2) a reduction of about 94 % is measured, compared to untwisted windings (R1, R2, R3). It has to be noted that the measurement accuracy in this case is low, due to the low losses as depicted in Figure 5.45. But the tendency shows the reduction.
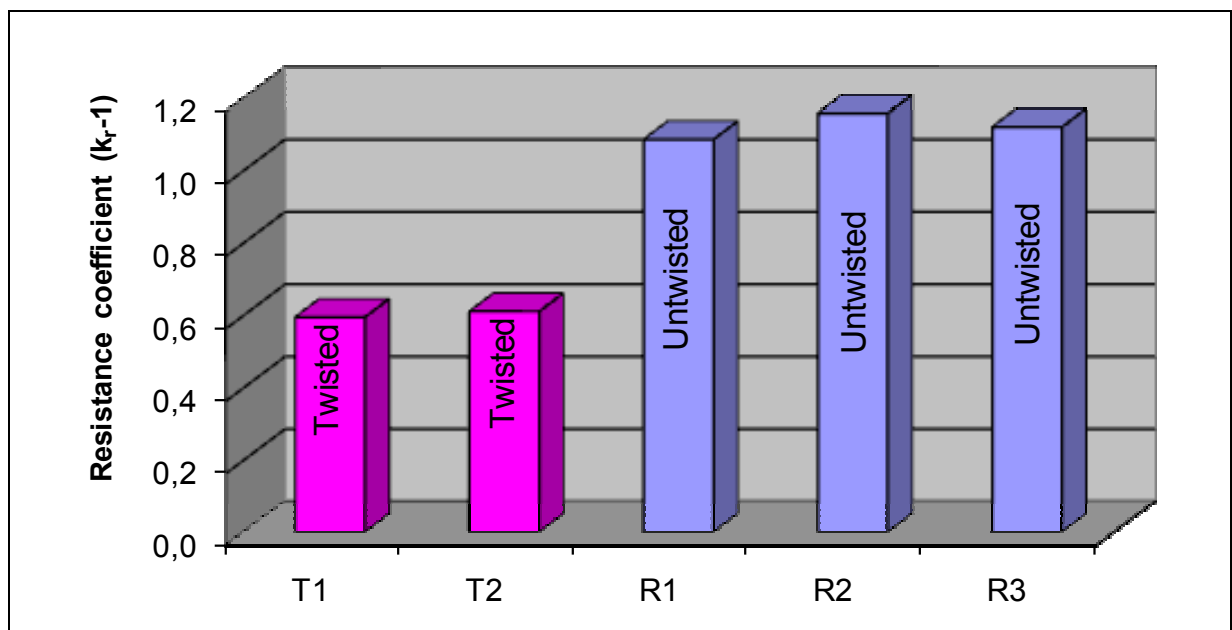
Figure 5.44: Reduction of the stator stray load losses with twist in the middle of the coil compared to untwisted winding for the two speeds round wire winding "A445-**4**6R" at 50 Hz
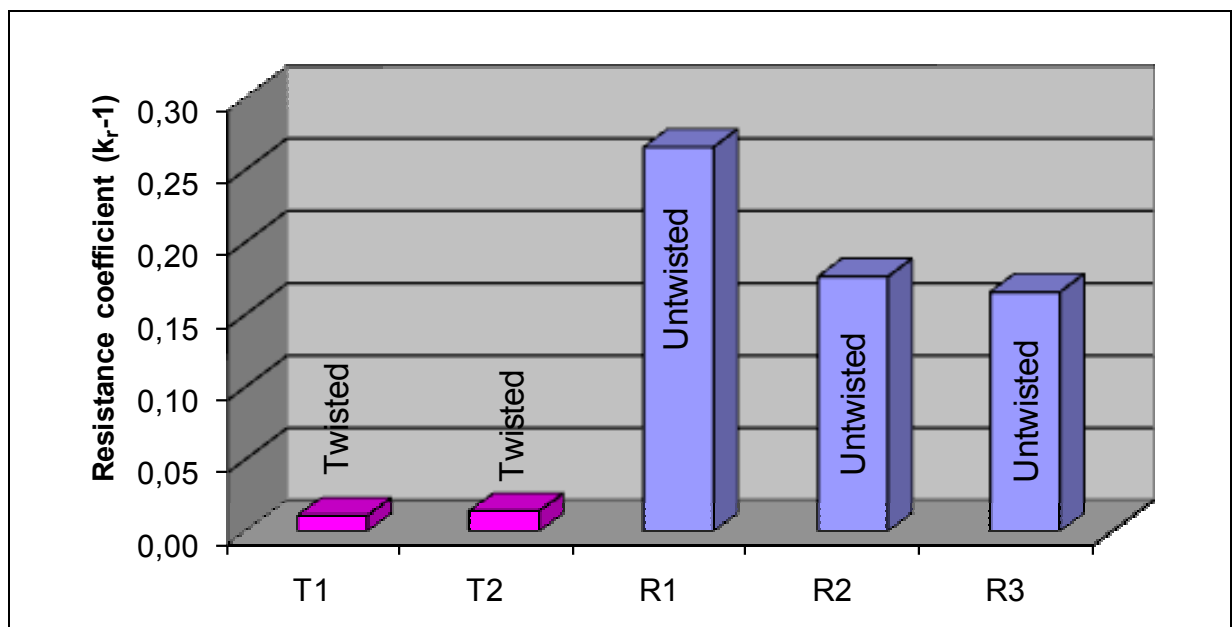
Figure 5.45: Reduction of the stator stray load losses with twist in the middle of the coil compared to untwisted winding for the round wire winding "A550-6R5" at 50 Hz

5.12 Calculation of the stray load losses in induction machine

In this section the analytically calculated stray load losses in 11 kW TEFC cage induction machines at sinusoidal supply will be compared with the measurements acc. to IEC 61972 [IEC 61972]/ IEC 60034-2 Ed. 4.0 draft [IEC 60034-2 draft] at different slip values *s*. The calculation tool for cage induction machines KLASYS [KLASYS], developed by *Binder* [Bind 1988], extended, improved and programmed in a Delphi Code by *Hagen* [Hage 2008], allows the calculation of different loss components like the losses in the stator winding due to the skin effect, due to harmonic rotor and inter-bar currents, due to tooth flux pulsations and eddy currents in the rotor surface, at any given slip *s*, load and saturation level [Hage 2008]. The calculation methods are based on a thorough survey on existing methods for the different stray load loss components, e. g. [Wepp 1964, Jord 1965, Sche 1969].

The calculation is done for the 11 kW, 4-pole motors A160-4...E160-4. The following calculated stray load loss components on the stator side are very small for all investigated motors and therefore neglected in the comparison:

- in the stator winding due to the skin effect,

- in the delta-connected stator winding due to the circulating currents generated by the third field harmonic,

- iron losses in the stator core due to the third field harmonic, caused by the deformation of the field distribution due to iron saturation,

- eddy current losses in the conductive stator frame, in the press plate and in the end shield.

5.12.1 Theoretical background of calculated loss components

The calculation of the stray load losses in the stator winding, due to the skin effect, is done with more or less the some formulas described in the section above, but for the single layer winding. Based on the classical induction machine theory for the harmonic field effects, published mainly by *Weppler*, *Schetelig*, *Taegen* et al., the harmonic losses are estimated.

The stator slot harmonics due to the stator current I_s of frequency f_s induce the rotor cage. The harmonic rotor currents cause additional losses in the rotor cage and as inter-bar currents in the stack. This is an essential part of stray load losses.

$$B_{s,v}(x_s,t) = B_{s,v} \cdot \cos(v \cdot \frac{x_s \pi}{\tau_p} - \omega_s t); \quad v = 1 + 6 \cdot g, \ g = 0, \pm 1, \pm 2, \dots \quad (5.83)$$

τ_p is the pole pitch, v are the ordinal numbers of the stator harmonics. With the number of the stator slots Q_s and the pole pair number p the dominating slot harmonics are

$$v_Q = 1 + (Q_s / p) \cdot g . \quad (5.84)$$

The rotor slot harmonics due to the rotor current I_r' of rotor frequency $f_r = s \cdot f_s$ induce the stator winding and cause additional losses in the stator.

$$B_{r,\mu}(x_r,t) = B_{r,\mu} \cdot \cos(\mu \cdot \frac{x_r \pi}{\tau_p} - s \cdot \omega_s t); \quad \mu = 1 + (Q_r / p) \cdot g \quad (5.85)$$

μ are the ordinal numbers of the rotor slot harmonics and Q_r the number of the rotor slots.

The stator harmonic currents $I_{s\mu}$ are induced by the rotor slot harmonics of frequency $f_{s\mu} = f_s \cdot [\mu \cdot (1-s) + s]$. At load with the slip $s = s_N$ the rotor current I_r' causes stator harmonic currents. At no-load, $s = 0$, with symmetric feeding the fundamental rotor current I_r' is zero, so no stator harmonic currents occur.

In Table 5.34 the slot harmonic amplitudes $B_{s,vQs}$ and $B_{r,\mu}$ are calculated with the influence of the winding parameters, the slot numbers Q_s, Q_r and the slot openings $s_{Q,s}$, $s_{Q,r}$. The dominating first pair of the slot harmonics for the stator and the rotor is given. For closed rotor slots an equivalent slot opening $s_{Q,r,eq}$ is used acc. to theory [Bind 1988].

	A160-4	B160-4	C160-4	D160-4	E160-4
Q_s/Q_r	48/40	36/28	48/40	48/36	36/28
$s_{Q,s}/\delta$, $s_{Q,r,eq}/\delta$	6.2 , 3.3	6.6 , 2.7	5.6 , 2.7	7.0 , 3.8	8.6 , 4.6
$B_{\delta 1}$ /T	0.91	0.81	0.9	1.0	0.93
ν_{Qs}	-23, +25	-17, +19	-23, +25	-23, +25	-17, +19
$B_{s,\nu Qs}$ /T	0.2 / 0.045	0.4 / 0.19	0.35 / 0.21	0.47 / 0.3	0.59 / 0.29
μ	-19, +21	-13, +15	-19, +21	-17, +19	-13, +15
$B_{r,\mu}$ /T	0.18 / 0.018	0.19 / 0.06	0.18 / 0.018	0.2 / 0.002	0.32 / 0.04

Table 5.34: Motor design data and their influence on the harmonics at 50 Hz for 11 kW, 4-pole motors

The influence of the motor design on the harmonics and consequently on the stray load losses is well shown in the Table 5.34. The slot harmonic amplitudes increase with decreasing ratio of "slot number per pole" and with increasing ratio of "slot opening/air gap". The skewing shall reduce the harmonic voltage induction, but increases the inter-bar currents. This causes additional losses in the rotor. In the motor "A160-4" with the lowest harmonic amplitudes and small skewing the stray load losses are small, whereas in the motor "E160-4" with small air gap and low slot number the slot harmonic amplitudes and the stray load losses are bigger.

5.12.1.1 High frequency tooth pulsation losses in the stator

The flux pulsations in the stator teeth due to rotor slotting [Sche 1969] causes high frequency tooth eddy currents and hysteresis losses $P_{p,s}$. Calculating the harmonic content of the air-gap zig-zag stray flux up to a certain maximum ordinal number μ_{max} of the rotor field harmonics yields the time function of the flux pulsation in the stator teeth. The sum of the rotor harmonic field waves with ordinal numbers $\mu = \nu + g_r \cdot Q_r$, $g_r = \pm 1, \pm 2,...$ is considered. All waves with a certain value $g_r \neq 0$ contribute to a pulsation in the stator tooth with the frequency $f_s \cdot |1 + g_r \cdot (Q_r / p) \cdot (1 - s)|$. Generally the eddy current losses increase with the square of the frequency, which is considered along with the (minor) field displacement in the laminations, which also depends on the effective

permeability. Anomalous (excess) eddy current losses are of minor importance in non-oriented steel sheets and are neglected. The increase of the hysteresis losses due to flux pulsations, resulting in minor sub-loops, is approximately calculated by means of the additional hysteresis factor [Leve 1978]. So the eddy current loss calculation depends strongly on the input of the specific iron losses $P_{1.5}$ (in W/kg at 50 Hz, 1.5 T) of the used sheet material and its increase due to the manufacturing process (punching...), which was assumed to be 30 %.

5.12.1.2   High frequency tooth pulsation losses in the rotor

The stator field harmonic waves cause flux pulsations in the rotor teeth and finally high frequency tooth eddy current losses $P_{p,r}$. Depending on the rotor skewing the flux is damped by the cage harmonic currents [Jord 1965]. Also these losses depend on the specific iron losses $P_{1.5}$ in the same way as the component in the stator $P_{p,s}$. As all motors investigated here have a skewed rotor cage, the rotor is divided into 10 parts in axial direction. In each axial section the cage flux between two bars is calculated with respect to the inter-bar currents. Expressions for the bar and inter-bar currents at the axial position y are taken from [Wepp 1966] to calculate the damping of the pulsating rotor tooth flux. The slot stray flux of the vth bar current harmonic, induced by the vth stator field harmonic, is added to the tooth flux. Due to the flux damping the "minor loop" hysteresis losses are negligible.

5.12.1.3   High frequency surface losses in the rotor

The machined rotor surface may have thin conductive areas, where the insulated rotor iron sheets are bridged by the tooling process. Here eddy currents may flow, being caused by the stator field waves, which enter and leave the rotor tooth within its tooth pitch $\tau_{Q,r}$, without penetrating the tooth body [Rao 1969]. The generated high frequency surface eddy current losses $P_{sur,r}$ are sensitive to the machining process. Usually the bridging of the sheets is not very pronounced in modern manufacturing processes with sharp tool cutting edges, so these losses are calculated, taking an intact core lamination into account [Kesa 1967]. Two

components are considered:

-   the surface flux caused by the stator field harmonics and

-   the zig-zag flux entering and leaving the rotor tooth tip as well as the stator tooth tip (see Figure 5.51).

5.12.1.4   Harmonic losses in the rotor

The harmonic I^2R losses $P_{c+q,r}$ in the squirrel cage and in the rotor iron stack play a decisive role especially at load due to the inter-bar currents. *Weppler* [Wepp 1966] introduced a complex skewing factor to take the inter-bar currents into account, which assumes a constant average value for the rotor cage inter-bar resistance R_q due to the iron oxidation. As can be seen in Figure 5.46 the calculated results depend strongly on the chosen value R_q [Engl 2006] at given slip s, which was assumed as in [Wepp 1966] with 0.01 $\Omega \cdot cm^2$ for all motors. Due to the manufacturing process at different manufacturers the value R_q should be different in reality.
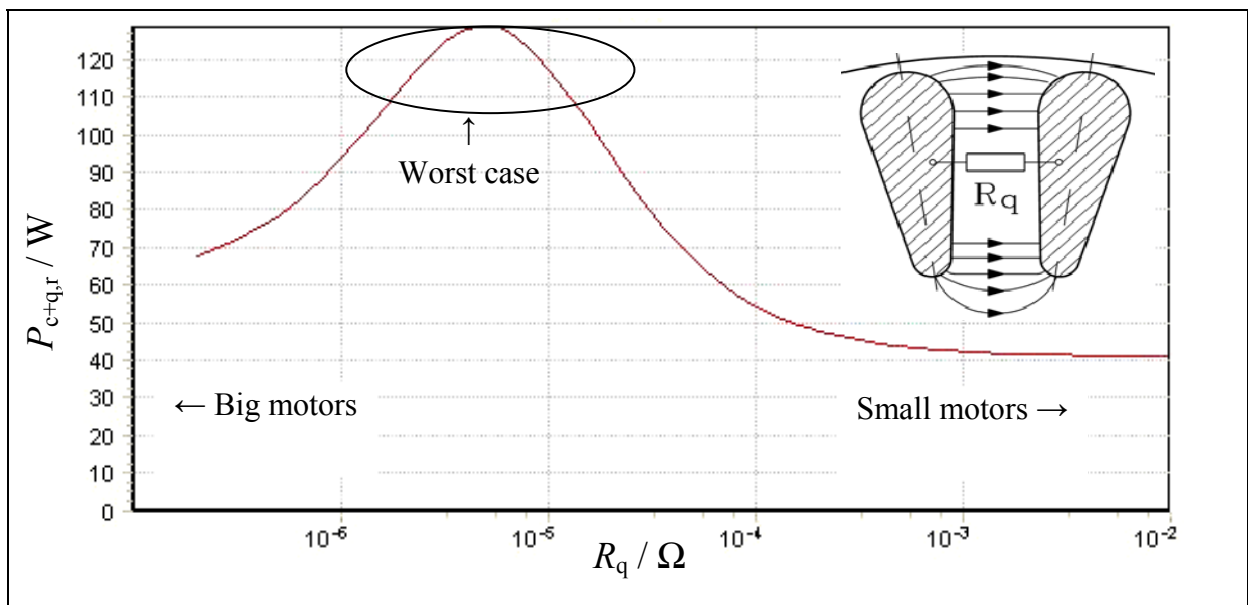
Figure 5.46: Calculated influence of inter-bar resistance on additional rotor cage losses for 11 kW, 4-pole motor "C160-4"; Inter-bar resistance R_q and inter-bar currents.

Especially the amplitudes of the stator slot harmonic fields with the ordinal

numbers ν_Q, are considerably amplified by the ratio of the stator slot opening vs. air-gap $s_{Q,s}/\delta$. Even in case of semi-closed stator slots these amplitudes are increased by a factor 2 … 3. The amplitudes decrease with $1/\nu_Q$. In [Wepp 1969] a simplified method was presented to consider the stator and the rotor slot openings $s_{Q,s}$ and $s_{Q,r}$, which was experimentally checked by testing the harmonic asynchronous starting torque. Even closed rotor slots saturate in the closing iron bridges at a rather low bar current, so an equivalent rotor slot opening is calculated iteratively. Both methods [Wepp 1966] and [Wepp 1969] are combined for the determination of the harmonic rotor bar and inter-bar currents, which – together with the rotor bar skin effect and the inter-bar resistance – yield the rotor losses.

5.12.2 Calculated stray load losses at no load

Already at no-load the stray load losses $P_{ad,0}$ are acting mainly as eddy current and hysteresis losses in the iron and conductive parts, especially at high saturation of the main flux. The amount of the skin effect in the winding is negligible due the low no-load current.

The calculated stray load losses at no-load $P_{ad,0}$ versus the measured iron losses P_{Fe} at no-load and rated voltage is presented in Figure 5.47.

The calculation results show for the motors "A160-4" and "C160-4", with the same stator and rotor slot numbers and the smallest ratio Q_s/Q_r, higher no-load stray load losses. As mentioned previously, the calculations are done – for all motors – with the same magnetising $B(H)$- curve and the specific iron losses, which are different in reality.
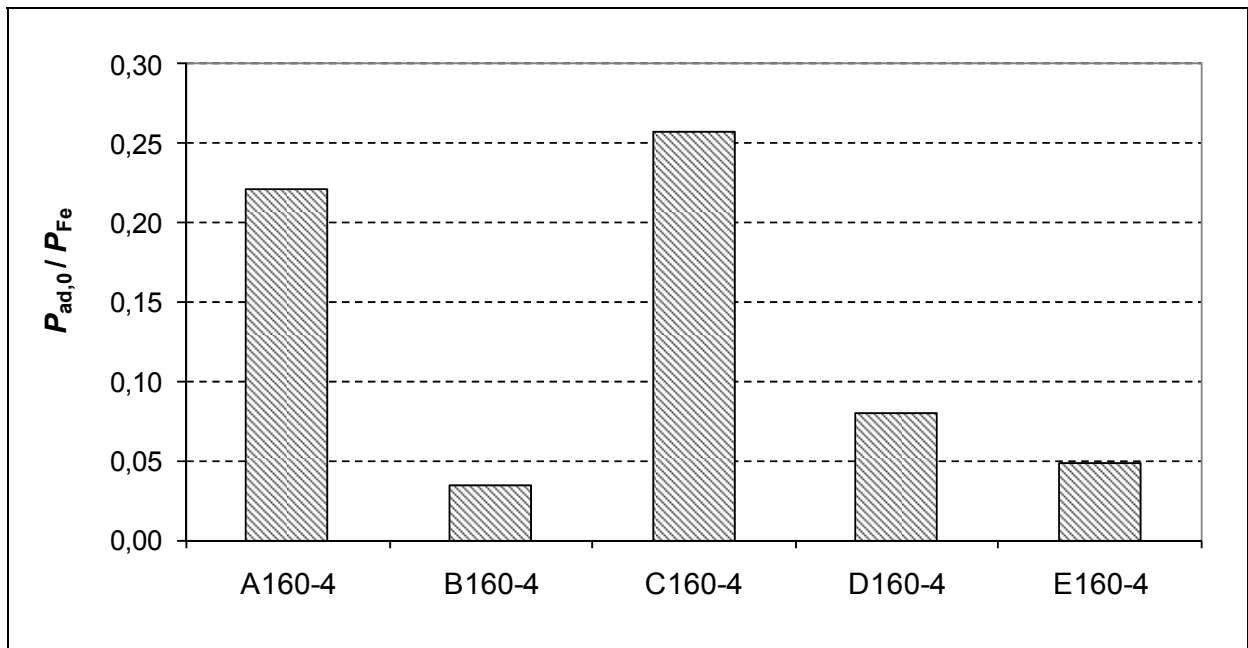
Figure 5.47: Calculated additional no-load losses $P_{ad,0}$ versus the measured iron losses P_{Fe} at no-load, rated voltage for 11 kW, 4-pole motors "X160-4"

5.12.3 Calculated stray load losses at rated slip

The calculated stray load losses P_{ad} for rated output power P_N are compared to the measured stray load losses at rated slip in Figure 5.48. As shown the calculation results for most motors are in the range of the measurements and for the motor "E160-4" agree quite well with the measurements. For the motors "A160-4" and "D160-4" the calculated stray load losses are overestimated. The calculations are done with the same $B(H)$- curve and based on several assumptions like the value of the inter-bar resistance R_q, the rotor surface impedance, the manufacturing (punching, tooling..) influence on pulsation losses etc..
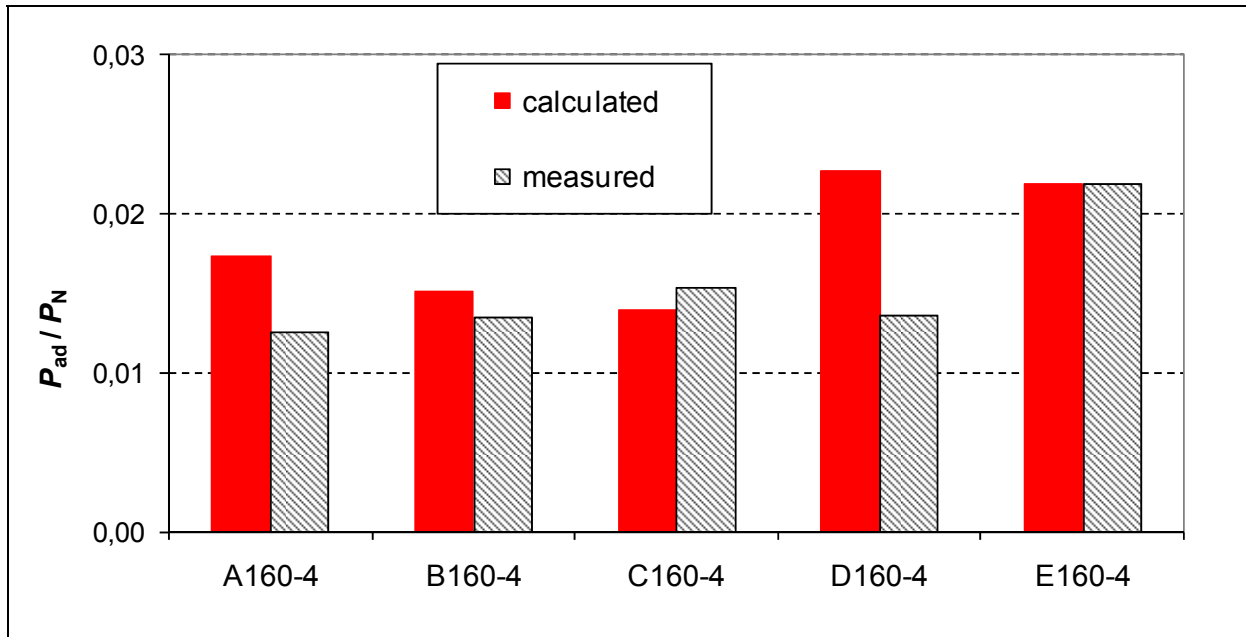
Figure 5.48: Comparison of calculated and measured stray load losses at rated slip related to
the rated output power for 11 kW, 4-pole motors "X160-4"

In Figure 5.49 the calculated stray load loss components $P_{p,s}$, $P_{p,r}$, $P_{sur,r}$, $P_{c+q,r}$
are shown at no-load and rated load for the 11 kW, 4-pole motor "B160-4" with
closed rotor slot opening and for the motor "C160-4" with semi closed rotor slot
opening, where the impact of the rotor slot opening – semi closed, open – on the
calculated stray load loss components can be seen. The rotor high frequency iron
losses $P_{sur,r}$ due to the stator field harmonics are damped by the high frequency
rotor bar current harmonics at no-load as well as at load [Ober 2000], so they do
not increase very much. The increase of the pulsation losses in the rotor $P_{p,r}$ at
closed rotor slots is higher than for semi closed rotor slots. The strongest
increase with load is visible for the cage and inter-bar harmonic losses $P_{c+q,r}$, as
the stator field harmonics increase by the ratio of the no load current to the rated
current I_N/I_0. This ratio is on average 2.2 for 11 kW-motors and increases with
increasing power. Hence the increase of this loss component is strongest for the
big motors.
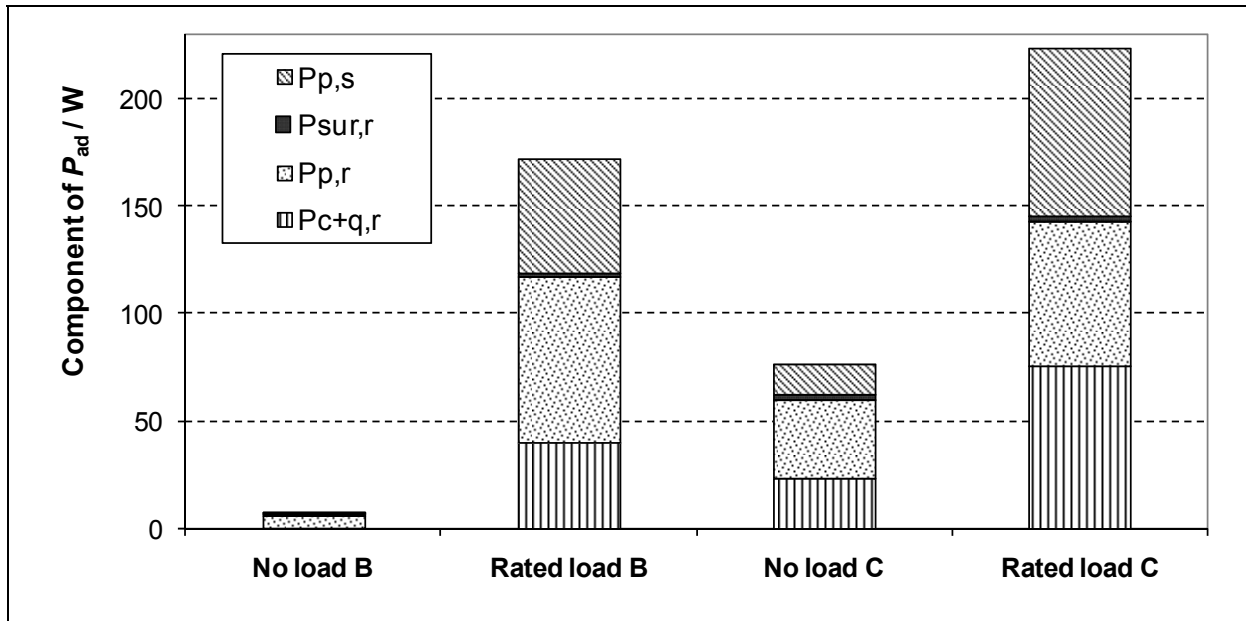
Figure 5.49: Comparison of calculated component of stray load losses at no load and at rated
load for 11 kW, 4-pole motors "B160-4" with closed rotor slot opening and
"C160-4" with semi closed rotor slot opening.

$P_{p,s}$, $P_{p,r}$: Stator and rotor high frequency pulsation losses, $P_{sur,r}$: Rotor surface
losses, $P_{c+q,r}$: Rotor cage and inter-bar harmonic losses. The stray load losses in
the stator winding $P_{ad,s}$ are not considered.

5.12.4 Calculated stray load losses at reverse rotation test

The calculated stray load losses P_{ad} versus the rated output power P_N are
compared to the measured stray load losses at slip $s = 2$ in Figure 5.50. As
shown the calculation results for the motors "B160-4" and "D160-4" fit well
with the measurements. For the remaining motors the stray load losses at slip
$s = 2$ are underestimated. The calculations are based on several assumptions like
the value of the inter-bar resistance, the rotor surface impedance, the
manufacturing (punching, tooling..) influence on pulsation losses etc. With
higher slip s the stray inductances are reduced due to increased saturation of the
tooth tips (reduction of the relative magnetic permeability) through the zig-zag
stray flux. At slip $s = 1$ the magnetic field is displaced from the rotor towards the
air gap due to the skin effect. A "flux compensation" occurs where the rotor and

the stator current are almost opposite in phase, $\underline{I}_s \approx -\underline{I}'_r$. The main flux saturation is strongly reduced. These effects are higher at slip $s = 2$. Therefore the analytical calculation is complicated and can be only an estimation.
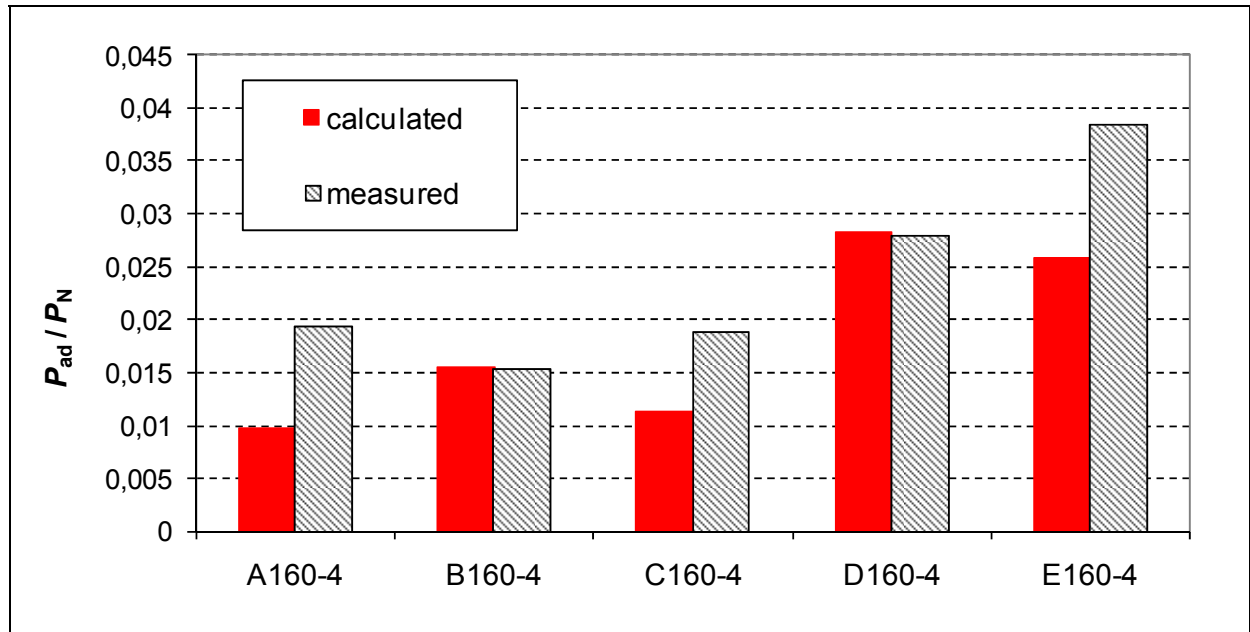
Figure 5.50: Comparison of calculated and measured stray load losses at reverse rotation test related to the rated output power for 11 kW, 4-pole motors "X160-4"

In Figure 5.51 a comparison of calculated components of the stray load losses $P_{p,s}$, $P_{p,r}$, $P_{sur,r}$, $P_{c+q,r}$ for locked rotor test ($s = 1$) and for reverse rotation test ($s = 2$) for the 11 kW, 4-pole motor "B160-4" with closed rotor slots and for the motor "C160-4" with semi closed rotor slot openings is presented. Also the zig-zag stray flux is shown schematically. Due to the slot-frequency at slip $s = 2$, the pulsation losses $P_{p,s}$ in the stator and $P_{p,r}$ in the rotor are higher, whereas at slip $s = 1$ they are negligibly small.
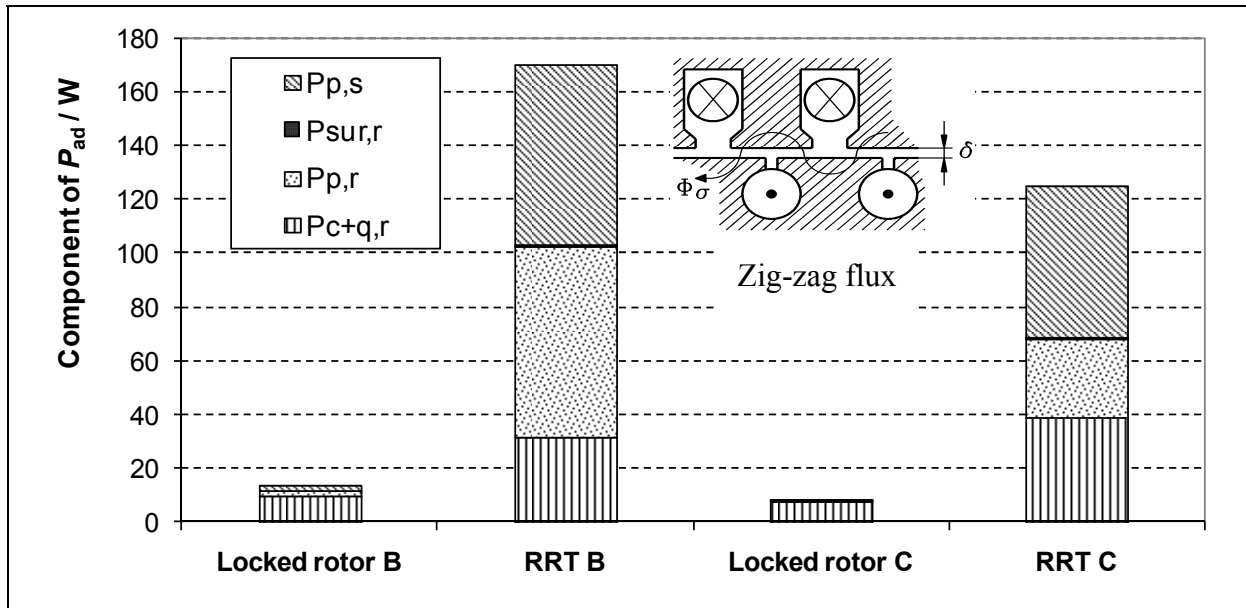
Figure 5.51: Comparison of calculated component of stray load losses at locked rotor test and at reverse rotation test for 11 kW, 4-pole motors "B160-4" with closed rotor slot opening and "C160-4" with semi closed rotor slot opening; Zig-zag stray flux.

$P_{p,s}$, $P_{p,r}$: Stator and rotor high frequency pulsation losses, $P_{sur,r}$: Rotor surface losses, $P_{c+q,r}$: Rotor cage and inter-bar harmonic losses. The stray load losses in the stator winding $P_{ad,s}$ are not considered.

5.13 Conclusion

The origin, the theoretical background, the measurement and the analytical estimation of the stator winding stray load losses due to the skin effect in grid-operated cage induction generators were shown. Different influence parameters like the number of wires per bundle, the pitching, the insertion of the wires in the slots etc., were investigated. Also some practicable measures to reduce this kind of losses were presented and tested. The analytical calculation of this loss component agrees quite well with the measurement for the profiled and the litz wire winding, but not always for the round wire winding, due to the random wire distribution in the slots. For some examples this loss component can be so high, that the generator will be overheated at continuous full load operation. The removed rotor test is a useful indicator for this.

From the comparison of the measured magnetic flux densities at rated

voltage, no-load current and full load current it can be seen that the measured iron losses from the standardized no-load test are smaller for the efficiency determination than the real iron losses at full load.

In addition, an overview on main loss components in cage induction machines and their analytical calculation, based on the classical induction machine theory for harmonic field effects, was shown. With some assumptions for material parameters such as the inter-bar resistance, the rotor surface resistance, the specific iron losses, the determination of the stray load losses is possible in a fast and satisfying way. This is especially useful for the simulation and optimisation of grid-operated machines, where a quite satisfying coincidence with measured stray load losses according to IEC 61972/ IEC 60034-2 Ed. 4.0 draft was found.

6   CONCLUSIONS AND OUTLOOK

The main findings of the present work "*Experimental Determination of Stray Load Losses in Cage Induction Machines*" are summarized in this chapter. The thesis is based on two research projects and deals with the measurement methods to determine the stray load losses and the efficiency of grid-operated low-voltage squirrel-cage induction machines. The strengths and weaknesses of different test methods were investigated and compared for water-cooled wind generators of 1.5 MW and 27 standard TEFC cage induction motors of different design in the power range 0.37 kW, 0.55 kW, 1.1 kW, 5.5 kW, 11 kW and 315 kW. Some analytical calculations were presented.

Methods to determine the losses and efficiency of electrical machines are either by direct or by indirect measurement. A direct measurement is the input-output test by measuring the input power $P_{e,in}$ and the output power $P_{m,out}$, yielding the total losses which include the stray load loss. Because of unavoidable measurement errors the direct determination of the efficiency is generally not accurate enough in case of machines of efficiencies above 95 %. For machines of higher efficiency indirect methods are preferred, especially the summation of separate losses. They imply the separate identification of the stray load losses, which is helpful for optimizing the machine design.

The efficiency determined of an induction motor depends, apart from the motor design, on the test method, the instrumentation and measurement accuracies, and on many parameters such as the load condition (full or partial load), the temperature and the quality of the power supply. It depends also on the interpretation of the standards by the users.

The methods for determining the efficiency of induction machines vary greatly in terms of their complexity, overall performance and their suitability for the test field conditions. These methods are based on different theoretical models

and different assumptions. Therefore it is difficult to compare the efficiency values obtained by different methods.

As the direct determination of the efficiency (measurement of the input and output power e.g. acc. to IEEE 112-method A) suffers from the measurement uncertainty, it is – naturally – limited for motors of high efficiency. The indirect method (e.g. residual loss method acc. to IEEE 112-method B) is less sensitive to measurement errors and seems to be, depending on the measurement accuracy of the total power losses P_d, useful also for higher efficiency machines.

The stray load losses have a considerable impact on the performance of the machine including the heating. By a tested example it was shown that, due to the stray load losses the generator could not run continuously at full load. To avoid insulation destruction, the practical consequence of this effect of overheating is the derating !

Prominent for determining the stray load loss is the residual loss method (consisting of a load test with torque measurement and a calculation procedure with smoothing the stray load loss by linear regression analysis), as standardized in IEC 60034-2-1 or IEEE 112-method B.

Because of the unavoidable measurement errors, the indirect determination of the stray load losses P_{ad} via measuring the input power $P_{e,in}$ and the output power $P_{m,out}$ (e.g. residual loss method acc. to IEEE 112-method B) is generally not accurate enough in case of only a small value of the stray load losses P_{ad}, e.g. for machines of efficiencies above 95 %. Therefore the direct measurement method of the stray load losses P_{ad} (e.g. eh-star method or RRT) can be useful in case of high efficiencies. Other advantages of this method are the separate identification of the stray load losses in the stator and in the rotor, which is helpful for optimizing of the machine design. In contrast, the residual loss method e.g. acc. to IEEE 112-method B and the calorimetric method determine the stray load losses as a sum.

In addition the influence of different parameters such as the instrumentation accuracy, the temperature, the resistive losses, the iron losses and the friction and windage losses on the determination of the stray load losses and the efficiency was shown.

It has been shown that the iron losses measured in the standardized no-load test are smaller than the real iron losses at full load. That means that the remaining part of the iron losses will be charged to the stray load losses when using the indirect measurement of the stray load losses (input-output test with segregation of the losses) acc. to [IEC 61972] and IEEE 112-method B, whereas it is left out of consideration when using the allowance for the stray load losses acc. to e.g. IEC 61972-2 and IEEE 112-method E1 during the efficiency determination !

A survey on cheap and simple methods to measure the stray load losses in squirrel-cage induction motors, apart from the standardized methods, resulted in finding three equivalent "no-load" methods, where no coupling and no dynamometer or torque-meter are needed. The strengths and weaknesses of these measurement methods were investigated and compared with the standardized residual loss methods (input-output test) and the reverse rotation test (RRT); their practically existing limitations were discussed. The eh-star method has been found to be a simple and fast test, yielding results comparable with the input-output test, fitting the purpose better than the RRT. Such a simple and fast test is required for the measurement of the stray load losses P_{ad}, e.g. during the process of motor design optimization.

The theoretical background and the test procedure of the eh-star method, as an equivalent test method to determine the stray load losses, are described in detail. Different evaluation methods A, A1, B and C were compared by theoretical and measured examples, showing the usefulness of the evaluation methods C and A. The influence of different parameters (e.g. the unbalanced auxiliary impedance $\underline{Z}_{eh}$, the temperature, …) on the stray load losses was shown.

Method A is proposed for the new standard IEC 60034-2 Ed. 4, 2nd CDV [IEC 60034-2 draft], as the calculation algorithms are simple for the standard-users (May 2007 it was accepted and published on Sept. 2007 in IEC 60034-2-1, Edition 1.0 [IEC 60034-2-1]).

The experimental determination of the stray load losses for 5.5 kW and

11 kW motors with pole count 2, 4 and 6 showed good coincidence between the residual loss methods and the eh-star method, whereas the RRT method gave bigger stray load losses.

For power rating less than 1.1 kW the RRT method yields – unlike in case of bigger motors – the same or less stray load loss values than the residual loss methods for the investigated motors. The eh-star method yields also lower losses than the input-output methods.

No good correlation was found between the results as well of the equivalent no-load method of *Bourne* as of the equivalent no-load method of *Rawcliffe* and the residual loss methods.

Main issues of the present PhD work were also investigations on the origin, the theoretical background, the measurement and the analytical estimation of the fundamental frequency stray load losses in the stator winding due to the skin effect. Different influence parameters such as the number of wires per bundle, the pitching of the winding, the method to insert the wires in the slots etc. ... were investigated. Other topics during regarding the removed rotor test like the eddy current losses in the press plates, the iron losses and the reactance quantities were also discussed.

For some round wire winding samples the fundamental frequency stray load losses in the stator winding can be so high that the generator cannot operate continuously at full load. The practical consequence to avoid endangering the generator is derating. Through the direct measurement of the stray load losses, separately in the stator and in the rotor, the source of the heating can be identified. By the input-output test e.g. acc. to IEEE 112-method B and the calorimetric method this would not be possible. Some practicable measures to reduce this part of the losses were presented and successfully tested. Thanks to these proven techniques the round wire winding is competitive to other more expensive winding types.

It has been shown that the result of analytical calculation of this loss component agrees quite well with the measurement for profiled and litz wire winding but not always for round wire winding, due to the randomly distributed wires in the slots.

With increasing winding resistance due to the skin effect the inductance

decreases, and consequently the "filter" effect of the winding decreases also, which leads to larger high-frequency stray load losses.

In addition, an overview was shown on main loss components in cage induction machines and their analytical calculation, based on the classical induction machine theory for harmonic field effects. With some assumptions regarding material parameters such as the inter-bar resistance, the rotor surface resistance and the specific iron losses, the determination of the stray load losses was possible in a fast and satisfying way. This is especially useful for the simulation and optimization of grid-operated machines, where a quite satisfying coincidence of measurement and calculation was found.

The measured stray load losses are for all cases larger than those obtained from the assigned value of 0.5 % of the electrical input power acc. to IEC 60034-2. For a fair competition the stray load losses must be measured and cannot be replaced by any kind of fixed assumption.

Outlook

The fundamental frequency stray load losses in the stator winding of the 1.5 MW round wire winding generators due to circulating currents can be high. They can be suppressed by some practicable measures. The press plate losses in the end region were found negligible for this power rating.

The iron losses must be regarded as load dependent for the stray load losses and the efficiency determination.

Motors of power rating 1.1 kW proved to be still good measurable in the lab, but need a careful testing. For power ratings less than 1.1 kW the stray load losses are very small (only some Watt), leading to increased measurement uncertainty.

For small motor rating of less than 0.55 kW the eh-star method should not be used for the determination of the stray load losses, due to measurement uncertainty.

The input-output test e.g. acc. to IEEE 112-method B determine the stray load losses as residual losses from the load characteristic. As the slip s and the speed n change during the load test together with the friction and windage losses

P_{fw}, this part of losses should be taken into account for more accurate determination of the stray load losses P_{ad}, especially for machines of high speed and high slip !

This contribution addresses many issues in terms of measurement, calculation and theory of the stray load losses and the efficiency of induction machines. Nevertheless, each research work can only cover a limited number of aspects related to its topic. The following items might indicate topics for further investigation:

Improvement of analytical models by means of FEM for estimation of the eddy current losses, and comparison with measurements.

Estimation of temperature distribution and temperature rise by means of thermal equivalent networks or by FEM, and comparison with the measurement.

Methods to take the load/speed dependent friction and windage losses into account for standardised determination of the stray load losses and the efficiency, using empirical formulae, with exponents tabled as functions e.g. of frame size, speed, pole count, rotor volume and fan design (number of blades, one or two directions of rotation).

7 BIBLIOGRAPHY

[Ange 2007]   Angers, P.; Friesen, D.: *Comparison of Test Methods for the Determination of Measured Efficiency*, Motor Summit (SEEM), 9-11 April 2007, Zürich, Switzerland.

[Aoul 2005]   Aoulkadi, M.; Binder, A.: *The Eh-star Method for Determination of Stray Load Losses in Cage Induction Machines*, Proc. of the 4th International Conference Energy Efficiency in Motor Driven Systems, EEMODS, 5-8 Sept. 2005, Heidelberg, Germany, 2005, Vol. 1, p. 130-140.

[Auin 1999]   Auinger, H.: *Determination and designation of the efficiency of electrical machines*, Power Engineering Journal, Vol. 13, Issue 1, February 1999, p. 15-23.

[Auin 2001]   Auinger, H.; Bunzel, E.: *Wirkungsgradermittlung von Elektromotoren, Bringt der Normentwurf IEC 61972/CDV Verbesserungen für den europäischen Markt ?*, Antriebstechnik 40, 2001, Nr. 11, p. 65-70.

[Bert 2005]   Bertoldi, P.: *The European Motor Challenge Program*, Proc. of the 4th International Conference Energy Efficiency in Motor Driven Systems, EEMODS, 5-8 Sept. 2005, Heidelberg, Germany, 2005, Vol. 1, p. 7-18.

[Bind 1988]   Binder, A.: *Vorausberechnung der Betriebskennlinien von Drehstrom-Kurzschlußläufer-Asynchronmaschinen mit besonderer Berücksichtigung der Nutung.* PhD Thesis, Vienna University of Technology, 1988.

[Bind 2000]   Binder, A.: *Analytical calculation of eddy current losses in massive rotor parts of high-speed permanent magnet machines*, Proc. of the International Symposium on Power Electronics, Electrical Drives, Automation and Motion, SPEEDAM, 13-16 June 2000, Ischia, Italy, 2000, pp. C2-1 – C2-6.

[Bind 2006c]   Binder, A.: *CAD and System Dynamics of Electrical Machines*. Lecture script, Institute of Electrical Energy Conversion, Darmstadt University of Technology, 2006.

[Bind 2006g]   Binder, A.: *Large Generators and High Power Drives*. Lecture script, Institute of Electrical Energy Conversion, Darmstadt University of Technology, 2006.

[Bind 2006m]   Binder, A.: *Motor Development for Electrical Drive Systems*. Lecture script, Institute of Electrical Energy Conversion, Darmstadt University of Technology, 2006.

[Bird 1964]   Bird, B.M.: *Measurement of Stray Load Losses in Induction Motors with Cast Aluminium Rotors*. IEE Proceedings, Vol. 111, 1964, p. 1697-1705.

[Bird 1967]   Bird, B.M.; Holgate, A.: *Discussion on Determination of Load Losses and Torque in Squirrel Cage Induction Motors*, by Christofides, N. and Adkins, B., IEE Proceedings, Vol. 114, 1967, p. 1085-1088.

[Böde 1962]   Bödefeld, Th.; Sequenz, H.: *Elektrische Maschinen, eine Einführung in die Grundlagen*. 6. Auflage, Springer -Verlag, Wien, 1962.

[Bogl 2004]   Boglietti, A.; Cavagnino, A.; Lazzari, M.; Pastorelli, M.: *International Standards for the Induction Motor Efficiency Evaluation: A Critical Analysis of the Stray Load Loss Determination*, IEEE Transactions on Industry Applications, Vol. 40, No. 5, 2004, p. 1294-1301.

[Bonf 1962]   Bonfert, K.: *Betriebsverhalten der Synchronmaschine, Bedeutung der Kenngrößen für Planung und Betrieb elektrischer Anlagen und Antriebe*. Springer -Verlag, Berlin/ Göttingen/ Heidelberg, 1962.

[Bour 1989]   Bourne, R.: *No-load method of estimating stray load loss in small cage induction motors*, IEE Proceedings, Vol. 136, Pt. B, No. 2, March 1989, p. 92-95.

[BWE 2008]   Hermann, A.: Bundesverband WindEnergie; *Windenergie nach dem neuen EEG;*. November 2008, Mitglieder-vesammlung BWE-Regionalverband Nordfriesland, 12. November 2008.

[Chal 1963]   Chalmers, B.J.; Williamson, A.C.: *Stray losses in squirrel-cage induction motors. Validity of the reverse rotation test method*, Proc. Instn. Electr. Eng., Vol. 110, 1963, p. 1773-1777.

[Drey 1928]   Dreyfus, L.: *Theorie der zusätzlichen Eisenverluste in Drehstromasynchronmotoren*, Archiv für Elektrotechnik, Vol. 20, 1928, p. 37-89, 188-210, 273-298.

[Durand-Kerner]   Durand, E.; Kerner I.; Weierstraß, K.
                  http://en.wikipedia.org/wiki/Durand-Kerner_method.

[Engl 2006]   Englebretson, S.; Kirtley, J.; Molina, K.: *Induction Motor Inter-bar Resistance Measurements*. Proc. of the Int. Conf. on El. Machines (ICEM), 2006, Chania, Greece, paper no. 367, 6 pages CD-ROM.

[Gera 2005]   Gerada, C.; Bradley, K.; Arellano-Padilla, J.: *An investigation into the suitability of unbalanced motor operation, the eh-star-circuit for stray load loss measurement*. 2005 IEEE Industry Applications Conference, 40th IAS Annual Meeting, Hong Kong, 2-6 Oct. 2005, 8 Pages.

[Guid 2005]   Aoulkadi, M.; Binder, A.: *Eh-Star-Guideline*. Version 1.4, 09.03.2005, Institute of Electrical Energy Conversion, Darmstadt University of Technology, 2005.

[Hage 2008]   Hagen, R.; Binder, A.; Aoulkadi, M.; Knopik, T.; Bradley, K.: *Comparison of measured and analytically calculated stray load losses in standard cage induction machines.* Proc. of the Int. Conf. on El. Machines (ICEM) 2008, 6-9 September, 2008, Vilamoura, Algarve, Portugal, paper ID 1389, 6 pages CD-ROM.

[Hill 1914]   Hillebrand F.: *Über zusätzliche Kupferverluste bei Wechselstrommaschinen.* Archiv für Elektrotechnik, III. Band, 1914, 5. Heft, p. 120.

[Hose 1923]   Hoseason, D.B.: *Tooth frequency losses in slip-ring induction motors,* Electrician, 1923, Vol. 91, p. 240.

[IEC 60034-1]   IEC 60034-1: Rotating electrical machines - Part 1: *Ratings and performance,* Geneva, Switzerland

[IEC 60034-2]   IEC 60034-2: Rotating electrical machines - Part 2: *Methods for determining losses and efficiency of electrical machinery from tests,* Geneva, Switzerland, 1972 (Amendment 1: 1995, Amendment 2: 1996).

[IEC 60034-2 draft]   IEC 2/1367/CDV, Project IEC 60034-2 Ed. 4: Rotating electrical machines - Part 2: *Methods for determining losses and efficiency from tests,* Geneva, Switzerland, 2005-12.
Note: This document eventually became IEC 60034-2-1

[IEC 60034-2-1]   IEC 60034-2-1, Edition 1.0: Rotating electrical machines - Part 2-1: *Standard methods for determining losses and efficiency from tests (excluding machines for traction vehicles),* Geneva, Switzerland, Sept. 2007.

[IEC 60034-4]   IEC 60034-4: Rotating electrical machines - Part 4: *Methods for determining synchronous machine quantities from tests,* Geneva, Switzerland, 1985.
Note: Current edition is Ed. 3: 2008-05

[IEC 61972]   IEC 61972: Rotating electrical machines - *Method for determining losses and efficiency of three-phase cage induction motors,* Geneva, Switzerland, July 2000.
Note: This document was withdrawn 2007-12; contents

included in IEC 60034-2-1

[IEEE 112]   IEEE Std 112-1996: *IEEE standard test procedure for poly-phase induction motors and generators*, New York, USA, 1997.

[Jimo 1985]   Jimoh, A.A.; Findlay, R.D.; Poloujadoff, M.: *Stray losses in induction machines: Part I. Definition, origin and measurement. Part II. Calculation and reduction*, IEEE Trans. PAS-104, 1985, p. 1500-1512.

[Jord 1965]   Jordan, H.; Taegen, F.: *Zur Messung der Zusatzverluste von Asynchronmaschinen*, ETZ-A, Vol. 86, 1965, p. 167-171.

[Jord 1967]   Jordan, H.; Richter, E.; Röder, G.: *Ein einfaches Verfahren zur Messung der Zusatzverluste in Asynchronmaschinen.* ETZ-A, Vol. 88, 1967, no. 23, p. 577-583.

[Jord 1970]   Jordan, H.; Weis, M.: *Synchronmaschinen I, Vollpolmaschine.* Braunschweig, Vieweg, 1970.

[Kesa 1967]   Kesavamurthy, N.; Basu, A. K.: *Effects of travelling field on ferromagnetic plates of finite thickness.* IEEE Transactions on power apparatus and systems, Vol. 86, no. 12, 1967, p. 1565-1570.

[Kett 1984]   Ketteler, K.H.: *Über den Einfluss der Wicklungsschaltung in Induktionsmaschinen auf die Zusatzverluste und den einseitigen magnetischen Zug.* ETZ- A, Vol. 106(3), 1984, pp. 99-106.

[Keul 2005]   De Keulenaer, H.; De Almeida, et al.: *Energy Efficient Motor Driven Systems*, Proc. of the 4th International Conference Energy Efficiency in Motor Driven Systems, EEMODS, 5-8 Sept. 2005, Heidelberg, Germany, 2005, Vol. 1, p. 170-180.

[Keve 1973]   Keve, Th.: *Die Bedeutung der Last-Zusatzverluste von Asynchronmotoren und ihre Bestimmung*, Bull. SEV 64, 1973, no. 6, p. 369-376.

[KLASYS]   KLASYS05: Simulation tool for cage induction machines, developed by A. Binder, improved and programmed in a Delphi Code by R. Hagen, Institute of Electrical Energy Conversion, Darmstadt University of Technology, 2008.

[Klau 2005]   Klaus, G.: *Numerical Method for the Integral Calculation of Eddy Current Losses and Temperature Rises Caused by Magnetic Fields in the Stator Core End Region of Air-cooled Turbine Generators*. PhD Thesis, Dresden University of Technology, 2005.

[Kova 1962]   Kovacs, K.P.: *Symmetrische Komponenten in Wechselstrommaschinen*, Birkhäuser-Verlag, Basel & Stuttgart, 1962, Switzerland / Germany.

[Kron 1969]   Kron, A.W.; Pfau, D.: *Beitrag zur Kenntnis der Zusatzverluste großer Asynchronmotoren*. ETZ- A Bd. 90, H.21, pp. 531-534, 1969.

[Kuče 1956]   Kučera, J.; Hapl, J.: *Wicklungen der Wechselstrommaschinen*. VEB –Verlag Technik, Berlin, 1956.

[Lamm 1966]   Lammeraner, J.; Štafl, M.: *Eddy currents*, liffe Books Ltd, London, 1966.

[Leve 1978]   Levers, J. D.; Biringer, P.; Hollitscher H.: *A Simple Method of Estimating Minor Loop Hysteresis Loss in Thin Laminations*. IEEE Trans. on Magnetics 14, 1978, no.5, p. 386-388.

[Link 1907]   Linke, W.: *Zur Trennung der Verluste in Asynchronmaschinen*, Elektrotechnische Zeitschrift, Vol. 28, 1907, p. 964.

[Mand 1962]   Mandi, A.: *Ein Vorschlag zur Bestimmung des Wirkungsgrades und der Erwärmung von Induktionsmotoren*, E und M, Jahrgang 79, 1962, Heft 15/16, p. 399-405.

[Morg 1939]   Morgan, Th.; Brown, W.E.; Schumer, A.J.: *Reverse Rotation Test for the determination of stray load loss in induction machines*, Trans. Amer. Inst. Electr. Eng., Vol. 58, 1939, p. 319-324.

[Müll 1956]   Müller, G.: *Die Stromverdrängungsverluste in Dreiphasenwicklungen aus unterteilten Leitern*. Deutsche Elektrotechnik, Jahrgang 10, Heft 6, 1956, pp. 225 – 229.

[NEMA]   NEMA Standards Publication Number MG1, *National Electrical Manufactures' Association (NEMA)*, Washington DC, USA, 1993.

[Neuh 1964]   Neuhaus, W.: *Über die Entstehung von asynchronen Oberfeldmomenten durch zusätzliche Eisenverluste in Drehstromasynchronmachinen mit Käfigläufern*. PhD Thesis TH Hannover, 1964.

[Ober 1969]   Oberretl, K.: *13 Regeln für minimale Zusatzverluste in Induktionsmotoren*. Bulletin Oerlikon Nr. 389/390, pp. 1-11, 1969.

[Ober 2000]   Oberretl, K.: *Eisenverluste, Flusspulsation und magnetische Nutkeile in Käfigläufermotoren*, Archiv für Elektrotechnik 82, pp. 301-311, 2000.

[Rao 1969]   Rao, V.S.; Butler, O.I.: *Stray losses of poly-phase cage-induction motors with particular reference to the condition of imperfect rotor-bar-iron insulation*. Proc. IEE, Vol. 116, no. 5, May 1969, p. 737-751.

[Rawc 1952]   Rawcliffe, G.H.; Menon, A.M.: *A simple new test for harmonic-frequency losses in a.c. machines*, Proc. IEE, 1952, Vol. 99, Pt. II, p. 145-150.

[Rich 1936]   Richter, R.: *Elektrische Maschinen*, Vol. 4: *Die Induktionsmaschinen*. Springer -Verlag, Berlin, 1936.

[Rich 1953]   Richter, R.: *Elektrische Maschinen*, Vol. 2: S*ynchronmaschinen und Einankerumformer*. Birkhäuser-Verlag, Berlin, 1953.

[Rich 1967]   Richter, R.: *Elektrische Maschinen*, Vol. 1. Birkhäuser-Verlag, Stuttgart, 1967.

[Rogo 1925]   Rogowski, W.; Vieweg, V.: *Zusätzliche Verluste in kleinen Drehstrommotoren*, Archiv für Elektrotechnik, Vol. 14, 1925, p. 574-594.

[Sand 2005]   Sander, J.: *Activities of CEMEP to Promote Efficient Motor Driven Systems*, Proc. of the 4th International Conference Energy Efficiency in Motor Driven Systems, EEMODS, 5-8 Sept. 2005, Heidelberg, Germany, 2005, Vol. 1, p. 21-23.

[Sche 1909]   Schenkel, M.: *Beitrag zur Bestimmung der Streuung von Wechselstromwicklungen*, Zeitschrift E und M, Selbstverlag des Elektrotechnischen Vereins Wien, 1909, p. 201-208.

[Sche 1969]   Schetelig, H.: *Die Berechnung der magnetischen Flüsse in Drehstrom-Asynchronmaschinen mit Käfigläufer*. PhD Thesis, Hannover University, 1969.

[Schw 1964]   Schwarz, K.K.: *Survey of basis stray losses in squirrel-cage induction motors*, Proc. IEE, 1964, Vo. 111, no. 9, p. 1565-1574.

[Taeg 1987]   Taegen, F.; Walczak, R.: *Experimental verification of stray load losses in cage induction motors under no-load, full-load and reverse rotation test conditions*. Archiv für Elektrotechnik 70, pp. 255-263, 1987.

[Trax 2003]   Traxler-Samek, G.: *Zusatzverluste im Stirnraum von Hydrogeneratoren mit Röbelstabwicklung*. PhD Thesis, Vienna University of Technology, 2003.

[VDE 2008]   VDE- Studie, Studie der Energietechnischen Gesellschaft im VDE (ETG): *Effizienz- und Einsparpotentiale elektrischer Energie in Deutschland; Perspektive bis 2025 und Handlungs-bedarf*. Januar 2008.

[Vogt 1974]   Vogt, K.: *Elektrische Maschinen, Berechnung rotierender elektrischer Maschinen*, VEB Verlag Technik Berlin, 2. Auflage 1974.

[Walt 1995]   Walters, D G.; Williams, I J.; Jackson D C.; Brook, H.: *The case for a new generation of high efficiency motors - some problems and solutions*, IEE, Electrical Machines and Drives, 11-13 Sept. 1995, Conference Publication no. 412, 1995, p. 26-31.

[Wepp 1964]   Weppler, R.: *Grundsätzliches zur Berechnung der Spaltstreuung bei Kurzschlussläufermotoren mit Berücksichtigung der Eisensättigung.* ETZ- A, Vol. 85, 1964, p. 402-407.

[Wepp 1966]   Weppler, R.: *Ein Beitrag zur Berechnung von Asynchronmotoren mit nichtisoliertem Läuferkäfig.* Archiv für Elektrotechnik 50, 1966, p. 238-252.

[Wepp 1969]   Weppler, R.; Neuhaus, W.: *Der Einfluss der Nutöffnungen auf den Drehmomentenverlauf von Drehstrom-Asynchronmotoren mit Käfigläufer.* ETZ- A, Vol. 90, 1969, p. 186-191.

[Zwan 2004]   Zwanziger, P.: *Elektrische Antriebstechnik – ein Beitrag zum Energiesparen*, ZVEI-Mitgliederversammlung des Fachverbandes Automation, TA-Kolloquium, 24. September 2004.

[Zwan 2006]   Zwanziger, P.: *Motor Systems in the Machinery Industry – a Manufacturer's Perspective from Point of View of CEMEP LV Motors*, Proc. of the Industrial Electric Motor Systems Efficiency Workshop, International Energy Agency, IEA, Paris, 15-16 May 2006.

7.1 List of Publications

[1] Aoulkadi, M.; Binder, A.: *Reverse Rotation Test for the Measurement of Stray load losses in 1.5 MW Squirrel-Cage Induction Generators*, Proc. of the International Symposium on Power Electronics, Electrical Drives, Automation and Motion, SPEEDAM, 16-18 June 2004, Capri, Italy, 2004, Vol. 2, p. F4B-1-F4B-4, 6 pages CD-ROM.

[2] Aoulkadi, M.; Binder, A.: *The eh-star method for determination of stray load losses in cage induction machines*, Proc. of the 4th International Conference Energy Efficiency in Motor Driven Systems, EEMODS, 5-8 Sept. 2005, Heidelberg, Germany, 2005, Vol. 1, p. 130-140.

[3] Aoulkadi, M.; Binder, A.: *Comparison of different measurement methods for stray load losses in cage induction machines: input-output method, rrt-method and eh-star-method*, Proc. of the 40th International Universities Power Engineering Conference, UPEC, 7-9 September 2005, Cork, Ireland, 2005, paper ID 75, 5 pages CD-ROM.

[4] Aoulkadi, M.; Binder, A.; Joksimović, G.: *Additional losses in high-speed induction machine - removed rotor test*, Proc. of the 11th European Conference on Power Electronics and Applications, EPE, 11-14 Sept. 2005, Dresden, Germany, 2005, paper ID 610, 10 pages CD-ROM.

[5] Aoulkadi, M.; Binder, A.: *Evaluation of Different Measurement Methods to Determine Stray Load Losses in Induction Machines*, Proc. of the International Symposium on Power Electronics, Electrical Drives, Automation and Motion, SPEEDAM, 23-26 May 2006, Taormina, Italy, 2006, p. S1-13-S1-18.

[6] Aoulkadi, M.; Binder, A.: *Comparison of different evaluation methods to determine stray load losses in induction machines with eh-star method*, Proc. of the 6th International Electric Machines and Drives Conference, IEMDC, 3-5 May 2007, Antalya, Turkey, 2007, Vol. 1, p. 519-524.

Published also in: IEEE Transactions on Industry Applications, Vol. 44, Issue 6, Nov.-dec. 2008, p. 1675-1682.

[7]   Aoulkadi, M.; Binder, A.: *Influence of auxiliary impedance on stray load loss determination with eh-star method*, Proc. of the 5th International Conference Energy Efficiency in Motor Driven Systems, EEMODS, 10-13 June 2007, Beijing, China, 2007.

[8]   Aoulkadi, M.; Binder, A.: *Die Eh-Stern-Methode - ein alternatives Messverfahren für die lastabhängigen Zusatzverluste in Asynchron-maschinen*, 6.Technischer Tag der VEM Gruppe in Wernigerode, 04-05 September 2007, Wernigerode, Deutschland, 2007.

[9]   Aoulkadi, M.; Binder, A.: *When loads stray, Evaluation of Different Measurement Methods to Determine Stray Load Losses in Induction Machines*, IEEE Industrial Electronics Magazine, Vol. 2, Issue 1, March 2008, p. 21- 30.

[10] Hagen, R.; Aoulkadi, M.; Binder, A.; Knopik, T.; Bradley, K.: *Comparison of measured and analytically calculated stray load losses in standard cage induction machines*. Proc. of the Int. Conf. on El. Machines (ICEM) 2008, September 6-9, 2008, Vilamoura, Algarve, Portugal, paper ID 1389, 6 pages CD-ROM.

7.2 Supervised Master Thesis (Diplomarbeit)

[1]   Gail, G.: *Einsatz der Bohrungsfeldmessung für die Bestimmung der Wicklungserwärmung und der lastabhängigen Zusatzverluste im Ständer von Asynchronmaschinen*. Diplomarbeit Nr. 604, September 2003.

[2]   Popescu, M.: *Determination of stray load losses in cage induction machines*. Master thesis Nr. 621, Juni 2006.

8 LIST OF SYMBOLS AND ABBREVIATIONS

Symbols

Symbol	Unit	Name
$\hat{a}_\mathrm{e}$	A/m	exciting current loading
$\underline{a}$	-	complex unity phasor: $\underline{a} = e^{j \cdot 2\pi / 3}, \underline{a}^2 = e^{j \cdot 4\pi / 3}, \quad \underline{a}^3 = 1$
a	-	number of parallel winding branches
$A_\mathrm{Cu,solid}$	m^2	copper cross section of the solid profiled partial conductor
a_p	-	number of parallel wires in bundle (partial conductors) per turn
A_Q	m^2	slot cross section
A_s	A/m	stator current loading
B	T	magnetic flux density
b_bot	m	slot width of the oval-shaped slot at the bottom edge
B_Q	T	magnetic flux density in slot (stray flux)
b_Q	m	slot width
$b_\mathrm{Q,e}$	m	equivalent slot width
b_TL	m	width of partial conductor
b_top	m	slot width of the oval-shaped slot at the top edge
d_Cu	m	diameter of the wire (without insulation)
$d_\mathrm{Cu,insl}$	m	diameter of the insulated wire
d_e	m	air gap between excitation and massive body
d_E	m	penetration depth
$d_\mathrm{insl,TL}$	m	insulation thickness of the wire (both sides)
$d_\mathrm{lin,insl}$	m	thickness of the slot lining
D_si	m	diameter of the stator bore

f	Hz	frequency
g	-	integer number
H	A/m	magnetic field strength
h_c	m	coil height
h_Q	m	slot height
h_{TL}	m	partial conductor height (without insulation)
h_w	m	height of the turn per coil
h_{wedge}	m	wedge height
I	A	current (rms)
I_0	A	no-load current at rated voltage
I_1	A	positive sequence current
I_2	A	negative sequence current
I_b	A	bar current
I_c	A	coil current
I_{Ft}	A	*Foucault* current (eddy current)
I_i	A	inner phase current "behind" the iron resistance R_{Fe}
$I_{i,1}$	A	inner phase current of positive sequence system
$I_{i,2}$	A	inner phase current of negative sequence system
I_N	A	rated current
I_{tN}	A	rated test current
j	-	$j = \sqrt{-1}$ imaginary unit
J	A/m^2	electric current density
k	-	coefficient between positive and negative sequence system
k_{Bind}	-	pitching coefficient considered acc. to *A. Binder*
k_{f1}	-	filling factor of the high power winding "winding 1"
k_{f2}	-	filling factor of the low power winding "winding 2"
k_{HF}	-	extension factor considering the turn height in the low filled slot
k_{LF}	-	litz filling factor
k_r	-	average increase of AC resistance
k_w	-	winding factor
$k_{w,coil}$	-	winding factor of the bore-coil ($k_{w.coil} = 1$)
l	m	axial length

l_{b1}	m	length of the conductor in the straight part of the winding overhang
l_{b2}	m	length of the conductor in the curved part of the winding overhang
l_{Fe}	m	length of the iron stack
L_{Fe}	m	total length of the iron stack (with radial ventilation ducts)
l'_{Fe}	m	corrected length of the iron stack
l_k	m	length (thickness) of the radial ventilation ducts
l_m	m	length of the conductor ($l_m = l_{Fe} + l_{b1} + l_{b2}$)
m	-	number of phases
M, M_δ	Nm	internal (air gap) torque
M_{ad}	Nm	additional loss torque
M_E	Nm	error in harmonic torque for eh-star method evaluation
M_{fw}	Nm	friction and windage torque
M_s	Nm	shaft torque
n	1/s	rotational speed
N	-	number of turns per phase
N_c	-	number of turns per coil
n_k	-	number of the radial ventilation ducts
n_n	-	number of wires (partial conductors) side by side (horizontal) per slot
$n_ü$	-	number of wires (partial conductors) one above the other per slot
$n_{ü/turn}$	-	number of wires (partial conductors) one above the other per turn
p	-	number of pole pairs
P	W	power
$P_{1.5}$	W/kg	specific iron losses at 1.5 T, 50 Hz
P_{ad}	W	additional losses (stray load losses)
$P_{ad,0}$	W	additional losses at no-load
$P_{ad,1}$	W	additional losses of positive sequence system
$P_{ad,2}$	W	additional losses of negative sequence system
$P_{ad,asym}$	W	additional losses at asymmetric feeding

$P_{ad,r}$	W	additional losses in the rotor
$P_{ad,s}$	W	additional losses in the stator
$P_{ad,s,1.O}$	W	first order skin effect additional losses in stator winding (circulating currents)
$P_{ad,s,2.O}$	W	second order skin effect additional losses in stator winding (within the conductor itself)
$P_{c+q,r}$	W	harmonic losses in the squirrel cage and in the rotor iron stack
P_{cont}	W	check input power (control)
$P_{Cu,s,dc}$	W	DC copper losses (without skin effect)
P_d	W	total losses (difference between input and output)
P_E	W	error in harmonic power for eh-star method evaluation
$P_{e,in}$	W	electrical input power
$P_{Fe,s}$	W	stator iron losses
$P_{Ft,1.O}$	W	first order eddy current losses in stator winding
$P_{Ft,2.O}$	W	second order eddy current losses in stator winding
P_{fw}	W	friction and windage losses
$P_{m,out}$	W	output power (mechanical power on the motor shaft)
$P_{p,r}$	W	high frequency pulsation losses in the rotor
$P_{p,s}$	W	high frequency pulsation losses in the stator
p_{pu}	-	number of the positive passes in upper layer
p_{slot}	-	number of passes through the slot ($p_{slot} = w_ü$ number of turns per slot for two-layer and $p_{slot} = 2 \cdot w_ü$ for single-layer winding)
$P_{sur,r}$	W	high frequency surface losses in the rotor
$P_{\delta,1}$	W	air gap power of positive sequence system
$P_{\delta,2}$	W	air gap power of negative sequence system
P_Σ	W	sum of the conventional losses
q	-	number of slots per pole and phase
Q	-	number of slots
R	Ω	resistance
R_{eh}	Ω	auxiliary resistance in eh-star-circuit
R_{Fe}	Ω	iron (core) resistance
R_m	-	magnetic *Reynolds* number
R_q	Ω	rotor cage inter-bar resistance

R_s	Ω	stator phase DC-resistance
$R_{s,ad}$	Ω	stator phase AC-resistance considering the stray load losses in the stator winding due to the skin effect
$R_{s,dc}$	Ω	stator phase DC-resistance (without skin effect)
s	m	distance
s	-	slip
s_1	-	slip of the positive sequence system
s_2	-	slip of the negative sequence system
s_Q	m	slot opening
s_w	-	number of mixed slots (different phases in upper and lower layer)
U	V	voltage (rms)
$\ddot{u}_U$	-	voltage transformation ratio between the stator winding and the bore-coil
U_i	V	inner phase voltage at the equivalent iron resistance R_{Fe}
$U_{i,1}$	V	inner phase voltage of positive sequence system
$U_{i,2}$	V	inner phase voltage of negative sequence system
U_{LL}	V	line to line voltage
U_s	V	stator phase voltage
$U_{s,1}$	V	positive sequence voltage
$U_{s,2}$	V	negative sequence voltage
W	m	coil width
w_{coil}	-	number of turns of the bore-coil
$w_{\ddot{u}}$	-	number of turns one above the other per slot
X	Ω	reactance
x	m	circumference co-ordinate
x	-	per unit inductance
X_{bore}	Ω	stator bore reactance (removed rotor test)
$X_{s\sigma b}$	Ω	stator winding overhang stray reactance
$X_{s\sigma Q}$	Ω	stator slot stray reactance
Z	Ω	impedance
Z_{eh}	Ω	auxiliary impedance in eh-star-circuit

Z_{sc}	Ω	stator short circuit impedance (at $s = 1$)

Greek

Symbol	Unit	Name
η	-	efficiency
Θ	A	ampere turns
δ	m	air gap width
ϑ	°C	temperature
$\Delta\vartheta$	K	temperature rise
κ	S/m	electric conductivity
ν	-	ordinal number of stator harmonic field
μ	-	ordinal number of rotor space harmonics, caused by the stator fundamental field $\nu = 1$
μ_ν	-	ordinal number of rotor harmonic field, caused by the νth stator harmonic field
μ	Vs/(Am)	magnetic permeability
μ_0	Vs/(Am)	magnetic permeability of empty space ($4\pi.10^{-7}$ Vs/(Am))
ξ	-	„reduced" conductor height
σ	-	stray (leakage) coefficient
σ_s	-	*Blondel's* stray coefficient
τ_Q	m	slot pitch (stator, rotor)
τ_p	m	pole pitch
$v_{Mü}$	-	number of positive sequences of the partial conductor
$\rho_{Mü}$	-	number of negative sequences of the partial conductor (transposed or twisted)
Φ	Wb	magnetic flux
φ	rad	phase angle
ω	1/s	angular frequency
∞	-	infinite

Subscripts

Symbol	Name
0	no-load
1	positive sequence
1.O	first order skin effect
2	negative sequence
2.O	second order skin effect
δ	air gap
ad	additional
av	average
b	winding overhang (bobinage)
c	coil, corrected (smoothed) data
Cu	copper
d	difference
dir	direct
e	electric, equivalent
eq	equivalent
Fe	iron
Ft	*Foucault* losses (eddy current losses)
fw	friction and windage
h	main, magnetizing (Hauptfeld)
hy	hysteresis
i	internal, inner, induced
in	input
indir	indirect
L	line
LL	line-to-line
m	mechanical, magnetic
max	maximum
mech	mechanical
N	rated (Nominal)
out	output

p	fundamental, pulsation
Q	slot
r	rotor
regr	regression (line)
ReRT	removed rotor test
s	stator
SC	Short circuit test or locked rotor test
t	test
TL	partial conductor (Teilleiter), wire
U, V, W	three phases
UV, VW, WU	line-to-line

Notation

Symbol	Name
i	lower-case letters: instantaneous value (e.g.: electric current) or per unit value
I	upper-case letters: r.m.s. or DC value (e.g.: electric current)
X, x	upper-case letter: value in physical units e.g. reactance in Ω, lower-case letter: per unit value
$\underline{I}$	underlined: complex values
$\underline{I}^*$	conjugated complex value of $\underline{I}$
$\hat{I}$	amplitude
I'	related to stator side winding
Re{.}	real part of ...
Im{.}	imaginary part of ...

Abbreviations

Symbol	Name
AC	Alternating Current

acc.	According
CDV	Committee Draft for Vote
CEMEP	European Committee of Manufacturers of Electrical Machines and Power Electronics
CO_2	Carbon dioxide
CSA	Canadian standard association
DC	Direct Current
DE	Drive end
e.g.	for example (latin: exempli gratia)
ECCP	European Climate Change Program
Ed	Edition
eh	single phase (*Einphasig*), auxiliary resistance (*Hilfswiderstand*)
FEM	Finite Element Method
i.e.	this means
I^2R	*Ohmic* losses
IEC	International Electrotechnical Commission
IEEE	Institution of Electrical and Electronic Engineers
IM	Induction machine
JEC	Japanese Electrotechnical Commission
L	Litz (braid) wire winding
NA	Not applicable
NDE	Non Drive end
NEMA	National Electrical Manufacturers Association
NM	Not measured
P	Profile conductor winding
p.u.	per unit
R	Round wire winding
ReRT	Removed rotor test
RRT	Reverse rotation test ($s = 2$)
SCT	Short circuit test or locked rotor test ($s = 1$)
TEFC	Totally enclosed fan cooled
vs.	versus

9   APPENDIX

9.1 Appendix A: Durand-Kerner method

Retrieved from "http://en.wikipedia.org/wiki/Durand-Kerner_method"

In numerical analysis, the *Durand-Kerner* method (established 1960-66) or method of *Weierstrass* (established 1859-91) is a root-finding algorithm for solving polynomial equations. In other words, the method can be used to solve numerically the equation

$$f(x) = 0 \tag{9.1}$$

where f is a given polynomial, which can be taken to be normed so that the leading coefficient is 1.

The explanation is for an equation of degree four. It is easily generalized to other degrees.
Let the normed polynomial f be defined by

$$f(x) = x^4 + a \cdot x^3 + b \cdot x^2 + c \cdot x + d \tag{9.2}$$

for all x.
The known numbers a, b, c, d are the coefficients.
Let the (complex) numbers P, Q, R, S be the roots of this polynomial f. Then

$$f(x) = (x - P) \cdot (x - Q) \cdot (x - R) \cdot (x - S) \tag{9.3}$$

for all x. One can isolate the value P from this equation,

$$P = x - \frac{f(x)}{(x-Q)\cdot(x-R)\cdot(x-S)}.$$ (9.4)

The substitution

$$x := x - \frac{f(x)}{(x-Q)\cdot(x-R)\cdot(x-S)}.$$ (9.5)

is a strongly stable fixed point iteration in that every initial point $x \neq Q, R, S$ delivers after one iteration the root P.

If one replaces the zeros Q, R and S by approximations q, r, $s \neq P$, then P is still a fixed point of the perturbed fixed point iteration since

$$P - \frac{f(P)}{(P-q)\cdot(P-r)\cdot(P-s)} = P - 0 = P.$$ (9.6)

Note that the denominator is still different from zero. This fixed point iteration is a contraction mapping, around P.

The clue to the method now is to combine the fixed point iteration for P with similar iterations for Q, R, S into a simultaneous iteration for all roots. Initialize p, q, r, s:

$$p_0 := (0.4 + 0.9\cdot j)^0;$$

$$q_0 := (0.4 + 0.9\cdot j)^1;$$

$$r_0 := (0.4 + 0.9\cdot j)^2;$$ (9.7)

$$s_0 := (0.4 + 0.9\cdot j)^3;$$

There is nothing special about choosing $(0.4 + 0.9\cdot j)$ except that it is neither a real number nor a root of unity.
Make the substitutions for $n = 1, 2, 3, \cdots$

$$p_n = p_{n-1} - \frac{f(p_{n-1})}{(p_{n-1} - q_{n-1}) \cdot (p_{n-1} - r_{n-1}) \cdot (p_{n-1} - s_{n-1})}$$

$$q_n = q_{n-1} - \frac{f(q_{n-1})}{(q_{n-1} - p_n) \cdot (q_{n-1} - r_{n-1}) \cdot (p_{n-1} - s_{n-1})}$$

(9.8)

$$r_n = r_{n-1} - \frac{f(r_{n-1})}{(r_{n-1} - p_n) \cdot (r_{n-1} - q_n) \cdot (r_{n-1} - s_{n-1})}$$

$$s_n = s_{n-1} - \frac{f(s_{n-1})}{(s_{n-1} - p_n) \cdot (s_{n-1} - q_n) \cdot (s_{n-1} - r_n)}.$$

Re-iterate until the numbers p, q, r, s stop essentially changing. Then they have the values P, Q, R, S in some order and in the chosen precision. So the problem is solved.

Note that you must use complex number arithmetic, and that the roots are found simultaneously rather than one at a time.

Example

$$f(x) = x^4 - 2 \cdot x^3 - 3 \cdot x^2 + 4 \cdot x + 5 = 0$$

(9.9)

As can be seen in Table 9.1 the first 6 iterations move p, q, r, s seemingly chaotically, but then the roots are located to 1 decimal. After the iteration number 7 we have 6 correct decimals, and the subsequent iteration number 9 confirms that the computed roots are fixed. This general behaviour is characteristic for the method.

	p	q	r	s
1.iter	0.567890-1.257574j	5.375121+1.7971371j	-2.83117249-0.24757577j	-1.111838-0.29198737j
2.iter	0.947011-1.128573j	3.578850+1.02767661j	-1.41127774+0.41594683j	-1.11458243-0.31505032j
3	1.363243-0.686370j	2.755792+0.58255052j	-1.06228266+0.43985696j	-1.05675176-0.33603752j
4	1.704446-0.356538j	2.354657+0.34629936j	-1.02051528+0.33580547j	-1.03858821-0.32556722j
5	1.947909-0.255583j	2.121741+0.25598039j	-1.03469917+0.32517503j	-1.03495096-0.3255729j
6	2.054696-0.313857j	2.015231+0.31385679j	-1.03496586+0.32574203j	-1.03496107-0.32574223j
7	2.034242-0.325300j	2.035681+0.32530047j	-1.03496163+0.32574103j	-1.03496163-0.32574104j
8	2.034963-0.325741j	2.034961+0.32574054j	-1.03496164+0.32574104j	-1.03496164-0.32574104j
9	2.034962-0.325741j	2.034962+0.32574104j	-1.03496164+0.32574104j	-1.03496164-0.32574104j
10	2.034962-0.325741j	2.034962+0.32574104j	-1.03496164+0.32574104j	-1.03496164-0.32574104j
11	2.034962-0.325741j	2.034962+0.32574104j	-1.03496164+0.32574104j	-1.03496164-0.32574104j
12	2.034962-0.325741j	2.034962+0.32574104j	-1.03496164+0.32574104j	-1.03496164-0.32574104j
13	2.034962-0.325741j	2.034962+0.32574104j	-1.03496164+0.32574104j	-1.03496164-0.32574104j
…				
20	2.034962-0.325741j	2.034962+0.32574104j	-1.03496164+0.32574104j	-1.03496164-0.32574104j

Table 9.1: The iterations and the roots of the example-polynomial

9.2 Appendix B: Measurement setup

Quantity	Instrument	Accuracy
Power	NORMA Wide Band Power Analyzer Type D6100	Voltage 0.07% at 50 Hz Current 0.07% at 50 Hz
	Shunts Norma Trax Shunt 1 ... 100 A	± 0.03%
Torque	Load cell HBM S2, 500 N	0.05%
	Load cell HBM S2, 50 N	0.05%
	Signal amplifier HBM MVD2555	0.1%
Speed	Heidenhain encoder ERN 120	TTL, 1024
Resistance	Burster Resistomat Type 2316	0.03% (resolution $0.1\mu\Omega$)
Resistance (cooling curve)	Yokogawa Analyzing recorder AR1100	0.2%
Current	Amperemeter	0.2%
Voltage	Voltmeter	0.1%
Time function of currents and voltages	FFT Analyzer Ono Sokki CF-5210	± 0.05 dB at <20 kHz ± 0.1 dB at 20 kHz ...100 kHz
Temperature	Thermocouple Type J, Type K	± 2.5°C
Flux density	Hall sensor Siemens type KSY 44	± 0.2% at $B = 0 \dots 0.5$ T ± 0.7% at $B = 0 \dots 1.0$ T

Table 9.2: Measurement instrument
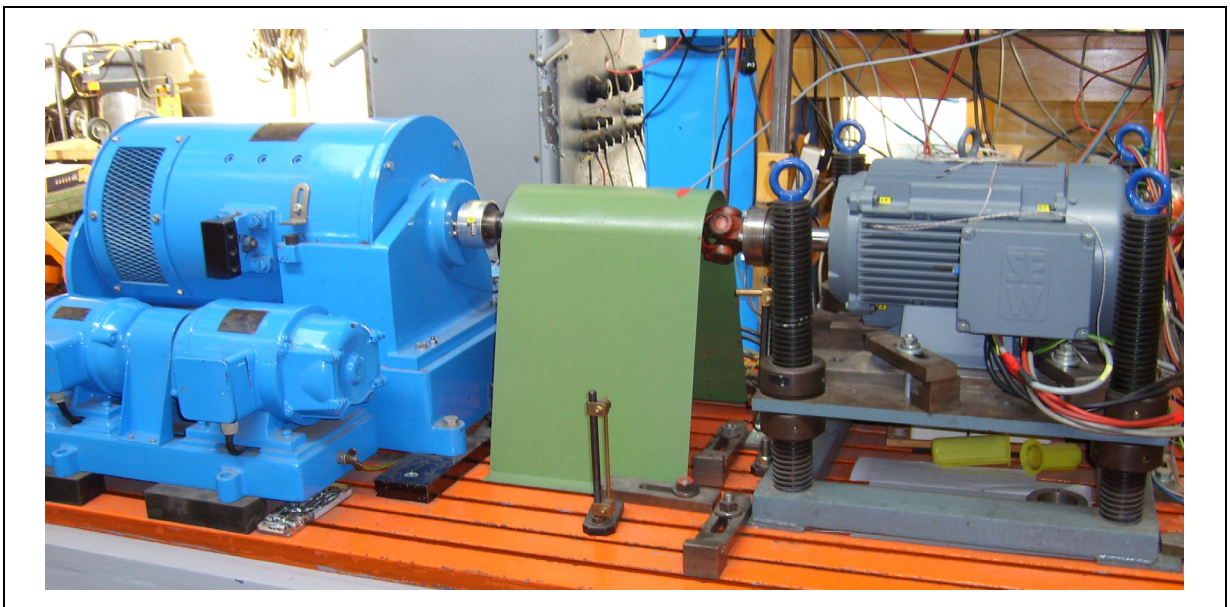
Figure 9.1: Test bench: coupled IM with dynamometer for frame size ≥132 mm

Figure 9.2: Test bench: Measurement instrument
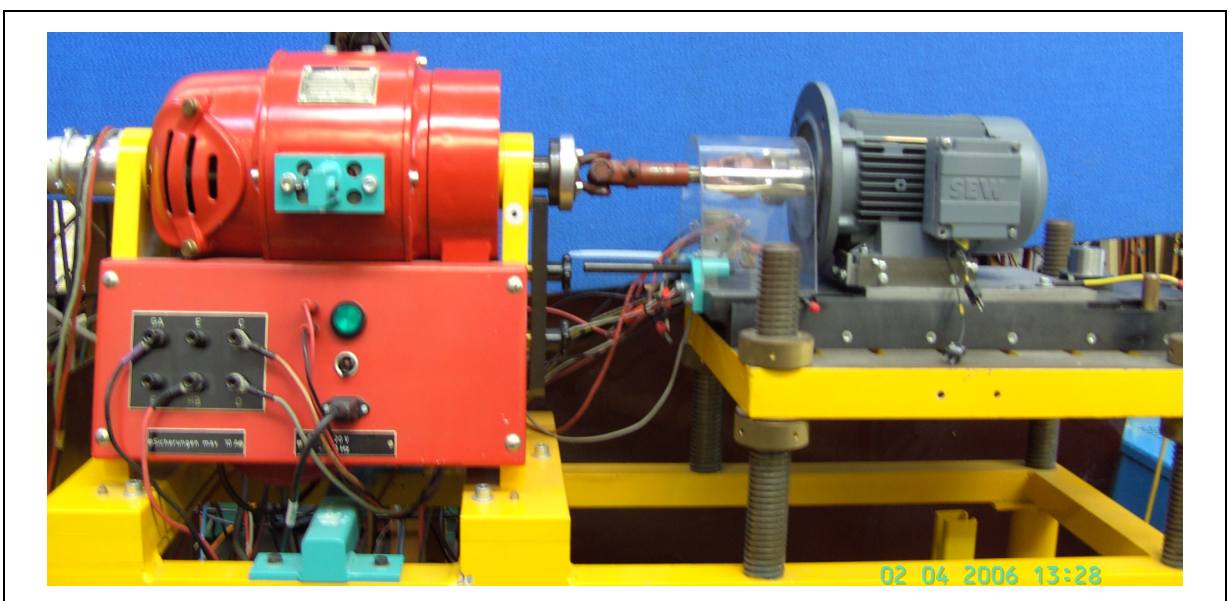
Figure 9.3: Test bench: coupled IM with dynamometer for frame size 80 mm

9.3 Appendix C: Tested motors

11 kW 4-pole motors	A160-4	B160-4	C160-4	D160-4	E160-4
Power / kW	11	11	11	11	11
Voltage / V; Connection Y	400	690	690	690	400
Current / A	21.4	12.1	12	12.4	22.5
Frequency / Hz	50	50	50	50	50
Speed / rpm	1455	1465	1450	1460	1440

Table 9.4: Rated data of tested 11 kW, 4-pole motors

11 kW 2- & 6-pole motors	A160-2	B160-2	C160-2	D160-2	A160-**6**
Power / kW	11	11	11	11	11
Voltage / V; Connection Y	690	400	690	400	690
Current / A	11.5	21.7	12.5	21.2	13.6
Frequency / Hz	50	50	50	50	50
Speed / rpm	2900	2940	2930	2880	967

Table 9.5: Rated data of tested 11 kW, 2-pole and 6-pole motors

5.5 kW 6- & 4-pole motors	A132-6	B132-6	C132-6	D132-6	A132-**4**
Power / kW	5.5	5.5	5.5	5.5	5.5
Voltage / V; Connection Y	690	400	690	400	690
Current / A	7	13.8	7.7	13.4	8.6
Frequency / Hz	50	50	50	50	50
Speed / rpm	955	960	950	960	1390

Table 9.6: Rated data of tested 5.5 kW, 6-pole and 4-pole motors

1.1 kW 2-pole motors	A80-2	B80-2	C80-2	D80-2
Power / kW	1.1	1.1	1.1	1.1
Voltage / V; Connection Δ	231	231	231	231
Current / A	4.43	4.27	4.32	4.9
Frequency / Hz	50	50	50	50
Speed / rpm	2835	2845	2845	2720

Table 9.7: Rated data of tested 1.1 kW, 2-pole motors

0.55 kW 4-pole motors	A80-4	B80-4	C80-4	D80-4
Power / kW	0.55	0.55	0.55	0.55
Voltage / V; Connection Δ	231	231	231	231
Current / A	2.89	2.76	2.65	2.67
Frequency / Hz	50	50	50	50
Speed / rpm	1400	1400	1390	1380

Table 9.8: Rated data of tested 0.55 kW, 4-pole motors

0.37 kW 6-pole motors	A80-6	B80-6	C80-6	D80-6
Power / kW	0.37	0.37	0.37	0.37
Voltage / V; Connection Δ	231	231	231	231
Current / A	2.14	2.2	2.22	2.16
Frequency / Hz	50	50	50	50
Speed / rpm	915	950	918	912

Table 9.9: Rated data of tested 0.37 kW, 6-pole motors

	A550-6	A317-4
	1500 kW 6-pole generator	315 kW 4-pole motor
Power / kW	1500	315
Voltage / V; Connection Δ	600	400
Current / A	1580	540
Frequency / Hz	60	50
Speed / rpm	1220	1488

Table 9.10: Rated data of tested 1500 kW, 6-pole generator and 315 kW, 4-pole motor

9.4 Appendix D: Example for measurement results

Stray load loss measurement results for 11 kW motor A160-4 acc. to IEC 60034-2 Ed. 4.0 draft / IEC 61972
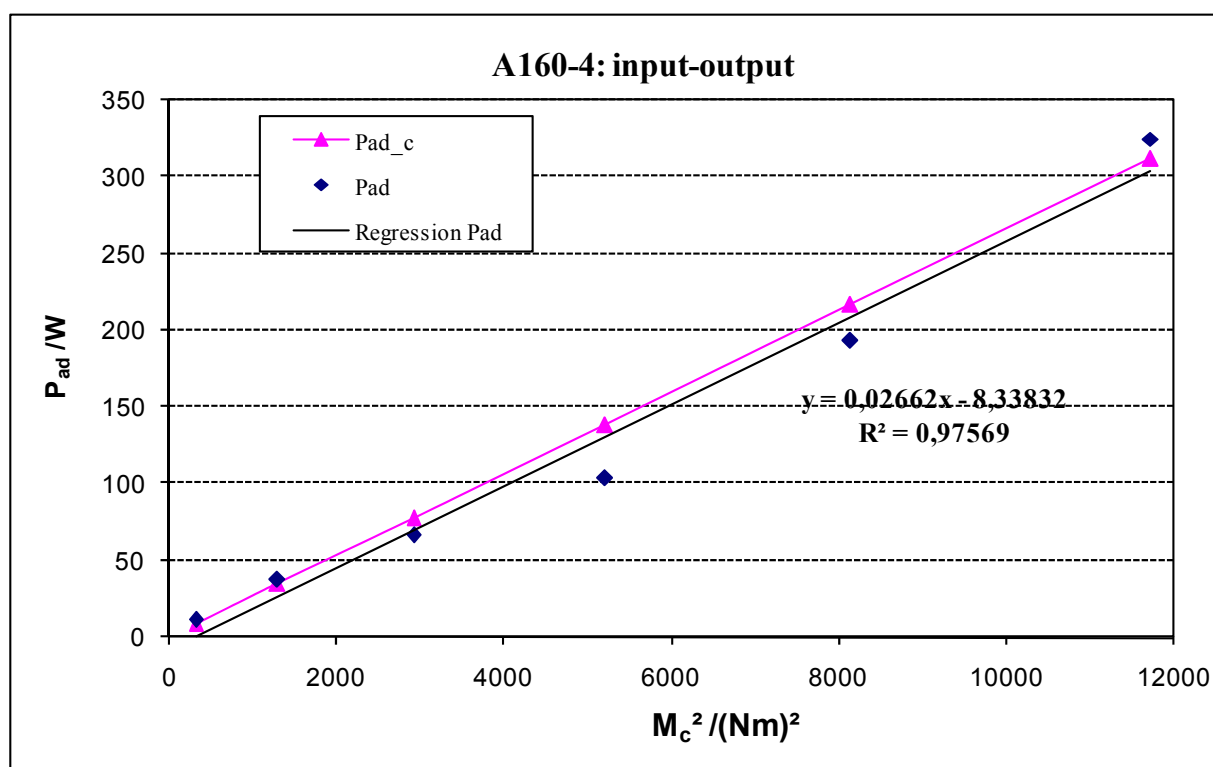

Figure 9.4: Residual loss method (Input-output test) acc. to IEC 60034-2 Ed. 4.0 draft

A160-4	$R_{LL, kalt}$ [Ω]	**0,7246**		400V Y		ϑ_{kalt} [°C]		20	
	$R_{LL, war}$ [Ω]	0,9228	ϑ_{wi} [°C]		89,75	ϑ_{Raum} [°C]		24	
Input-outpu	$R_{s, war\ 30s}$ [Ω]	0,9114	$\vartheta_{wi,\ 30s}$ [°C]		85,74				
	Heat run	1,5		1,25	1	0,75	0,5	0,25	
ϑ_{Raum} [°C]		24	24	23,9	23,9	23,9	23,8	23,76	
ϑ_{wi} [°C]		89,75	89,75	89,75	89,75	85,87	82,01	78,14	
f_s [Hz]		50	50	50	50	50	50	50	
n_{syn} [rpm]		1500	1500	1500	1500	1500	1500	1500	
Δn [rpm]		43,9	71,2	57,8	44,9	32,6	21	10	
n [rpm]		1456,1	1428,8	1442,2	1455,1	1467,4	1479	1490	
U_{LL} [V]		399,97	400,14	399,74	399,91	400,47	400,22	400,07	
I_L [A]		21,622	31,024	26,103	21,585	17,55	14,093	11,567	
$P_{el,in}$ [W]		12436,2	19044,3	15680,3	12462,8	9363,8	6355,9	3405,90	
P_{Fe_IEC} [W]		302,184	287,713	294,362	302,011	310,598	317,284	323,972	
$P_{Cu,s}$ [W]		647,40	1332,83	943,54	645,18	421,41	268,47	178,64	
P_δ [W]		11486,62	17423,76	14442,40	11515,61	8631,79	5770,15	2903,29	
$P_{Cu,r}$ [W]		336,18	827,05	556,51	344,70	187,60	80,78	19,36	
P_{R_IEC} [W]		70,15	70,15	70,15	70,15	70,15	70,15	70,15	
P_{total} [W]		1355,90	2517,74	1864,56	1362,04	989,76	736,69	592,12	
$P_{m,Norma}$ [W]		11013,00	16215,00	13636,00	11011,00	8321,60	5595,10	2816,10	
M [Nm]		72,12	108,27	90,19	72,16	54,05	36,03	17,95	
$M_{dyn\ Corr}$ [Nm]		0,010	0,010	0,010	0,010	0,010	0,010	0,010	
M_c [Nm]		72,134	108,282	90,198	72,171	54,064	36,035	17,958	
$P_{m,out}$ [W]		10999,23	16201,48	13622,36	10997,24	8307,72	5581,11	2802,01	
P_d [W]		1436,97	2842,82	2057,94	1465,56	1056,08	774,79	603,89	
P_{add} [W]		81,07	325,08	193,38	103,52	66,32	38,11	11,77	
$P_{add,ind}$ [W]		62,18	196,04	114,27	62,10	30,84	13,50	4,87	
$M_c{}^2$ [Nm²]		5203,37	11724,91	8135,73	5208,64	2922,87	1298,52	322,48	
Intercept B		-8,34	Slope A		0,02662	Correlat. Fact		0,988	Point Deleted	0
$P_{Cu,s\ c}$ [W]		649,39	1336,94	946,45	647,17	427,83	275,88	185,85	
Δn_c [rpm]		44,04	71,43	57,98	45,04	33,11	21,60	10,42	
n_c [rpm]		1456,0	1428,6	1442,0	1455,0	1466,9	1478,4	1489,6	
$P_{\delta\ c}$ [W]		11484,62	17419,65	14439,49	11513,62	8625,37	5762,74	2896,08	
$P_{Cu,r\ c}$ [W]		337,18	829,48	558,17	345,74	190,40	82,97	20,11	
$P_{add,c}$ [W]		138,50	312,08	216,55	138,64	77,80	34,56	8,58	
$P_{total,c}$ [W]		1497,41	2836,36	2085,68	1503,71	1076,77	780,85	608,66	
$P_{m,out,c}$ [W]		10938,79	16207,94	13594,62	10959,09	8287,03	5575,05	2797,24	
η [%]		87,96	85,11	86,70	87,93	88,50	87,71	82,13	
η_{dir} [%]		88,43	85,07	86,87	88,23	88,71	87,79	82,22	
$\eta_{indir0.5}$ [%]		88,60	85,75	87,38	88,57	89,10	88,20	82,47	
$\eta_{indirIEC-2}$ [%]		87,12	83,65	85,58	87,11	88,01	87,53	82,31	
$\eta_{indirIEEE-E1}$		87,50	84,26	86,07	87,49	88,28	87,70	82,37	
$p.f.$ [%]		83,03	88,57	86,76	83,36	76,92	65,06	42,49	

Table 9.11: Residual loss method (Input-output test) acc. to IEC 60034-2 Ed. 4.0 draft

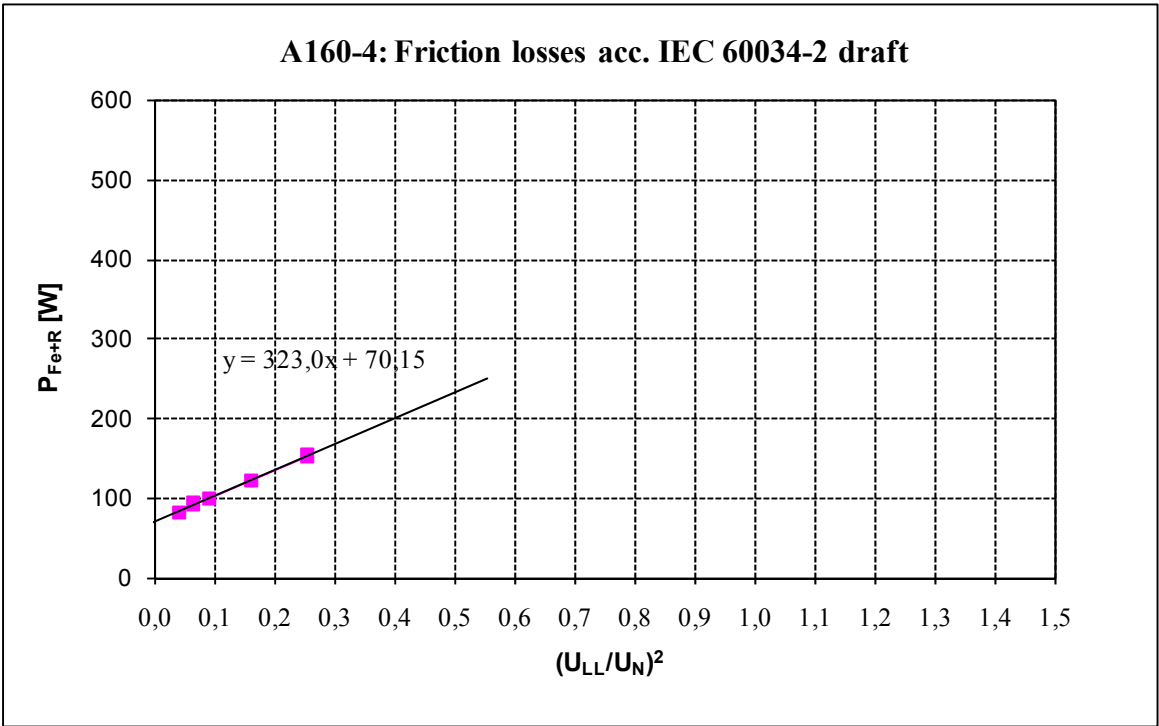No-load losses segregation acc. to IEC 60034-2 Ed. 4 draft.

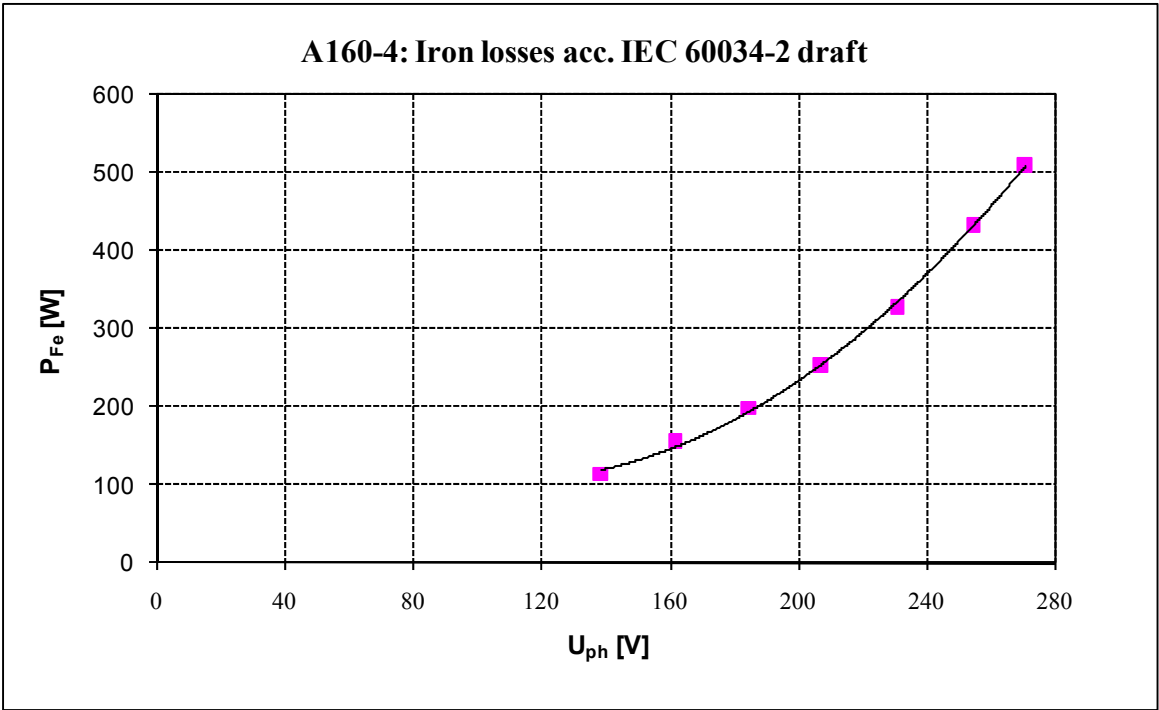Figure 9.5: Friction losses acc. to IEC 60034-2 Ed. 4.0 draft

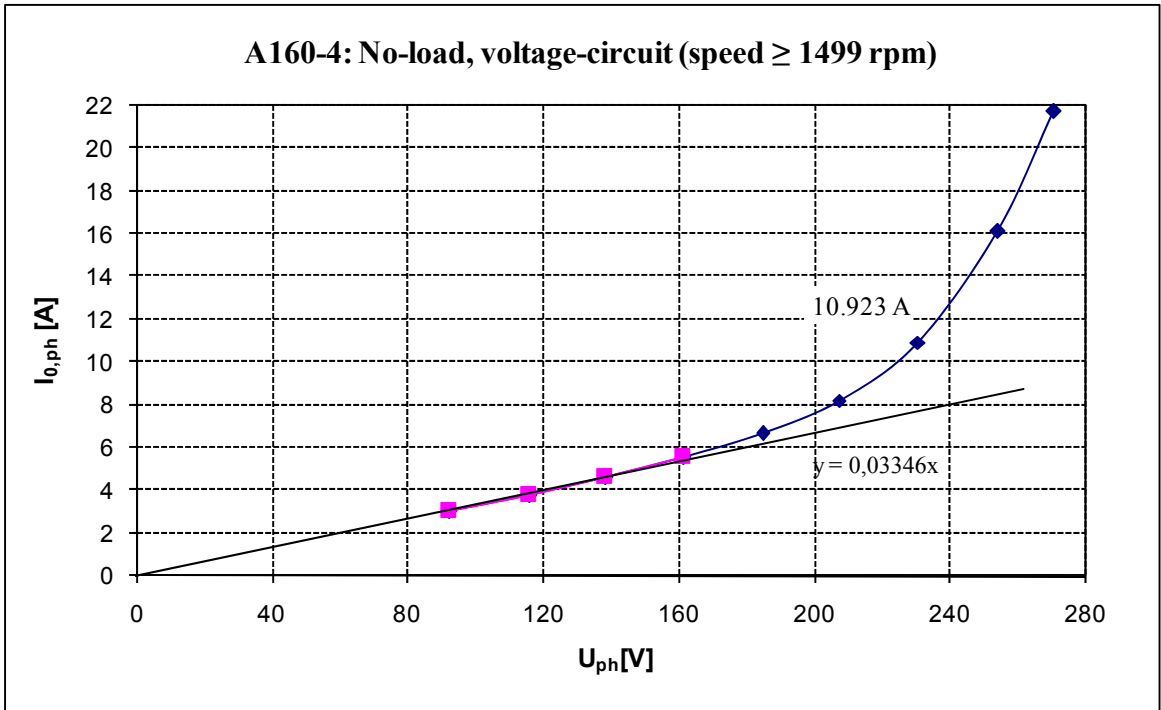Figure 9.6: Iron losses acc. to IEC 60034-2 Ed. 4.0 draft

Figure 9.7: No-load, voltage-current

U_{LL} [V]	I_L [A]	$P_{el,in}$ [W]	$\vartheta_{wi, mit}$ [°C]	$R_{s, war}$ [Ω]	$P_{Cu,s}$ [W]	P_{Fe+R} [W]	P_{Fe} [W]	n [rpm]
469,18	21,733	1152,6	49,65	0,4044	573,06	579,54	509,39	1500,5
440,89	16,141	818	49,65	0,4044	316,10	501,90	431,75	1500,2
399,72	10,923	541,3	49,65	0,4044	144,76	396,54	**326,39**	1500,1
359,28	8,234	404,32	48,44	0,4027	81,91	322,41	252,26	1500,1
320,55	6,682	323,79	47,29	0,4011	53,72	270,07	199,92	1499,4
280,11	5,538	261,77	46,08	0,3993	36,74	225,03	154,88	1499,5
240,41	4,608	210,54	44,89	0,3977	25,33	185,21	115,06	1499,6
201,37	3,804	168,7	43,72	0,3960	17,19	151,51		1499,9
160,42	3,042	133,64	42,50	0,3943	10,95	122,69		1499,9
120,10	2,334	106,37	41,29	0,3926	6,42	99,95		1498,7
101,32	2,035	95,9	40,73	0,3918	4,87	91,03		1497,6
80,54	1,723	85,81	40,11	0,3909	3,48	82,33		1496,3

No-load **A160-4** 400V Y $R_{s,20°C}$ [Ω] 0,36230

Table 9.12: No-load test acc. to IEC 60034-2 Ed. 4.0 draft
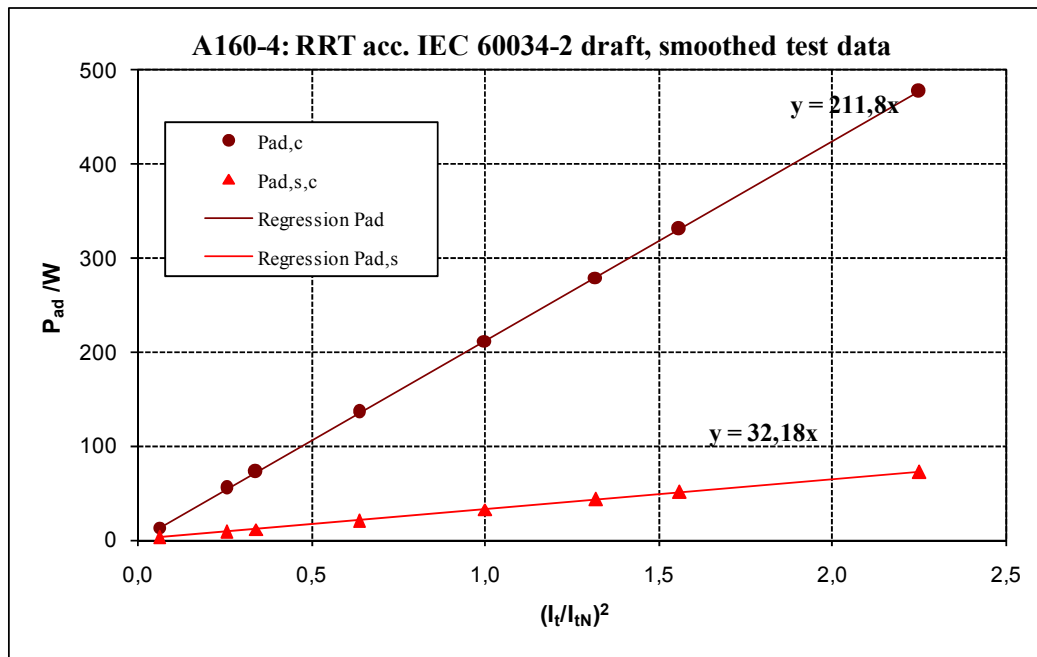
Figure 9.8: Reverse rotation test acc. to IEC 60034-2 Ed. 4.0 draft

| A160-4 | $R_{s,\,kalt}$ [Ω] | **0,3623** | | 400V Y | ϑ_{kalt} [°C] | 20 |
| | $R_{s,\,war}$ [Ω] | 0,4160 | ϑ_{wi} [°C] | 57,78 | ϑ_{Raum} [°C] | 25 |

RRT	1,5	1,25	I_N =21.62A	$I_{t,N}$ =18.66A	0,75	I_0 =10.92A	0,50	0,25	0
ϑ_{Raum} [°C]	23,5	23,5	23,5	23,6	23,6	24	24,5	25	
ϑ_{wi} [°C]	57,70	57,79	57,82	57,86	57,86	57,86	57,86	57,86	
ϑ_{Geh} [°C]	50,7	54,0	56,9	57,9	57,6	54,3	51,8	50,1	
n [rpm]	1500,3	1500,3	1500,1	1500,1	1499,7	1501,1	1500	1499,4	1500
U_{LL} [V]	75,20	65,24	61,01	54,41	45,06	34,72	30,87	18,29	
I_{tL} [A]	28,011	23,326	21,449	18,684	14,915	10,921	9,475	4,712	
$P_{el,in}$ [W]	1750,17	1242,84	1055,83	797,89	504,23	264,63	196,85	49,713	
M_c [Nm]	7,328	5,326	4,575	3,634	2,513	1,572	1,311	0,741	0,441
$P_{m,in}$ [W]	1151,29	836,71	718,62	570,82	394,61	247,05	205,99	116,32	69,20
$P_{m,in}$-P_0 [W]	1082,09	767,51	649,42	501,62	325,40	177,85	136,79	47,12	
$P_{Cu,s}$ [W]	978,88	679,02	574,21	435,77	277,69	148,88	112,07	27,72	
$P_{ad,r}$ [W]	428,68	281,48	231,57	184,77	123,03	69,06	54,05	15,89	
$P_{ad,s}$ [W]	117,9	77,8	63,8	45,3	24,2	7,0	2,0	-9,2	
P_{add} [W]	546,57	359,27	295,35	230,05	147,19	76,02	56,09	6,67	
M_c² [Nm²]	53,70	28,36	20,93	13,20	6,31	2,47	1,72	0,55	
$(I_t/I_{t,N})$²	2,25	1,56	1,32	1,00	0,64	0,34	0,26	0,06	
$P_{m,in}$-P_0 [W]	1031,98	744,25	640,70	500,75	334,87	191,93	148,93	42,78	
$P_{el,in}$ [W]	1782,94	1233,22	1041,50	788,75	501,04	267,45	200,91	49,20	
$P_{el,ReRT,c}$ [W]	1137,55	783,42	660,32	498,44	314,94	166,88	124,94	30,10	
$\vartheta_{wi,ReRT}$ [°C]	65,63	71,70	73,80	78,28	78,28	78,28	78,28	78,28	
$R_{s,\,ReRT}$ [Ω]	0,42713	0,43576	0,43874	0,44510	0,44510	0,44510	0,44510	0,44510	
$R_{s,\,RRT}$ [Ω]	0,41586	0,41599	0,41604	0,41610	0,41610	0,41610	0,41610	0,41610	
P_{add}' [W]	492,23	334,31	282,96	212,35	147,31	88,60	70,21	22,19	
$P_{ad,c}$ [W]	477,28	330,98	279,85	**212,35**	135,32	72,55	54,61	13,51	
$P_{ad,s,c}$ [W]	72,5	50,3	42,5	32,3	20,6	11,0	8,3	2,1	

Table 9.13: Reverse rotation test acc. to IEC 60034-2 Ed. 4.0 draft

Evaluation of eh-star-test, guideline, Version 1.5   A160-4
Algorithm written by M. Aoulkadi/Darmstadt University of Technology

	Star connection!	load point	1	2	3	4	5	6
Input data	rated line- line voltage	$U_{N,Y}$ [V]	400,0			Motor type	A160-4	
	rated phase current	I_N [A]	21,6			core losses	P_{FeN} [W]	312,4
	no-load phase current	I_0 [A]	10,9			friction & windage losses	P_{fwN} [W]	71,4
	number of poles	2p	4,0		Stator phase resistance @ 20°C		$R_{s, 20°C}$ [Ω]	0,4
	frequency	f [Hz]	50,0	50,0	50,0	50,0	50,0	50,0
	line- line voltage	U_{UV} [V]	152,5	140,2	125,0	120,1	107,2	82,7
	line- line voltage	U_{VW} [V]	166,3	152,8	136,3	130,9	116,8	89,9
	line- line voltage	U_{WU} [V]	47,5	42,8	37,3	35,6	31,0	22,3
	phase current	I_{Uph} [A]	27,3	24,7	21,7	20,7	18,2	13,8
	phase current	I_{Vph} [A]	32,5	29,5	25,8	24,6	21,7	16,4
	phase current	I_{Wph} [A]	22,4	20,1	17,5	16,6	14,4	10,4
	input power	$P_{e,in}$ [W]	2456,7	2050,5	1600,0	1469,4	1155,4	684,8
	speed	n [rpm]	1467,5	1466,7	1466,4	1466,3	1465,3	1461,3
					Comments:			
	line- line resistance @ 20°C	$R_{VW, 20°C}$ [Ω]	0,7		Measurement Aron_V, Evaluation method C			
	line- line resistance @ begin	$R_{VW, begin}$ [Ω]	0,7					
	line- line resistance @ end	$R_{VW, end}$ [Ω]	0,8					

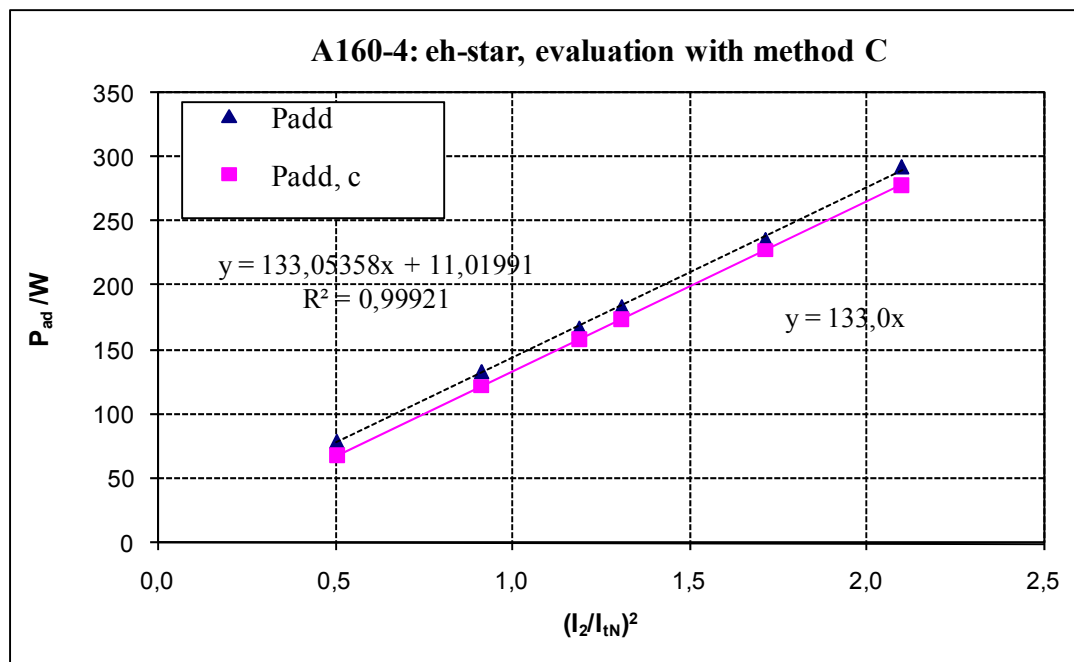|	eh-impedance (=U_{WU}/I_{Wph})	Z_{eh} [Ω]	2,1238	2,1268	2,1346	2,1393	2,1438	2,1502
Output data	winding temperature	temp [°C]	29,58	32,9830	37,01	38,30	41,54	41,54
	positive sequence current	I_1 [A]	5,8784	5,3658	4,7681	4,5857	4,1404	3,4453
	negative sequence current	I_2 [A]	27,0378	24,4424	21,3614	20,3620	17,8526	13,2873
	ratio (positive/negative)	I_1 / I_2	0,2174	0,2195	0,2232	0,2252	0,2319	0,2593
	rated test current	I_{tN} [A]	18,6595	18,6595	18,6595	18,6595	18,6595	18,6595
	stray load losses	P_{add} [W]	293,3285	236,6515	184,3855	167,8209	133,9670	79,7112
	check of real power	P_{cont} [W]	2456,70	2050,50	1600,00	1469,40	1155,42	684,81
		$(I_2 /I_{tN})^2$	2,0996	1,7159	1,3106	1,1908	0,9154	0,5071
		$P_{cont} /P_{e,in}$	1	1	1	1	1	1
	stray load losses @ I_{tN}	Intercept B	11,0199		Slope A	133,0536	Correlat. Fact	0,99961
	corrected stray load losses	$P_{add, c}$ [W]	279,362	228,304	174,376	158,441	121,795	67,468

Figure 9.9: Eh-star method